UNIVERSITY OF LEEDS

Modelling climate-ice sheet interactions during the Last and Penultimate Deglaciations (~21-9 ka and ~140-128 ka)

Violet Lorna Patterson

The University of Leeds

School of Earth and Environment

January 2025

Submitted in accordance with the requirements for the degree of

Doctor of Philosophy

Intellectual property

I confirm that the work submitted is my own, except where work which has formed part of jointly authored publications has been included. My contribution and the other authors to this work has been explicitly indicated below. I confirm that appropriate credit has been given within the thesis where reference has been made to the work of others.

Research from the publication Patterson et al., 2024, *Contrasting the Penultimate Glacial Maximum and the Last Glacial Maximum (140 and 21 ka) using coupled climate–ice sheet modelling*, Climate of the Past, 20(10), pp.2191–2218, https://doi.org/10.5194/cp-20-2191-2024, jointly authored with Lauren J. Gregoire, Ruza F. Ivanovic, Niall Gandy, Jonathan Owen, Robin S. Smith, Oliver G. Pollard, Lachlan C. Astfalck and Paul J. Valdes, has been included in this thesis as Chapter 2. VLP designed the simulations (along with LJG, RFI and NG), led the project and performed the majority of the work including preparing the initial and boundary conditions (alongside NG and support from OGP), running the simulations, analysing the results and writing the manuscript with comments and contributions from all co-authors. LJG, RFI and NG supervised the work and contributed to the interpretation of the results. LJG acquired the funding and conceptualised the project. LCA and NG designed and performed the wave 2 simulations the ensembles were sampled from, and JO did the sampling. RSS provided technical and scientific support and updates for FAMOUS-Glimmer. PJV provided the PGM HadCM3 sea surface temperature and sea ice dataset.

The work in Chapter 3 has been submitted to The Cryosphere, jointly authored by Violet L. Patterson, Lauren J. Gregoire. Ruza F. Ivanovic, Niall Gandy, Stephen Cornford, Jonathan Owen, Sam Sherriff-Tadano and Robin S. Smith with the provisional title: "*Exploring the sensitivity of the Northern Hemisphere ice sheets at the last two glacial maxima to coupled climate-ice sheet model parameters*". VLP lead the project and undertook the majority of the work. VLP designed the study (alongside LJG, RFI and NG), prepared the initial and boundary conditions, ran the simulations, analysed the results and wrote the manuscript with input from all co-authors and particular contribution from SST on the FAMOUS-ice coupling and elevcon description. LJG, RFI, and NG supervised the project and aided the interpretation of the results, and LJG acquired the funding. SC provided technical and scientific support in the set-up and updating of BISICLES. SST and RSS implemented and tested the elevcon height adjustment parameter. JO provided support on statistical methods including the Sobol′ analysis and

emulation. Any changes to the work presented in this thesis are due to the editorial and review process of the journal.

The work in Chapter 4 was led and undertaken by Violet L. Patterson and included contributions from Lauren J. Gregoire, Ruza F. Ivanovic and Niall Gandy. VLP designed the experiments (with support from LJG, RFI and NG), prepared the initial conditions and transient forcings, ran the simulations and analysed the results. LJG, RFI and NG supervised the work throughout, advised on the results and provided comments on the text.

Acknowledgements

Firstly, I would like to thank my supervisors Lauren Gregoire, Ruza Ivanovic and Niall Gandy for their continued support and feedback over the course of this PhD. I greatly appreciate all your encouragement and belief in me and feel lucky to have worked under your guidance and expertise.

I also could not have completed this work without the technical support and expertise of Robin Smith, Stephen Cornford, Julia Tindall and Richard Rigby. I would also like to thank Jonathan Owen for his invaluable statistical knowledge and teaching.

Thank you to Brooke, Yvan, Sam, Laura, Trys and Oliver and the rest of ICAS and the Climate-Ice research group in Leeds. They were always willing to help but also made the experience particularly enjoyable.

Finally, I am grateful to my friends and family for being there for me throughout, especially to my Mum and Dad, Nancy, and Huey the dog; thanks for always being so supportive and loving.

This project was funded by the "SMB-Gen" UK Research and Innovation (UKRI) Future Leaders Fellowship (grant no. MR/S016961/1).

Abstract

The Penultimate Deglaciation (PDG; ~140–128 thousand years ago; ka) is the transition from the Penultimate Glacial Maximum (PGM; ~140 ka) to the Last Interglacial (LIG; ~129–116 ka). The LIG experienced warmer temperatures than present day and it was the last time in Earth's history that sea levels were higher than todays, due to larger contributions from the Greenland and Antarctic ice sheets. Understanding the mechanisms that led to their retreat is important for accurately projecting future sea level rise, because large uncertainties remain in how the ice sheets will respond to a warming climate. The climate and ice sheets at the LIG were still responding to changes that occurred during the PDG, yet very little is known about their evolution during this period due to incomplete and highly uncertain geological data. However, from what records do exist, it is thought that the magnitude and sequence of events differed from the more recent and better constrained Last Deglaciation (LDG; ~21–9 ka). Numerical modelling of these two periods can help fill the gaps in the empirical record and provide a deeper understanding of the complex interactions that occurred between the ice sheets and climate during glacial-interglacial cycles. This will require the improvement of complex coupled climate-ice sheet models so that they are able to simulate all time periods well.

This thesis strives to contribute to this endeavour by examining the similarities and differences between the last two deglaciations through a series of coupled climate-ice sheet simulations using the model FAMOUS-ice. First, the model is tuned to produce realistic Northern Hemisphere ice sheets during the Last and Penultimate glacial maxima through large ensemble analyses and model-data comparison. This provides a range of initial Last Glacial Maximum and Penultimate Glacial Maximum ice sheet conditions for use in subsequent simulations. Error margins resulting from uncertain model parameters are explored, and the importance of different processes and feedbacks on the configuration of the glacial maximum ice sheets is quantified through sensitivity experiments and statistical analyses. Finally, transient simulations of the Last and Penultimate deglaciations are performed in which the rates and patterns of Northern Hemisphere ice sheet retreat are compared. It is shown that modelled rates of deglaciation occurred at a quicker rate during the PDG than the LDG, and the different Eurasian ice sheet configurations led to different patterns of retreat through varied instability mechanisms. Further sensitivity tests are undertaken to investigate the role of surface, sub-shelf and dynamic processes in the ice sheet retreat, as well as the relative importance of insolation, greenhouse gases and sea surface conditions in driving deglaciation. This work highlights the

high sensitivity of the surface mass balance to the albedo of the ice sheets, and its dominant role in determining the configuration of the simulated ice sheets during all stages due to the ice-albedo feedback. Accurate representation of ice dynamics becomes more important when simulating ice sheet retreat, but the ice sheet evolution is not as sensitive to the rate of sub-shelf melt, except when confined ice shelves form. This thesis also highlights the need for the tuning of coupled climate-ice sheet models across transient simulations to find sets of parameters that produce plausible ice sheet configurations at all phases of glacial-interglacial cycles, as well as for present and future scenarios, to increase the reliability of simulations of future sea level rise.

Contents

Intellectual property **ii**

Acknowledgements **iv**

Abstract **v**

Contents **vii**

List of Figures **xi**

List of Tables **xiv**

Abbreviations **xv**

Introduction **1**

1.1 Motivation 1
1.2 Context 3
1.2.1 Quaternary glacial-interglacial cycles 3
1.2.1.1 Ice sheet records 5
1.2.1.2 Climate records 6
1.2.2 Ice sheet-earth system interactions 8
1.2.2.1 Ice sheet – atmosphere interactions 8
1.2.2.2 Ice sheet – ocean interactions 9
1.2.2.3 Ice dynamics 11
1.2.2.4 Ice sheet – solid earth interactions 12
1.2.2.5 Other interactions 12
1.2.3 The Last Deglaciation versus the Penultimate Deglaciation 13
1.2.3.1 Ice sheets 13
1.2.3.2 Climate 21
1.2.4 Numerical modelling of glacial-interglacial cycles 25
1.2.5 Previous studies 31
1.3 Aims and approach of this study 36

Contrasting the Penultimate and Last Glacial Maxima (140 and 21 ka) using coupled climate-ice sheet modelling **40**

2.1 Abstract 40

2.2 Introduction 41
2.3 Methods 43
2.3.1 Model description 43
2.3.2 Experiment design 45
2.3.2.1 Climate boundary conditions 45
2.3.2.2 Ice sheet boundary and initial conditions 48
2.3.3 Ensemble design 50
2.3.4 Implausibility criteria 52
2.3.5 Sensitivity analysis 54
2.4 Results 55
2.4.1 Ensembles 55
2.4.2 Impact of initial ice sheet versus climate 58
2.4.3 Uncertainty due to model parameters 60
2.5 Discussion 62
2.6 Conclusions 67
2.7 Appendices 68
2.7.1 Eccentricity equation correction 68
2.7.2 Sea surface temperatures 69
2.7.3 Impact of different initial ice sheets 69
2.7.4 Wave 2 methodology 69
2.7.5 Metrics versus parameters plots 73

Exploring the sensitivity of the Northern Hemisphere ice sheets at the last two glacial maxima to coupled climate-ice sheet model parameters 76

3.1 Abstract 76
3.2 Introduction 77
3.3 Methods 81
3.3.1 Models 81
3.3.2 Ice dynamics in BISICLES 85
3.3.2.1 Temperature spin-up 86
3.3.2.2 Drain factor sensitivity tests 86
3.3.2.3 Spatial resolution sensitivity tests 87
3.3.3 Experiment design 88
3.3.3.1 Boundary and initial conditions 88
3.3.3.2 Ensemble design 89
3.3.4 Evaluating the ensemble 91

3.3.5 Gaussian process emulation and Sobol′ sensitivity analysis 93
3.4 Results and discussion 94
3.4.1 Initial ensemble 94
3.4.2 Non-implausible parameter sets 97
3.4.3 Sensitivity to parameters 102
3.4.4 Ice dynamics 107
3.5 Conclusions 110
3.6 Appendices 111
3.6.1 Implementation of the *elevcon* parameter 111
3.6.2 BISICLES spin-up 114
3.6.3 Sensitivity tests 117
3.6.4 Leave-one-out-cross-validation (LOOCV) 119
3.6.5 Parameter pairs plot 120

Comparing the Last and Penultimate Deglaciations using a coupled climate-ice sheet model 122

4.1 Abstract 122
4.2 Introduction 123
4.3 Methods 126
4.3.1 Models 126
4.3.2 Experiment design 127
4.3.2.1 Boundary and Initial Conditions 127
4.3.2.2 Sensitivity experiments 131
4.4 Results 133
4.4.1 Reference simulations 133
4.4.1.1 Rate of deglaciation 133
4.4.1.2 Pattern of deglaciation 135
4.4.1.3 Comparison of simulated climates 138
4.4.2 Parameter sensitivity tests 140
4.4.3 Forcing sensitivity tests 142
4.5 Discussion 143
4.5.1 Evaluation of reference ice sheets 143
4.5.2 Causes of ice retreat 145
4.5.3 Evaluation of reference climates 149
4.5.4 Parameter sensitivities 150
4.5.5 Forcing sensitivities 152

4.5.6 Limitations and future work 153
4.6 Conclusions 154
4.7 Appendices 155
4.7.1 Glacial maximum spin-ups 155
4.7.2 Control experiments 157
4.7.3 Surface ablation and ocean loss in the parameter sensitivity experiments 158

Discussion and conclusions **160**

5.1 Review of aims and research questions 160
5.1.1 RQ1. Why did the configuration of the Northern Hemisphere ice sheets differ during the Last Glacial Maximum and Penultimate Glacial Maximum? 161
5.1.2 RQ2. Which climatological and glaciological processes and feedbacks are important when simulating glacial periods? 162
5.1.3 RQ3. What are the similarities and differences between the last two deglaciations due to the different transient climate forcings (orbit, GHGs, sea surface conditions) and initial ice sheet states? 165
5.1.4 RQ4. What are the main drivers of ice sheet retreat during the last two deglaciations? 168
5.2 Limitations and future work 171
5.2.1 Initial ice sheet states 171
5.2.2 Climate forcing 172
5.2.3 Modelling limitations 173
5.2.3.1 Climate model 173
5.2.3.2 Ice sheet model 174
5.2.4 Techniques 177
5.3 Conclusions 180

Bibliography **183**

List of Figures

Figure 1.1: Structure of glacial-interglacial cycles over the past 500,000 years 4
Figure 1.2: Interactions between ice sheets and other components of the earth system. 9
Figure 1.3: Sea level evolution over the past two glacial cycles 14
Figure 1.4: Reconstructions of the extent of the NH ice sheets 17
Figure 1.5: Major ice streams and drainage routes of the LGM NH ice sheets 19
Figure 1.6: Proxy records of abrupt events over the Last and Penultimate deglaciations 23
Figure 1.7: Hierarchy of stress balance approximations available in ice sheet models 28

Figure 2.1: Coupling procedure between FAMOUS and Glimmer 45
Figure 2.2: LGM and PGM insolation and SSTs 48
Figure 2.3: FAMOUS topography and ice mask initial condition 49
Figure 2.4: LGM NAIS implausibility metric 54
Figure 2.5: FAMOUS-Glimmer LGM and PGM ensemble ice volume distribution 56
Figure 2.6: FAMOUS-Glimmer LGM and PGM ensemble ice volumes and southern areas. 57
Figure 2.7: LGM and PGM NROY ensemble members ice volume distribution 58
Figure 2.8: Sensitivity tests final ice thickness. 59
Figure 2.9: Sensitivity tests ice thickness, runoff and snowfall differences 60
Figure 2.10: Relationship between LGM southern area and influential parameters. 62
Figure 2.11: Evolution of climate proxies over the last two glacial-interglacial cycles 65
Figure 2.12: Effects of eccentricity error 68
Figure 2.13: LGM and PGM HadCM3 SSTs and LGM SST statisitcal reconstruction. 69
Figure 2.14: Impact of different initial ice sheets on ice thickness 69
Figure 2.15: Ice volumes in emulated sub-waves of simulations 72
Figure 2.16: LGM ensemble: southern area versus each of the 13 parameters 73
Figure 2.17: PGM ensemble: southern area versus each of the 13 parameters 74
Figure 2.18: LGM minus PGM southern area versus each of the 13 parameters 75

Figure 3.1: Resolution sensitivity tests results; ice thickness 88
Figure 3.2: LGM NAIS and EIS implausibility metric. 92
Figure 3.3: FAMOUS-BISICLES LGM and PGM ensemble ice volume distribution. 95
Figure 3.4: LGM and PGM ensemble mean SMB and variance 96
Figure 3.5: LGM NROY simulations; final ice thickness and SMB 99

Figure 3.6: PGM NROY simulations; final ice thickness and SMB 100
Figure 3.7: PGM NROY simulations versus other model reconstructions 101
Figure 3.8: FAMOUS-BISICLES LGM and PGM ensemble ice volumes and areas 102
Figure 3.9: Sobol′ sensitivity analysis results 105
Figure 3.10: Emulated mean ice sheet volumes versus influential parameters. 106
Figure 3.11: Sobol′ sensitivity indices for *beta* and relationship to ocean ice loss 107
Figure 3.12: LGM NROY simulations NAIS ice streams compared to reconstructions 108
Figure 3.13: LGM NROY simulations EIS ice streams compared to reconstructions 110
Figure 3.14: *Elevcon* sensitivity test results. 113
Figure 3.15: Effect of different values of *elevcon* on LGM NAIS SMB 113
Figure 3.16: LGM and PGM spin-ups initial SMB and ice surface temperature 114
Figure 3.17: LGM spin-up internal ice temperature 115
Figure 3.18: PGM spin-up internal ice temperature. 116
Figure 3.19: Till water drainage rate sensitivity tests results; ice velocity 117
Figure 3.20: Resolution sensitivity tests results; ice velocity 118
Figure 3.21: Resolution sensitivity tests results; difference in ice velocity 118
Figure 3.22: Leave-One-Out Cross Validation results 119
Figure 3.23: FAMOUS-BISICLES ensemble parameter pair plot 120
Figure 3.24: PGM NROY simulations NAIS ice streams 121
Figure 3.25: PGM NROY simulations EIS ice streams 121

Figure 4.1: LDG and PDG transient insolation and CO_2 forcings 128
Figure 4.2: LDG and PDG transient SST, sea ice and sub-ocean forcings 129
Figure 4.3: LDG_{ref} and PDG_{ref} simulations; ice volume evolution 134
Figure 4.4: LDG_{ref} and PDG_{ref} simulations; normalised ice volume evolution 135
Figure 4.5: Pattern of ice retreat and velocity during LDG_{ref} 136
Figure 4.6: LDG_{ref} simulation ice thickness compared to the reconstructions 137
Figure 4.7: Pattern of ice retreat and velocity during PDG_{ref} 138
Figure 4.8: LDG_{ref} and PDG_{ref} annual mean surface air temperature evolution 139
Figure 4.9: LDG_{ref} and PDG_{ref} global mean surface air temperature difference 140
Figure 4.10: Total ice shelf area in LDG_{ref} and LDG_{ssm} simulations. 141
Figure 4.11: LDG and PDG parameter sensitivity tests; ice volume evolution 142
Figure 4.12: LDG and PDG forcing sensitivity tests; ice volume evolution 143
Figure 4.13: LDG_{ref} and $PDG_{ref.}$ simulations; surface versus ocean mass loss 147
Figure 4.14: LDG and PDG bedrock difference, ice velocity and sub-shelf melt rate 148

Figure 4.15: PDG_{ssm} and PDG_{ref} simulations; difference in ice velocity. 151
Figure 4.16: LGM and PGM glacial maximum spin-up ice volume evolutions 156
Figure 4.17: Reference versus sub-shelf melt simulations initial ice thickness 157
Figure 4.18: LDG and PDG control experiment results..... 157
Figure 4.19: LDG_{ssm} and $PDG_{ssm.}$ simulations; surface versus ocean mass loss..... 158
Figure 4.20: LDG_{drain} and $PDG_{drain.}$ simulations; surface versus ocean mass loss 158
Figure 4.21: LDG_{alb} and $PDG_{alb.}$ simulations; surface versus ocean mass loss..... 159

Figure 5.1: FAMOUS-Glimmer versus FAMOUS-BISICLES ice volume distributions..... 175
Figure 5.2: Parameter pair plot; LGM NAIS and modern Greenland NROY simulations... 180

List of Tables

Table 1.1: Research objectives 37

Table 2.1: LGM and PGM climate boundary conditions 46
Table 2.2: FAMOUS-Glimmer experiments and initial conditions 50
Table 2.3: Description of parameters varied in the ensembles 51
Table 2.4: LGM and PGM NROY simulations; average ice sheet volumes and areas. 56
Table 2.5: Sensitivity experiments; final ice volumes 59

Table 3.1: Parameters varied in the ensemble and the ranges sampled. 90
Table 3.2: Ranges of values used in implausibility metric 93
Table 3.3: LGM and PGM NROY simulations; ice sheet volumes and extents 98
Table 4.1: List of experiments and the parameter values and transient forcing used 133

Table 5.1: Research objectives 160

Abbreviations

ACR Antarctic Cold Reversal

AIS Antarctic Ice Sheet

AMOC Atlantic Meridional Overturning Circulation

BA Bølling-Allerød

BIIS British-Irish Ice Sheet

BKIS Barents-Kara Ice Sheet

CIS Cordilleran Ice Sheet

EIS Eurasian Ice Sheet

ELA Equilibrium Line Altitude

EMIC Earth system Model of Intermediate Complexity

FIS Fennoscandian Ice Sheet

(AO)GCM (Atmosphere-Ocean) General Circulation Model

GHG Greenhouse Gas

GIA Glacial Isostatic Adjustment

GMT Global Mean Air Temperature

GrIS Greenland Ice Sheet

GP Gaussian Process

HS Heinrich Stadial

IRD Ice Rafted Debris

ISM Ice Sheet Model

ka thousand years before present

kyr thousand years

LDG Last Deglaciation

LGM Last Glacial Maximum

LIG Last Interglacial

LIS Laurentide Ice Sheet

MIS Marine Isotope Stage

NADW North Atlantic Deep-water

NAIS North American Ice Sheet

NH Northern Hemisphere

NROY Not Ruled Out Yet

PDG Penultimate Deglaciation

PGM Penultimate Glacial Maximum

PMIP4 Paleoclimate Modelling Intercomparison Project phase 4

RSL Relative Sea Level

SIA Shallow Ice Approximation

s.l.e. Sea Level Equivalent

SMB Surface Mass Balance

SSA Shallow Shelf Approximation

SST Sea Surface Temperature

YD Younger Dryas

Chapter 1

1 Introduction

1.1 Motivation

By the end of the 21st century, human induced climate change is projected to cause up to 4.8°C of atmospheric warming depending on the emissions scenario (relative to 1995-2014) (Intergovernmental Panel on Climate Change (IPCC), 2023b). This will have significant impacts globally, including sea level rise due to the melting of the Greenland and Antarctic ice sheets, which will threaten coastal environments, causing catastrophic economic, social and environmental losses. However, the magnitude of sea level rise, and therefore the severity of the impacts, is highly uncertain with projections ranging from 0.3-1.6 m depending on the emissions scenario. One of the biggest uncertainties stems from how ice sheets will respond to warming and the likelihood of processes such as marine ice sheet instability occurring (Bamber et al., 2022; Intergovernmental Panel on Climate Change (IPCC), 2023c; Kopp et al., 2017; Pattyn et al., 2018). Ice sheets can respond to changes in climate across millennial timescales for which direct observations are not available. However, in the past, the climate system has experienced huge shifts, albeit as a result of natural processes and not anthropogenic, causing significant changes in ice sheet extent and sea level. Thus, studying these past periods, through the palaeo-record and numerical modelling, could advance our understanding of how ice sheets respond to changes in climate forcing (such as solar insolation and greenhouse gases) and the processes and mechanisms responsible for higher sea levels, therefore helping constrain projections of future sea level rise (Fischer et al., 2018; Haywood et al., 2019; Masson-Delmotte et al., 2013; Stokes et al., 2015). In addition, model-data comparison will enable us to determine the robustness of the models when performing out-of-sample, i.e. in future projection scenarios.

In particular, the Last Interglacial period (LIG; ~129-116 thousand years ago; ka) was the most recent period in Earth's history where temperatures were higher than pre-industrial times. It is estimated that average global surface temperatures were ~1-2 °C higher (Otto-Bliesner et al., 2013a; Turney and Jones, 2010), with high latitude temperatures exceeding this (Capron et al., 2017a; Landais et al., 2016), causing a sea level 1-9 m higher than present day (Dutton and Lambeck, 2012; Dyer et al., 2021; Kopp et al., 2009). This implies there was significant ice

loss from the Greenland and Antarctic ice sheets but the individual contributions from each, as well as the total global mean sea level rise, is uncertain, largely due to a lack of understanding of the mechanisms involved in their retreat (Dutton et al., 2015; Quiquet et al., 2013; Stone et al., 2013). The LIG has therefore been the focus of numerous studies seeking to disentangle the interactions that occurred between the climate and the ice sheets during this period of substantial change, since it is seen as a partial analogue for future climate change (Gilford et al., 2020; Golledge et al., 2021).

Due to the response times of ice sheets being on the order of millennia, changes in sea level during the LIG were still responding to changes in the climate and ice sheets that took place during the deglaciation that preceded it; the Penultimate Deglaciation (PDG; ~140-128 ka) (Menviel et al., 2019). Not much is known about the evolution of the climate and ice sheets during the PDG due to the erasure of glaciological evidence during the more recent glacial advance and difficulties in dating older records (Capron et al., 2017b; Govin et al., 2015). Nevertheless, there is some evidence that the pace, magnitude and timing of changes during the PDG differed to the Last Deglaciation (LDG; ~21-9 ka), which preceded the current Holocene interglacial, possibly contributing to the different interglacial characteristics (Landais et al., 2013; Menviel et al., 2019). Thus, developing a deeper understanding of how and why these two deglaciations differed, will provide important knowledge on how the earth system responds to large changes in internal and external forcings.

Whilst the palaeo-data record can provide important constraints on how the components of the earth system changed over time, they do not easily explain what caused these changes or how these components interacted with each other (Harrison et al., 2016). This is therefore the motivation of this PhD project, as well as many others in the research community, who aim to fill in some of the gaps in the data record by using numerical models to simulate the evolution of the Last and Penultimate glacial cycles. For example, the Paleoclimate Modelling Intercomparison Project phase 4 (PMIP4) has produced protocols for performing simulations of the deglaciations, using complex climate models, to investigate the responses of the climate system to large changes in boundary conditions (Ivanovic et al., 2016; Menviel et al., 2019). This PhD project contributes to this modelling effort and uses the climate boundary conditions outlined in these protocols. However, it also seeks to capture the important feedbacks that occur between the climate and the ice sheets (outlined in Sect. 1.2.2) by coupling a general circulation model (GCM) to an ice sheet model (ISM). This will help further understanding on the evolution of the earth system during the last two glacial-interglacial cycles and how this may have contributed to the higher sea level during the Last Interglacial compared to present day.

In addition, comparing the results of these modelling studies to the available palaeo-data provides valuable information on the capabilities of the models used for future projections of sea level rise. This can then be utilised to provide estimates of the uncertainty in projections as a result of model limitations, as well as help improve the representation of certain processes in numerical models and increase their ability to robustly simulate all time periods (Braconnot et al., 2012; Harrison et al., 2016).

1.2 Context

1.2.1 Quaternary glacial-interglacial cycles

During the Quaternary (2.6 million years ago to present), the Earth's climate cycled between long, colder glacial and brief, warmer interglacial conditions (Lisiecki and Raymo, 2005; PAGES, 2016). The huge shifts in the climate and ice sheets that occurred during this period are documented in the palaeo-record (see Sects. 1.2.1.1 and 1.2.1.2) which shows how glacial periods involve a gradual cooling, a decreasing of greenhouse gases (GHGs) and the slow build up, over 70,000-90,000 years, of large ice sheets over the Northern Hemisphere (NH) continents. This caused sea levels to decrease by up to 130 m at the glacial maximum (Bintanja et al., 2005; Lambeck et al., 2014). In contrast, the transition to interglacial conditions, called deglaciations or terminations, happens relatively quickly (~10,000 years) causing the record of changes in climate to display a sawtooth pattern (Figure 1.1; Broecker and van Donk, 1970; PAGES, 2016). During deglaciations, temperatures and GHGs increase and the large continental ice sheets retreat, releasing large fluxes of meltwater into the oceans, causing a global mean sea level rise. These large scale shifts in climate are triggered by changes in summer insolation received at high northern latitudes due to variations in the Earth's orbit (the Milankovitch Theory; Berger, 1978, 1980; Hays et al., 1976). This includes changes to the shape of the Earth's orbit (eccentricity), the tilt of the Earth's axis (obliquity) and the direction the axis is pointed (precession). However internal amplifications mechanisms and feedbacks are needed to explain the magnitude and timings of the rapid deglaciations (Lisiecki, 2010).

After the long term build-up of ice sheets reaches a critical threshold, they can then become susceptible to rapid disintegration under a modest insolation forcing due to non-linear responses of the climate system (Abe-Ouchi et al., 2013; Barker and Knorr, 2021; Imbrie et al., 1993; PAGES, 2016). These mechanisms are related to increases in atmospheric CO_2, changes in atmospheric and oceanic circulation, and feedbacks related to the ice sheets themselves (Abe-Ouchi et al., 2013; Cheng et al., 2009; Denton et al., 2010; Stap et al., 2014). Additionally, within each deglaciation, there is evidence of abrupt millennial scale events in which the

climate oscillates between colder stadial and warmer interstadial conditions (Dansgaard et al., 1993; McManus et al., 1999; PAGES, 2016). Ice core isotope records from Greenland and Antarctica show large and abrupt changes in temperature and GHGs occurring asynchronously over the Northern and Southern Hemispheres (Barbante et al., 2006; Blunier et al., 1998; Blunier and Brook, 2001; Jouzel et al., 2007b) leading to the widely accepted theory that these events are related to a change in the strength of the Atlantic Meridional Overturning Circulation (AMOC) and thus the transport of heat across the equator. This concept is known as the "thermal bipolar seesaw" (Broecker, 1998; McManus et al., 2004; Stocker and Johnsen, 2003). AMOC weakening has been suggested to arise due to a reduction of North Atlantic Deep-water (NADW) formation as a result of increased meltwater into the North Atlantic from ice sheet disintegration (triggered by rising insolation) (Ivanovic et al., 2017; Ng et al., 2018). To support this, ice rafted debris (IRD) layers in North Atlantic sediment cores provide evidence of huge iceberg discharges from the North American ice sheet providing additional freshwater to the region (called Heinrich events) during some of the stadials (called Heinrich Stadials; Heinrich, 1988) which could be a consequence of and/or lead to a strengthening of these abrupt events (Barker et al., 2015; Broecker, 1994; Hemming, 2004).

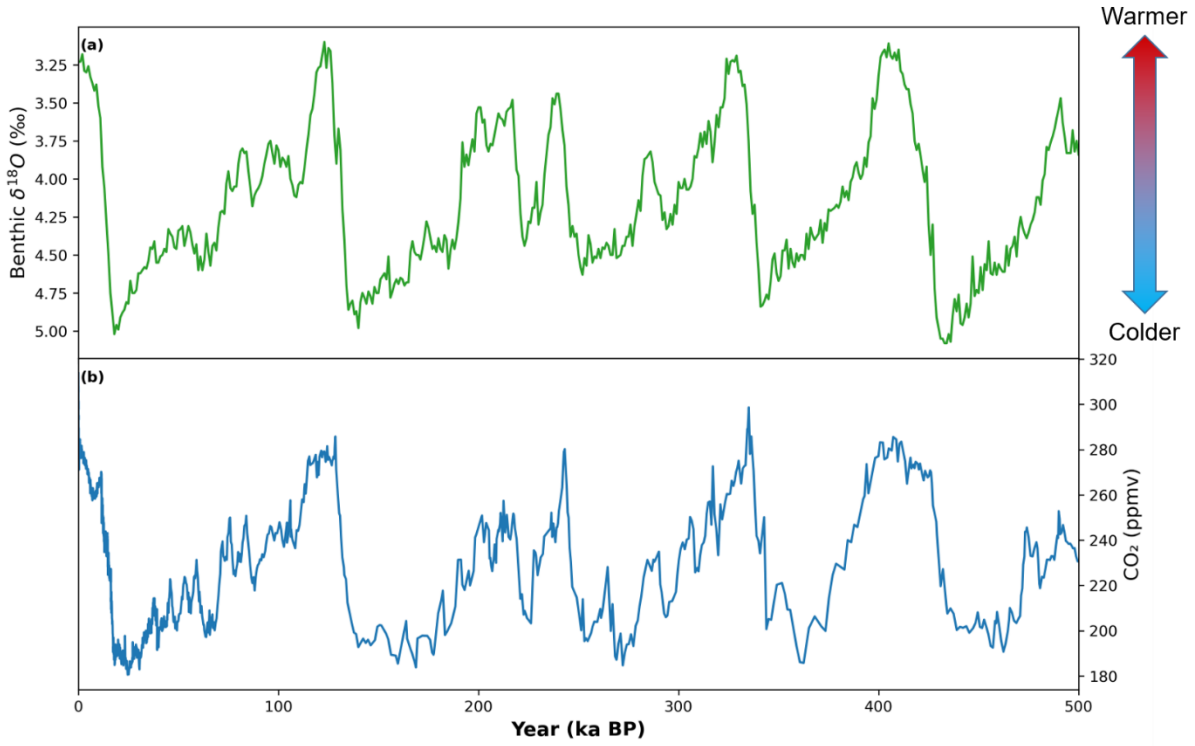

Figure 1.1: Structure of glacial-interglacial cycles over the past 500,000 years shown through (a) the benthic $\delta^{18}O$ record (a proxy for temperature and global ice volume; Lisiecki and Raymo, (2005)) and (b) EPICA Dome C CO_2 record (Bereiter et al., 2015).

The characteristics of each glacial-interglacial cycle differ as a result of variations in the evolution of external climate factors, such as insolation, and complex interactions between all components of the earth system, most of which are not yet fully understood (Hughes and Gibbard, 2018). To further our understanding of the Quaternary cycles, these processes need to be explored on all spatial and temporal scales. Some of the major interactions and feedbacks affecting the evolution of the climate and ice sheets that need to be considered are outlined in Sect. 1.2.2.

1.2.1.1 Ice sheet records

There are a number of lines of empirical evidence that can help determine the extent, dynamics and chronology of the ice sheets through glacial-interglacial cycles. This includes the use of landforms, such as drumlins and moraines, and properties of sediment deposits, which can also be dated using methods such as radiocarbon dating and cosmogenic exposure, to provide a geochronological record (Ely et al., 2021; Kleman et al., 2006; Kleman and Borgström, 1996; Stokes et al., 2015). For example moraine ridges can be mapped and dated to show change in ice sheet extent and flow direction over time (Clark et al., 2012a), benthic $\delta^{18}O$ isotope records from marine sediment cores are used as a proxy for changes in global ice volume and sea level (Lisiecki and Raymo, 2005), and sediment dropped from melting icebergs (IRD) can indicate the marine extent of ice sheets and periods of rapid ice sheet disintegration (Hemming, 2004; Knies et al., 2001).

The accuracy of reconstructions based on this empirical evidence is limited by the spatial and temporal resolution of geomorphological evidence and chronological controls, low precision of available dates, sample contamination, measurement uncertainty and contradictions and discrepancies between different lines of data (Dalton et al., 2020; Hughes et al., 2016; Patton et al., 2017). Nevertheless, several compilations of data have been produced to reconstruct the evolution of the extent of the ice sheets and ice streaming at the Last Glacial Maximum (LGM) and through the Last Deglaciation (e.g. Batchelor et al., 2019; Clark et al., 2022; Dalton et al., 2020; Dyke et al., 2002; Hughes et al., 2016; Margold et al., 2018), which have been used as boundary conditions and constraints for numerical models (e.g. Tarasov et al., 2012).

The Penultimate Deglaciation efforts have been limited to reconstructing the maximum extent through the whole Penultimate Glacial Cycle (Batchelor et al., 2019; Svendsen et al., 2004). This is because there are fewer constraints on periods predating the LGM as much of the glaciological evidence was erased by the last glacial advance, and there are also difficulties in dating older records (Hughes and Gibbard, 2018; Svendsen et al., 2004). In addition, the

thickness distribution and surface topography of the ice sheets during both glacials are more uncertain since there is little direct evidence from the empirical record and they must therefore be inferred from indirect constraints such as relative sea level (RSL) (Harrison et al., 2016; Stokes et al., 2015).

Whilst the addition of water into the ocean raises the global mean sea level, the spatial pattern of sea level change varies globally due to a few additional processes that act upon the oceans and land. The sea level measured at a specific location (relative to the local topography) is known as RSL. The main processes that can affect the RSL are changes to land ice volume (and hence global mean sea level) and changes to the height of the land due to glacial isostatic adjustment (GIA). GIA is the response of the solid earth, gravitational field and oceans to the loading of ice masses (Whitehouse, 2018; Yokoyama and Purcell, 2021). As an ice sheet grows it depresses the lithosphere and mantle beneath it and when it retreats the elastic lithosphere rebounds almost instantaneously whereas the viscous mantle has a delayed response, over thousands to hundreds of thousands of years (Fyke et al., 2018; Yokoyama and Purcell, 2021). This redistribution of mass also affects Earth's gravitational field and axis of rotation. A smaller ice sheet mass exerts a smaller gravitational influence on the ocean, causing a fall in local sea level (Yokoyama and Purcell, 2021).

RSL data can be obtained from coral reefs, raised shorelines and faunal assamblages on continental shelves and combined with GIA modelling, sometimes along with ice extent and chronological constraints, to reconstruct global sea level change (and therefore total ice volume change) and ice thickness over the deglaciations (Lecavalier et al., 2014). Global mean sea level change can also be measured from evidence at sites far from the past ice sheets and measurements can be supplemented by GPS data of present day vertical velocities of the land (Argus et al., 2014; Lambeck et al., 2006, 2017; Milne et al., 2002; Peltier et al., 2015). However, there are large uncertainties in the rheological structure of the earth and different earth models can produce multiple ice sheet configurations that fit the RSL data (Schmidt et al., 2014b). These methods can also not provide information on mechanisms of retreat and often produce ice sheets that are inconsistent with ice sheet physics and climate (Tarasov et al., 2012).

1.2.1.2 Climate records

The climatic conditions, and timing of changes, during glacial-interglacial cycles can be inferred from empirical evidence obtained from ice and sediment cores and speleothems. Measurements made from air bubbles in ice cores provide a direct record of the atmospheric

composition over time meaning GHG concentrations (including CO_2, N_2O and CH_4) over several glacial-interglacial cycles are relatively well known. Greenland ice cores (e.g. NGRIP) only span the last glacial cycle (~123,000 years) whereas ice cores from Antarctica (e.g. EPICA Dome C) go as far as 800,000 years before present (Andersen et al., 2004; Augustin et al., 2004). In addition, measurements of $\delta^{18}O$ and deuterium isotopes from ice cores can also provide a proxy for air temperatures over the ice sheets (Andersen et al., 2004; Jouzel et al., 2007b). Rates and amount of dust deposition can also be determined from ice cores, which also serve as a proxy for Antarctic air temperature during glacials, since dust deposition becomes increasingly positively correlated with Antarctic temperature as it gets colder (Lambert et al., 2008). The distribution and chemistry of microfossils (e.g. insects, pollen, foraminifera) and sediments found in cores and rocks in marine, lake and terrestrial environments can provide proxies for temperature, salinity and precipitation, and provide information on past vegetation (e.g. Martrat et al., 2014; Oppo et al., 2006). As well as providing a proxy for global ice volume, the marine oxygen isotope record is also affected by ocean temperatures (Lisiecki and Raymo, 2005). These can be disentangled to provide a record of sea surface temperatures (SSTs) and ice volume (Shakun et al., 2015). Speleothems are cave formations produced when mineral deposits are carried by ground water percolating through the rock and build up over tens of thousands of years. Similar to cores, measurements of isotopes and trace elements in the deposits can provide information on multiple climate variables (Drysdale et al., 2020; Wong and Breecker, 2015) and give relatively precise timings of climate events (Cheng et al., 2009).

As with empirical data on palaeo-ice sheets, uncertainties arise from unreliable chronologies, irregular sampling, different techniques used and discrepancies between different datasets (Govin et al., 2015; Harrison et al., 2016). In addition, palaeoclimate proxies can be controlled by multiple factors making it difficult to disentangle the influence from a single variable of interest. They can also be influenced by non-climatic factors (e.g. CO_2), and rely on the assumption that relationships observed between the proxy and the climate variable held throughout the past (Braconnot et al., 2012). Therefore, multiple proxies are usually combined to reconstruct past climate variables (e.g. Waelbroeck et al., 2009) and numerical climate models can be employed to further our understanding and fill in gaps by constraining the physical processes that lead to the spatial and temporal patterns seen in records (Jonkers et al., 2021). These models are usually forced with appropriate insolation values which can be calculated from the orbital parameters (eccentricity, obliquity and precession).

1.2.2 Ice sheet-earth system interactions

Whilst it is mostly changes in summer insolation and atmospheric CO_2 that drives changes in the climate, pacing the waxing and waning of the ice sheets through glacial-interglacial cycles, the ice sheets themselves also exert a large influence on the climate and other components of the earth system, which in turn modulate the response of the ice sheets to the external climate forcings (Figure 1.2; Clark et al., 2009; Fyke et al., 2018). Feedbacks that result from these two-way interactions can be positive (amplify the response) or negative (have a dampening effect) and can have a significant effect on the volume and extent of an ice sheet by changing its mass balance (Fyke et al., 2018). The mass balance is primarily determined by the mass change of ice in contact with the atmosphere (surface mass balance; SMB), which is the net balance of accumulation (i.e. from snow and freezing rain) and ablation from melt and sublimation at the surface of the ice sheet, and the mass change of ice in contact with the ocean where ice can be lost to calving and ocean driven basal melt. There is also a small contribution from bottom melt of grounded ice by geothermal heat flux, but this is minor compared to atmospheric and oceanic losses (Vizcaino, 2014). Changes in summer air temperatures, precipitation patterns, ocean temperatures and circulation, and ice dynamics affect this balance.

1.2.2.1 Ice sheet – atmosphere interactions

Ice sheets affect atmospheric conditions in many ways. They have high surface elevations and a high albedo (reflect a large proportion of the incoming shortwave radiation). This leads to global and local cooling of surface air temperatures and changes in large-scale atmospheric circulation, which in turn affect wind and precipitation patterns (Beghin et al., 2015; Le clec'h et al., 2019; Manabe and Broccoli, 1985; Roe and Lindzen, 2001). For example, it has been shown that the large ice sheet that covered North America during the last glacial period, may have been high enough to cause a zonalisation and strengthening of the jet stream and a shift in stationary waves, which could have caused a warming over the Arctic and a reduction of precipitation over parts of Eurasia (Kageyama and Valdes, 2000; Liakka et al., 2016; Liakka and Lofverstrom, 2018; Ullman et al., 2014). These ice sheet properties also lead to important feedbacks including the ice-albedo feedback. As snow and ice start to melt, the surface darkens and the albedo decreases. This allows more absorption of incoming solar radiation, warming the surface and causing more melt, especially in summer (Abe-Ouchi et al., 2007; Pritchard et al., 2008; Stap et al., 2014). This is a main contributor to present and future mass loss across Greenland (Box et al., 2012; Zeitz et al., 2021). The same effect occurs if the melting snow exposes the underlying firn or bare ice, produces melt pools or, over longer timescales, is replaced by rocks, soil or vegetation, since these all have lower albedos than fresh snow and

ice (Box et al., 2012; Stone and Lunt, 2013; Tedesco et al., 2011). Changes to dust deposition on the ice sheet can also lower the albedo and enhance surface melt (Bar-Or et al., 2008).

Another important positive feedback is the temperature-elevation feedback (Abe-Ouchi et al., 2007). An increase in ablation will lower the elevation of the ice sheet into warmer air temperatures due to the lapse rate effect, this in turn enhances the ablation further (Levermann and Winkelmann, 2016). The impact of this increases with greater levels of elevation change and larger ablation areas. This has been shown to trigger large areas of rapid deglaciation during glacial periods as a threshold in geometry is reached (Gregoire et al., 2016). However, elevation change also results in a negative feedback since warmer air holds more moisture, leading to higher precipitation/accumulation in the so called elevation-desert effect (Masson-Delmotte et al., 2013). Another negative elevation feedback occurs when an ice sheet gains mass causing a larger advance into the ablation area, warmer lower latitudes, or the marine margins where further growth is then inhibited (Fyke et al., 2018). Already, from this first section, it is clear that earth system interactions are numerous, bi-directional, and complex.

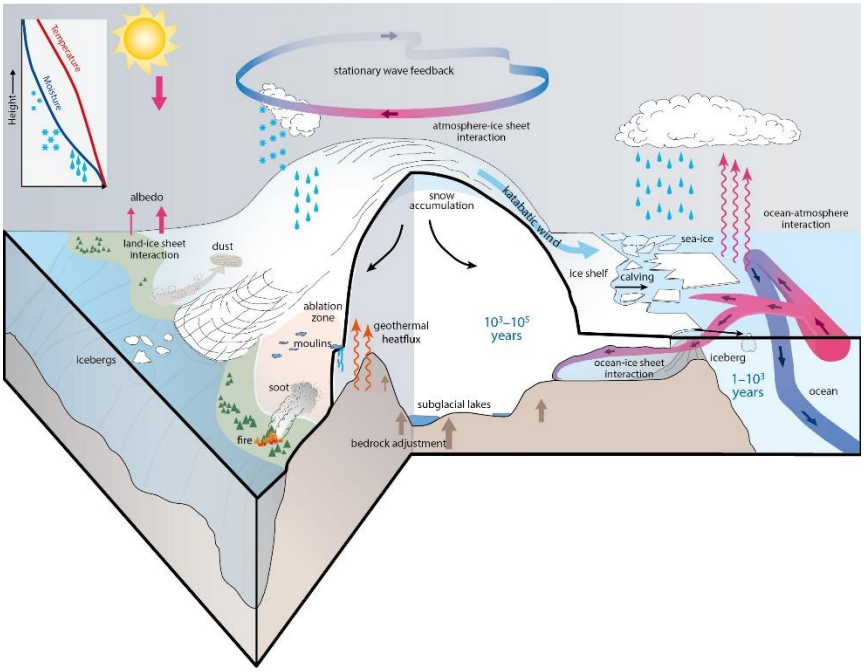

Figure 1.2: Schematic of interactions between ice sheets and other components of the earth system from IPCC AR5 (Masson-Delmotte et al., 2013).

1.2.2.2 Ice sheet – ocean interactions

Ice sheets also affect oceanic conditions through the input of freshwater as a result of surface meltwater runoff and melting of icebergs, outlet glaciers and ice shelves. This acts to freshen and cool the ocean which affects the ocean circulation through reducing deep-water formation. This in turn impacts the transfer of heat across the globe and shifts temperature and

precipitation patterns (An et al., 2024; Li et al., 2023b). For example, evidence suggests that the AMOC has slowed down over the twentieth century which may be due to the addition of meltwater from Greenland causing a reduction in surface ocean density and thus the formation of North Atlantic Deep-water (Bakker et al., 2016; Rahmstorf et al., 2015). The atmospheric cooling caused by the presence of ice sheets also contributes to cooler sea surface temperatures which leads to a larger expansion of sea ice cover in the North Atlantic. This in turn reduces global temperatures further through the ice-albedo feedback which again influences atmospheric circulation (Colleoni et al., 2011).

Moreover, where ice sheets discharge into the ocean, either through outlet glaciers or floating ice shelves (for ice sheets that lie on bedrock that is below sea level) at marine margins, interactions with the ocean can have a significant impact on the mass balance of the ice sheet. The two main processes that lead to ice mass loss by the ocean are sub-shelf melt and calving of icebergs, which are closely linked to the ice sheet dynamics through the transport of ice from the interior to the marine margins. However, both of these processes are poorly understood since they difficult to observe and measure and are affected by many complex processes and feedbacks (Benn et al., 2007; Truffer and Motyka, 2016). Sub-shelf melting is largely controlled by the temperature of the subsurface ocean water at the front of the glaciers and in the ice shelf cavities, and it is therefore affected by global ocean temperatures and transport of water onto the continental shelf (Benn et al., 2007; Fyke et al., 2018; Joughin et al., 2012; Rignot and Jacobs, 2002). One positive feedback related to this process occurs when increased freshwater flux leads to stratification of the water column and reduced vertical mixing. This increases temperatures on the continental shelf and thus increases the melting of ice shelves. This process may have contributed to the production of massive icebergs and rapid ice sheet retreat during Heinrich events (Alvarez-Solas et al., 2010; Marcott et al., 2011). Calving of ice by the ocean occurs as a result of mechanical processes that cause fracturing, which can be exacerbated by increases in ocean temperatures through the thinning and weakening of ice shelves and thermal undercutting of the terminus (Benn et al., 2007).

In addition to directly decreasing the mass of the ice sheet, ice sheet-ocean interactions impact the stability of an ice sheet. The presence of confined ice shelves (i.e. in an embayment or has pinning points) provides buttressing that restricts the flow of grounded ice from upstream of ice streams and glaciers (Hanna et al., 2013). Therefore, if an ice shelf starts to thin or disintegrate through sub-shelf melt or calving, a series of positive feedbacks can be set up. Loss of buttressing leads to increased strain rates, acceleration and thinning of grounded glaciers (Dupont and Alley, 2005; Liu et al., 2015). This results in an increase in the discharge of ice

across the grounding line (the zone where ice transitions from the grounded ice sheet to the floating ice shelves) and groundling line retreat which can further reduce basal traction (Benn et al., 2017; Gudmundsson et al., 2019). Observations under Pine Island Glacier in Antarctica have provided evidence of this processes occurring here over the past few decades due to changes in heat transport under the ice shelf, resulting in the largest contribution to sea level rise from any Antarctic glacier over this time (Jenkins et al., 2010; Rignot et al., 2019). Furthermore, increased speeds can lead to more rifting and calving and retreating grounding lines lead to a larger areas being subjected to warmer ocean temperatures (Joughin et al., 2012). Grounding line retreat can also become unstable, leading to irreversible and rapid ice sheet collapse, if it occurs across bedrock that slopes down towards the interior of the ice sheet. This is because it will retreat into deeper water and thicker ice which results in an increased ice flux, which in turn further thins the ice leading to continued retreat and so on. This process is referred to as marine ice sheet instability (Hanna et al., 2013; Joughin et al., 2012; Pattyn et al., 2018; Schoof, 2007) and is the cause for much of the uncertainty related to ice sheet response to climate change. The West Antarctic ice sheet is particularly vulnerable to this instability owing to the retrograde bed that is present under many of its large outlet glaciers. There is evidence that this process may have led to periods of accelerated retreat across Pine Island Glacier from 1940s-1990s (Reed et al., 2024) which causes concern for the future rate of ice mass loss and sea level rise as grounding line retreat continues across potentially unstable glaciers around Antarctica (Joughin et al., 2014).

1.2.2.3 Ice dynamics

The dynamics of an ice sheet is also influenced by its mass balance and in turn plays a role in its evolution and stability over the glacial cycles. Ice sheets flow under gravity and speeds vary from a few meters per year in the interior to a few kilometres per year in fast flowing outlet glaciers, ice streams and ice shelves. The gravity driven movement of thick ice from where it has accumulated in the interior to the thinner ice at the edges where ablation occurs, controls the ice sheet geometry and therefore its impact on the earth system (Fyke et al., 2018). The flow of ice to the margins can also lead to feedbacks that result in deglaciation. For example, as more ice flows into ablations zones and to the marine margins, the height of the ice sheet in the interior decreases (initiating a temperature-elevation feedback) and more ice is lost through ablation and calving (Marshall and Clark, 2002).

The rate of ice flow through deformation and basal sliding is a partly a function of ice temperature and displays an oscillatory behaviour. Warmer ice flows faster which results in thinning of the ice sheet leading to cooling through advection and the potential for ice to freeze

to the bed. This slows down the ice flow allowing ice thickness to increase again until melting point is reached again at the ice base (Marshall and Clark, 2002). The presence of water at the ice-bedrock interface is also important for determining the ice flow since basal sliding increases with the subglacial water pressure (Hoffman and Price, 2014).

1.2.2.4 Ice sheet – solid earth interactions

GIA processes can control the ice sheet response to atmospheric and oceanic forcings. For example, as an ice sheet grows and the bedrock lowers so does the elevation of the ice sheet, which decreases the SMB through the temperature-elevation feedback. Therefore, once the ice sheet reaches a certain height it only requires a small change in insolation to trigger rapid retreat due to delayed isostatic rebound (Abe-Ouchi et al., 2013). When a marine ice sheet retreats, the elastic uplift reduces the sea level in the region of the ice shelves which can slow down grounding line retreat and help prevent marine ice sheet instabilities (Gomez et al., 2010, 2015; Konrad et al., 2015).

1.2.2.5 Other interactions

Other earth system feedbacks also alter the pace of glacial-interglacial cycles, e.g. vegetation feedbacks (Horton et al., 2010; Willeit et al., 2024). For instance, the northern boreal treeline shifts southward with decreases in summer insolation and is replaced by tundra which has a higher albedo, enhancing orbitally induced summer cooling and promoting ice expansion (Kageyama et al., 2004; Stone and Lunt, 2013; Willeit et al., 2024).

Interactions with large proglacial lakes that form in front of terrestrial ice sheet margins as they retreat and meltwater fills in the depressions left behind, can affect the rate of deglaciation. For example, they increase the subglacial water pressure, reduce basal friction, accelerate sliding and promote the formation of ice streams. Also, ice shelves can form on the proglacial lakes and can therefore undergo similar processes to marine ice shelves, leading to grounding line retreat and potentially instabilities, which may have caused the collapse of the ice saddle over Hudson Bay during the LDG (Carrivick and Tweed, 2013; Hinck et al., 2022; Quiquet et al., 2021b; Scherrenberg et al., 2023a). However, the rates of calving and sub-shelf melt differ due to differences in circulation of the freshwater compared to ocean water and they tend to have less of an impact on mass balance and dynamics than the atmospheric mass loss (Quiquet et al., 2021b; Truffer and Motyka, 2016). These large lakes also impact the SMB of the ice sheets through their effects on the energy budget since they have low albedos and high thermal heat capacities which causes a reduction in summer ablation (Carrivick and Tweed, 2013; Hostetler et al., 2000).

It is clear that these interactions do not act in isolation as all parts of the system are connected and a change in one will impact others in complex ways. For example, changes in wind patterns can affect the ocean circulation (Davini et al., 2015; Sherriff-Tadano et al., 2018). Surface melt and rainwater can percolate through ice shelves causing them to thin, cause hydrofracturing and penetrate to the ice bed where it acts to increase ice flow to marine margins and ablation zones through basal sliding (DeConto and Pollard, 2016; Parizek and Alley, 2004; Zwally et al., 2002). Freshwater that discharges into the ocean from surface melt can also form buoyant plumes that carry warmer ocean water to the shelf front, enhancing ice loss through oceanic processes (Hewitt, 2020). Reduced basal friction causes higher velocities and the formation of ice shelves which lowers the surface elevation, increasing surface melt. This is turn can accelerate mass loss through marine/proglacial lake instabilities (Hinck et al., 2022; Scherrenberg et al., 2023a).

1.2.3 The Last Deglaciation versus the Penultimate Deglaciation

The last two deglaciations differed in terms of the conditions under which they were initiated, the evolution of the climate and ice sheets and the characteristics of the following interglacials (Menviel et al., 2019). The Last Deglaciation (~21-9 ka) occurred during Marine Isotope Stage 2 (MIS 2; ~29-14 ka) and began after the Last Glacial Maximum (LGM; ~21 ka) which is the period during the glacial cycle in which sea level records show the largest drop (i.e. global ice volume was at its largest) (Hughes et al., 2013; Ivanovic et al., 2016). A retreat of the ice sheets was then triggered leading to a rise in sea levels and a transition into the current Holocene interglacial (~11 ka). The Penultimate Deglaciation (~140-128 ka) occurred during Marine Isotope Stage 6 (MIS 6; ~190-130 ka). It began after the Penultimate Glacial Maximum (PGM; ~140 ka) and led into the Last Interglacial (~129-116 ka) (Menviel et al., 2019). This thesis uses the dates 21 ka and 140 ka, as in the PMIP4 modelling protocols, to be the LGM and PGM, respectively. However, it is important to note that marine isotope and sea level records show a low in global sea level spanning ~26-19 ka (Clark et al., 2009; Clark and Mix, 2002) and ~155-140 ka (Rohling et al., 2017).

1.2.3.1 Ice sheets

Studies based on proxy data, RSL records and GIA modelling suggest that the LGM sea level was around 120-130 m lower than present day (Austermann et al., 2013; Clark et al., 2009; Clark and Mix, 2002; Grant et al., 2014). The PGM shows more uncertainty with some estimates from Red Sea and Mediterranean RSL and palaeo-shoreline records suggesting the sea level drop was 21 ± 14 m lower than the LGM (Grant et al., 2014; Rabineau et al., 2006;

Rohling et al., 2017) and so global ice volume was also smaller. However, reconstructions based on the marine benthic $\delta^{18}O$ record suggest a sea level drop of similar or even larger value than the LGM (up to 150 m below present day) (Bintanja et al., 2005; Shakun et al., 2015; Waelbroeck et al., 2002), and some sources state the presence of larger ice sheets overall during MIS 6 (e.g. Batchelor et al., 2019; Margari et al., 2014).

The sea level evolution determined from a number of these studies is shown in Figure 1.3 and displays the large spread in these estimates. These discrepancies may be due to inaccurate estimates of GIA, uncertainties in the effect of temperature on $\delta^{18}O$ data or measurements of RSL data.

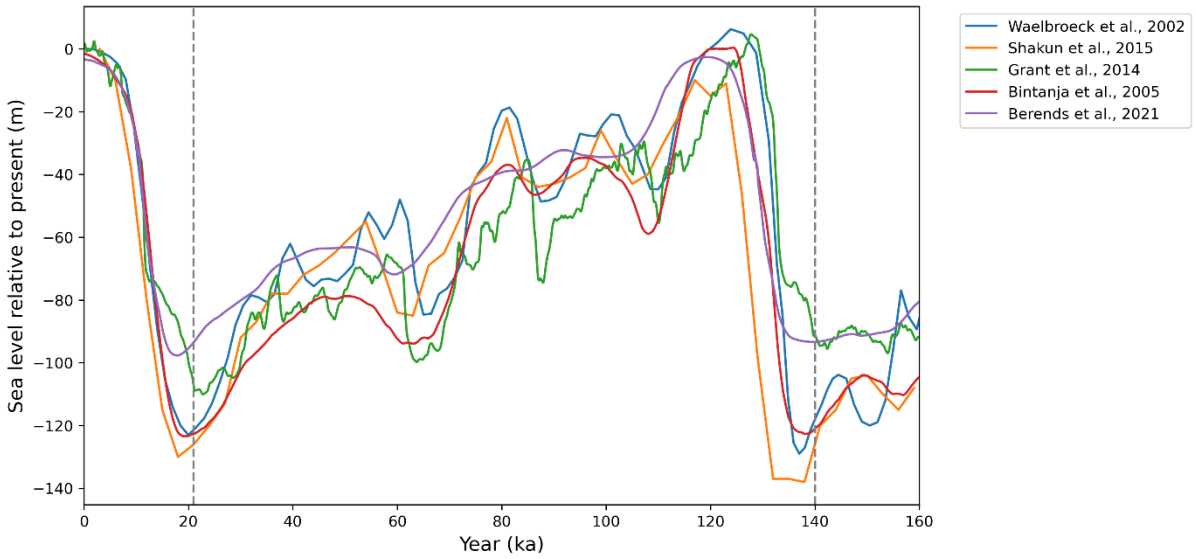

Figure 1.3: Sea level evolution over the past two glacial cycles relative to present day from a number of different studies (Berends et al., 2021; Bintanja et al., 2005; Grant et al., 2014; Shakun et al., 2015; Waelbroeck et al., 2002).

Since the determination of ice sheet configuration from empirical evidence and GIA-based constraints is difficult (see Sect. 1.2.1.1), they can be combined with physics-based ice sheet modelling, to help fill in some of the data gaps and provide further constraints on the ice sheet evolution, especially in regards to ice volume and thickness of specific ice sheets and ice dynamics (e.g. Sejrup et al., 2022; Tarasov et al., 2012; Tarasov and Peltier, 2004). As such, in recent years there has been significant improvements in our understanding of the evolution of the Northern Hemisphere ice sheets, especially through the Last Deglaciation (Patton et al., 2017; Tarasov et al., 2012). Numerical modelling has also been employed to help understand the contribution of different processes to the ice sheet retreat and the individual ice sheet contributions to sea level (e.g. Abe-Ouchi et al., 2013; Golledge et al., 2021; Quiquet et al., 2021a). From all these available data sources, it is clear that the ice sheet configurations, timing

and patterns of changes, and the processes that cause them, differ between the last two glacial maxima and deglaciations but how and why is still very uncertain.

The Eurasian Ice Sheet (EIS) comprises the largely marine based British-Irish Ice Sheet (BIIS) and Barents-Kara Ice Sheet (BKIS), and the largely terrestrial Fennoscandian Ice Sheet (FIS), which were all connected during the glacial maxima and extended out to the continental shelf along most of the marine margin (Figure 1.4; Clark et al., 2012a, 2022; Hughes et al., 2016). During the LGM, the southern extent reached to around 53º N and reconstructions show a maximum extent of 5.48 x 10^6 km^2 (Figure 1.4a), however the ice did not reach this maximum in all areas at the same time (Hughes et al., 2016; Patton et al., 2016). For example, parts of the BIIS may have reached their maximum as early as 27-26 ka before starting their retreat before 21 ka (Clark et al., 2012a, 2022), but the eastern margins may have continued to advance until 20 ka (Hughes et al., 2016; Patton et al., 2017). Numerical and GIA modelling studies estimate that the LGM EIS volume was around 13-24 m sea level equivalent (m s.l.e.). (Lambeck et al., 2006; Patton et al., 2016; Peltier et al., 2015; Simms et al., 2019). Retreat started after 19 ka mostly from the BKIS, with the BIIS and FIS separating by 18 ka, and then was relatively constant across the whole EIS until 14-12 ka where it slowed for the FIS and BKIS. The FIS and BKIS separated by 15 ka and after 11 ka only significant portions of the FIS remained. By 9 ka the EIS was almost entirely deglaciated (Hughes et al., 2016). Studies have suggested that the majority of initial retreat of the marine based sectors of the BIIS and BKIS are controlled by glacio-isostatic loading aided by instabilities triggered by increased sea levels, ice stream acceleration and temperature-elevation feedbacks (Clark et al., 2022; Gandy et al., 2018, 2021; Petrini et al., 2020). Climate warming then melted the remaining terrestrial regions.

The glaciation of Eurasia during MIS 6 was likely the largest since MIS 12 (478-424 ka) (Hughes and Gibbard, 2018) and reconstructions show an EIS ~50% larger than during the last glacial cycle, extending 200 km further south and 1000 km further east in Siberia (Figure 1.4b; Batchelor et al., 2019; Hughes and Gibbard, 2018; Svendsen et al., 2004). Some suggested contributing factors to this include; warmer global oceans causing enhanced precipitation over Eurasia, lower rates of dust deposition increasing albedo, different vegetation cover, presence of large proglacial lakes and less extensive and seasonally open sea ice cover in the North Atlantic and Arctic (Rohling et al., 2017).

During MIS 6 there were two major ice advances in Europe, the more extensive Drenthe (~160 ka), which was followed by partial melting and up to 30 m s.l.e. sea level rise ~157-154 ka, under increasing summer insolation, and then a readvance after 150 ka during the less extensive

Warthe. After this, global mean sea level records indicate that global ice volume reached its maximum extent ~140 ka, reflecting the growth of the North American ice sheet, and perhaps expansion in Russia and Siberia (Hughes and Gibbard, 2018; Margari et al., 2014). Thus, the extent of the EIS during the PGM is not well known and evidence may correspond to previous advances during MIS 6. Similarly, the volume of the EIS is very uncertain but most estimates from modelling studies fall between 40–70 m s.l.e. (Colleoni et al., 2016; Lambeck et al., 2006; Pollard et al., 2023; Rohling et al., 2017; Wekerle et al., 2016).

Few geological records are available to constrain the pattern of retreat of the Penultimate Glacial ice sheets but GIA modelling suggests that by around 135 ka, ice over Russia had retreated to the Kara Sea and there was also substantial retreat over Scandinavia. By 129 ka, the majority of the ice sheet had disappeared (Lambeck et al., 2006).

Geological evidence suggests that North East Siberia was ice free around the LGM but that there was extensive ice cover present at some point in time, likely during MIS 6 (Niessen et al., 2013). It has been suggested that the dust deposition rate can influence the presence of ice in this region and high rates during the LGM contributed to Siberia being ice free due to lowering the albedo and thus increasing melt (Colleoni et al., 2009a; Krinner et al., 2006). The EPICA Dome C Antarctica cores show dust deposition rates were ~40% lower at PGM (Delmonte et al., 2004). This feature is also reproduced in numerical models of the PGM which show that summer temperatures in Siberia are very sensitive to changes in stationary wave fields and associated northward heat transport. Therefore, small changes in glacial climates and ice sheet configurations can cause large differences in Siberian temperatures allowing the formation of an extensive ice cap and shelf over this region in some glacial simulations but not in others (Bakker et al., 2020; Colleoni et al., 2016; Colleoni and Liakka, 2020). In addition, Jakobsson et al., (2010, 2016) describe evidence of a thick ice shelf extending into the Arctic Ocean from the Barents and East Siberian margins dating to MIS 6 that was not present during MIS 2. This could explain some of the discrepancies between sea level reconstructions during MIS 6 (Gasson et al., 2018). However, both of these features are highly uncertain and debated (Stein et al., 2017).

There is evidence for the existence of large proglacial lakes at the terrestrial margins of the EIS during the Last Deglaciation, including the Baltic Ice Lake and White Sea Ice Lake which rapidly drained large amounts of freshwater into the North Atlantic and Arctic Ocean, likely affecting the ocean circulation and global climate (Jakobsson et al., 2007; Patton et al., 2017). There were several ice streams draining the EIS, the main ones being the Norwegian Channel Ice Stream which flowed from the FIS into the North Sea until around 18 ka (Patton et al.,

2017; Sejrup et al., 2009) and the Bjørnøyrenna Ice Stream draining the BKIS (Andreassen and Winsborrow, 2009) (Figure 1.5a).

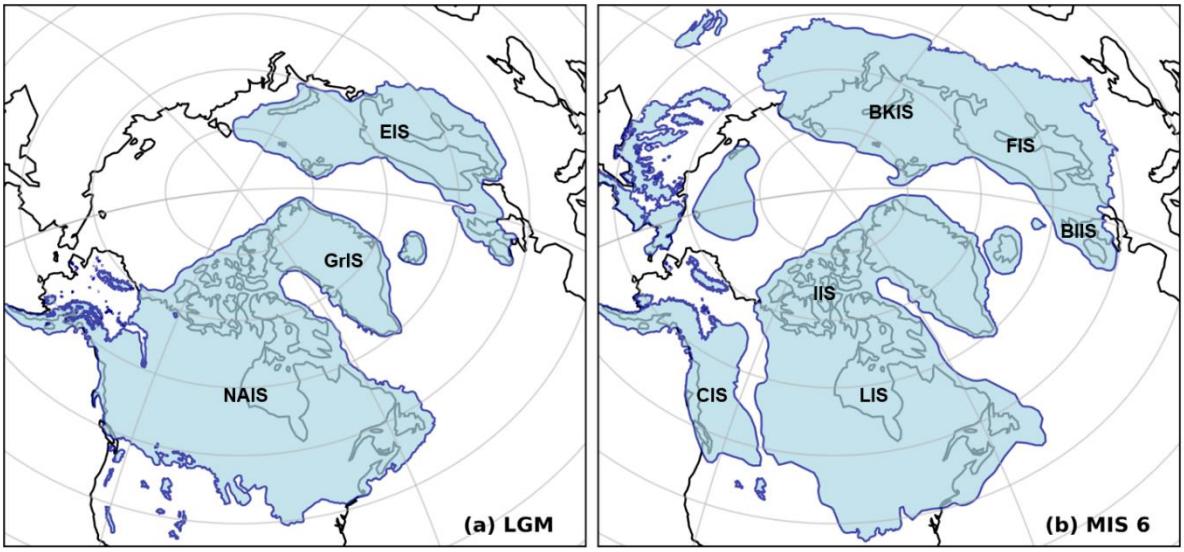

Figure 1.4: Reconstructions of the extent of the Northern Hemisphere ice sheets based on empirical and model data for (a) LGM (Dalton et al., 2020; Hughes et al., 2016) and (b) MIS 6 (Batchelor et al., 2019). The three large ice sheet complexes are labelled on panel (a); NAIS = North American Ice Sheet, EIS = Eurasian Ice Sheet, GrIS = Greenland Ice Sheet. The individual ice sheets that make up these complexes are labelled on panel (b); LIS = Laurentide Ice Sheet, CIS = Cordilleran Ice Sheet, IIS = Innuitian Ice Sheet, BIIS = British-Irish Ice Sheet, FIS = Fennoscandian Ice Sheet, BKIS = Barents-Kara Ice Sheet.

The North American Ice Sheet (NAIS) was a largely terrestrial based ice sheet composed of the Laurentide (LIS), Cordilleran (CIS) and Innuitian Ice Sheets (IIS) (Figure 1.4). At the LGM, all three ice sheets coalesced and extended to the continental shelf in many regions, with a total area of 15.47 x 10^6 km^2. Ice lobes (formed by extensions of terrestrial ice streams) extended from the southern margin reaching a latitude of around 40º N (Figure 1.4a; Batchelor et al., 2019; Dalton et al., 2020, 2023). However, as with Eurasia, the timing of the local glacial maximum was asynchronous across the different areas of the ice sheet and some sections reached a maximum extent prior to the LGM (Dalton et al., 2020, 2023; Hughes et al., 2013). The volume of the NAIS at the LGM is estimated by a number of different studies to be ~68-88 m s.l.e. (e.g. Lambeck et al., 2017; Peltier et al., 2015; Rohling et al., 2017; Simms et al., 2019; Tarasov et al., 2012). Deglaciation began at around 18 ka with a slow retreat of the southern and eastern margins. The LIS and CIS gradually separated from the north and south from ~17.5-14 ka. The CIS was deglaciated by ~11 ka while ice remained over the Hudson Bay until ~8 ka (Dalton et al., 2023).

In general, there is a lack of evidence for the extent of the NAIS during the PGM and the following deglaciation. There is some evidence that, at some point during MIS 6, it extended 150 km further south in Illinois and 30 km in Wisconsin compared to the LGM but the timing is uncertain (Figure 1.4b; Batchelor et al., 2019; Hughes and Gibbard, 2018). Overall, the limited data suggests that the LGM advance was larger in most areas compared to the PGM (Dyke et al., 2002), with reconstructions also suggesting that the LIS and CIS were disconnected at the PGM (Batchelor et al., 2019). A smaller volume PGM NAIS is backed up by additional empirical evidence such as IRD layers in sediment cores in the North Atlantic. They show reduced levels during the Penultimate Glacial Cycle compared to the last, which suggests less iceberg discharge into the North Atlantic (Hemming, 2004; Naafs et al., 2013; Obrochta et al., 2014). Additionally, climate and ice sheet simulations using a smaller NAIS (~30 m s.l.e.) and a larger EIS give the best fit to global environmental proxy data (Colleoni et al., 2016; Wekerle et al., 2016), and GIA modelling combined with palaeo-sea-level data across The Bahamas has demonstrated a 98% probability that the LIS was between 16 and 23 m s.l.e. smaller than at the LGM (Dyer et al., 2021). In addition, given the constraints on the EIS and the global mean sea level drop, the NAIS must have been smaller to match the global ice volume. The volume has thus been estimated to have been around 39-59 m s.l.e. (Rohling et al., 2017).

Proglacial lakes also existed at the southern margin of the NAIS during the Last Glacial Period, the largest one being Lake Agassiz (Carrivick and Tweed, 2013). This may have accelerated the retreat of the NAIS due to grounding line instability triggered by negative SMB (Quiquet et al., 2021b). The drainage of this lake into the Arctic Ocean could have triggered the Younger Dryas cool period due to its impact on ocean circulation (Norris et al., 2021). It also may have caused a regional cooling and reduced precipitation at the southern Laurentide ice sheet at 11ka which would have impacted the deglaciation (Hostetler et al., 2000). The ice streams of the Laurentide ice sheet have been reconstructed from geomorphological and geological records, the main ones persisting through much of the deglaciation being; the Hudson Strait, Amundsen Gulf and M'Clure Strait ice streams (Figure 1.5b; Margold et al., 2018).

The different topographies of the NAIS has been shown to have a large impact on the climate of each glacial due to its location in the westerly mean flow, and therefore some studies have concluded that it has an influence on the size and configuration of the EIS during that period (Beghin et al., 2015; Liakka et al., 2016). For example, atmospheric modelling shows a larger LGM-like NAIS causes changes to planetary waves that yield a cooling over Europe but warmer surface air temperatures over Siberia and Beringia. This prevents the expansion of

snow and sea ice in NE Asia, resulting in a decrease in albedo, and contributes to the more westward migration of the EIS. This could explain the lack of evidence of glaciation in Eastern Siberia during the LGM (Liakka et al., 2016; Löfverström et al., 2014; Löfverström and Lora, 2017; Ullman et al., 2014). The more western EIS may have also blocked moisture from the Atlantic, further inhibiting ice accumulation in the East (Krinner et al., 2011). A larger NAIS also enhances the stationary waves downstream which causes an acceleration, zonalisation and southward displacement of the jet stream and associated storm tracks in the North Atlantic. This shifts precipitation to the south of Europe in winter, further starving the EIS of moisture (Hofer et al., 2012; Löfverström and Lora, 2017; Merz et al., 2015). In contrast, a smaller PGM-like NAIS causes a more meridional Jetstream and a shift in stationary waves that allow cold Arctic air to penetrate downstream and cause colder temperatures across Siberia and Beringia and enhanced snow and sea ice cover, consistent with evidence of more extensive glaciation over this region during MIS 6 (Colleoni et al., 2016; Ullman et al., 2014). There is also increased storm track activity and precipitation seen over North Atlantic and the EIS, allowing the growth of the ice sheet (Colleoni et al., 2016; Löfverström and Lora, 2017). Positive SMB values induced by a smaller NAIS could have also contributed to the large Arctic ice shelf that may have been present during the Penultimate Glacial Cycle (Jakobsson et al., 2016; Liakka and Lofverstrom, 2018).

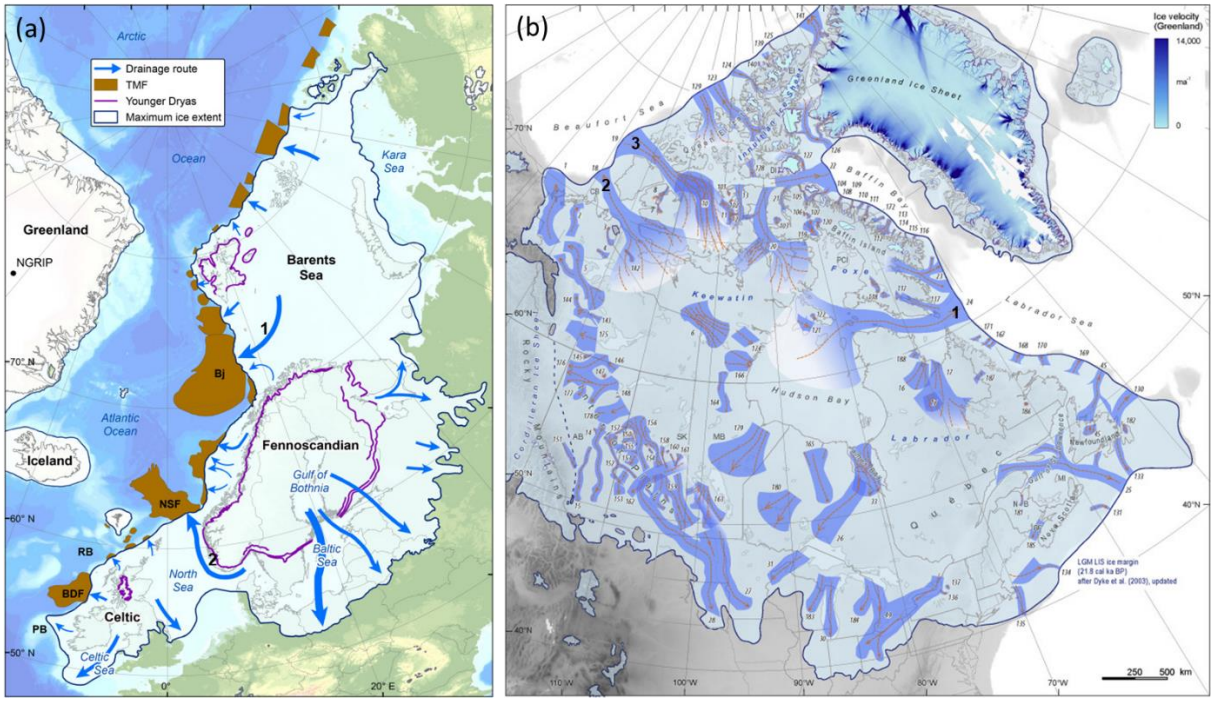

Figure 1.5: Major ice streams and drainage routes of the (a) LGM Eurasian Ice Sheet from Patton et al. (2017) and references therein. 1 = Bjørnøyrenna Ice Stream; 2 = Norwegian Channel Ice Stream. TMF: Trough Mouth Fans; PB: Porcupine Bank; BDF: Barra and Donegal Fans; RB: Rosemary Bank; NSF: North Sea Fan; Bj: Bjørnøyrenna Fan; and (b) LGM Laurentide Ice Sheet from Margold et al. (2018) and

references therein. 1 = Hudson Strait; 2 = Amundsen Gulf; 3 = M'Clure Strait Ice Stream. AB: Alberta; BF: Bay of Fundy; CB: Cape Bathurst; DI: Devon Island; EI: Ellesmere Island; MB: Manitoba; MI: Magdalen Islands; NB: New Brunswick; PCI: Prince Charles Island; SK: Saskatchewan.

The Greenland Ice Sheet (GrIS) and Antarctic Ice Sheet (AIS) extended onto the continental shelves in many areas during the glacial maxima but again the local glacial maxima was not synchronous (Bentley et al., 2014; Hughes et al., 2013; Vasskog et al., 2015). Studies show that the GrIS reached its maximum volume during the Last Glacial Cycle ~18-16 ka (Vasskog et al., 2015) and was connected to the IIS during both glacial periods. Reconstructions based on empirical and model data estimate the GrIS was 2-5 m s.l.e. larger at the LGM than present day (present volume of 7.4 m s.l.e.) (Lecavalier et al., 2014; Simms et al., 2019; Vasskog et al., 2015) and the AIS 7-15 m s.l.e. larger (present volume of 58 m s.l.e.) (Simms et al., 2019). During the LDG, the eastern GrIS margin started to retreat before the maximum volume was reached whilst the southern margin started to retreat ~16-14 ka. In the west, ice did not retreat from the shelf edge until around 13.8-12.2 ka. The volume then decreased continuously after ~13.5 ka until ~4 ka (Lecavalier et al., 2014; Vasskog et al., 2015). Whilst some areas of Antarctica started to retreat by ~18 ka, most of the deglaciation took place later on and through the Holocene, between 15-6 ka (Argus et al., 2014; Bentley et al., 2014; Briggs et al., 2014; Mackintosh et al., 2014).

Since there is limited preservation of offshore geomorphological evidence from the PGM, most modelling studies assume both ice sheets were similar to the LGM configurations (Bradley et al., 2018). However, there is some evidence that suggests that the maximum volume of the GrIS was larger during MIS 6 than MIS 2, including glacial deposits showing some surfaces have not been glaciated since MIS 6 (Roberts et al., 2009) and marine deposits showing sea water moved further inland at the LIG than the Holocene as a result of more ice causing a larger isostatic depression during MIS 6. This data is sparse and there could be alternative explanations, for example sea level being already higher when the GrIS started to melt due to earlier melting of ice sheets elsewhere (Alley et al., 2010).

Sea level records indicate that the LIG sea level was higher than present day. Whilst previous geological data-based estimates put the peak value between 6-9 m higher (Dutton et al., 2015; Dutton and Lambeck, 2012; Grant et al., 2014; Kopp et al., 2009), new revised estimates lower this to between 1.2-5.3 m, peaking at 127 ka (Dyer et al., 2021). Since thermal expansion and mountain glaciers contributed less than 1 m to this rise (McKay et al., 2011), the rest must have come from the Antarctic and Greenland ice sheets (Dutton and Lambeck, 2012). The magnitude and drivers of individual contributions are very uncertain, but there is evidence in ice core and

marine records that the GrIS was smaller than present day, with most palaeo-data and modelling based estimates converging on around a 1-2 m s.l.e. contribution occurring after 125 ka (range from ~0.4-5.5 m) (Quiquet et al., 2013; Rohling et al., 2019). The AIS contribution ranges from ~3.6-7.4 m s.l.e. (DeConto and Pollard, 2016; McKay et al., 2011) with the timing of peak contribution occurring before 126 ka (Rohling et al., 2019). This large range of values makes it difficult to determine whether sections of the AIS collapsed during the LIG (Dutton and Barlow, 2019). There is some evidence from ice cores that the East AIS persisted throughout the LIG but the West AIS is less certain (Chandler and Langebroek, 2021).

1.2.3.2 Climate

The orbital configurations and evolution of solar insolation differed between the Last and Penultimate Glacial Cycles. The average incoming insolation was similar at both glacial maxima (Berger and Loutre, 1991) but the seasonal and latitudinal patterns differed due to the orbital configurations. Eccentricity was larger at the PGM (0.033) compared to the LGM (0.019) which enhances the effects of precession (Berger, 1978). This causes cooler and longer springs and early summers, but shorter and warmer late summers and autumns in the NH high latitudes (Colleoni et al., 2011). The colder springs reduce the melting of snow accumulated in winter which could explain some of the differences in ice sheet configuration. The GHG concentrations were also similar with a CO_2 concentration of ~190 ppm at the LGM (Bereiter et al., 2015) and ~191 ppm at the PGM (Köhler et al., 2017).

Due to the presence of the large continental ice sheets and lower atmospheric CO_2 concentration, the global mean air temperatures were cooler during glacial periods compared to present day, and precipitation was decreased (Bartlein et al., 2011). However, the magnitude of this cooling is still very uncertain with a combination of modelling studies and global climate proxy compilations estimating a LGM cooling of between 1.7-8.0 ºC relative to the pre-industrial (e.g. Annan et al., 2022; Tierney et al., 2020a). There are much fewer constraints on the PGM due to low resolution climate records and challenges with establishing chronologies for these records (Govin et al., 2015). However, $\delta^{18}O$ records and modelling suggests a smaller global cooling than the LGM, which modelling has attributed to the different orbital configurations (Colleoni et al., 2016; Menviel et al., 2019; Quiquet and Roche, 2024).

One recent LGM SST reconstruction from proxy data has a global average cooling of 1.7 ºC compared to the present day (GLOMAP; Paul et al., 2021) whereas another that combined proxies with modelling produced a larger global cooling of 3.6 ºC (Tierney et al., 2020a). Surface ocean fields can also be extracted from GCM simulations that produce a range of

values and spatial patterns depending on the model used (Kageyama et al., 2021). In comparison, no similar global reconstructions have been produced for the PGM but it has been suggested that SSTs may have been warmer, and sea ice thinner and smaller in extent, during MIS 6 compared to MIS 2 which could have allowed greater moisture supply leading to the larger NH ice sheets (Hughes and Gibbard, 2018). Comparison of individual marine sediment core records supports this (Martrat et al., 2014) as do modelling studies (Quiquet and Roche, 2024). A synthesis of Southern Ocean SST proxies for the Penultimate Glacial Cycle shows that annual/summer cooling at the PGM reached -3.6±1 ºC/-4.0±1.2 ºC, which is similar to the LGM (Chandler and Langebroek, 2021).

The evolution of the climate and the sequence of abrupt millennial scale events differed between the last two deglaciations. The Last Deglaciation began around 19 ka following an increase in 65º N summer insolation after the LGM (Ivanovic et al., 2016). From ~17.5 ka, as CO_2 concentrations also rose, the NH ice sheets started to disintegrate draining large amounts of freshwater into the North Atlantic, weakening the formation of NADW and therefore the AMOC (Clark et al., 2012b; McManus et al., 2004). This led to a cooling and drying in the NH but an increase in temperatures over Antarctica, due to the thermal bipolar seesaw effect, and rapidly increasing CO_2 potentially due to release from the warming Southern Ocean (Barbante et al., 2006; Buizert et al., 2014, 2015; Marcott et al., 2014; Stocker and Johnsen, 2003). Since IRD layers have been found in North Atlantic sediment records during this time indicating the discharge of large ice bergs from the Laurentide ice sheet, this cold NH period is known as Heinrich Stadial 1 (HS1) (Hemming, 2004). This lasted until around 14.7 ka, when the AMOC strengthened once again, possibly due to a reduction in the meltwater input or a shift in the threshold for a weakened AMOC as a result of rising CO_2 levels (Barker and Knorr, 2021), causing an abrupt warming over Greenland and in the North Atlantic known as the Bølling-Allerød (BA) interstadial (Buizert et al., 2014). A rapid rise in sea level of 14-18 m in less than 500 years, coincided with (and possibly triggered), the BA warming, referred to as Meltwater Pulse 1A (MWP-1A; ~14.5 ka; Deschamps et al., 2012). Following this, a period of cooling in the Antarctic region occurred until ~12.8 ka, called the Antarctic Cold Reversal (ACR), and there was a pause in the increasing atmospheric CO_2 (Jouzel et al., 2007b). This may have been caused by the resumption of NADW enhancing northward heat transport from the southern hemisphere or a meltwater pulse from the AIS (Menviel et al., 2011). However, more recent GIA modelling constrained by sea level data disproves this latter cause (Lin et al., 2021). The NH returned to cooler stadial conditions during the Younger Dryas (YD) between ~12.8-11.7ka (Alley, 2000a; Buizert et al., 2014), possibly due to further increases in meltwater into the NH

oceans, whilst the warming resumed in Antarctica along with the increase in CO_2. The end of the YD was marked by a rapid warming into the Holocene interglacial (Figure 1.6; Ivanovic et al., 2016).

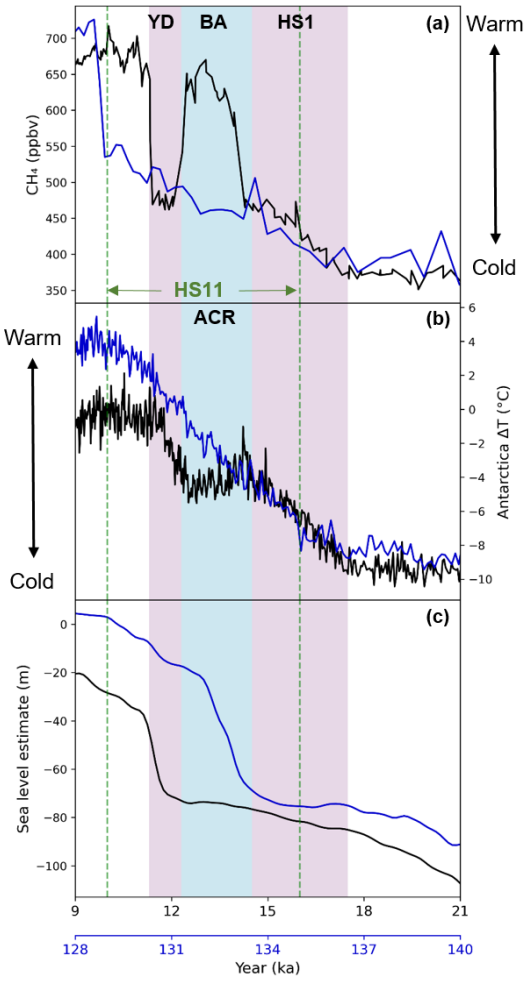

Figure 1.6: Records of (a) atmospheric CH_4 from the EDC ice core, Antarctica (Loulergue et al., 2008) which reflects abrupt AMOC changes during deglaciation, (b) Antarctic temperature anomalies relative to present day from the EDC ice core (Jouzel et al., 2007a), and (c) global mean sea level estimate from Red Sea RSL records, compared to present day (Grant et al., 2014). Pink shaded areas show the HS1 and YD stadials and the blue shaded area shows the BA interstadial/ACR. The green dashed lines denote the approximate start and end of the HS11 stadial. Time spans 9-21 ka for the LDG (black x-axis) and 128-140 ka for the PDG (blue x-axis).

In contrast to the two abrupt climate changes during the LDG (HS1 and the YD), most sources of evidence point to only one abrupt climate event during the PDG, Heinrich Stadial 11 (HS11), towards the end of the deglaciation and start of the interglacial, which lasted longer than HS1 (~135-129 ka) (Cheng et al., 2009; Jiménez-Amat and Zahn, 2015; Marino et al., 2015). This has been linked to cold, dry conditions over the North Atlantic, as a result of a weakened AMOC from freshwater perturbation (Martrat et al., 2014), a gradual Antarctic warming to

~2°C higher than pre-industrial and associated CO_2 rise of ~60 ppm (Capron et al., 2017a; Landais et al., 2013; Obase et al., 2021), and a sea level rise of ~80 m (Grant et al., 2014). Following this the AMOC strengthened again in the LIG (Figure 1.6).

The cause of the differences between the two deglaciations is not yet well known. Some have suggested that the disintegration of the NH ice sheets could have caused a larger freshwater input during the PDG, thus allowing the weakened AMOC to persist for longer and only recover at the start of the LIG (Carlson, 2008; Obase et al., 2021). The additional freshwater may be a result of the varying continental ice sheet configurations and orbital forcing scenarios that each deglaciation is initiated under. For example, NH summer insolation rose much quicker during the PDG and peak anomalies reached more than 70 Wm^{-2} compared to ~50 Wm^{-2} during the LDG (Menviel et al., 2019). This may have caused faster disintegration of the LIS explaining the faster sea level response to insolation forcing seen for the LIG (Berger, 1978; Carlson, 2008; Obase et al., 2021; Parker et al., 2022; Stirling et al., 1998; Stoll et al., 2022). The larger EIS at the PGM could also be a source of this additional meltwater (Clark et al., 2020; Stoll et al., 2022). In contrast, during the Last Deglaciation there was a relatively small amount of meltwater which allowed the AMOC to strengthen again before the onset of the current interglacial, thus causing the BA warming. The BA warming and following ACR was critical in causing lower Antarctic temps during LDG as the following YD warming in this region was not large enough to compensate for the 2000 years of cooling (Obase et al., 2021). However, even when the different size of the PGM ice sheets is not considered, the higher summer insolation during the PDG has been shown to have increased the rate of ice sheet melt (Obase et al., 2021; Quiquet and Roche, 2024). Thus, Obase et al., (2021) suggest that during the early stage of the PDG the large EIS was an important source of additional meltwater causing the stronger and longer HS11 but during the later stages the higher insolation becomes important for maintaining this meltwater input and allowing the weakened AMOC to persist for longer, into the later stages of the deglaciation and start of the LIG, which was more important for the peak Antarctica temperatures. This indicates that differences in orbital forcing were an important factor in the occurrence of abrupt events during the deglaciations and the temperature of Antarctica in the following interglacials (Govin et al., 2015; Landais et al., 2013; Obase et al., 2021). More recent records have indicated that there may have been a period of AMOC recovery during the beginning of HS11 (~134.5 ka), in contrast to what has been previously reported (Stoll et al., 2022). This could be due to strong temporal variations in the meltwater forcing.. More investigation into the mechanisms behind the rapid AMOC shifts during both deglaciations is needed to come to a conclusion.

As mentioned in Sect. 1.1, evidence from ice and sediment cores indicates that the LIG global mean air temperature was 1-2 ºC higher than the current interglacial (Otto-Bliesner et al., 2013b; Turney and Jones, 2010) and peak global sea surface temperatures were around 0.2-1ºC higher (Hoffman et al., 2017; Shackleton et al., 2020; Turney et al., 2020a). Arctic temperatures have been measured to be even higher (4-5 ºC; Anderson et al., 2006), as have Greenland surface temperatures (5-8 ºC; Anderson et al., 2006; Dahl-Jensen et al., 2013) and Antarctic surface and Southern Ocean temperatures (~1-2 ºC; Capron et al., 2017a; Chandler and Langebroek, 2021). However, the difference in mean annual radiative forcing is only $+1.4 Wm^{-2}$ which is not high enough to explain these temperature differences (Bova et al., 2021). The differing deglaciation pathways have therefore been hypothesised to be the main driver of the different interglacial climates that followed, rather than forcings within the interglacials themselves. For example, the weaker AMOC persisting into the LDG has been proposed to be a significant contributor to the higher Antarctic and Southern Ocean temperatures (Obase et al., 2021). Additionally, the faster Penultimate Deglaciation compared to the Last Deglaciation, with ice sheets reaching near modern levels by the onset of the LIG compared to only half of the retreat occurring by the start of the Holocene, may have also contributed to the warmer LIG, since greater ice extent during the Holocene would act to cool the planet through higher albedo, starting the Holocene off at lower temperature (Bova et al., 2021).

Some studies have suggested that the increase in Southern Hemisphere temperatures at the onset of the LIG led to a significant mass loss from the AIS through increased subsurface ocean warming, contributing to the higher LIG sea levels (Clark et al., 2020; Marino et al., 2015; Turney et al., 2020b). This is supported by recent studies suggesting an asynchronous contribution to the LIG high stand (Dyer et al., 2021; Rohling et al., 2019). The reconstructions show a peak between ~129.5 to 124.5 ka mostly derived from Antarctica, a low centred on 125-124 ka, and then variable influences from both the AIS and GrIS from ~124 to 119 ka (Rohling et al., 2019). If this warming led to areas of the AIS collapsing through marine ice sheet instabilities, the contribution to the sea level high stand could have been significant. Improving the representation of processes such as marine ice sheet instability in models and modelling ice sheet dynamics during past periods such as the LIG, will therefore be vital in constraining projections of sea level rise under climate change.

1.2.4 Numerical modelling of glacial-interglacial cycles

It is clear that understanding the evolution of the climate and ice sheets during past glacial-interglacial cycles is important for understanding the response of these components of the earth

system to changes in climate forcing. Due to limitations of empirical data in terms of resolution, accuracy and precision and what it can tell us, numerical models are a vital tool that can be employed to help us make sense of these data and improve understanding of the processes and mechanisms of glacials and deglaciations. In turn, the empirical data from past periods can be used to help improve models through comparison of model output with constraints on climatic conditions and ice sheet configurations (Ely et al., 2021; Haywood et al., 2019). In particular, since the two-way interactions between ice sheets and all other components of the earth system are so important, the use of climate and ice sheet models coupled together is needed to capture the relevant processes leading to the changes observed, and improve our knowledge of the climate system. There are several types of climate and ice sheets models that have been developed that range in complexity that can be chosen depending on the purpose of the study.

Energy Balance Models can range from zero to two dimensional and are the simplest numerical climate models that represent the Earth's temperature by calculating the radiation budget from incoming and outgoing energy (Edwards, 2011). The transport of heat from the tropics to the polar regions is then approximated based on the horizontal temperature gradient across a single level and ice cover is parameterised by increasing albedo where temperatures are below a certain value. Since the equations that are resolved are so simple, these models can be run for millions of years, but they can only capture large scale variations in temperatures and do not simulate other atmospheric processes such as precipitation. As such, they are useful for understanding how the Earth's temperature responds to changes in orbital forcing but cannot provide much information on changes to other components of the earth system (Budyko, 1969; Pollard, 2010).

Earth System Models of Intermediate Complexity (EMICs) contain all the basic components of the global climate system in two to three dimensions at a level of complexity that allows integration over a wide range of temporal and spatial scales (Claussen et al., 2002). Therefore, they are often used to simulate and explore slow climate changes associated with feedbacks over millennial time scales, such as ice sheets and vegetation (Crucifix and Loutre, 2002; Petoukhov et al., 2005; Weber, 2010). This is possible as many processes are parameterised or not included, such as the radiative effect of clouds (Stokes et al., 2015), or are modelled at a relatively coarse spatial resolution. This reduces computational costs and increases the flexibility of EMICs, enabling more freedom to tune the model to remove potential biases. However, it also limits the scope of the information they can provide, for example they are unsuitable for modelling small scale or high frequency climate variations (e.g. wind driven ocean circulation; Intergovernmental Panel on Climate Change (IPCC), 2014; Weber, 2010).

Furthermore, the highly simplified nature of some processes means that parameter calibration may be limited in improving biases if there are model structural problems (Shi et al., 2019).

General Circulation Models (GCMs) are three dimensional and provide the most complex representation of the Earth's climate, explicitly resolving many of the relevant processes, although some sub-grid scale processes, such as those related to cloud formation, are still parameterised (Gordon et al., 2000; McGuffie and Henderson-Sellers, 2005). They can consist of models of the atmosphere (AGCM) or ocean (OGCM) or both can be combined to fully interact with each other (AOGCM) (McGuffie and Henderson-Sellers, 2005). In addition, over time, other components have been coupled to AOGCMs making them even more complex (e.g. vegetation, sea ice, carbon cycle) creating integrated multi-system models called earth system models (ESMs) (Edwards, 2011). They have a relatively fine resolution of 1-5º allowing the simulation of smaller scale ocean and atmospheric circulation patterns, which enables the investigation of mechanisms responsible for the large scale climate response (McGuffie and Henderson-Sellers, 2005). However, the large computational expense means that they are largely restricted to performing snapshot simulations (i.e. LGM) or shorter timescales of a few hundreds to thousands of years at a time (e.g. Charbit et al., 2007), rather than full glacial cycles.

Ice sheet models (ISMs) are able to simulate the 3D dynamic and thermodynamic evolution of ice at a variety of scales and solve equations of ice flow through several approximations (Figure 1.7). The simplest ones use shallow ice (SIA) and shallow shelf approximations (SSA). SIA models are a relatively good approximation for slow moving, large areas of grounded ice (i.e. ice sheets) that have a small depth-to-width ratio and where vertical deformation in response to gravity is important. Whilst SIA is computationally cheap to run, it cannot represent ice flow in key regions such as ice domes, ice streams and ice shelves since it does not consider longitudinal stresses or vertical stress gradients (Pattyn, 2003; Rutt et al., 2009). In contrast, SSA is suitable for modelling floating ice shelves and low drag ice streams where longitudinal stresses dominate. However, it vertically integrates ice velocity and so cannot accurately simulate regions where there are large vertical variations in speeds, such as across the grounding line (Bueler and Brown, 2009). There are also hybrid models, such as the Schoof-Hindmarsh model (L1L2), which combine SSA and SIA to enable the simulation of entire ice sheets. For example, SIA can be used to model the interior of the ice sheet, SSA for the ice shelves and a combination of both for areas of ice streaming across the grounding line (Pollard and DeConto, 2012; Schoof and Hindmarsh, 2010). A step up from this are higher order models, such as the Blatter-Pattyn type models or second order models (Blatter, 1995; Pattyn,

2003). These incorporate additional stresses making them a better representation of whole ice sheet systems than hybrid models but they still may not perform well in grounding zones and they are also much more computationally expensive. The most complex models use no approximations and resolve the full Stokes equations that include all relevant stresses. As such, these models are very computationally expensive and can only feasibly be used to model small areas of ice flow over short timescales (e.g. at a specific grounding line) (Blatter et al., 2011; Kirchner et al., 2016).

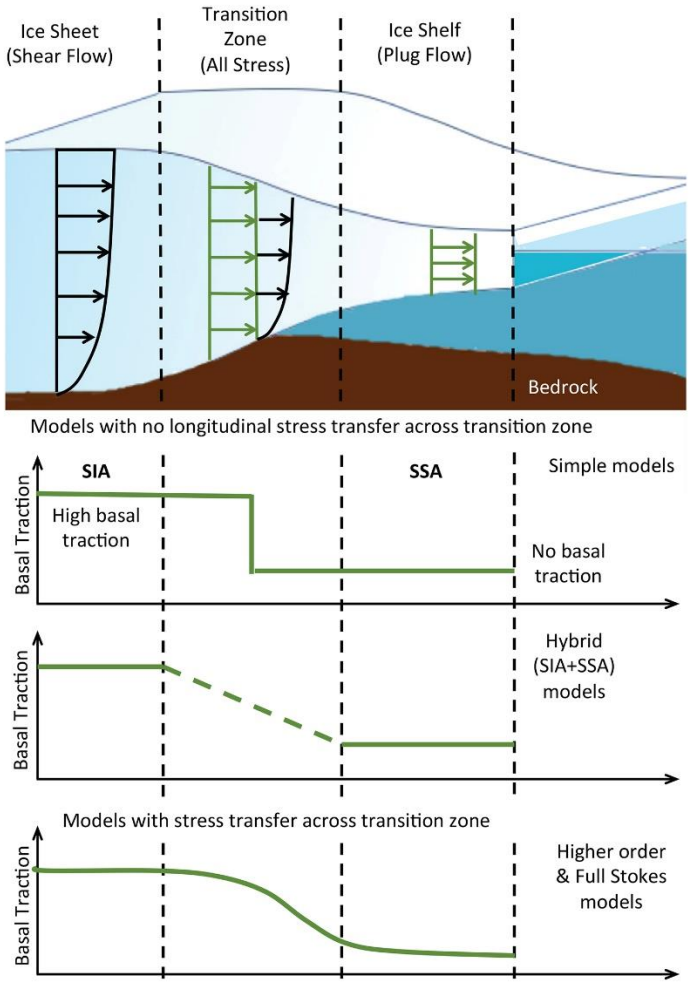

Figure 1.7: Illustration of the hierarchy of stress balance approximations available in ice sheet models. From Nowicki and Seroussi, (2018).

Whilst modelling techniques and the processes represented in them have improved significantly over the past few decades, there are still many challenges that scientists face that introduce large uncertainties in the modelled output. Firstly, model structural uncertainty arises due to limited knowledge of climate and ice sheet processes and computational constraints. This means that each model differs in terms of spatial resolution, governing physical equations, initialisation methods and parameterisations of processes, producing a spread in model output

and leading to large biases in simulated climates and ice sheets (Ely et al., 2021; Li et al., 2023a). For example, the relationship between ocean temperatures and sub-shelf melt rates is uncertain and ice sheet models implement several different parameterisations, ranging from simple linear relations to complex ice shelf cavity models. Studies comparing rates of ice sheet retreat using these different methods have shown they produce a large range of results (Berends et al., 2023; Burgard et al., 2022; Favier et al., 2019). Similarly, climate model intercomparison studies have demonstrated the wide range of simulated climates obtained by the different models despite using the same boundary conditions (Harrison et al., 2015). They have also shown how model development does not always guarantee increased confidence in the results, evidenced by the larger range in equilibrium climate sensitivity of the newer set of models in the Coupled Model Intercomparison Project (CMIP6) compared to the previous generation (CMIP5) (Meehl et al., 2020). The numerical schemes used by the models require input parameters which can also be very uncertain leading to parametric uncertainty. Thus models need to be tuned to find values of these parameters that produce reliable representations of the processes being modelled (Gregoire et al., 2011). Another large source of uncertainty arises from the choice of boundary conditions including ice sheet topography and meltwater forcing, which have been shown to significantly impact the modelled output (Izumi et al., 2023; Kapsch et al., 2022; Snoll et al., 2024). In addition, palaeo simulations often require a spin-up to allow the boundary conditions to adjust which requires extra computational time (Haywood et al., 2019).

To this end, many researchers employ techniques of uncertainty quantification to account for these model limitations and quantify the uncertainties that arise. The main approach employed to evaluate parametric uncertainty is a perturbed physics ensemble (PPE) in which a selection of model parameters are varied systematically across their plausible ranges to produce multiple combinations of model inputs to be evaluated by the model. The spread in the resulting outputs highlights the model sensitivity to the input parameters and each ensemble member can then be compared to empirical constraints to find the sets of parameters that produce plausible simulations in order to tune the model (e.g. Gandy et al., 2023; Gregoire et al., 2011, 2016; Hopcroft et al., 2021). The number of samples needed increases with the number of parameters being tested leading to the use of efficient sampling techniques such as Latin Hypercube Sampling, which generates statistically efficient random samples across multi-dimensional distributions (McKay, 1992; Williamson, 2015). The extent to which parametric uncertainty can be reduced through tuning is limited by the complexity of the model and the computational

resources available to run ensemble members, as well as the number of reliable observational constraints against which to compare the model output.

The structural uncertainty of a model can also be quantified by evaluating the discrepancy between model output and observational constraints. Many studies summarise one or more output fields into a metric, such as ice sheet volume and extent, which can be compared against empirical and model reconstructions and used as a measure of structural uncertainty (e.g. Gregoire et al., 2011). Multi-model ensembles have been performed to assess the structural uncertainty of a range of models frequently used for climate projections, in which these models are employed to simulate past climates under most of the same boundary conditions and benchmarked against palaeoclimate data syntheses (Braconnot et al., 2012; Harrison et al., 2015).

To assess the individual impact a specific parameter or boundary condition has on the modelled output, sensitivity analyses can be performed. This can involve local approaches where one input is varied at a time whilst keeping everything else constant (e.g. Zweck and Huybrechts, 2005), or global methods such as Sobol′ Sensitivity Analysis (Sobol′, 2001; Zeng et al., 2021), which calculates the relative contribution of each parameter to the overall output variance and considers the interactions between parameters.

Methods of sensitivity analysis can be extended through history matching which involves identifying areas of the parameter space that cannot be ruled out based on empirical and model constraints taking into account model and data uncertainty (Gardner et al., 2020; Williamson et al., 2013, 2015). Usually, a sensitivity analysis is performed first to find the parameters that are responsible for most of the variation in model output in order to reduce the dimensions of the parameter space, so that a larger sample of each parameter can be explored in a PPE. Once this PPE has been run, many groups utilise emulation methods in order to increase the number of samples able to be evaluated further. An emulator (e.g. Gaussian Process (GP) emulator) is a statistical approximation of a numerical model that is trained on the ensemble model output but can then be used to evaluate many more inputs using only a fraction of the computational costs. The resulting emulated outputs are compared to the constraint data, usually in the form of a singular implausibility metric, which identifies areas of the parameter space that are “Not Ruled Out Yet” (NROY). These areas can then be resampled for additional waves of ensemble simulations and history matching to refine the space further (Gardner et al., 2020; Li et al., 2019).

Other challenges arise due to technological and computational limitations that make the coupling of ice sheet and climate models problematic. Most AOGCMs resolve weather and climate processes on spatial scales of tens to hundreds of kilometres, and temporal scales of minutes to days, since this is the characteristic length scale of atmospheric and oceanic circulation. However, ISMs need to resolve much smaller scale features (a few kilometres or less) such as gradients of SMB on ice sheet slopes, grounding line migration and ice streaming (Pattyn et al., 2017), many of which evolve over millennial timescales. Running a GCM over these long glacial-interglacial timescales and at high enough spatial resolutions is not computationally feasible and has therefore led to a number of different strategies by modelling groups to account for this (Pollard, 2010).

Despite these challenges, significant advancements to our understanding of the last two glacial-interglacial cycles has occurred thanks to numerical modelling. The next section reviews some of these studies, which use a range of models and techniques to look at a variety of aspects of these time periods, and gives an overview of what current technological capabilities has enabled us to conclude.

1.2.5 Previous studies

Before recent technological advances made coupling of climate and ice sheet models feasible, many studies treated these components independently and either prescribed the ice sheet forcing in climate models or the climate forcing in ice sheet models. These methods have been used to simulate the ice sheet evolution over multiple glacial-interglacial cycles for use as forcings in the PMIP4 protocols for the Last and Penultimate Deglaciations (Abe-Ouchi et al., 2013; Briggs et al., 2013, 2014; Tarasov et al., 2012). There is also an extensive literature using these methods aiming to reconstruct the ice sheets and climate of the Last Glacial Cycle and investigate the mechanisms behind the sequence of events (e.g. Patton et al., 2017).

Many of these studies also explore the sensitivity of the results to modelling choices such as model parameters and boundary conditions. For example, Petrini et al., (2020) performed an ensemble of simulations using a 3D ISM of the Last Deglaciation of the BKIS forced by climate fields from AOGCM snapshot simulations of the LGM and pre-industrial, interpolated using a climate index, and a global mean sea level curve. They found that ocean forcing is the main driver of the retreat of the ice sheet and its sensitivity to sub-shelf melting is amplified by the global mean sea level rise. Conversely, van Aalderen et al., (2023) performed some similar ISM simulations of the EIS forced by LGM climate fields from five different PMIP simulations, to test its sensitivity to different drivers of deglaciation. They find that atmospheric

warming is the primary trigger of retreat with increasing atmospheric temperatures amplifying the ice sheet's sensitivity to sub-shelf melt. They argue that these different conclusions result from the methodologies used to generate the initial LGM ice sheet.

Several other studies show how the choice of AOGCM used to generate the climate fields that drive ISMs causes significant variations in the simulated ice sheet evolution due to the dominant role of atmospheric conditions on SMB. They also highlight how, although the main features of ice sheet evolution are captured, there are still large discrepancies when compared to geological reconstructions, likely as a result of missing climate-ice sheet interactions, missing processes in the ice sheet model itself or the choice of ice sheet reconstruction used as a boundary condition (Alder and Hostetler, 2019; Blasco et al., 2021; Charbit et al., 2007; Niu et al., 2019; Scherrenberg et al., 2023b). The sensitivity of the NH ice sheets during the Last Glacial Cycle to the representation of the climate is also highlighted by Zweck and Huybrechts, (2005) who vary 11 parameters in an ice sheet model, the GCM climate used as forcing and the glacial index used to scale it. The uncertainty in parameters controlling climate conditions over the ice sheet dominate the variability in the results but ice rheology and basal processes are also important for simulated ice sheet thickness. The importance of the climate forcing, as well as the interpolation method, used is further explored by Scherrenberg et al., (2023b). They force an ISM over the LDG using output from several climate models and two interpolation methods; climate matrix and glacial index. The GCM used to generate the climate forcing was much more important than the method used to interpolate the snapshots, with the majority of models resulting in unrealistic LGM ice volumes. However, the interpolation method used impacted the pattern of glacial inception and rate of deglaciation due to the representation of the ice-albedo feedback. The glacial index method does not include the effects on temperature due to albedo. This leads to biases in regions with particularly high and low albedos, which impacts the ice sheet evolution and produces a worse match to geological constraints. They use the results of these experiments to select a climate forcing for ISM simulations over several glacial cycles and show that proglacial lakes accelerate the deglaciation of ice sheets (Scherrenberg et al., 2023a).

Abe-Ouchi et al., (2007) evaluated the influences of different feedbacks on the climate at the LGM through performing sensitivity tests in which they drive a GCM using different initial ice sheet and climate conditions. The results of these GCM simulations are then used to drive an ISM over the Last Glacial Cycle. They show that the ice-albedo feedback, temperature-elevation feedback and desertification effect significantly influenced the ice sheet mass balance and therefore must be treated carefully when simulating glacial-interglacial cycles. Other

studies have also investigated possible mechanisms responsible for the abrupt events recorded in proxy records during the LDG. For example, it has been proposed that the NAIS could have had a significant contribution to MWP-1A through a saddle collapse triggered by the BA warming (Gregoire et al., 2012, 2016). In addition, simulations of the LDG using an EMIC forced by transient ice sheet and freshwater forcings show that the North Atlantic is a key driver in the observed millennial scale variability due to freshwater input varying the strength of deep-water formation (Menviel et al., 2011). However, the ice sheet reconstruction and meltwater distribution used to force climate models has also been found to significantly impact the simulated millennial scale variability in transient simulations (Kapsch et al., 2022; Smith and Gregory, 2012). The former is largely because differences in topographies have a large impact on the atmospheric circulation (Liakka et al., 2016; Ullman et al., 2014).

Fewer studies have focused on the Penultimate Glacial Cycle but several attempts have been made to model the PGM ice sheets in order to provide better constraints on their configurations. They find that using a smaller PGM NAIS to force a GCM results in a PGM climate that is more in line with proxy records (Colleoni et al., 2016). Similarly, using a climate field produced using a smaller prescribed NAIS to force an ISM results in global ice volumes that are more in line with sea level reconstructions (Wekerle et al., 2016). This supports the evidence that the NAIS was smaller during the PGM than the LGM. The last two deglaciations have been compared in transient simulations using an AOGCM with prescribed ice sheets and freshwater forcing. One study showed that a greater ice sheet discharge is needed during the PDG to simulate the abrupt change of HS11 compared to the LDG, highlighting the importance of the different orbital forcings in causing different patterns of ice mass loss and meltwater flux (Obase et al., 2021). Another showed that the longer period of reduced AMOC during HS11 caused a greater subsurface warming in the Atlantic and lead to the more rapid sea level rise during the PDG compared to the LDG. They then used these two GCM climate outputs to drive an ISM, which they first optimised by performing ensembles of the better constrained LDG, and found that this greater subsurface warming, along with the greater glacial isostatic depression by the EIS, contributed to the excess ice loss from the AIS and GrIS during the LIG (Clark et al., 2020). However, both of these studies used an LGM ice sheet configuration as a starting point for both deglaciations which neglects any affects the different ice sheet configurations may have on the climate.

Technological developments have permitted several solutions to the computational limitations of directly coupling climate and ice sheet models. As such, fully coupled simulations of the last two glacial periods can now be undertaken, which reduces some of the uncertainties related

to missing feedbacks, choice of climate or ice sheet forcing or inconsistencies between the simulated components. To get around the issue of different atmospheric and ice sheet grid resolutions, the surface mass balance calculated by the coarser atmospheric model is downscaled onto the finer ice sheet model grid by splitting each atmosphere grid box into several sub-grid scale tiles representing a different elevation range (Ganopolski et al., 2010; Smith et al., 2021b; Ziemen et al., 2014). These tiles are then used separately to provide finer scale information to the ice sheet model.

One approach to dealing with the mismatch in temporal scales between climate and ice sheet processes is to use an EMIC. These much simpler models are capable of simulating longer timespans with minimal computational effort and have therefore been coupled with ISMs to perform simulations of glacial cycles. These studies have provided insights into the physical mechanisms and feedbacks that drove the Last Deglaciation through the performance of sensitivity tests. For example, in support of the Milankovitch theory, the primary trigger for ice sheet retreat has been shown to be an increase in insolation as a result of changing orbit, however CO_2 concentration provides a key contribution especially in terms of modulating the timing of melt (Charbit et al., 2005; Ganopolski and Brovkin, 2017; Heinemann et al., 2014; Quiquet and Roche, 2024). In addition, simulations that include the effects of dust deposition and snow ageing have found it to be an important feedback in producing a full deglaciation of the NH during the LDG (Ganopolski et al., 2010; Willeit and Ganopolski, 2018).The magnitude of the freshwater forcing has also been shown to be important in whether millennial scale variability is simulated in the models due to the sensitivity of the AMOC, and thus also impacts the deglaciation of the ice sheets (Charbit et al., 2005; Ganopolski and Brovkin, 2017; Quiquet et al., 2021a). For example, simulations of the LDG using a coupled EMIC-ISM by Quiquet et al., (2021a) do not produce any abrupt changes when a realistic freshwater forcing is used since it causes a complete shutdown of the AMOC. Similarly, in the absence of this forcing there are also no abrupt changes as the AMOC remains strong. This also causes a more rapid deglaciation of the ice sheets, especially for North America. However, when the magnitude of the forcing is reduced, abrupt changes in AMOC state are simulated leading to abrupt changes in temperature over Greenland. This highlights that some models can be too sensitive to freshwater input. Additional sensitivity tests also showed that model parameters that affect basal sliding can impact the rate of retreat of the ice sheets due to affecting the sensitivity of the grounding line, but the effect on the climate evolution is limited. Changes to parameters controlling the SMB impact the overall size of the ice sheets but maintain similar retreat patterns. Finally, they show that the retreat is mostly driven by the magnitude of surface

ablation and is relatively insensitive to sub-shelf melt rates. This study was followed by one that performed equivalent simulations of the Penultimate Deglaciation in which they compared the two (Quiquet and Roche, 2024). They revealed that NH insolation is the main driver of retreat for both periods but the difference in solar insolation leads to a different rate of ice retreat, despite both sets of simulations starting from the same LGM ice sheet configuration. Warmer air temperatures and subsurface Southern Ocean temperatures are also simulated during the PDG, as are different AMOC sensitivities between both periods even without the inclusion of freshwater forcing, with the PDG circulation being more prone to collapse. They also highlight the importance of vegetation changes in simulating a full deglaciation due to its impact on albedo.

The atmospheric and oceanic dynamics in EMICs are highly parameterised providing an oversimplified representation of many processes that can lead to biases in the model output and limit confidence in the results. Therefore, it is preferable to use AOGCMs which have a much more detailed representation of these processes, reducing some of these uncertainties, but are much more expensive. To overcome this, many simulations are performed asynchronously whereby the climate model is run for a short period of time and the output is then used to drive the ice sheet model for a much longer period which is then fed back to the climate model and so on (e.g. Niu et al., 2021). This decreases the computational expense since the climate model does not have to run for the entire simulation length required. In addition, several studies use low resolution versions of AOGCMs to further reduce costs and enable longer transient simulations or large ensembles to be performed. Ziemen et al., (2014) performed steady state LGM simulations using an AOGCM-ISM coupled model which produced NH ice sheets that agreed reasonably well with reconstructions. A subsequent study using the same model investigates the characteristics of Heinrich events over the Last Deglaciation through several transient simulations. They show a two-step response of the climate system to the events; first to the freshwater discharge which strengthens the stratification of the North Atlantic reducing deep-water formation. This weakens ocean circulation and cools the North Atlantic. Second, once the freshwater discharge ends, and the NAIS surface elevation is at a minimum, the lower elevation allows the Jetstream to expand northwards, weakening the subpolar gyre and cooling Europe. The effects of ice sheet topography on atmospheric circulation provides an explanation for the observed two-stage behaviour during Heinrich events, which experiments using uncoupled climate models have been unable to simulate (Roberts et al., 2014; Ziemen et al., 2019). The importance of climate-ice sheet interactions is further highlighted in a study by Gregory et al., (2012) who simulated the Last Glacial Inception over North America. They

found that the ice-albedo feedback has a dominant role on the initial expansion of ice over the continent, with the temperature elevation feedback also becoming important for the thickening of the ice sheets later on in the glacial period. There are also topographic influences on atmospheric circulation which affects the cloud and temperature patterns and therefore the ice sheet growth.

These studies all used one set of model parameters, the values of which can be very uncertain, causing uncertainty or error in the results, as has been shown in ensemble and sensitivity experiments performed by uncoupled models (Gregoire et al., 2011; Pittard et al., 2022; Pollard et al., 2016). As such, more recent efforts to simulate the LGM NAIS and GrIS have tried to quantify this uncertainty in coupled GCM-ISM ensemble experiments. Gandy et al., (2023) found that the value of parameters controlling the surface albedo of the NAIS determined the majority of the uncertainty in the LGM configuration and that different values are needed to produce realistic modern day Greenland configurations. Sherriff-Tadano et al., (2024) expanded on this by including a slab ocean model and a more complex ice sheet model able to better simulate ice dynamics. They also show the importance of albedo parameters on the NAIS volume but find that Greenland is more affected by the rate of basal sliding due to the larger contribution from calving on its mass balance.

The coarse resolution of the climate and ice sheet models used in these studies leads to some biases in the simulated climates and the underestimation of some smaller scale features such as ice lobes and ice streams. For example, simulations tend to grow too much ice over Alaska and Northern Siberia due to a cold bias over this region which is then amplified by albedo and altitude feedbacks (Gandy et al., 2023; Sherriff-Tadano et al., 2024; Ziemen et al., 2014). Ziemen et al., (2014) also suggest that these discrepancies could be due to the effects of dust feedbacks not being included in the model or too long integration times under a constant LGM boundary condition. They highlight that in reality the ice sheet and climate state at the LGM were not in equilibrium and transient simulations over the last glacial would produce a better representation. Many coupled simulations also underestimate the southern extent of the ice sheets possibly due to an underestimation of the stationary wave effect that cools these areas (Abe-Ouchi et al., 2007; Roe and Lindzen, 2001; Sherriff-Tadano et al., 2024).

1.3 Aims and approach of this study

The overall aim of this thesis is to understand the evolution of the Northern Hemisphere ice sheets during the Last and Penultimate Deglaciations and why they differed. This will be achieved by performing the first transient simulations of these two time periods using a GCM

coupled to an ISM under the different climate forcings and initial ice sheet conditions. The following four research questions will be investigated to help achieve the aim:

RQ1. Why did the configuration of the Northern Hemisphere ice sheets differ during the Last Glacial Maximum and Penultimate Glacial Maximum?

RQ2. Which climatological and glaciological processes and feedbacks are important when simulating glacial periods?

RQ3. What are the similarities and differences between the last two deglaciations due to the different transient climate forcings (orbit, GHGs, sea surface conditions) and initial ice sheet states?

RQ4. What were the main drivers of ice sheet retreat during the last two deglaciations?

In order to answer these questions there are a number of steps that must be performed that direct the approach that this thesis has taken. Thus, the next three chapters of this thesis tackle four main objectives outlined in Table 1.1.

Table 1.1: Research objectives and the relevant thesis chapters in which they are addressed.

Objective	Chapter(s)
OBJ1. Develop implausibility metrics to constrain the model output and find simulations that produce plausible LGM and PGM Northern Hemisphere ice sheets	2, 3
OBJ2. Assess the uncertainty in the simulated ice sheets that arises from model parameter and boundary condition uncertainties	2, 3, 4
OBJ3. Determine the sensitivity of the individual ice sheet evolutions to model parameters	2, 3, 4
OBJ4. Evaluate the importance of different drivers in the deglaciations through sensitivity tests	4

The strong, diverse interactions between the atmosphere and ice sheets have a large influence on the surface mass balance of the ice sheets (e.g. through albedo and topography feedbacks) and therefore their evolution through glacial-interglacial cycles. They thus need to be explicitly modelled in order to understand the differences between the last two glacial-interglacial cycles and answer the research questions. This requires the use of a fully coupled atmospheric-ice

sheet model to perform simulations of these periods. In this thesis we use a version of the FAMOUS general circulation model that has been developed to enable the bi-directional coupling to an ice sheet model (FAMOUS-ice; Smith et al., 2021b). Since the research questions and objectives require running multi-millennial simulations and large ensembles, the use of a high resolution AGCM is unfeasible. FAMOUS uses the same physics as the HadCM3 AGCM but at a lower resolution, making it more computationally efficient. Whilst it runs at similar resolutions to many EMICs, it has a much more complex representation of many atmospheric processes reducing the uncertainty from simplified parameterisations.

We use two 3D ice sheet models that are suitable for different applications. Glimmer is a fast, low resolution dynamical ISM that uses the shallow ice approximation making it adequate for simulating continental ice sheets over glacial-interglacial scales (Rutt et al., 2009). We also employ the more complex ISM, BISICLES, which uses L1L2 physics and allows smaller areas of interest to be simulated at higher resolution through adaptive mesh refinement, making it more suitable for simulating ice streaming across grounding lines which could be important for the largely marine based Eurasian ice sheet (Cornford et al., 2013).

The coupling procedure and representation of albedo in the latest version of FAMOUS-ice used in this thesis, also give it advantage over other model approaches for the representation of SMB. Surface mass balance is calculated using a multi-layer surface snow scheme on sub-grid scale tiles at set elevations within each glaciated grid box in FAMOUS, enabling it to be effectively downscaled onto the finer ice sheet model grid (Smith et al., 2021b). This scheme calculates SMB based on the surface energy budget and snowfall making it more realistic compared to empirical parameterisations based on surface air temperatures and precipitation, that are often used (e.g. Gregory et al., 2012; Quiquet et al., 2021a). In addition, the snow and ice albedo is a prognostic quantity in FAMOUS-ice, rather than prescribed, calculated using the age, density and temperature of the snow or ice at the surface.

Simulations of deglaciations must start from a spun-up glacial maximum condition with the different ice sheet configurations consistent with the different glacial climates. Starting from the different glacial maximum conditions is important because the configuration of the ice sheets impacts the interactions they have with the climate, as discussed in Sects. 1.2.2 and 1.2.3.1. However, as we have seen, the ice sheet configuration is sensitive to the choice of model parameters. Gandy et al., (2023) performed simulations using FAMOUS coupled to Glimmer and found that the model was overtuned to fit present day Greenland conditions and deglaciated under LGM conditions. So, work first needed to be done to tune the model to

simulate a plausible NAIS at the LGM. This was done by performing an ensemble of simulations varying 13 climate and ice sheet parameters over their range of possible values and ruling out any simulations that do not have a reasonable match to volume and extent constraints. By doing this they obtain a small set of plausible spun up LGM North American ice sheets. However, we still lack a PGM NAIS initial condition. This forms the basis of **Chapter 2** of this thesis, expanding the work of Gandy et al., (2023) by running ensembles of simulations of the LGM and PGM North American ice sheets under their respective climate boundary conditions (i.e. orbital parameters and GHGs) to equilibrium. **Chapter 3** develops this work further by including the Eurasian ice sheet in the simulations and using the more complex ice sheet model, BISICLES, to perform additional LGM and PGM ensembles varying 12 parameters. **Chapter 4** then uses the glacial maxima equilibrium simulations produced from Chapter 3 as initial conditions for transient simulations of the Last and Penultimate Deglaciations.

Chapter 2

2 Contrasting the Penultimate and Last Glacial Maxima (140 and 21 ka) using coupled climate-ice sheet modelling

This chapter has been published as Patterson et al., 2024, *Contrasting the Penultimate Glacial Maximum and the Last Glacial Maximum (140 and 21 ka) using coupled climate–ice sheet modelling*, Climate of the Past, 20(10), pp.2191–2218, https://doi.org/10.5194/cp-20-2191-2024

2.1 Abstract

The configuration of the Northern Hemisphere ice sheets during the Penultimate Glacial Maximum differed to the Last Glacial Maximum. However, the reasons for this are not yet fully understood. These differences likely contributed to the varied deglaciation pathways experienced following the glacial maxima and may have had consequences for the interglacial sea level rise. Therefore, a better understanding of how and why these two glacial maxima differed is crucial for developing the full picture on why the Last Interglacial sea level was up to 9 meters higher than today, and thus may help constrain future sea level rise. To understand the differences between the North American ice sheet at the Last and Penultimate glacial maxima (21 and 140 ka), we perform two perturbed-physics ensembles of 62 simulations using a coupled climate-ice sheet model FAMOUS-ice, in which the North American and Greenland ice sheets are dynamically simulated with the Glimmer ice sheet model. We select six ensemble members that match reconstructed ice extent and volumes at the Last and Penultimate glacial maxima. To understand the role of orbit, greenhouse gases and initial conditions on the final ice sheet configurations, we use a factor decomposition technique. This reveals that the initial ice sheet conditions used in the model are extremely important in determining the difference in final ice volumes between both periods due to the large effect of the ice-albedo feedback. In contrast to evidence of a smaller Penultimate North American ice sheet, our model shows that the climate boundary conditions at these glacial maxima, if considered in isolation, imply a larger Penultimate Glacial Maximum North American ice sheet than at the Last Glacial

Maximum, of around 6 meters sea level equivalent. This suggests the growth of the ice sheet prior to the glacial maxima is key in explaining the differences in North American ice volume.

2.2 Introduction

The Penultimate Glacial Maximum (PGM) occurred around 140 thousand years ago (ka), within Marine Isotope Stage 6 (MIS 6). Greenhouse gas (GHG) concentrations and global average insolation were similar to the Last Glacial Maximum (LGM; ~21 ka) (Bereiter et al., 2015; Berger and Loutre, 1991; Loulergue et al., 2008) but the orbital configuration differed, affecting the seasonal and latitudinal distribution of incoming shortwave radiation (Berger, 1978; Colleoni et al., 2011). The global total ice sheet volume, and thus the global mean sea level, was likely similar between the two glacial maxima (~120-130 m below present), with larger uncertainty at the PGM (Masson-Delmotte et al., 2010; Rabineau et al., 2006; Rohling et al., 2017). Both geological evidence and numerical modelling suggest that despite the similarities in total ice volume between the PGM and the LGM, the configurations of the Northern Hemisphere (NH) ice sheets differed significantly (e.g. Batchelor et al., 2019; Colleoni et al., 2016; Svendsen et al., 2004).

Some reconstructions suggest the Eurasian ice sheet (EIS) may have been up to ~50% larger during the Penultimate Glacial Cycle (MIS 6: ~190-130 ka) than during the Last Glacial Cycle (~115-12 ka) (Svendsen et al., 2004). However, evidence of multiple advances and uncertainties in dating proxy records means that the maximum extent mapped at 140 ka could correspond to previous advances during MIS 6 (Colleoni et al., 2016; Ehlers et al., 2018; Margari et al., 2014; Svendsen et al., 2004). The extent of the North American ice sheet (NAIS) during the PGM is even less well constrained due to a lack of glaciological evidence (e.g. moraines and till). The scarcity of empirical data in itself suggests that it was smaller in most areas than at the LGM because the subsequent larger ice sheet could have largely erased the evidence of prior glaciations (Dyke et al., 2002; Rohling et al., 2017). Additionally, evidence of reduced ice rafted debris (IRD) discharge from the Hudson Strait in the North Atlantic IRD belt (e.g. Hemming, 2004; Naafs et al., 2013; Obrochta et al., 2014), relative sea level assessment studies (e.g. Rohling et al., 2017) and climate, ice sheet and glacial isostatic adjustment modelling (e.g. Colleoni et al., 2016; Dyer et al., 2021) all point to a smaller volume PGM NAIS. For example, assuming a similar global mean sea level fall (and Antarctic ice sheet volume) at the PGM as at the LGM but with a larger volume EIS at the PGM (estimated at 33-53 m sea level equivalent (m s.l.e.) versus 14-29 m s.l.e. at the LGM), this follows that

the NAIS must have been smaller than at the LGM to compensate (39-59 m s.l.e. versus 51-88 m s.l.e.) (Rohling et al., 2017).

The reason for these differences is likely complex and is not yet fully understood. The evolution and surface mass balance (SMB) of ice sheets depends on many factors such as; background climate, climate and ice sheet histories, dust deposition, vegetation, ice albedo and sea surface temperatures (SSTs), as well as the interactions and feedbacks between them all (Colleoni et al., 2009a, 2011; Kageyama et al., 2004; Krinner et al., 2006, 2011; Liakka et al., 2012; Stone and Lunt, 2013). The ice sheets themselves also strongly influence the climate through their interactions with atmospheric and oceanic circulation and the energy balance. This alters global and local temperature and precipitation patterns which in turn affects ice sheet ablation and accumulation (i.e. SMB) (Abe-Ouchi et al., 2007; Beghin et al., 2014, 2015; Gregoire et al., 2015, 2018; Izumi et al., 2023; Kageyama and Valdes, 2000; Liakka et al., 2016; Snoll et al., 2022; Ullman et al., 2014). These interactions between the vast ice sheets and other components of the climate system exerted an important control on the initial climate state for the deglaciations, and hence on the subsequent chain of events, thus impacting the climate, ocean and sea level evolution during deglaciation. Thus, the contrasting configurations of the NH ice sheets at the glacial maxima may have contributed to the different deglaciation pathways that followed. The timings and magnitudes of the climate and ocean circulation changes that occurred during the Penultimate Deglaciation (~140-128 ka) differed to the Last Deglaciation (~21-9 ka) (Landais et al., 2013; Menviel et al., 2019). For example, the Last Deglaciation experienced two abrupt climate changes associated with a weakened Atlantic Meridional Overturning Circulation; Heinrich Stadial 1 and the Younger Dryas (Denton et al., 2010; Ivanovic et al., 2016), compared to evidence of only one, much longer abrupt change towards the end of the Penultimate Deglaciation, Heinrich Stadial 11 (Cheng et al., 2009; Govin et al., 2015; Jiménez-Amat and Zahn, 2015; Marino et al., 2015). The deglaciations also led to interglacials with very different characteristics to one another, including average global surface temperatures 1-2 °C higher and sea level up to 9 m higher than the pre-industrial during the Last Interglacial (~129-116 ka) (Dutton et al., 2015; Dutton and Lambeck, 2012; Dyer et al., 2021; Grant et al., 2014; Kopp et al., 2009; Otto-Bliesner et al., 2013b; Turney and Jones, 2010).

In this context, it is important to examine the complex physical interactions between the climate and the ice sheets to better understand why the last two glacial maxima had different ice sheet configurations and evaluate the ice sheets' sensitivities to changes in climate in relation to different orbits and GHG concentrations.

Despite the challenges in coupling atmosphere-ocean general circulation models (AOGCMs) with ice sheet models due to the mismatch between the required spatial and temporal scales, recent technical advances have meant that this is now possible. A combination of increased computer power, the development of more computationally efficient, lower resolution AOGCMs and sub-grid scale schemes translating ice sheet relevant atmospheric processes onto the higher resolution ice sheet grid, has made bi-directional, coupled climate-ice sheet simulations over longer timescales, and in large ensembles, feasible (Fyke et al., 2011; Sellevold et al., 2019; Smith et al., 2021b; Vizcaíno et al., 2013; Ziemen et al., 2014).

This study uses a coupled climate-ice sheet model, called FAMOUS-ice (Smith et al., 2021b), to perform ensemble simulations of the PGM and LGM to explore input climate and ice sheet parameter uncertainties, their effects on the North American ice sheet volume during each period, and find parameter combinations that give a reasonable ice sheet configuration for both glacial maxima. The ensembles are also constrained based on volume and extent metrics and the "Not Ruled Out Yet" (NROY) simulations are analysed to try and understand the similarities and differences between both periods. We find that the initial conditions used in the LGM and PGM experiments played an important role in some of the differences seen and we quantify this impact through the use of sensitivity tests and factor decomposition analysis.

2.3 Methods

2.3.1 Model description

FAMOUS is a fast, low resolution AOGCM that is based on Hadley Centre coupled model, HadCM3, and therefore retains all the complex processes represented in an AOGCM but uses only half the spatial resolution and a longer time step. Since it requires only 10% of the computational costs of HadCM3, it has been successfully used for long transient palaeo simulations (Dentith et al., 2019; Gregoire et al., 2012; Gregory et al., 2012; Roberts et al., 2014; Smith and Gregory, 2012) and large ensembles for uncertainty quantification (Gandy et al., 2023; Gregoire et al., 2011). This study uses the atmospheric component, which is a quasi-hydrostatic, primitive equation grid point model with a horizontal resolution of 7.5° longitude by 5° latitude with 11 vertical levels and a 1-hour time step (Williams et al., 2013). Land processes are modelled using the MOSES2.2 land surface scheme (Essery et al., 2003), which uses a set of sub-gridscale tiles in each grid box to represent fractions of nine different surface types, including land ice (Smith et al., 2021b). Whilst this study prescribes sea surface

temperatures (SSTs) and sea ice concentrations, FAMOUS can also be run fully coupled with a dynamical ocean (e.g. Dentith et al., 2019).

FAMOUS now allows the direct two way coupling to an ice sheet model in the configuration FAMOUS-ice (Smith et al., 2021b). Here, we use FAMOUS in combination with Glimmer to interactively simulate the North American and Greenland ice sheets at 40 km resolution. Glimmer is a fast running, 3D thermomechanical ice sheet model which uses the shallow ice approximation. This allows it to model ice sheet evolution over long timescales as it is more computationally efficient, and therefore has been used to simulate continental ice sheets over glacial-interglacial cycles (Gregoire et al., 2016; Rutt et al., 2009).

FAMOUS-ice accounts for the mismatch between atmosphere and ice sheet grid sizes by using a multi-layer surface snow scheme to calculate SMB on "tiles" at 10 set elevations within each grid box that contains land ice in FAMOUS. This SMB is then downscaled from the coarse FAMOUS grid to the much finer Glimmer grid at each model year (Smith et al., 2021b). Glimmer uses this SMB field to calculate ice flow and surface elevation and passes this back to FAMOUS in which orography and ice cover is updated. In this study, to reduce computational costs further, FAMOUS-ice runs at 10 times ice sheet acceleration: for every year of climate integrated in FAMOUS, the simulated SMB field forces 10 years of ice sheet integration in Glimmer. Figure 2.1 shows a simplified diagram of this coupling process and full details can be found in Smith et al. (2021b). The current computational cost of this set-up is around 50 decades (of climate years) per wallclock day using 8 processors.

FAMOUS-ice has been shown to perform well in simulations of past and future ice sheets including Greenland and North America (Gandy et al., 2023; Gregory et al., 2020; Smith et al., 2021b). In particular, the LGM North American ice sheet study of Gandy et al. (2023) was able to utilise the useful constraints of the LGM to infer the importance of parameters controlling ice sheet albedo on ice sheet configuration in this model.

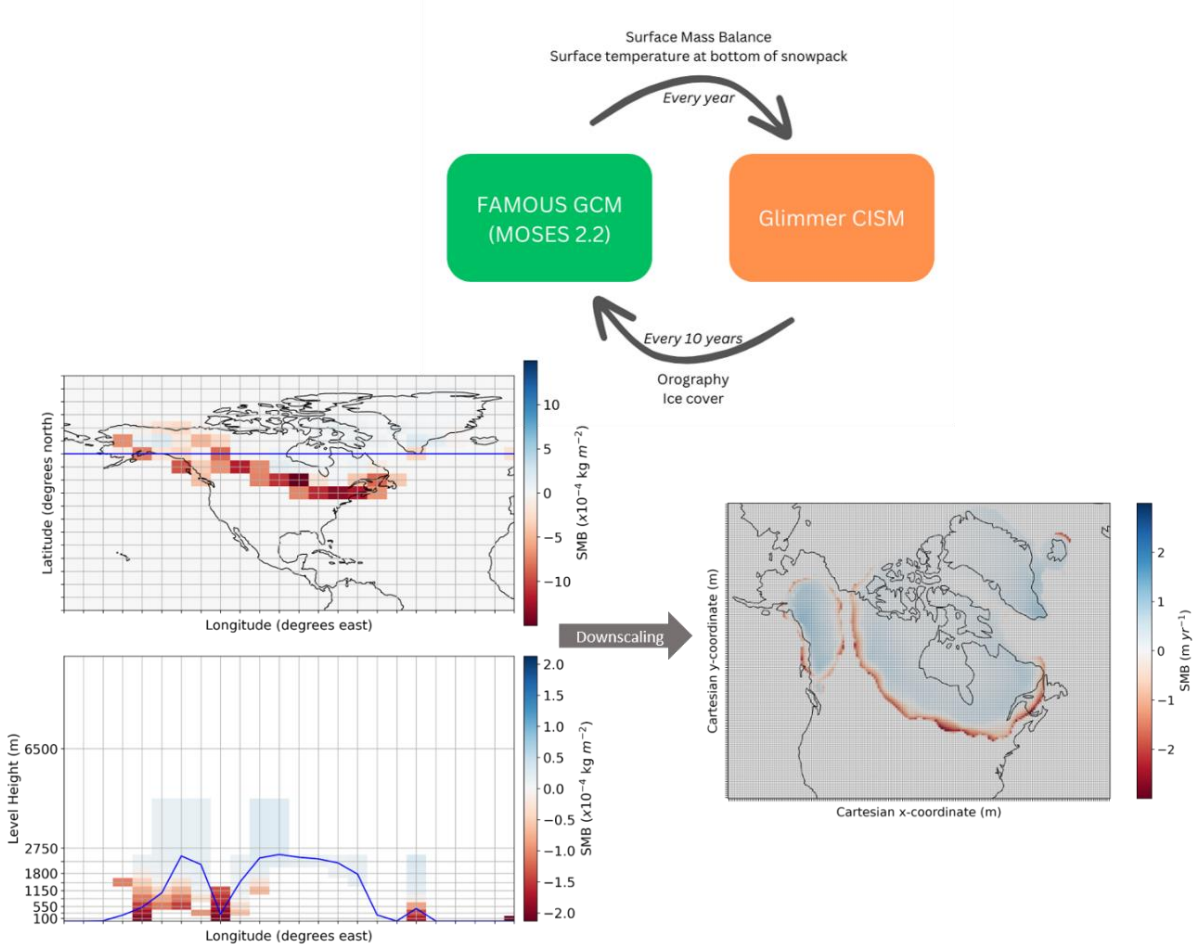

Figure 2.1: Schematic illustrating the calculation of SMB at different elevations on the FAMOUS grid followed by downscaling onto the Glimmer grid.

2.3.2 Experiment design

2.3.2.1 Climate boundary conditions

With the exception of including dynamic North American and Greenland ice sheets, our FAMOUS-ice simulations are set up following the Paleoclimate Modelling Intercomparison Project Phase 4 (PMIP4) protocols for the LGM (Kageyama et al., 2017) and PGM (Menviel et al., 2019). These protocols prescribe climatic boundary conditions, including orbital parameters and GHG concentrations, the values of which can be found in Table 2.1. Concentrations of CO_2, CH_4, and N_2O are very similar between the LGM and PGM, but orbital parameters are significantly different. The larger eccentricity at the PGM enhances the effect of precession compared to the LGM, which affects the seasonal and latitudinal distribution of insolation. These changes are important for ice sheet surface mass balance since melting is particularly sensitive to spring and summer temperatures (Huybers, 2006; Niu et al., 2019). The PGM received lower insolation in the Northern Hemisphere in late winter to early summer but higher levels in late summer to early winter compared to the LGM (Figure 2.2a). Subsequent to the completion of this work, it was discovered that the equation for the role of

eccentricity on solar insolation was incorrect in the model code. The magnitude of the error is larger for periods with higher eccentricity values, and so a sensitivity test was run to determine the effect this correction has on SMB and ice volume at the PGM. Details of this error and the results of the sensitivity test can be found in Sect. 2.7.1, but the impact was shown to be minimal, and it has been corrected for the work in Chapters 3 and 4 of this thesis (Figure 2.12).

Table 2.1: Climate boundary conditions used in the LGM and PGM experiments as prescribed by the PMIP4 protocols for each period (Kageyama et al., 2017; Menviel et al., 2019).

	Eccentr-icity	Obliquity (°)	Perihelion – 180 (°)	Solar Constant (Wm^{-2})	CO_2 (ppm)	CH_4 (ppb)	N_2O (ppb)	Orography and ice extent
LGM (21 ka)	0.019	22.949	114	1360.7	190	375	200	GLAC-1D (Briggs et al., 2014; Ivanovic et al., 2016; Tarasov et al., 2012)
PGM (140 ka)	0.033	23.414	73	1360.7	191	385	201	Combined reconstruction (Abe-Ouchi et al., 2013; Briggs et al., 2014; Tarasov et al., 2012)

In the climate model, the global orography (including the Eurasian and Antarctic ice sheets) and land-sea mask for the LGM are calculated from the GLAC-1D 21 ka reconstruction (Briggs et al., 2014; Ivanovic et al., 2016; Tarasov et al., 2012), which is one of three recommendations in the PMIP4 protocol (Kageyama et al., 2017). For the PGM simulations we used the 140 ka combined reconstruction (Abe-Ouchi et al., 2013; Briggs et al., 2014; Tarasov et al., 2012) detailed in the PGM PMIP4 protocol (Menviel et al., 2019). Vegetation is prescribed based on a pre-industrial distribution and kept constant. As ice cover changes, the fractions of grid cells that are land ice versus other surface types changes proportionally, altering albedo. However, since there is no dynamical vegetation component, some important climate-ice-vegetation feedbacks are neglected, which could have a significant impact on ice sheet evolution (Stone and Lunt, 2013).

Because of the low resolution of the FAMOUS model, using a dynamical ocean and sea ice can introduce large biases in the simulated climate (Dentith et al., 2019). By prescribing SST and sea ice, we are able to limit the amplification of climate biases arising from atmosphere-ocean-sea ice interactions. Thus, SSTs and sea ice concentration are also prescribed and constant and are taken from higher resolution HadCM3 simulations of 21ka (Figure 2.13a; see

details in Izumi et al. (2023) and 140 ka (Figure 2.13b). The 140 ka simulation is part of a suite of simulations covering the last 140,000 years (Allen et al., 2020). It was performed using a version of HadCM3 (specifically HadCM3B-M2.1aD, see Valdes et al. (2017), which was the same version as used by Izumi et al. (2023) for the LGM and Davies-Barnard et al. (2017)). The simulation was forced with 140 ka orbital configuration (Berger and Loutre, 1991) and greenhouse gases (Loulergue et al., 2008; Petit et al., 1999; Spahni et al., 2005). Ice sheet forcing and land sea mask were from de Boer et al. (2013) who modelled the evolution of all the major ice sheets. It was run as a "snapshot" simulation for 3070 years which allowed the deeper ocean to attain near equilibrium.

FAMOUS atmosphere-ocean GCM has not been run for the PGM, and we lack sufficient data density for precisely dated PGM SSTs and sea-ice to produce statistically varied reconstructions, as in Gandy et al. (2023). Thus, for physical consistency between the LGM and PGM periods, HadCM3 output was used for the surface ocean boundary conditions. Of all possible options, HadCM3 output is the most appropriate choice for this because it is the parent model for FAMOUS; they share the same physics, differing mainly in their resolutions, and HadCM3 was used as the tuning target for FAMOUS during model development (Smith et al., 2008). We take the multi-year monthly mean "climatology" of SSTs and sea ice concentrations from the final 100 years of the simulations. These 12-month climatologies are repeated throughout the duration of the simulations to provide a seasonal forcing with no long-term trend and no interannual variability.

The modelled annual average SSTs are cooler at the LGM than at the PGM, everywhere, except in the North Atlantic due to less sea ice cover in this region (Figure 2.2b). However, the summer SSTs are warmer in the Northern Hemisphere at the LGM compared to the PGM (Figure 2.2c). The HadCM3 LGM SSTs are colder on average than the reconstruction in Gandy et al. (2023), with the largest differences, of up to 6 ºC, occurring in the tropics and mid-latitudes (Figure 2.13c).

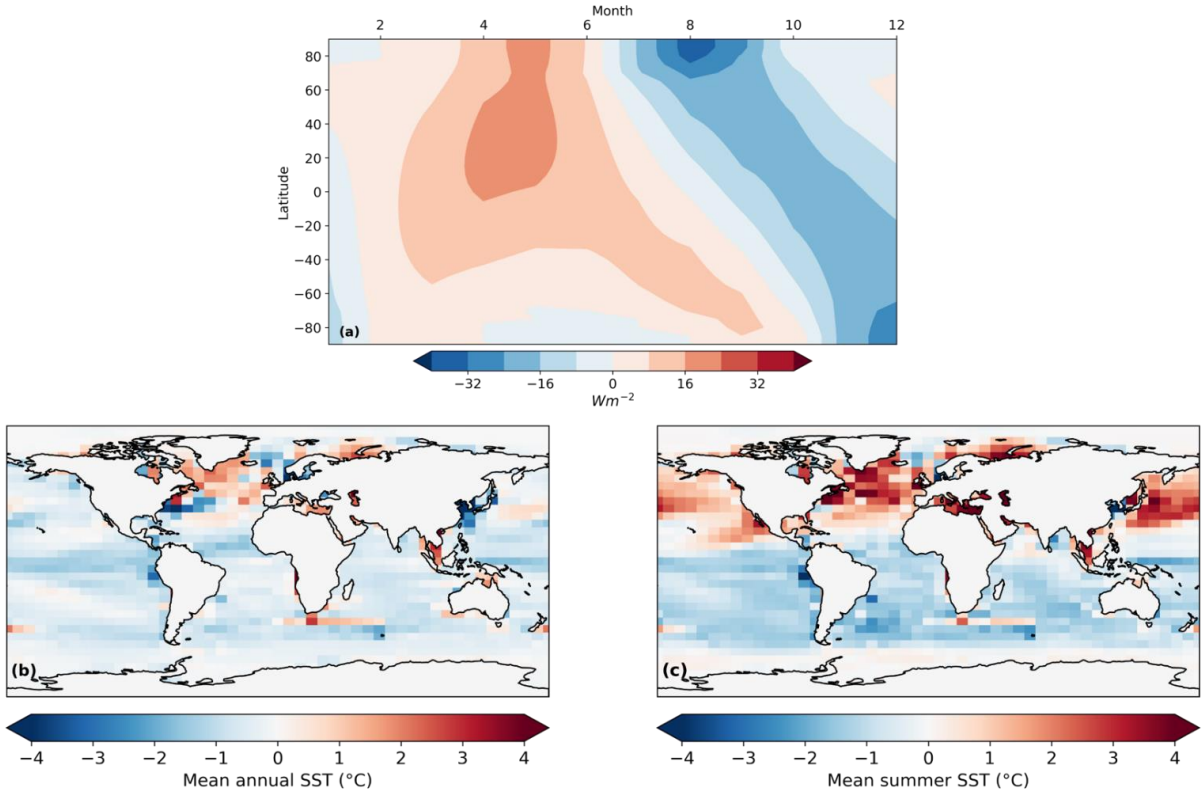

Figure 2.2: Difference between the LGM and PGM (a) latitudinal distribution of incoming top of the atmosphere shortwave radiation each month (b) modelled annual sea surface temperatures and (c) modelled summer (JJA) sea surface temperatures.

2.3.2.2 Ice sheet boundary and initial conditions

In all our simulations, the ice sheet extent is set to the PMIP4 boundary conditions for the LGM and PGM as described in Table 2.1, except in the interactive ice sheet model domain, which covers North America and Greenland. Here, we describe how the ice extent and elevation is initialised in FAMOUS and Glimmer over the interactive domain in our ensemble of PGM and LGM simulations and sensitivity experiments.

In our ensemble of LGM and PGM simulations, Glimmer is initiated from an 18.2 ka NAIS taken from a previous Last Deglaciation ensemble (Gregoire et al., 2016). This smaller intermediate (MIS 3-like) ice sheet was used in Gandy et al. (2023) as an approximate pre-glacial maximum extent from which to grow the ice sheet towards an equilibrium ice volume. For consistency, we used the same initial ice sheet conditions as in Gandy et al. (2023) when running our ensembles of LGM and PGM simulations. The coupling between the models passes this orography field from Glimmer to FAMOUS, updating the PMIP4 boundary condition that FAMOUS was initiated from. However, due to the technical formulation of the coupling, where entire gridboxes were initialised as covered in ice at all elevations in FAMOUS, the tiles in such gridboxes would not subsequently update to reflect the existence

of any non-glaciated fractions that might exist in the Glimmer state. This means that when the initial conditions are radically different in FAMOUS and Glimmer (as in our ensemble of simulations), the FAMOUS ice extent over the North American continent is not updated to match the Glimmer initial conditions. Thus, in our ensemble of LGM simulations, the albedo remains high throughout the saddle region (the area between the Laurentide and Cordilleran ice sheets) because the FAMOUS ice extent remains as large as the atmospheric model's initial conditions (i.e. the GLAC-1D 21 ka reconstruction) for the duration of the simulations (Figure 2.3). This coupling procedure has since been improved to allow tile fractions to update to match those in the ice sheet model despite drastically different initial ice cover. The different ice sheet configurations used in FAMOUS and Glimmer in the ensembles, are outlined in our table of experiments, Table 2.2 (experiments 1 and 2). The impact of this set-up compared to an ice sheet configuration matched in FAMOUS and Glimmer is explored in Sects. 2.4.2 and 2.7.3.

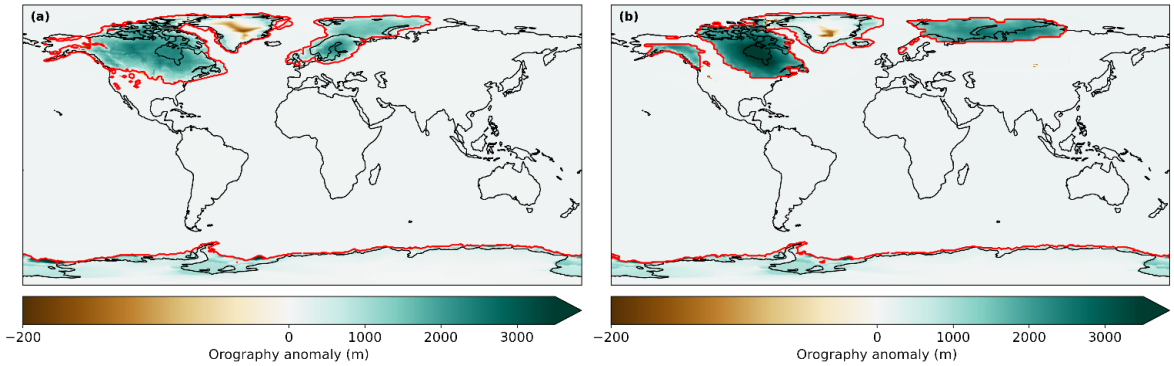

Figure 2.3: Topography anomaly from present day used as the initial condition in FAMOUS and the ice masks (red lines) for (a) the LGM and (b) the PGM.

We perform two sets of sensitivity experiments to understand the relative impact of the initial ice sheet conditions and the climate forcing on the resulting LGM and PGM NAIS volumes. The first set of experiments uses matching ice sheet configurations in FAMOUS and Glimmer, set either to the LGM GLAC-1D reconstruction or to the end of one of our PGM coupled simulations (Table 2.2; experiments 3–6). The second set uses the same initial ice sheet configurations as in the ensemble, i.e. GLAC-1D and PMIP4 reconstructions in FAMOUS and the 18.2 ka ice sheet in Glimmer (Table 2.2; experiments 7-10). A full description of the initial conditions and methods used in these sensitivity experiments can be found in Sect. 2.3.5.

Table 2.2: Table of experiments performed in this study detailing the "climate forcing" (orbital configuration, trace gases and global orography as outlined in Table 2.1 and SSTs/sea ice from HadCM3), initial ice extent set in FAMOUS over Greenland and North America, initial Glimmer ice sheet conditions and input parameter values. NROY are the simulations that are "Not Ruled Out Yet" after applying the implausibility metric described in Sect. 2.3.4.

Experiments	Climate forcing	FAMOUS initial ice extent	Glimmer initial condition	Input parameter values
1) LGM ensemble	LGM	PMIP4 LGM (GLAC-1D)	18.2 ka ice sheet	Randomly sampled from Table 2.3 ranges (See Sect. 2.3.3)
2) PGM ensemble	**PGM**	**PMIP4 PGM**	18.2 ka ice sheet	Randomly sampled from Table 2.3 ranges (See Sect. 2.3.3)
3) $V_{\_1}$ (full LGM)	LGM	PMIP4 LGM (GLAC-1D)	PMIP4 LGM GLAC-1D	Matching NROYa simulation xpken/xpkyn (See Sect. 2.3.4 and 2.4.1)
4) V_{c_1}	**PGM**	PMIP4 LGM (GLAC-1D)	PMIP4 LGM GLAC-1D	
5) V_{i_1}	LGM	**PGM NROYa (xpkyn)**	**PGM NROYa (xpkyn)**	
6) V_{ci_1} (full PGM)	**PGM**	**PGM NROYa (xpkyn)**	**PGM NROYa (xpkyn)**	
7) $V_{\_2}$ (NROYa LGM)	LGM	PMIP4 LGM (GLAC-1D)	18.2 ka ice sheet	
8) V_{c_2}	**PGM**	PMIP4 LGM (GLAC-1D)	18.2 ka ice sheet	
9) V_{i_2}	LGM	**PMIP4 PGM**	18.2 ka ice sheet	
10) V_{ci_2} (NROYa PGM)	**PGM**	**PMIP4 PGM**	18.2 ka ice sheet	

2.3.3 Ensemble design

The ensemble by Gandy et al. (2023) showed that uncertainty in parameters controlling SMB, ice sheet dynamics and climatic conditions over the ice sheets had a significant influence on the extent and volume of the LGM NAIS, with albedo parameters explaining the majority of the variation in model output. Since these parameters needed re-tuning from simulations of the present day Greenland ice sheet to produce an acceptable LGM NAIS configuration in FAMOUS-ice under LGM climate conditions, the PGM may also show different sensitivities

to the uncertain parameters. Therefore, we ran new ensembles of the LGM and PGM in order to explore uncertainties and identify combinations of climate and ice sheet parameters that perform well for both periods.

Following on from Gandy et al. (2023), a second wave of simulations was performed and compared to reconstructions of ice sheet extent and volume to identify "Not Ruled Out Yet" (NROY) parameter combinations (see methodology in Sect. 2.7.4), the results of which formed the basis of the ensemble design in this study. We re-ran the LGM ensemble to allow for slight changes in the experiment design compared to Gandy et al. (2023): we use orbital parameters for 21 ka rather than 23 ka and HadCM3 SSTs instead of a statistical reconstruction (see Sect. 2.3.2.1). Table 2.3 details the 13 parameters that were varied in these simulations. Out of the 176 NROY parameter combinations from the Wave 2, a representative subset of 62 were selected which provided adequate coverage of the NROY space (see Sect. 2.7.4 for details). Each was run for 1000 climate years (10,000 ice sheet years) for both the LGM and PGM experiments until the majority of the ice sheet reached close to equilibrium. Despite differences in the model set-up between this study and Gandy et al. (2023), we expect the 62 samples chosen from their design to be a good estimate to an optimal parameter design for our experiment design (Sect. 2.7.4).

Table 2.3: Description of parameters varied in the ensembles. Adapted from Gandy et al. (2023).

Parameter	Range	Description
lapse rate (tgrad)	-0.01 – -0.002 K m^{-1}	Prescribed lapse rate for air temperature used to downscale FAMOUS near-surface ice sheet climate onto surface elevation tiles. Down welling longwave radiation is also adjusted for consistency. More negative values lead to stronger lapse rate effects (Smith et al., 2021b).
daice	-0.4 – 0 K^{-1}	Sensitivity of bare-ice albedo to surface air temperatures once the surface is in a melt regime. Albedo reduced to as low as 0.15 with minimum value (Smith et al., 2021b).
fsnow	350 – 800 kg m^{-3}	The threshold in surface snow density at which the FAMOUS albedo scheme switches from a scattering paradigm appropriate for a conglomeration of snow grains to one more appropriate for a solid surface. Higher values correspond to using brighter albedos for denser snow, increasing ice sheet albedo (Smith et al., 2021b).

av_gr	0 – 0.01 μ m^{-1}	Sensitivity of the snow albedo to variation in surface grain size. Higher values enhance the darkening of snow over time, decreasing the albedo (Smith et al., 2021b).
rhcrit	0.6 – 0.9 Pa^{-1}	The threshold of relative humidity for cloud formation (Smith, 1990). A higher value means clouds can form less easily.
vf1	1 – 2 m s^{-1}	The precipitating ice fall-out speed (Heymsfield, 1977).
ct	$5x10^{-5}$ – $4x10^{-4}$ s^{-1}	The conversion rate of cloud liquid water droplets to precipitation (Smith, 1990).
cw	$1x10^{-4}$ – $2x10^{-3}$ kg m^{-3}	The threshold values of cloud liquid water for formation of precipitation (Smith, 1990). Only the value for the land is varied.
entrainment coeff	1.5 – 6	Rate of mixing between environmental air and convective plume. Higher values enhance mixing of convective plumes with ambient dry air.
alpham	0.2 – 0.65	The sea ice lowest albedo (Crossley & Roberts, 1995).
basal sliding	0.5 – 20 mm yr^{-1}	The basal sliding rate. A higher value allows increased ice velocity.
mantle relaxation time	300 – 9000 yrs	The relaxation time of the mantle, a lower value making the mantle less viscous, thus allowing a quicker topographic rebound.
flow enhancement factor (flow factor)	1 – 10	Glen's Flow Law enhancement factor. Increasing the factor makes the ice softer and more deformable (Rutt et al., 2009).

2.3.4 Implausibility criteria

To filter out implausible ice sheet configurations in the results, a set of constraints, based on southern ice sheet extent and volume, were applied to the LGM ensemble. Both ensembles were filtered based on the LGM results since the extent of the NAIS is very well constrained by geological data and there are more estimates of ice volume for the LGM than the PGM. This is because there is a lack of empirical data (over both space and time) on ice sheet configuration at the PGM due to destruction of evidence by subsequent glaciations and difficulties with dating what is available (Parker et al., 2022). Thus, most of the reconstructions of NAIS PGM extent are actually the maximum extent reached over the whole of MIS 6 (190-130 ka) and are mostly based on numerical modelling combined with this scarce proxy data (e.g. Batchelor et

al., 2019; Colleoni et al., 2016). This leaves a set of plausible or "Not Ruled Out Yet" (NROY) LGM simulations that can then be compared to the corresponding PGM simulations to determine whether parameters that performed well for the LGM also give plausible PGM results. LGM ice extent was assessed against the reconstruction by Dalton et al. (2020). We focus our evaluation of ice extent on the southern NAIS area and chose to disregard regions of known model bias. This includes marine margins that are subject to processes not included in Glimmer and the Alaskan regions where small climate model biases lead to ice sheet overgrowth (e.g. Ganopolski et al., 2010; Gregoire et al., 2016; Sherriff-Tadano et al., 2024; Ziemen et al., 2014). Additionally, ice lobes are not well captured in many models as they are likely to be transient, short-lived features that may be caused by complex ice dynamics (e.g. Zweck and Huybrechts, 2005). Therefore, we do not expect our simulations to perfectly match the reconstructed Southern NAIS extent. To account for the expected mismatch between model and data, we applied a tolerance on the Southern ice sheet area of 1.79×10^6 km^2, equivalent to three-times the area of the lobes (Figure 2.4). We thus calculate the Southern NAIS ice area as the integrated area within the large box shown in Figure 2.4 at the end of each LGM simulation and selected simulations that matched the reconstructed area from Dalton et al. (2020) within plus or minus 1.79×10^6 km^2. The volume of the NAIS is not as well constrained by proxy data and so estimates rely on ice sheet, glacial isostatic adjustment and sea level modelling studies. Based on a number of these studies (Batchelor et al., 2019; Gowan et al., 2021; Lambeck et al., 2014; Marshall et al., 2002; Peltier et al., 2015; Rohling et al., 2017; Tarasov et al., 2012; Tarasov and Peltier, 2002, 2004), a minimum NAIS (including Greenland) volume of 70 m s.l.e. (2.8×10^7 km^3) was applied to the ensemble. The translation of ice volumes into meters of sea level equivalent are calculated based on present day ocean area.

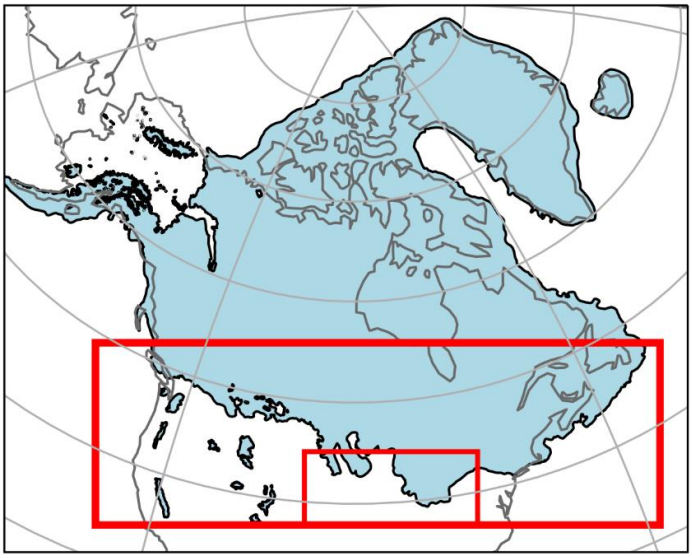

Figure 2.4: Outline of the LGM North American ice sheet by Dalton et al. (2020). The large red box shows the region used to calculate reconstructed and modelled Southern NAIS area. The small red box shows the region used to calculate the area of the lobes from which we set the upper and lower target bounds for southern ice extent (See Sect. 2.3.4).

2.3.5 Sensitivity analysis

We choose one of the resulting NROY parameter combinations, NROYa (specifically experiments xpken/xpkyn), which has LGM and PGM ice volumes lying in the middle of estimated ranges and the least excess ice growth over Alaska, to investigate the relative impact of the initial conditions versus the climate on the resulting ice sheet configurations. This is achieved through a sensitivity analysis along with factorisation based on the method used by Gregoire et al. (2015) and Lunt et al. (2012). We divided the differences in inputs between LGM and PGM into two factors; the initial ice sheet configurations used in FAMOUS and Glimmer and the climate boundary conditions (orbital parameters, greenhouse gases and SSTs/sea ice). Thus, the total difference in final ice volume (ΔV) between the LGM and the PGM can be written as Eq. (2.1):

$$\Delta V = dV_{ice} + dV_{climate} \,, \tag{2.1}$$

where dV_{ice} is the difference in final ice volume due to the different initial ice sheet configurations and $dV_{climate}$ is the difference due to the difference climate boundary conditions used.

The factorisation method requires 2^N simulations (where N is the number of different components) to determine the contribution of each component to ice volume difference, therefore $2^2 = 4$ experiments are needed that systematically change one variable. These

experiments are listed in Table 2.2. The relative contributions of the initial conditions and climate can be calculated by Eqs. (2.2) and (2.3):

$$dV_{ice} = \frac{1}{2}\big((V_i - V) + (V_{ci} - V_c)\big), \quad (2.2)$$

$$dV_{climate} = \frac{1}{2}\big((V_c - V) + (V_{ci} - V_i)\big), \quad (2.3)$$

To properly understand the effect of the initial conditions, we performed two sets of sensitivity experiments. In the first set, labelled $V_{\_1}$, V_{c_1}, V_{i_1} and V_{ci_1} (Table 2.2; experiments 3–6), both the topography and ice cover are set to be consistent between the climate and ice sheet model components. Specifically, for the LGM, the Glimmer initial bedrock topography and ice surface elevation was prescribed from the GLAC-1D reconstruction used in the FAMOUS LGM boundary condition. For the PGM, the ice thickness data needed for the PMIP4 reconstruction to be converted to the Glimmer initial condition were not available. Instead, both Glimmer and FAMOUS were initialised with the final timestep of the NROYa PGM (xpkyn) experiment since it closely resembles the PMIP4 reconstruction. Experiment $V_{\_1}$ corresponds to a full LGM simulation and V_{ci_1} corresponds to a full PGM simulation. In the second set of sensitivity experiments, we use the initial Glimmer ice sheet used in the ensembles, i.e. the 18.2 ka mid-size ice sheet, only varying the FAMOUS initial ice sheets to see how this difference in orography between the climate and ice sheet models may have impacted the result. These experiments are labelled $V_{\_2}$, V_{c_2}, V_{i_2} and V_{ci_2} (Table 2.2; experiments 7–10), with $V_{\_2}$ corresponding to the LGM NROYa (xpken) and V_{ci_2} corresponding to the PGM NROYa (xpkyn).

2.4 Results

2.4.1 Ensembles

Our ensembles of 62 North American ice sheet configurations spans uncertainty in model parameters and reveals the wide range of possible modelled ice sheet evolutions. Over the full ensembles, we find that the set-up of the original Wave 2 meant that the albedo values were too high and so the use of more realistic albedos in these ensembles led to many of the runs deglaciating to very low volumes as shown in Figure 2.5 (see Sect. 2.7.4 for more detail).

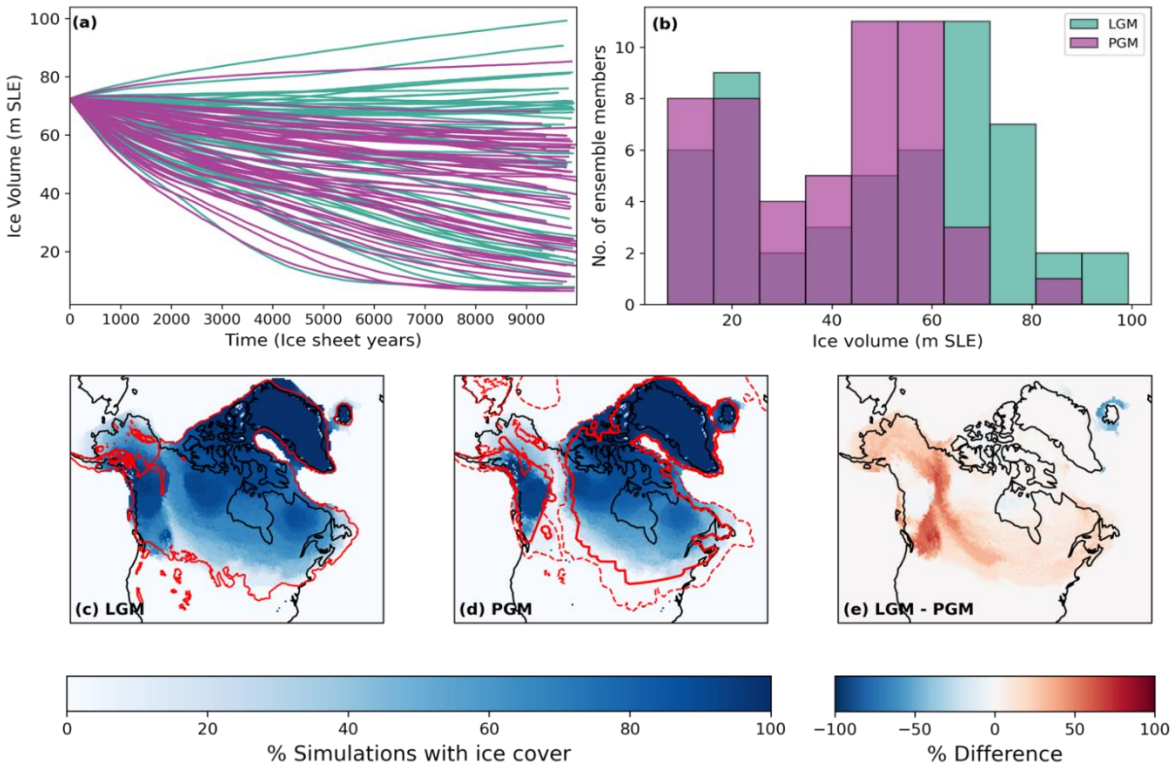

Figure 2.5: (a) Ice volume evolution over modelled time, and (b) density distribution of final ice volumes for the full LGM and PGM ensembles. Percentage of simulations with ice cover for (c) LGM (with the Dalton et al. (2020) reconstructed margin shown in red); (d) PGM (with the PMIP4 PGM modelled margin shown in solid red and the Batchelor et al. (2019) reconstructed maximum MIS 6 margin shown in dashed red), and (e) the difference between the LGM and PGM, at the end of the simulations.

Table 2.4: Average volumes (NAIS + Greenland) and southern NAIS areas and their standard deviations (SD) of the NROY LGM and PGM simulations. Also shown are estimated values from literature for comparison.

	Mean Total Volume (SD), m s.l.e.	Estimated Total Volume, m s.l.e.	Mean Southern Area (SD), x 10^6 km^2	Estimated Southern Area, x 10^6 km^2
LGM	82.1 (8.29)	61-98 (Rohling et al., 2017)	5.55 (0.33)	6.28 (Dalton et al., 2020)
PGM	62.3 (10.3)	49-69 (Rohling et al., 2017)	3.64 (0.82)	3.32 (Menviel et al., 2019)

After applying our implausibility criteria (Sect. 2.3.4), six non-implausible or NROY LGM simulations remained. Table 2.4 gives the average volumes and areas of these six simulations and the corresponding six PGM ice sheets compared to estimated values from empirical and model data. All six LGM simulations show an overgrowth of ice in Alaska of varying

magnitudes, as a result of the previously mentioned climate model bias. However, in other regions the simulations display a very similar ice extent, with the southern area only varying by 9.7 x 10^5 km^2. None of the simulations form ice lobes, as expected, but they do show a close match to reconstructed ice extent in our target area, although towards the lower end of the plausible range, and in the marine regions (Figure 2.6a and Figure 2.7a). There is a minimum ice volume of 73.9 m s.l.e. and a maximum of 97.1 m s.l.e.. The maximum ice thickness varies by around 300 m but the overall shapes of the ice sheets remain the same, with the thickest ice towards the east of the ice sheet over Hudson Bay.

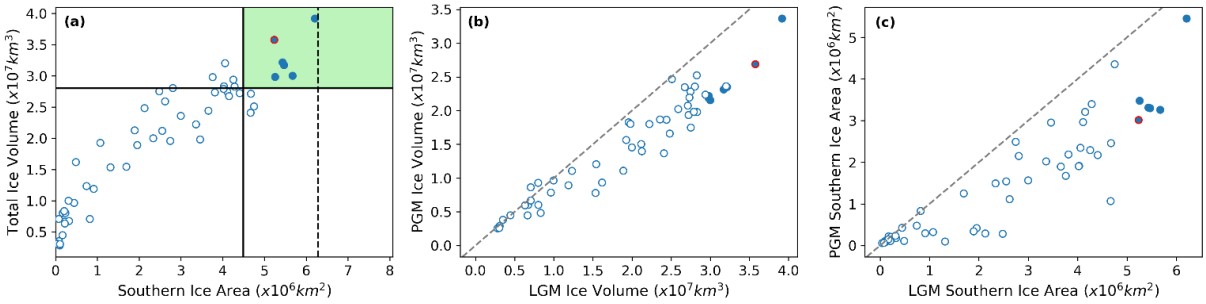

Figure 2.6: (a) The relationship between final ice volume and southern area for the LGM ensemble, and the relationship between the LGM and PGM (b) final ice volume, and (c) final southern areas. The filled in blue dots represent the six NROY LGM simulations and the solid lines on panel (a) show the minimum volume and area constraints applied to the ensemble. The ensemble member chosen as NROYa is outlined in red (Sect 2.3.5).

All the PGM ice sheets were smaller in volume than their LGM counterpart (Figure 2.6 and Figure 2.7) and displayed a smaller extent in the southern margin and the saddle region between the western Cordilleran ice sheet and eastern Laurentide ice sheet. However, the PGM simulations also displayed more variability in their ice extent and volumes. The ice volumes range from 53.4 m s.l.e. to 83.37 m s.l.e. and the southern extent varies by 2.44 x 10^6 km^2. The range in maximum ice thickness is also over double the LGM, varying by around 613 m. These PGM configurations also look plausible compared to the less well constrained extent data available, including previous empirical and modelled reconstructions of the PGM/MIS 6 extent (Batchelor et al., 2019; Menviel et al., 2019; Figure 2.7b). For example, all the simulations maintain an ice-free corridor between the Laurentide and Cordilleran ice sheets which is a common feature in these PGM reconstructions. In addition, the excess Alaskan ice seen in LGM simulations is also present at the PGM, however the growth is not as excessive.

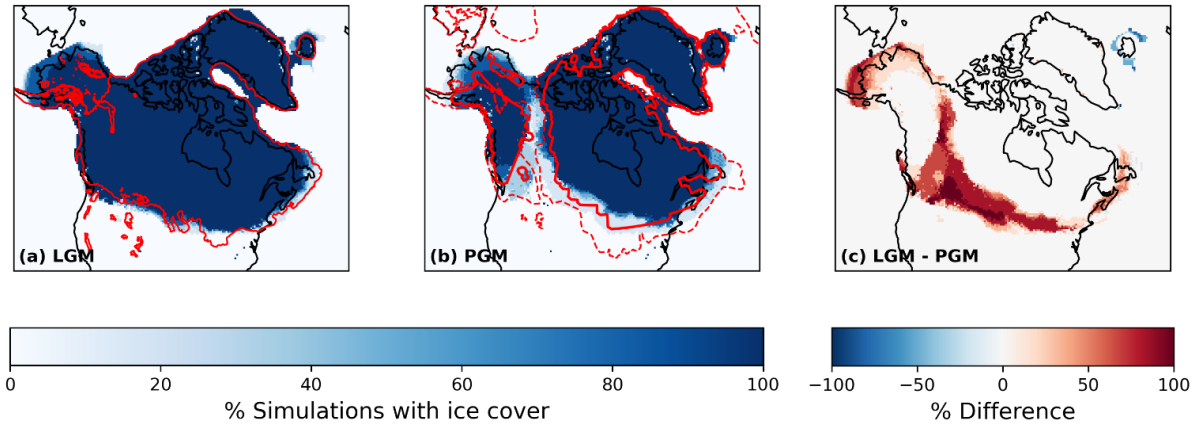

Figure 2.7: Percentage of simulations with ice cover for (a) LGM with the Dalton et al. (2020) reconstructed margin shown in red; (b) PGM with the PMIP PGM modelled margin shown in solid red and the Batchelor et al., (2019) reconstructed maximum MIS 6 margin shown in dashed red, and (c) the difference between the LGM and PGM, at the end of the simulations for the six NROY ensemble members.

2.4.2 Impact of initial ice sheet versus climate

Out of our six NROY model configurations, we selected the parameters of a pair of LGM and PGM experiments xpken/xpkyn (NROYa; Figure 2.6) to perform two sets of four sensitivity experiments to decompose the effects of climate forcing and initial conditions on the final ice sheet volume. This included repeating xpken and xpkyn using matching FAMOUS and Glimmer LGM and PGM initial conditions respectively (Table 2.2, experiments 3 and 6). For both glacial maxima, using the matching initial conditions resulted in more excess ice over Alaska (Figure 2.14), though the southern ice extents are relatively similar between the two sets of experiments. Overall, for the LGM, using the GLAC-1D reconstruction in Glimmer ($V_{\_1}$) resulted in an ice sheet 9.7 m s.l.e. larger than if the 18.2 ka ice sheet was used ($V_{\_2}$) (Table 2.5; Figure 2.14a). For the PGM, the matching initial conditions (V_{ci_1}) resulted in only 0.45 m s.l.e. increase from the NROYa simulation (V_{ci_2}) due to a decrease in ice volume over the Laurentide ice sheet (Table 2.5; Figure 2.14b).

Table 2.5: Final ice volumes of the four sensitivity experiments performed with matching climate model and ice sheet model ice sheets and the equivalent four performed with different initial ice sheets in each model.

Experiment	Final ice volume (m s.l.e.)	Experiment	Final ice volume (m s.l.e.)
$V_{\_1}$ (full LGM)	100.3	$\mathbf{V_{\_2}}$	90.6
V_{c_1} (LGM ice , PGM climate)	104.2	$\mathbf{V_{c\_2}}$	97.1
V_{i_1} (PGM ice, LGM climate)	64.7	$\mathbf{V_{i\_2}}$	63.0
V_{ci_1} (full PGM)	68.6	$\mathbf{V_{ci\_2}}$	68.1

The final ice sheet volumes from the first set of four sensitivity experiments (Table 2.2; experiments 3–6) are displayed in Table 2.5 and shown in Figure 2.8. The results of the second set of four experiments (Table 2.2; experiments 7–10) are also included in Table 2.5. The results of the factor decomposition analysis show that the simulated ice volume at the PGM was 31.7 m s.l.e. (1.25 x 10^7 km^3) lower than at the LGM ($dV_{\_1}$). The initial ice sheet configuration (dV_{i_1}) alone caused a 35% decrease in volume, but this was partially offset by the climatic conditions (dV_{c_1}), which resulted in an increase in volume of 4%. The result was similar for the second set of experiments, with the initial ice sheet configuration (dV_{i_2}) causing a decrease of 31% in ice volume at the PGM compared to the LGM, but the climate (dV_{c_2}) caused a 6% increase in volume.

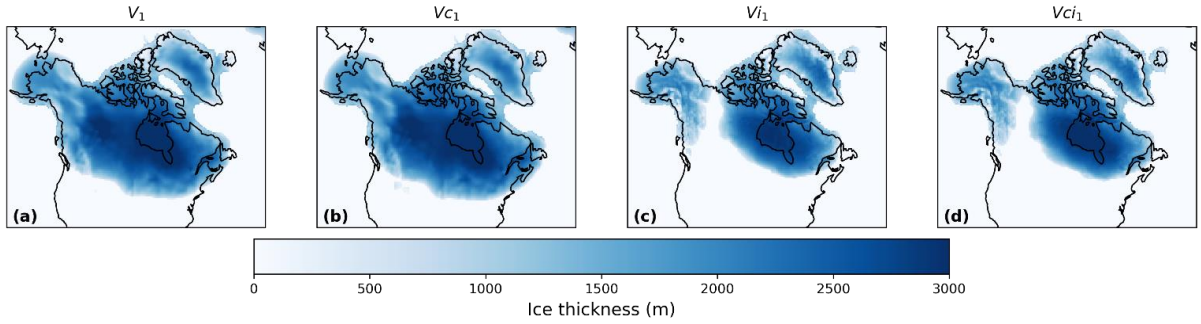

Figure 2.8: Final ice thickness in the sensitivity tests using (a) LGM ice sheets and LGM climate; (b) LGM ice sheets and PGM climate; (c) PGM ice sheets and LGM climate, and (d) PGM ice sheets and PGM climate.

The PGM climate is conducive to growing a larger ice sheet (Figure 2.9a) because the orbital configuration results in the Northern Hemisphere receiving less incoming solar radiation in spring and early summer (Table 2.1; Figure 2.2a). This reduces the melting of snow that has accumulated in winter (Figure 2.9b). The winter snow accumulation is also higher at the PGM

than at the LGM (Figure 2.9c) due to the PGM having warmer air temperatures in autumn and winter, because of the orbital forcing, leading to a wetter climate. Summer SSTs are also cooler at the PGM (Figure 2.2c) due to lower spring insolation, further contributing to reduced runoff. In contrast, the Greenland ice sheet decreases in size due to PGM climate conditions (Figure 2.9a), likely due to higher sea ice concentration south of Greenland reducing the moisture source available for precipitation.

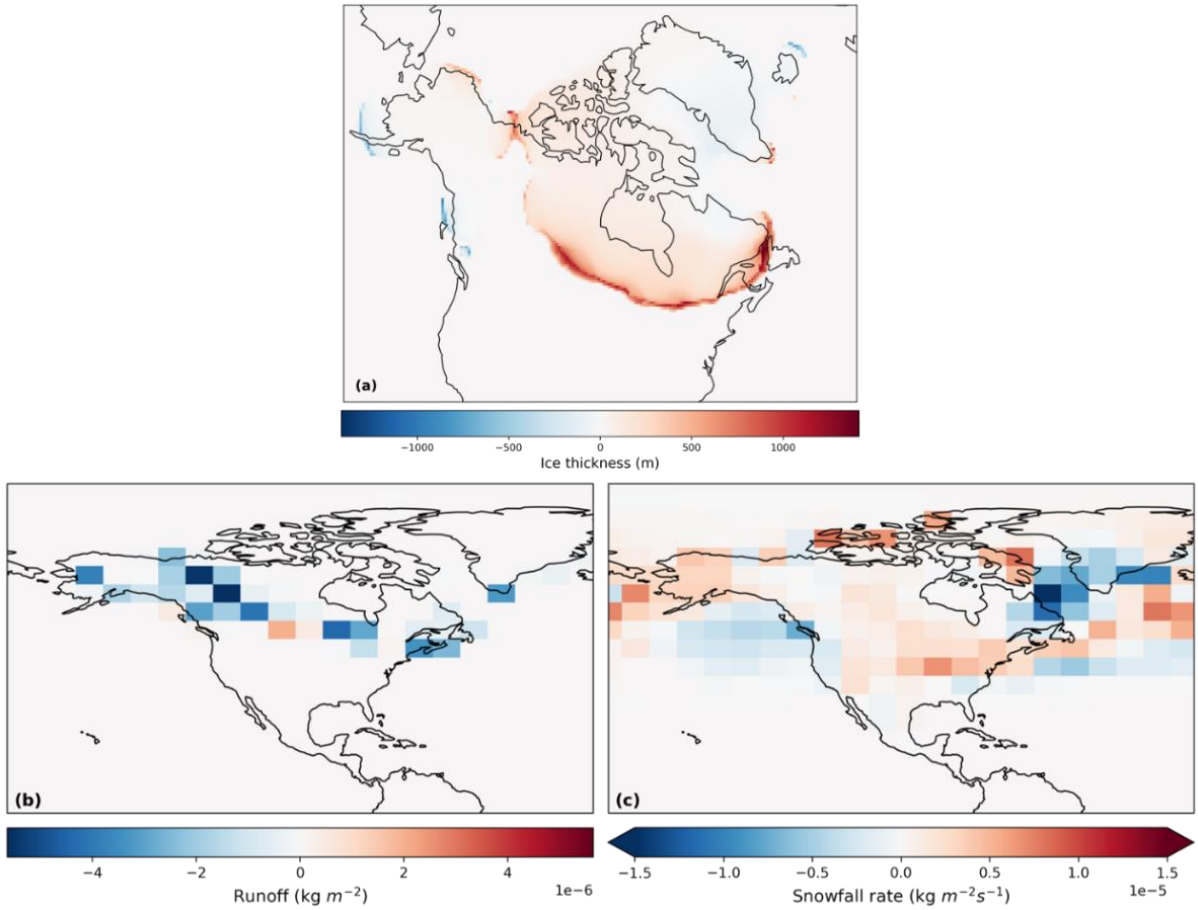

Figure 2.9: Difference between experiment Vci_1 (full PGM) and Vi_1 (PGM ice sheet with LGM climate) isolating the effect of LGM climate vs PGM climate on (a) final ice thickness simulated by Glimmer and (b) spring (MAM) runoff and (c) winter (DJF) snowfall over the first 10 years.

2.4.3 Uncertainty due to model parameters

Due to the sampling strategy, this ensemble does not have an optimal design for analysing the sensitivity of the ice sheets during the two time periods to the different model parameter values because our ensemble of simulations does not uniformly span the uncertain parameter space. For this, we refer the reader to the studies of Gandy et al. (2023) and Sherriff-Tadano et al., (2024) and Chapter 3 of this thesis, which present larger ensembles of experiments. Here, we first evaluate if our results are consistent with these two studies before examining if the difference between the PGM and LGM ice sheets is sensitive to specific model parameters.

Based on correlations between the parameters and ice sheet area and volume, we find that the LGM and PGM behave similarly across the parameter ranges (Figure 2.16 and Figure 2.17) and most of the uncertainty in the results for both periods can be explained by parameters that affect the surface albedo of the ice sheet; *daice, av_gr* and to a lesser extent, *fsnow.* Higher values of *daice* and f*snow* and lower values of *av_gr* cause higher albedos and lead to larger ice sheets (Table 2.3). *Basal sliding* also influences the volume of the ice sheet, with less impact on the area, with lower values and thus lower ice velocities causing larger volume ice sheets. The cloud parameter *cw* also shows a relatively high positive correlation for the PGM (Figure 2.10). This is consistent with the findings of previous studies and current understanding on the importance of albedo for ice sheet evolution (Gandy et al., 2023; Sherriff-Tadano et al., 2024; Willeit and Ganopolski, 2018).

Additionally, there is a negative correlation between the difference in ice volume and area between the LGM and PGM and the parameters *av_gr, basal sliding,* and *rhcrit.* Conversely, there is a positive correlation between the LGM-to-PGM difference in ice volume/area and *daice* (Figure 2.18). This suggests that lower values of *av_gr* and higher values of d*aice* and thus a higher albedo, as well as lower ice sheet velocity and more cloud, make the ice sheet more sensitive to changes in radiative forcings from the orbital boundary conditions.

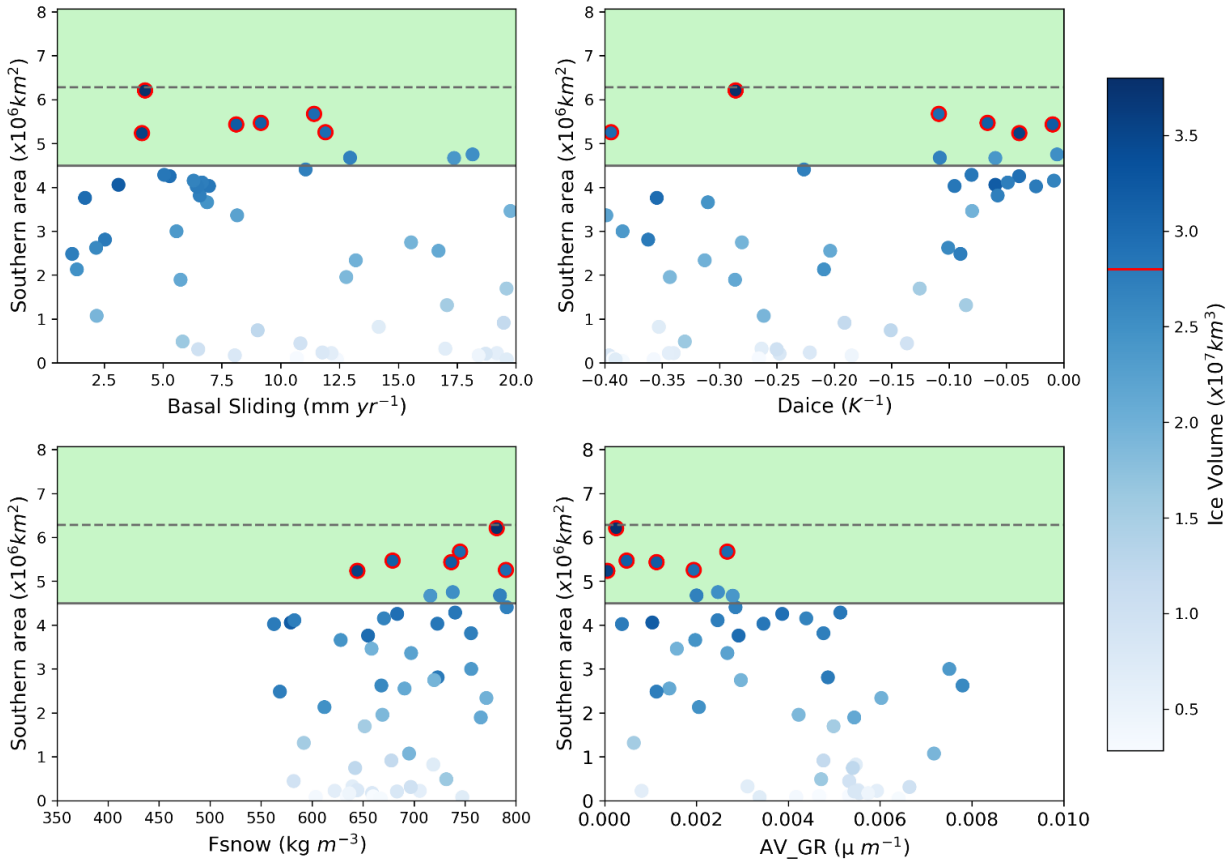

Figure 2.10: Relationship between LGM southern area and the four most influential parameters. The green shaded region shows the southern area constraint applied with the dotted line showing the exact area of the reconstruction and the solid line the minimum bound applied. The colour scale represents ice volume and the dots outlined in red are the six NROY LGM simulations with the red line on the colour bar showing the volume constraint.

2.5 Discussion

After constraining our ensembles based on the available empirical and model data for the LGM, we find that the model was able to successfully simulate the ice sheet at both periods under different LGM and PGM climate boundary conditions (orbital parameters, SSTs and global orography) and initial ice sheets. However, the southern extents of the constrained LGM simulations all fall towards the lower end of the plausible range, which is a common feature seen in other simulations using a low resolution atmosphere model due to biases that cause a reduced stationary wave effect over this region (Gandy et al., 2023; Sherriff-Tadano et al., 2024; Ziemen et al., 2014). Additionally, the ice lobes that are present over the Great Lakes of North America are not captured in these simulations. Again, this is common in ice sheet models and is likely a result of missing subglacial processes or the low resolution of the climate and ice sheets models.

Analysis of the behaviour of the modelled ice sheets across the parameter spaces reveals that both the LGM and PGM ice volume and extent have similar sensitivities to parameter uncertainties. We therefore conclude that parameters that produce a good LGM NAIS also produce a plausible PGM NAIS under PGM boundary conditions and thus similar model parameters are appropriate for use when modelling both periods. Our simulations can thus be compared and analysed to understand the causes of the different configurations between the two periods. However, since the ice volume is most sensitive to surface albedo and most simulations deglaciate under low values of *daice*, this suggests that the value of bare ice albedo in the model may need to be increased for future work.

The results of the sensitivity analysis show that the difference in initial ice sheet boundary conditions overwhelmingly determined the difference in final ice volume between the LGM and PGM in the ensemble of simulations. We tested the impact of starting from LGM and PGM ice sheet configurations in Glimmer instead of the 18.2 ka ice sheet and found that this caused an even larger difference in ice volume between the two glacials. Comparing the simulations that use the same initial ice topography in FAMOUS and Glimmer (first set of experiments), to those that use different topographies (second set of experiments), whilst keeping the ice cover consistent, reveals that the relative contribution from the initial ice sheet boundary conditions, compared to the climate conditions, to the simulated differences between the LGM and PGM ice sheets, remains similar. This suggests that the dominant feedback responsible for this result is the ice-albedo feedback rather than the temperature-elevation feedback. A similar conclusion was obtained by Abe-Ouchi et al. (2007) who studied the relative contribution to climate over ice sheets from the ice sheet itself and the orbital parameters and CO_2 concentration. They found the cooling caused by the ice sheet themselves was the dominant effect, mostly due to albedo feedbacks, which increase with ice sheet area. Kageyama et al. (2004) also highlighted in their study the importance of the albedo feedback on the maximum modelled North American ice volume. They show that changes in vegetation are needed to initiate glaciation over North America which is then accelerated by the ice-albedo feedback. The North American ice sheet was larger at the LGM than at the PGM. However, this sensitivity analysis reveals that the difference in orbital parameters, GHGs and SSTs (climate) between the LGM and PGM encourages the growth of a larger North American ice sheet at the PGM (Figure 2.9a). This effect would likely be even stronger if we had used the orbit at 137 ka (the timing of the minimum in Northern Hemisphere summer insolation; Figure 2.11a-c) since the PGM would have received even lower insolation in spring and early summer.

This result highlights the importance of the evolution of these climate factors and the ice sheets during the preceding glacial cycles in determining the glacial maxima configurations. For example, during the start of the Last Glacial Cycle (MIS 5; ~115-80 ka), the variation in 65º N summer insolation was relatively large as a result of changes in orbital parameters (Figure 2.11a-c), which resulted in multiple cycles of growth and recession of the North American ice sheets during this period, but total ice volume remained low (Bonelli et al., 2009; Dalton et al., 2022; Ganopolski et al., 2010). Insolation then reaches a minimum at ~70 ka (Figure 2.11c) which, combined with decreasing concentrations of CO_2 (~190 ppm at ~65 ka; Figure 2.11f), led to a significant increase in ice sheet volume to almost LGM extent (Fig. 2.11d) and a switch to more widespread glacial conditions at the MIS 5/MIS 4 transition (Bonelli et al., 2009; Dalton et al., 2022). The size of the NAIS at this time was large enough to induce positive feedbacks, such as the ice-albedo feedback, allowing its maintenance throughout MIS 4 and MIS 3 (~70-30 ka) despite an increase in insolation from ~50-30 ka (Figure 2.11c). This was also supported by a continued decrease in CO_2 (Figure 2.11f). Growth of the ice sheet could then continue to its glacial maximum extent following a further insolation and CO_2 decrease during MIS 2 (~30-21 ka) (Figure 2.11c-f). In contrast, prior to the PGM there were peaks in insolation at ~172 and ~148 ka that reached higher levels than were reached prior to the LGM during MIS 4 and MIS 3 (Figure 2.11c; Berger, 1978). This may have inhibited an initial significant build-up of ice over North America, as during MIS 4, preventing the initiation of an ice-albedo feedback strong enough to enable the continued growth towards a larger LGM configuration and/or maintain its volume through the second insolation peak. In addition, there was more time between the LGM and the insolation maximum at ~50-30 ka compared to the PGM and the maximum at ~147 ka. Therefore, the PGM NAIS may have not had enough time to regrow before insolation started to increase again. Thus, investigation of the processes and interactions that took place prior to the glacial maxima will be needed to fully understand why the LGM and PGM NAIS configuration differed.

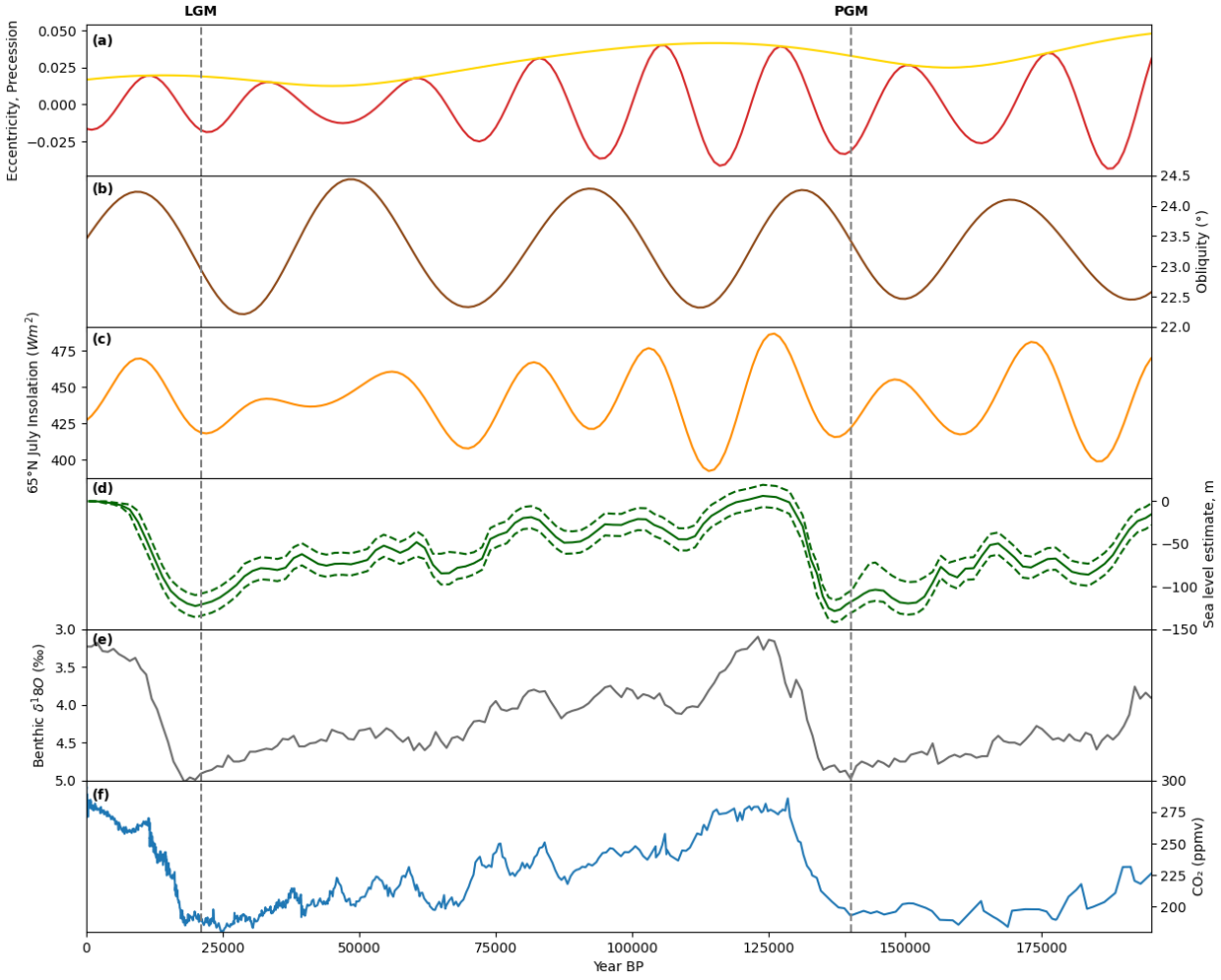

Figure 2.11: Evolution of climate proxies over the last two glacial-interglacial cycles: (a) precession index (red) with eccentricity as an envelope (yellow); (b) obliquity (Berger, 1978); (c) July insolation at 65° N (Berger and Loutre, 1991); (d) reconstruction of global mean sea level and uncertainty estimate (dotted lines) (Waelbroeck et al., 2002); (e) benthic δ18O global stack record (Lisiecki and Raymo, 2005), and (f) EPICA Dome C carbon dioxide ice core records (Bereiter et al., 2015; Lüthi et al., 2008). The PGM and LGM are indicated by the dotted line.

Additional feedbacks that played a role in the development of glacials into either an LGM-like or PGM-like mode are also missing in these simulations due to computational constraints. For example, the low resolution of the atmospheric component of FAMOUS means that it is capable of performing ensembles and long palaeo runs while directly coupled to an ice sheet model. However, it also means that many small-scale atmospheric processes (e.g. stationary wave response) caused by and affecting the ice sheet topography are not represented well (Beghin et al., 2014, 2015; Kageyama and Valdes, 2000; Liakka et al., 2012, 2016; Liakka and Nilsson, 2010). Additionally, the shallow ice approximation used in Glimmer means that the ice sheet will not be able to simulate marine instabilities of advance and retreat (Pattyn et al., 2012). This effect will be minimal for the NAIS, but a more advanced ice sheet model would be required to simulate a marine ice sheet like the EIS.

As a reminder, the vegetation was kept fixed at pre-industrial distributions, but the vegetation prior to and next to the ice cover has been shown to be very important for determining ice sheet expansion in models through the vegetation-albedo feedback (Colleoni et al., 2009b; Horton et al., 2010; Kageyama et al., 2004; Stone and Lunt, 2013). Therefore, implementing glacial maxima distributions or dynamical vegetation may affect the results since the reduction in forest and expansion of tundra/shrubs compared to present day would increase the albedo of the surface next to the ice and affect the climate (Meissner et al., 2003). Similarly, the prescribed SSTs and sea ice concentrations used introduce an additional source of uncertainty. As well as impacting the global mean temperature and precipitation patterns in the simulations, the SSTs and sea ice used can have local climate impacts that affect the simulated ice sheets. This includes causing a warming or cooling over the more coastal areas affecting the melt rate, and impacting evaporation rates, which affects the amount of snowfall the ice sheets receive. The SSTs used in this study are cooler (as a global average) than the multi-proxy and data assimilation LGM SST reconstructions of Tierney et al. (2020b) and Paul et al. (2020) and the constrained statistical reconstruction of Gandy et al. (2023) and Astfalck et al. (2024). HadCM3 also tends to simulate cooler SSTs compared to other PMIP4 models, although they are similar to CESM1.2 (Kageyama et al., 2021). Therefore, the use of colder SSTs in this study causes lower global mean temperature overall, but also would have caused a cooling next to the ice sheets and reduced snowfall, which would have impacted the ice sheet growth in different ways (Astfalck et al., 2024; Hofer et al., 2012; Marsiat and Valdes, 2001). The latter impact was shown to be most dominant in the study by Astfalck et al. (2024), suggesting that our simulated ice sheet volumes may have been larger had we used their warmer LGM SST reconstruction, due to increased evaporation. Prescribing the ocean forcing also neglects any effects changes in ocean conditions and ice sheets have on each other (e.g. Colleoni et al., 2011; Sherriff-Tadano et al., 2018, 2021; Timmermann et al., 2010; Ullman et al., 2014). Using a dynamical ocean would include the effects of meltwater and changes in atmospheric circulation, arising from the ice sheets, on ocean circulation and temperature, which would in turn affect the climate, feeding back onto the ice sheets themselves. Further work will be required to investigate the feedbacks between ice sheets and sea surface at the PGM, but this is beyond the scope of this study. We recommend the use of a fully coupled atmosphere-ocean-vegetation-ice sheet model to further investigate these feedbacks. The effect of dust deposition and ice dammed lakes have also been shown to have a large influence on the build-up of ice (e.g. Colleoni et al., 2009a; Krinner et al., 2004, 2006; Naafs et al., 2012) however further model developments would be needed to investigate these effects.

Finally, the Eurasian ice sheet also displayed important differences between the LGM and PGM and had a large influence on the climate. It is likely that some of the differences in the configurations of the NAIS and EIS between the two glacial maxima resulted from their interactions with each other (Beghin et al., 2014, 2015; Liakka et al., 2016). To investigate the EIS at the PGM, we recommend the use of an efficient marine ice sheet model such as BISICLES that uses adaptive mesh refinement (AMR) to refine the processes occurring at marine margins that are more important for the marine based Eurasian ice sheet (Cornford et al., 2013; Gandy et al., 2019).

2.6 Conclusions

We have performed and compared ensemble simulations of the LGM and PGM using a coupled atmosphere-ice sheet model (FAMOUS-ice) with prescribed surface ocean conditions and interactive North American and Greenland ice sheets. We tested the relative importance of the initial ice sheet configuration versus the climate boundary conditions on the resulting ice sheet volumes through sensitivity tests and factor decomposition analysis. The main conclusions of this study are as follows:

1. Successful simulations of the LGM and PGM North American and Greenland ice sheets are produced using a coupled climate-ice sheet model. We find that uncertain model parameters tuned to produce a plausible LGM North American ice sheet also perform well for the PGM.

2. The initial ice extents used as boundary conditions in coupled climate-ice sheet simulations have a much larger impact on the modelled NAIS than the climate boundary conditions, causing a ~30% decrease in ice volume at the PGM compared to the LGM. This is due to the ice-albedo feedback.

3. The climate of the PGM causes an increase in NAIS ice volume of ~6% compared to the LGM due to the orbital configuration causing the Northern Hemisphere to receive less insolation in spring and early summer. Since the LGM ice sheet was larger than the PGM, this suggests that the climate and ice sheet evolution prior to the glacial maxima contributes to the differences seen between the LGM and PGM ice sheets.

2.7 Appendices

2.7.1 Eccentricity equation correction

The equation for the role of eccentricity on solar insolation used in the simulations in this paper was:

$$S(t) = S_o((1 + \frac{e^2}{2})(1 + e\cos v)/(1 - e^2))^2 \quad (2.4)$$

However, this is incorrect and has now been corrected in the model to:

$$S(t) = S_o((1 + e\cos v)/(1 - e^2))^2 \quad (2.5)$$

where; S(t) is the incoming solar insolation, S_o is the solar constant, e is the eccentricity of the Earth's orbit and *v* is the true anomaly (the angle of Earth's current position on its orbit).

The PGM experiment "xpky0" was re-run with the correct equation and shows that on average the SMB was slightly lower in our simulations than it should have been (decreased by 16% at the end of the simulations), leading to slightly smaller ice sheets (Figure 2.12). However, the impact is small (and would be even smaller for the LGM given the lower eccentricity) and does not affect our overall conclusions.

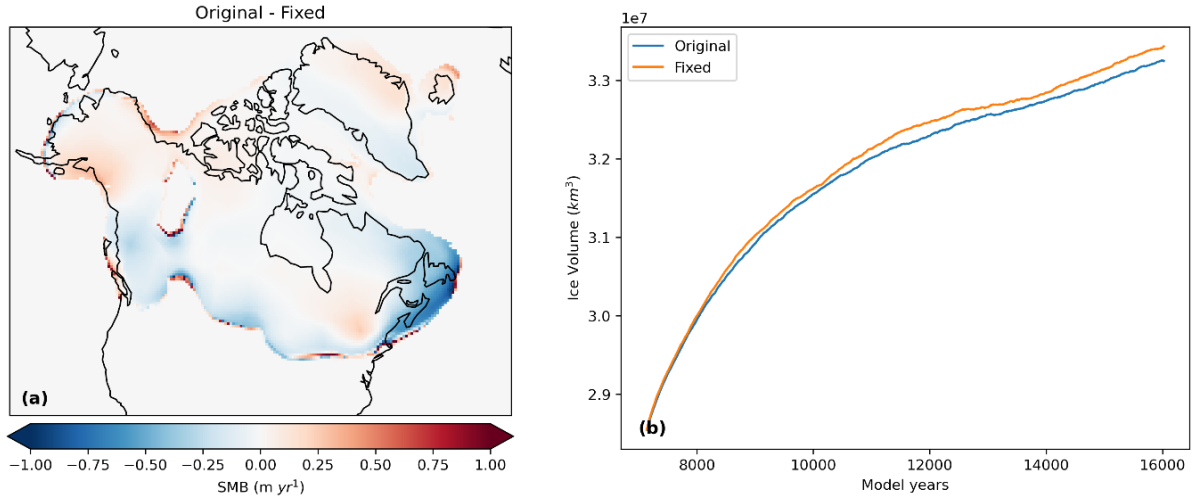

Figure 2.12: (a) Difference between the SMB at the end of the experiments between the original simulation and the simulation using the corrected eccentricity equation and (b) the evolution of ice sheet volume for both experiments.

2.7.2 Sea surface temperatures

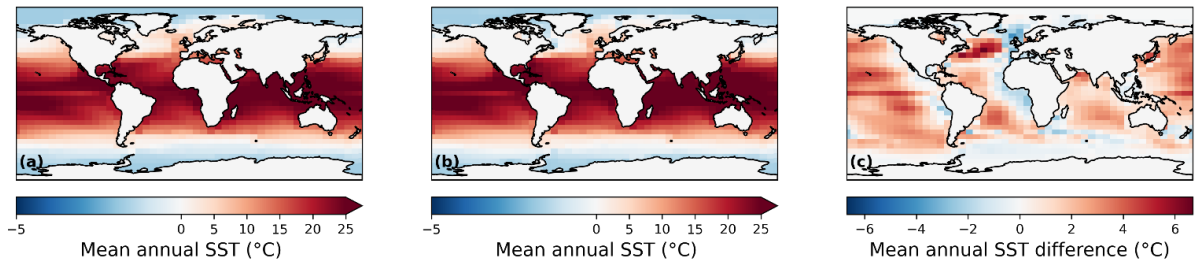

Figure 2.13: Mean annual SSTs used in this study from HadCM3 for (a) LGM and (b) PGM and (c) the difference between the LGM SST reconstruction used in Gandy et al. (2023) and the HadCM3 LGM SSTs.

2.7.3 Impact of different initial ice sheets

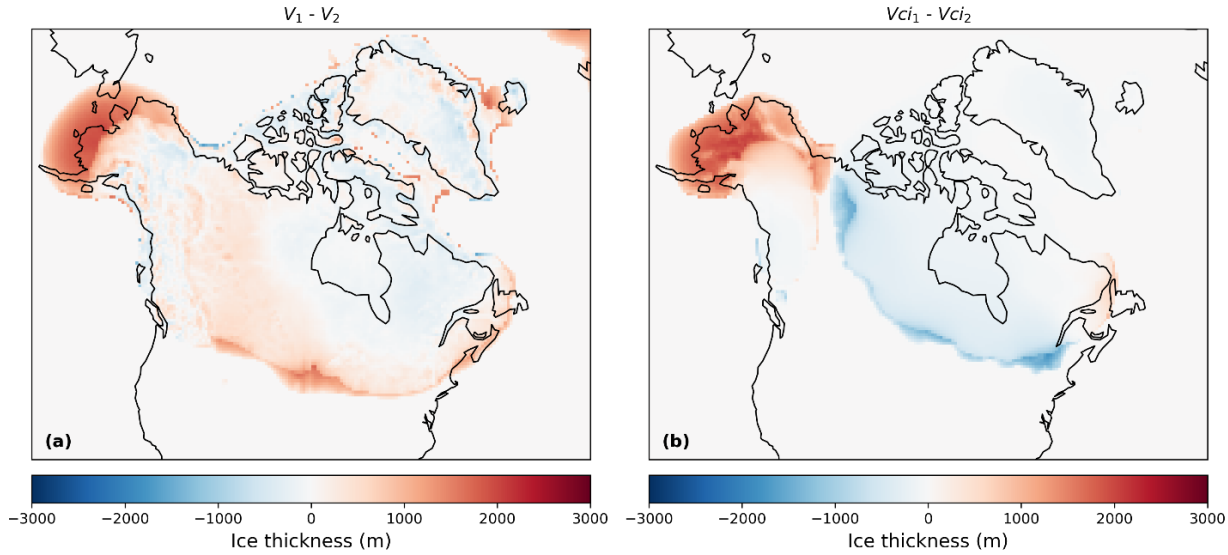

Figure 2.14: Difference in the final ice thickness between the simulations with matching initial conditions in FAMOUS and Glimmer and the NROYa ensemble member for (a) the LGM and (b) the PGM.

2.7.4 Wave 2 methodology

The ensemble design in this study was based on the "Not Ruled Out Yet" (NROY) parameter combinations from a second wave of ensemble members that followed on from the 280 member ensemble performed in Gandy et al. (2023). From the first wave of simulations, only 18 out of these 280 members produced a large enough LGM North American ice sheet to meet the volume and extent criteria they imposed (see details in reference). Further work was thus performed to augment the ensemble of simulations that met the NROY criteria. We used

statistical emulation to identify plausible regions in the parameter space. As there was limited information to constrain the domain of plausibility in the parameter space, we instead implemented an early-stopping criteria that allowed us to prevent the full execution of model runs that were not expected to produce good ice sheets. To do this we first modelled, from Wave 1, the predicted equilibrium area of the ice sheet from the value of the initial surface mass balance. Mathematically, we specified;

$$A = f(b) + \epsilon, \tag{2.6}$$

where A is the "equilibrium" ice sheet area after 10,000 ice sheet years, b is the 20 year averaged SMB value over the ice sheet and $f(\cdot)$ may be any function. We considered f to be either linear or sampled from a Gaussian Process (GP) and found the linear model gave more conservative uncertainty estimates which was desired since the Wave 2 runs needed to bound the NROY space. The predictive interval for the model is $P(b) = [f(b) + 3\sqrt{\text{var}(\epsilon)}, f(b) - 3\sqrt{\text{var}(\epsilon)}]$ and we targeted equilibrium ice sheet areas in the interval $T = [1.5\times10^7 \text{ km}^2, 2\times10^7 \text{ km}^2]$. The interval T is analogous to the target interval defined using Pukelsheim's 3-sigma rule in standard history matching (Pukelsheim, 1994). Plausible values of b satisfy the condition that $P(b) \cap T$ is non-zero, that is, for b to be plausible, the predictive bound $P(b)$ and the plausible equilibrium ice sheet area T must intersect. It was found that the 20-year averaged SMB had to be at least positive to produce a plausible ice sheet.

To further improve efficiency, we used Gaussian Process emulation to produce plausible values of b (and hence equilibrium ice sheet areas); iterating the training data of the emulator with each wave of simulator runs. Define by $\boldsymbol{x}$ the multivariate vector of parameters that they build the emulator over: here $\boldsymbol{x}$ comprised of the 4 most influential parameters *fsnow, av_gr, daice,* and *flow factor*. We model b with a random error process, $b \sim GP(x) + \eta$, where the effects of the parameters not explicitly represented in $\boldsymbol{x}$ are handled by the stochasticity of the process represented by η. Values of b were sampled using a stratified k-extended Latin Hypercube design (Williamson, 2015) and three sub-waves were executed, from which, a candidate set for the Wave 2 ensemble was extracted.

The first sub-wave (Wave 1.1) samples 200 ensemble members, which are predicted from the emulator to have non-negligible probability of positive SMB. This results in around 50% of simulations in this sub-wave having a positive SMB, an increase from 15% in the original wave (Figure 2.15, Wave 1.1). We attempt to refine the predictive bounds on the GP model twice more (Figure 2.15, Wave 1.2 and 1.3), with no improvement. This is likely due to the inherent

stochasticity of the climate model and cumulative effects of the parameters that they absorb into the predictive error term. At the end of this process of iterative short waves, the candidate set contains over 1000 20-year long simulations that have a positive SMB over the North American ice sheet. From this candidate set, and again using stratified k-extended Latin Hypercubes, we select an optimal (with respect to space-filling and accounting for the previous Wave 1 runs) design of 200 ensemble members to continue for a full 10,000 years to an equilibrium North American ice sheet. These 200 simulations make up the Wave 2. For context, this workflow of GP model sub-waves saved around 230,000 core hours (or about two months of real time) compared to running a full second ensemble wave.

Out of these 200 Wave 2 simulations, 176 members were identified to be NROY based on the original volume and extent thresholds. It is based on these results that we sub-sampled 62 parameter combinations for our simulations. This number of simulations was selected to enable us to run long equilibrium LGM and PGM simulations over a full ensemble within reasonable computational requirements. From the 176 NROY parameter combinations we randomly generated 10^7 candidate designs of size 62 from which we selected an approximate maximin design. This is obtained by: first linearly transforming each parameter onto the same range of [0, 1] to aid comparability; before computing the minimum distance between a parameter vector and its nearest neighbour; and then selecting the candidate design that maximised this distance. The resulting design possesses parameter vectors which are well-spaced and thus adequately cover the NROY space.

Our simulations use slightly different orbital parameter values and sea surface conditions to that of Gandy et al. (2023) (see Sect. 2.3.3). Thus, we do not expect the sample of 62 parameter combinations to provide full coverage of the NROY space but, as seen in Sect. S2 of the supplementary information in Gandy et al. (2023), the output trends are sufficiently similar that we expect this to be close enough to an optimal sample. Whilst we may have also sampled some parameter combinations outside of the NROY space, we feel these will still provide valuable information about uncertainty in outputs at the LGM and PGM. Our detailed comparison to empirical evidence and other model data (see Sect. 2.3.4 and 2.4.1) identified six parameter combinations that match our criteria for LGM and PGM ice extent and volume, thus demonstrating the success of this approach. Further exploration of the parameter space may produce NROY simulations in a different part of the parameter space but would not change the conclusion of this paper.

Upon analysing the results, we found a technical error in the original Wave 2 ensemble which resulted in the values of the parameter *daice* being shifted from its intended range of –0.4-0 K^{-1} to 0-0.4 K^{-1}, this means that the albedo of the bare ice was increasing with melting, which is likely not the case. This produced larger values of surface albedo and thus larger ice sheets in these Wave 2 simulations (not shown here). In the ensemble of simulations presented here, we corrected the *daice* values to match the intended parameter range. In some simulations, the switch of *daice* value from a large positive number to a large negative number would have resulted in a decrease in surface albedo and resulting ice sheet volume. This effect is negligible for values of d*aice* closer to zero.

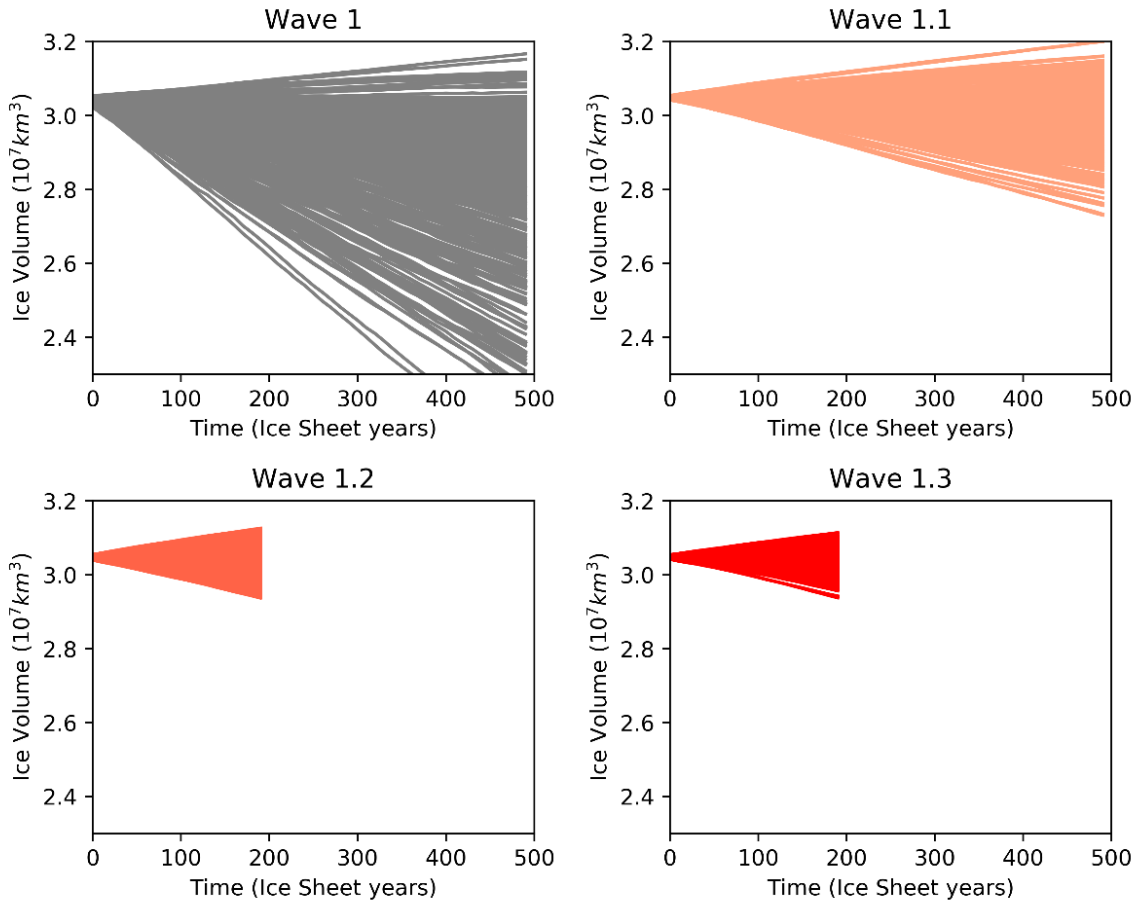

Figure 2.15: Ice volumes simulated in the successive ensemble sub-waves of simulations sampled to have a positive initial surface mass balance using the Gaussian Process emulator.

2.7.5 Metrics versus parameters plots

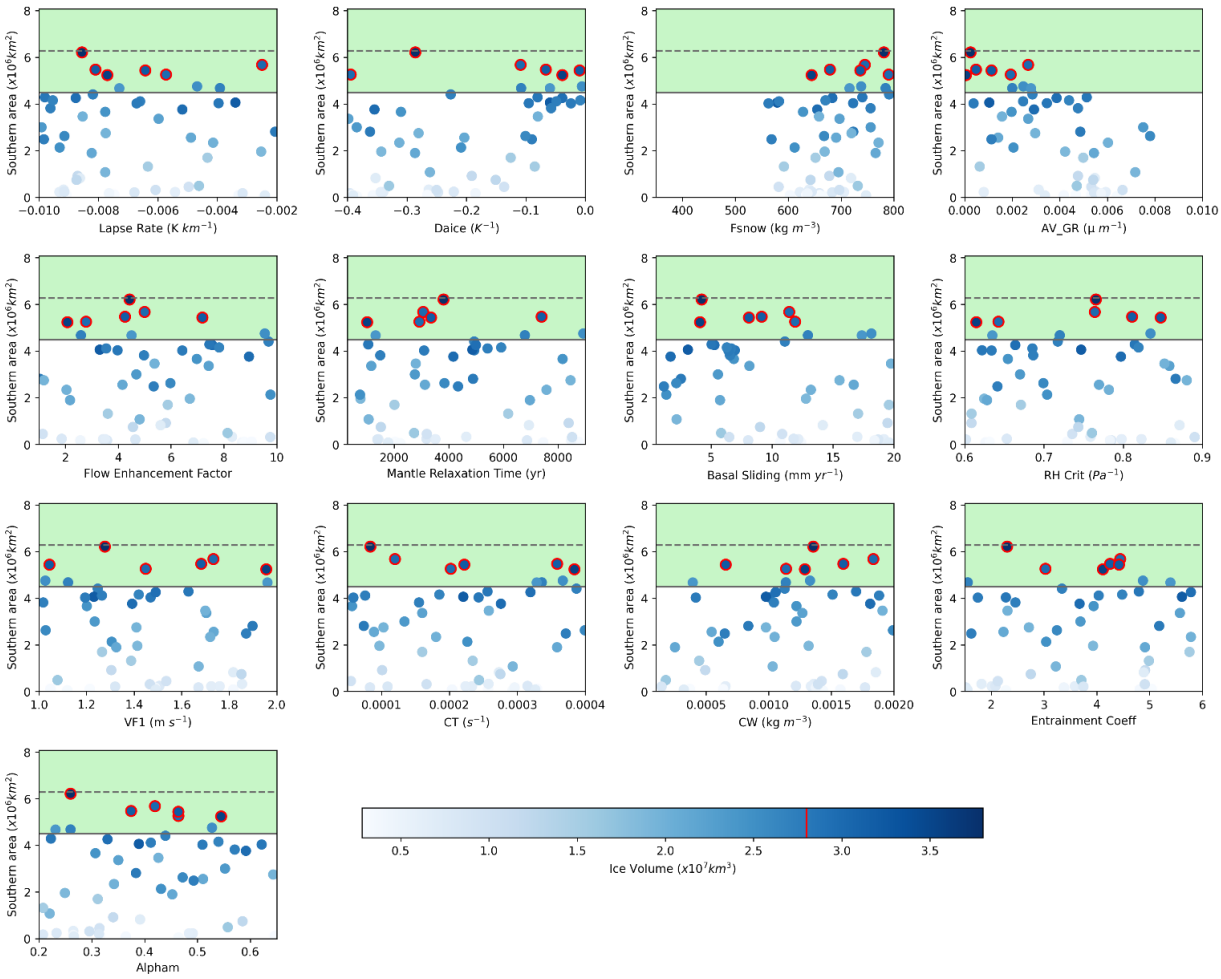

Figure 2.16: Southern area versus each of the 13 parameters varied for the LGM ensemble. The green shaded region shows the southern area constraint applied with the dotted line showing the exact area of the reconstruction and the solid line the solid line the minimum bound applied. The colour scale represents ice volume and the dots outlined in red are the six NROY LGM simulations with the red line on the colour bar showing the volume constraint.

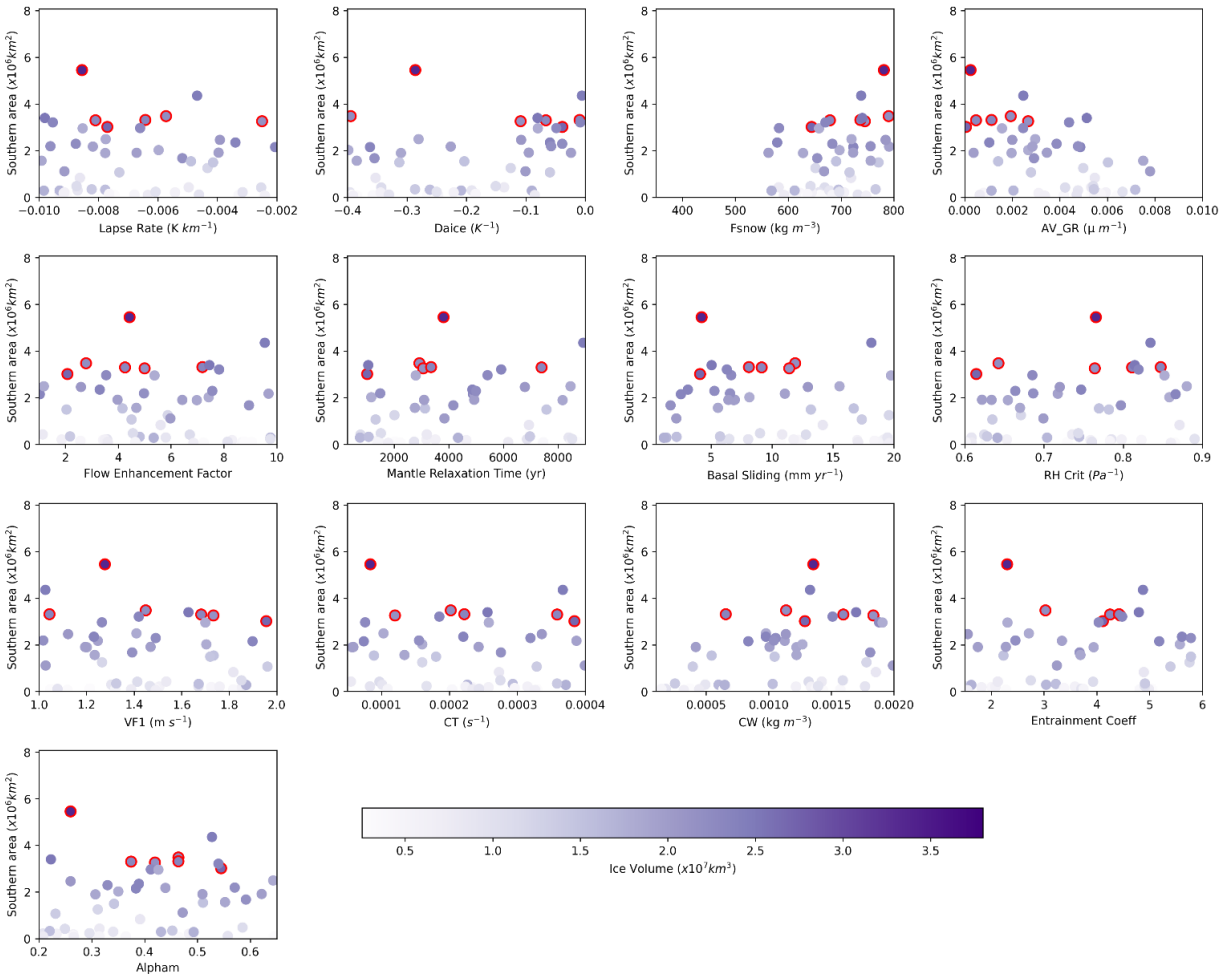

Figure 2.17: Southern area versus each of the 13 parameters varied for the PGM ensemble. The colour scale represents ice volume and the dots outlined in red are the corresponding six NROY PGM simulations.

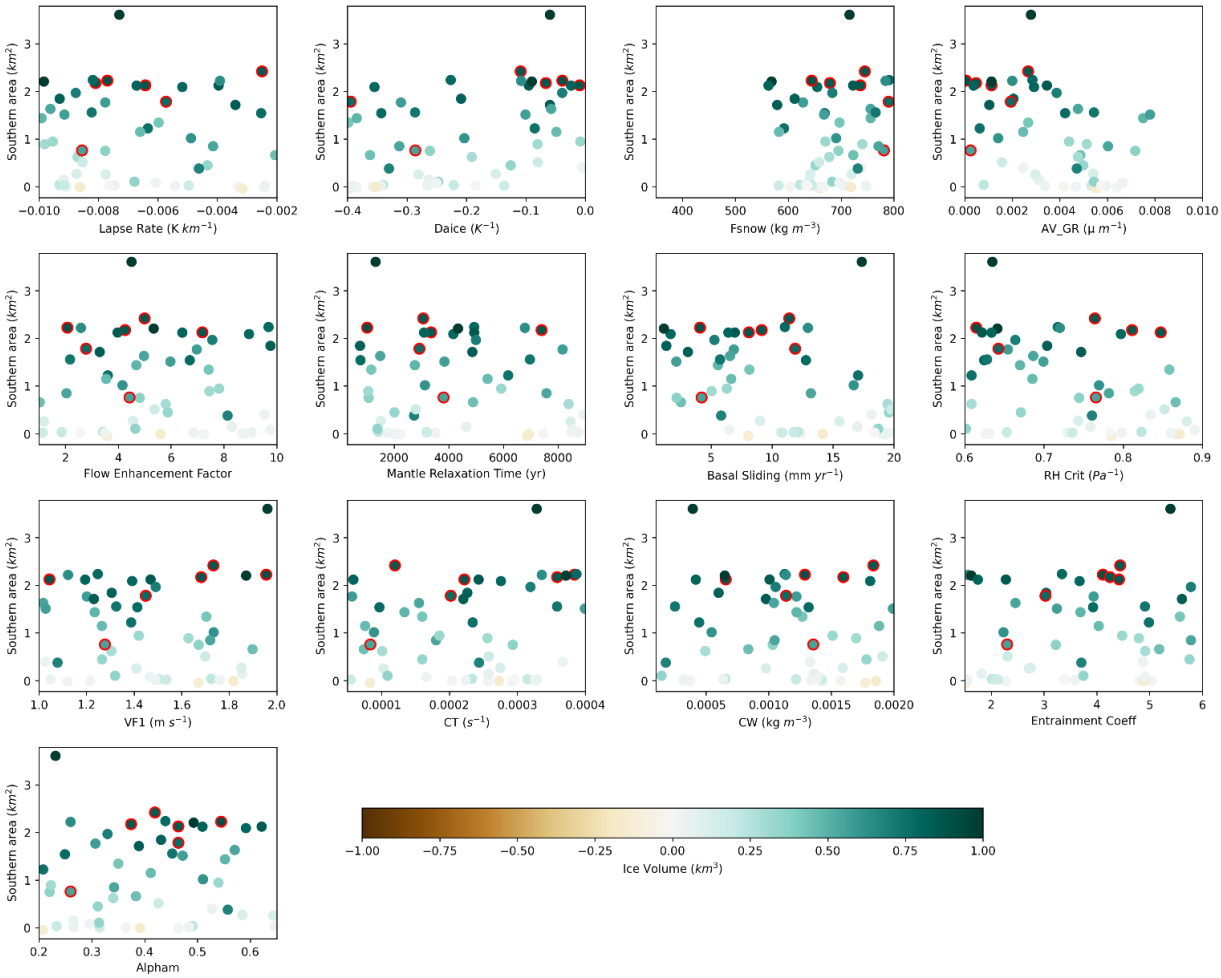

Figure 2.18: Difference in southern area versus each of the 13 parameters varied between the LGM and PGM ensemble members. The colour scale represents difference in ice volume and the dots outlined in red are the six NROY simulations.

Chapter 3

3 Exploring the sensitivity of the Northern Hemisphere ice sheets at the last two glacial maxima to coupled climate-ice sheet model parameters

3.1 Abstract

Simulations of past glacial periods are useful for testing the ability of numerical models to simulate ice sheet changes under significantly different climate conditions to present day. This can help improve projections of future sea level rise made by these same models, and avoid over-tuning to particular (e.g. modern) climate conditions. The Last Glacial Maximum (LGM; ~21 thousand years ago; ka) has been extensively used for this purpose since it is relatively well constrained by empirical evidence. However, less is known about the Penultimate Glacial Maximum (PGM; ~140 ka) and why the vast ice sheets covering much of the Northern Hemisphere, differed to the LGM. The answer likely lies, at least in part, in the different orbital configurations between the two periods, and the resulting impact on climate-ice sheet interactions.

Here, we perform and compare the first large ensembles of coupled climate-ice sheet (FAMOUS-BISICLES) simulations of the LGM and PGM to better understand how Northern Hemisphere ice sheets interact with the climate. We also quantify how sensitive the simulations are to the choice of uncertain model inputs, including physical parameter values. Specifically, we vary 12 uncertain parameters that control the model representations of ice sheet albedo, ice dynamics and climate. The ensembles are evaluated against palaeo-evidence of global mean temperature, ice volume and extent, to calibrate the model and find combinations of parameters that simultaneously yield plausible ice sheets and climates for both periods. The sensitivity of the North American ice sheet and the Eurasian ice sheet during the LGM and PGM, to each of the 12 parameter values, is explored using a combination of Gaussian Process emulation and Sobol′ sensitivity analysis. From the whole ensemble of 120 simulations, we find two simulations that meet our evaluation constraints for the LGM ice sheets. The parameter values

that influence the albedo of the ice sheet have the largest influence on the resulting ice sheet volumes, but several other parameters display different sensitivity indices depending on the ice sheet (North American versus Eurasian) and time period (PGM versus LGM). This includes parameters that affect the cloud liquid water, lapse rate, basal sliding and downscaling elevation heights.

3.2 Introduction

During glacial periods of the last 800,000 years, large ice sheets built up over the Northern Hemisphere (NH) continents (Ehlers et al., 2018), impacting the climate through their interactions with atmospheric circulation, oceanic circulation and the energy budget (Lambeck et al., 2014; Scherrenberg et al., 2023b). However, the evolution of the NH ice sheets differed between each glacial period, leading to different geometries at the glacial maxima - the periods during the glacials in which global ice volume is at its largest and global mean sea level is at its lowest (Ehlers et al., 2018).

Geological evidence and numerical simulations of the last two glacial maxima, the Penultimate Glacial Maximum (PGM; ~140 ka) and the Last Glacial Maximum (LGM; ~21 ka), for example, suggest very different configurations of the North American ice sheet (NAIS) and the Eurasian ice sheet (EIS) (Svendsen et al., 2004; Colleoni et al., 2016; Batchelor et al., 2019) despite similarities in greenhouse gas (GHG) concentrations (CO_2 ~190 ppm), global average insolation and global ice volume (~130 meters sea level equivalent (m s.l.e.)) (Berger and Loutre, 1991; Loulergue et al., 2008; Rabineau et al., 2006; Masson-Delmotte et al., 2010; Bereiter et al., 2015; Rohling et al., 2017). Geomorphological evidence suggests that the extent of the Penultimate EIS could have been ~50% larger than during the Last Glacial Cycle and expanded 200 km further south and 1000 km further east in Siberia (Batchelor et al., 2019; Knies et al., 2001; Svendsen et al., 2004). However, there are large uncertainties in its maximum extent at the PGM since there is evidence of two major ice advances in Europe, the more extensive Drenthe (~160 ka), which was followed by partial melting and sea level rise ~157-154 ka under increasing summer insolation, and then a readvance after 150 ka during the less extensive Warthe (Hughes and Gibbard, 2018). Thus, current reconstructions of the maximum may incorrectly incorporate previous advances during Marine Isotope Stage 6 (MIS 6; 195-123 ka) (Ehlers et al., 2018; Margari et al., 2014; Svendsen et al., 2004).

Since the volume of ice sheets cannot be directly inferred from empirical evidence, it must be indirectly estimated from datasets such as relative sea level proxies through glacial isostatic adjustment (GIA) inversion modelling and numerical ice sheet modelling (e.g. Lambeck et al.,

2006; Tarasov et al., 2012; Rohling et al., 2017). Consequently, there is even larger uncertainty in volume estimates than there are in extent estimates. Nonetheless, ice volume estimates support the ice extent-derived evidence that EIS volume was indeed larger at the PGM, with most estimates ranging from ~40-70 m s.l.e. compared to ~13-24 m s.l.e. at the LGM (Lambeck et al., 2006; Peyaud, 2006; Pollard et al., 2023; Rohling et al., 2017; Simms et al., 2019; Tarasov et al., 2012).

In contrast, whilst there is some evidence that, during the PGM, the NAIS extended slightly further south into the states of Illinois and Wisconsin (Batchelor et al., 2019; Hughes and Gibbard, 2018), most available evidence suggests that the NAIS was smaller in extent and volume compared to the LGM. This includes relative sea level assessment studies (e.g. Rohling et al., 2017), reduced ice rafted debris layers in the North Atlantic (pointing to reduced iceberg discharge from the Hudson Bay region; Hemming, 2004; Naafs et al., 2013; Obrochta et al., 2014), climate and ice sheet modelling studies (Abe-Ouchi et al., 2013; Colleoni et al., 2016; Wekerle et al., 2016) and GIA modelling studies (Dyer et al., 2021; Wainer et al., 2017). The relative lack of geomorphological evidence of the PGM NAIS further supports the hypothesis that PGM NAIS was smaller than LGM NAIS because it implies a larger ice advance at the LGM destroyed most traces of the previous glacial maximum (Dalton et al., 2022; Dyke et al., 2002; Rohling et al., 2017). Therefore, the footprint of the PGM NAIS remains very uncertain, while LGM NAIS ice extent is relatively well constrained from a range of glacial geological evidence, which has been updated in recent years (e.g. Dalton et al., 2020). As with the EIS, the volume of the NAIS is more difficult to assess from empirical evidence and mostly relies on modelling, which estimates it at being between ~39-59 m s.l.e. at the PGM compared to ~68-88 m s.l.e. at the LGM (Rohling et al., 2017; Simms et al., 2019).

The differences in the shape and size of the ice sheets between the LGM and PGM are not well understood. They result from complex interactions occurring between different components of the earth system (e.g. atmosphere, ocean, ice sheets, and solid earth) leading up to and at the glacial maximum. Despite similar levels of average global incoming solar radiation between the LGM and PGM, the seasonal and latitudinal patterns differed between the two periods, as did its evolution prior to the maxima, as a result of different orbital situations (Berger, 1978; Berger and Loutre, 1991). The orbital forcing, along with concentrations of GHGs, would have altered the radiative balance between the periods. As well as affecting the ice sheet evolutions directly, this also would have influenced the sources and pathways of moisture advection (Hughes and Gibbard, 2018; Krinner et al., 2011; Rohling et al., 2017), sea surface temperatures (SSTs) and sea ice concentration (Clark et al., 2009; Colleoni et al., 2011;

Kageyama et al., 1999; Kageyama and Valdes, 2000), vegetation distribution (Colleoni et al., 2009b; Kageyama et al., 2004; Stone and Lunt, 2013), dust deposition (Colleoni et al., 2009a; Krinner et al., 2006; Naafs et al., 2012b) and proglacial lake coverage (Colleoni et al., 2009a; Krinner et al., 2004), which all have important feedbacks onto the climate. Additionally, feedbacks on the climate from the ice sheets themselves are very important in regulating ice sheet surface mass balance (SMB), for example through the influence of the ice-albedo and temperature-elevation feedbacks on surface temperature and energy balance (Abe-Ouchi et al., 2007; Patterson et al., 2024), and interactions between atmospheric and oceanic circulation, surface temperature and precipitation patterns (Beghin et al., 2014, 2015; Liakka et al., 2012). Some studies have also concluded that the topography of the NAIS had a large influence in the size and configuration of the EIS through its effect on the jet stream and stationary waves (Beghin et al., 2015; Liakka et al., 2016).

Direct observations of processes occurring during glacial cycles are not available and while proxy evidence can provide important constraints on how the ice sheets changed, it cannot reveal the mechanisms behind these changes. Numerical modelling is therefore required to understand the response of the NH ice sheets to external and internal forcings and unpack why they differed between glacial periods. This is an important source of information in the context of understanding how ice sheets may respond to future climate change (Gregory et al., 2012). Currently there are large uncertainties in projections of future sea level rise (Edwards et al., 2021; Intergovernmental Panel On Climate Change, 2021) mainly as a result of limited knowledge of several important ice sheet processes, such as non-linear behaviours of the ice sheet system, and climate and ice sheet interactions (Golledge et al., 2019; Gregoire et al., 2012; Kopp et al., 2017). Simulations of past periods can help improve our understanding of these processes as well as help evaluate and refine the numerical models used for these projections (Braconnot et al., 2012; Gandy et al., 2018; Harrison et al., 2016; Masson-Delmotte et al., 2013; Schmidt et al., 2014a). The LGM has been extensively used for this purpose because the climate and ice sheet states are relatively well constrained by empirical evidence and thus allow evaluation of model performance, helping constrain climate and ice sheet models and future sea level projections (Gandy et al., 2023; Ziemen et al., 2014). Furthermore, the EIS has large marine based sectors in the Barents-Kara and North Sea regions, and thus it is often considered an analogue of the current West Antarctic ice sheet (Winsborrow et al., 2010). Modelling and identifying the mechanisms responsible for the different EIS evolutions might help with understanding the processes in effect in West Antarctica and its vulnerabilities to climate change (van Aalderen et al., 2023; Gandy et al., 2018).

Many previous studies simulating the NH LGM and PGM climate and ice sheets have treated the components independently. Either prescribing the ice sheets as a boundary condition in a climate model, which neglects any affects the climate has on the ice sheets (Beghin et al., 2015; Colleoni et al., 2016; Hofer et al., 2012; Merz et al., 2015; Ullman et al., 2014), or forcing ice sheet models with climate output from general circulation models (GCMs), which introduces large uncertainties depending on the model used and can produce unrealistic ice sheets (Abe-Ouchi et al., 2013; Alder and Hostetler, 2019; Charbit et al., 2007; Gregoire et al., 2016; Niu et al., 2019; Scherrenberg et al., 2023b; Wekerle et al., 2016; Zweck and Huybrechts, 2005). Thus, the use of directly coupled climate-ice sheet models to perform these simulations will explicitly resolve some of these important feedbacks and interactions between the climate and the ice sheets, reducing some of the uncertainties and inconsistencies caused by prescribing one of the components, and provide a better understanding of these processes (Abe-Ouchi et al., 2013; Niu et al., 2019; Quiquet et al., 2021a; Ziemen et al., 2014).

Recent developments have allowed the two-way coupling between GCMs and ice sheet models (ISMs), but previous studies using this method have focused on just one time period and/or one ice sheet and there have so far been no coupled GCM-ISM simulations of the NH ice sheets at the PGM (Gandy et al., 2023; Gregory et al., 2012; Patterson et al., 2024; Quiquet et al., 2021a; Sherriff-Tadano et al., 2024; Ziemen et al., 2014). Additionally, it has been shown that uncertainties in certain model parameters can have a large influence on the resulting ice volumes simulated by the coupled model through altering the strength of important climate-ice sheet feedbacks (Gandy et al., 2023; Patterson et al., 2024; Sherriff-Tadano et al., 2024). The work presented in Chapter 2 evaluated a range of model parameter values based on whether they produced plausible NAIS configurations for both the LGM and PGM. However, the different processes operating on the Eurasian ice sheet (see Sect. 3.3.1), the interactions that may occur between both ice sheets and the use of a different ice sheet model with more advanced physics and an updated experimental design, require additional uncertainty quantification to be carried out. This can be done through a large ensemble analysis, to re-evaluate the collection of parameter combinations that yield model output consistent with observation data (up to the assessed uncertainties), referred to as the "Not Ruled Out Yet" (NROY) parameter space (Williamson et al., 2013).

The aim of this work is therefore to perform and compare ensemble simulations of the NH ice sheets at the LGM and PGM using a coupled climate-ice sheet model (FAMOUS-BISICLES). After performing some sensitivity tests to optimise the model for ice streaming in the NH ice sheets, we assess the ability of the model to produce reasonable simulations of both the NAIS

and EIS for both periods. We evaluate the impact of uncertainty in model parameters on the resulting ice sheets and whether both ice sheets show similar sensitivities to the parameters. The model is evaluated against an implausibility metric based on ice sheet volume and extent data, and the representation of ice streams is assessed.

3.3 Methods

3.3.1 Models

The climate model used in this study, FAMOUS, is sufficiently efficient that it is suitable for running long (multi-millennial) palaeo simulations (e.g. Gregory et al., 2012; Gregoire et al., 2012; Roberts et al., 2014; Dentith et al., 2020) and large ensembles for uncertainty quantification (Gandy et al., 2023; Gregoire et al., 2011; Sherriff-Tadano et al., 2024), whilst still resolving the same complex processes as represented in an atmosphere-ocean general circulation model (AOGCM). It is based on HadCM3 AOGCM (Gordon et al., 2000; Pope et al., 2000) but has half the spatial resolution and a longer time-step, thus requiring only 10% of the computational costs of the parent GCM.

We use the atmospheric component of FAMOUS, which is a hydrostatic, primitive equation (i.e. resolves the fundamental governing equations of atmospheric dynamics) grid point model with a horizontal resolution of 7.5° longitude by 5° latitude with 11 vertical levels and a 1-hour time step (Williams et al., 2013). FAMOUS can also be run coupled with a dynamical ocean (e.g. Dentith et al., 2020), however, in this study, we prescribe sea surface temperatures and sea ice (see Sect. 3.3.3.1). The land surface scheme MOSES2.2 (Essery et al., 2003) is used to represent land processes on a set of sub-grid scale tiles in each grid box representing fractions of nine different surface types, including land ice (Smith et al., 2021b).

This study uses a version of FAMOUS developed to have bi-directional coupling to an ice sheet model (FAMOUS-ice; Smith et al., 2021b) accounting for the mismatch between the atmosphere and ice sheet grid sizes by using sub-grid scale elevation tiles. The atmospheric surface air temperature and long wave radiation is calculated in FAMOUS at the mean elevation within each grid cell and for ice sheet grid cells, these quantities are downscaled onto 10 vertical “ice tiles" with different elevations; 100 m, 300 m, 550 m, 850 m, 1150 m, 1450 m, 1800 m, 2250 m, 2750 m, 3600 m. The air temperature downscaling is done by using a constant lapse rate (*tgrad*) to adjust for the differences in the elevation between each tile and the mean elevation, and humidity and downwelling longwave are adjusted to be consistent with the temperature adjustment. No downscaling is applied to precipitation and shortwave radiation in this version of the model. The surface energy fluxes and SMB are calculated on the 10 ice tiles

based on the energy budget equation and a multi-layer deep snowpack model. Then the SMB is passed onto the ice sheet model, which projects and linearly interpolates this coarse SMB field onto the higher resolution ice sheet surface. The resulting changes in ice extent and surface elevation simulated by the ice sheet model are passed back to FAMOUS to update the fraction of ice present within each ice tile and the orography fields. Within FAMOUS, the mean of the surface fluxes weighted by ice fraction within the ice tiles sets the land-atmosphere exchanges within FAMOUS. In this study, this process is run at 10 times ice sheet model acceleration meaning one year of climate integrated in FAMOUS is used to force 10 years of ice sheet integration in the dynamical ice sheet model before the ice cover and orography fields are passed back (Gregory et al., 2020).

In Chapter 2, FAMOUS was coupled to the Glimmer ice sheet model to simulate the North American ice sheet. However, the coarse resolution and the use of shallow ice approximation (SIA) in the Glimmer ice sheet model used in that study does not resolve the small-scale processes or longitudinal stresses required to accurately simulate ice stream evolution or grounding line migration. Whilst these processes are not as important to capture in an equilibrium spin-up of a continental size terrestrial ice sheet, such as NAIS, they have a large influence on the behaviour, configuration and stability of a marine ice sheet (Hubbard et al., 2009; Pattyn et al., 2012; Stokes and Clark, 2001). In particular, the Eurasian ice sheet has many ice streams within marine sectors (e.g. North Sea and Barents Sea) that are vulnerable to processes that may cause instabilities of retreat, for example Marine Ice Sheet Instability (MISI), and are likely to have been important in its evolution and deglaciation (Kopp et al., 2017). These processes are similar to those in operation today in West Antarctica, currently forming a large source of uncertainty in future sea level projections (van Aalderen et al., 2023; Alvarez-Solas et al., 2019; Edwards et al., 2019; Gandy et al., 2019, 2021; Petrini et al., 2020).

BISICLES is well suited to simulating marine ice sheet dynamics due to its use of the L1L2 physics for approximating the sliding and flow of the ice sheet, instead of SIA (Cornford et al., 2013). The L1L2 approximation is a variant of Glen's flow law that includes longitudinal and lateral stresses and approximates vertical shear strains in vertically integrated models (Schoof and Hindmarsh, 2010). This makes it able to represent ice-shelves and fast-flowing ice streams (Hindmarsh, 2009). Additionally, some ice sheet processes, such as ice streaming and grounding line migration, require high resolution to simulate accurately. BISICLES enables this to be feasible in millennial scale and large ensemble simulations through its adaptive mesh refinement (AMR). Where required, the model can simulate at high resolution, whilst the rest of the domain (i.e. the slower moving interior of ice sheets) remains at a lower resolution, thus

increasing the efficiency of the model (Cornford et al., 2013). With these features, BISICLES is a model well suited to simulate the past evolution of marine ice sheets such as the Eurasian ice sheet. It also allows for better physical accuracy in the representation of ice streams within the North American ice sheet. BISICLES has previously been used to successfully simulate the ice streams and retreat of the marine based British-Irish ice sheet (BIIS) at the Last Deglaciation (Gandy et al., 2018, 2019, 2021), the final retreat of the NAIS during the early Holocene (Matero et al., 2020), produce an initial condition of the present-day Greenland ice sheet (Lee et al., 2015) and model the future evolution of the Antarctic ice sheet (Cornford et al., 2015; Siahaan et al., 2022). Additionally, FAMOUS-BISICLES has been used to explore the sensitivity of the NAIS and Greenland ice sheet at the LGM to model parameter values through large ensemble analysis (Sherriff-Tadano et al., 2024).

We use the updated version of BISICLES developed by Gandy et al., (2019), which implements a pressure limited basal sliding law that is sensitive to the presence of till water. This is mostly found to be applicable near the grounding line, and the inclusion of the Coulomb sliding law has been shown to have an effect on ice sheet stability in models, with greater grounding line retreat occurring in simulations that include this law than those without (Nias et al., 2018; Schoof, 2006; Tsai et al., 2015).The upper surface temperature boundary condition in the ice sheet model (surface heat flux) is determined by the climate model and the basal boundary condition (basal heat flux) is set as a constant flux (3×10^6 J a^{-1} m^{-2}). The effective pressure, and therefore the basal sliding, depends on the basal water pressure and thus the depth of the till water layer. Once the englacial drainage water fraction grows beyond a certain value (0.01) it is drained to a till layer at a rate proportional to the water fraction, up until a maximum water fraction (0.05). The till water is lost vertically at a rate proportional to the till water depth which is determined by the specified till water drain factor (*drain*) (Van Pelt and Oerlemans, 2012). This basal hydrology scheme is therefore non-mass conserving. A maximum till water thickness of 2 m is set following previous studies (Bueler and van Pelt, 2015; Gandy et al., 2019; Moreno-Parada et al., 2023). A recent comparison study by Drew and Tarasov (2023) shows that this simplified “leaky bucket” hydrology scheme produces similar results to more complete models over centennial or longer timescales and continental scale ice sheets. Additionally, the implementation of this basal sliding scheme coupled with this hydrology parameterisation allows the simulation of spontaneous ice stream generation and evolution (Gandy et al., 2019, 2021).

The upper surface thickness flux (i.e. accumulation/melt) is calculated by the climate model and the lower surface (basal) thickness flux (i.e. oceanic melt) is set to zero for grounded ice and is proportional to the SSTs for floating ice, according to the linear relationship;

$$Subshelf\ melt\ rate\ (myr^{-1}) = c(T_{ocn} - T_f), \quad (3.1)$$

where c is a constant, T_{ocn} is the prescribed sea surface temperature and T_f is the freezing point of seawater, assumed to be -1.8 ºC at the surface (Alvarez-Solas et al., 2019; Beckmann and Goosse, 2003; Gandy et al., 2018; Martin et al., 2011; Rignot and Jacobs, 2002). Since the freezing point of sea water varies with depth of the ice shelf base and with salinity, and the surface temperatures are used rather than subsurface, this is a highly idealised parameterisation. In addition, many studies have found a quadratic relationship to be a better fit to present-day observations (e.g. DeConto and Pollard, 2016; Favier et al., 2019; Holland et al., 2008). However, the lack of constraints on ice shelves, ocean temperatures, and sub-shelf melt rates for the periods covered in this study makes this a large source of uncertainty in our modelling. In this context, it is preferable to choose a simple linear representation of sub-shelf melt over a more complex quadratic relationship. We account for this uncertainty in the wide range of sub-shelf melt constant (c) values used (1–50 m yr^{-1} $°C^{-1}$). This relationship produces an average sub-shelf melt rate across the ice shelves of between around 1.6–28 m yr^{-1}, which are not unrealistic when compared to the estimates from present-day Antarctica of 0–43 m yr^{-1} (Depoorter et al., 2013; Jourdain et al., 2022; Rignot et al., 2013). However, some regions in some simulations display very large rates of 100s of metres per year.

Glacial isostatic adjustment of bedrock topography due to changes in the ice sheet load is included through coupling BISICLES to a simple Elastic Lithosphere Relaxing Asthenosphere (ELRA) model, which approximates this response by assuming a fully elastic lithosphere above a uniformly viscous asthenosphere (Kachuck et al., 2020). A relaxation time of 3000 years is applied in this model based on previous studies (Pollard and DeConto, 2012). This method does not account for changes in the gravitational pull that ice sheets exert on sea level or adjustments in global mean sea level caused by changing global ice sheet volume (e.g. Gomez et al., 2010).

Sherriff-Tadano et al. (2024) found that some of the FAMOUS-BISICLES simulations of the NAIS at the LGM exhibit a strong local melting of the ice sheet from parts of the interior. This phenomenon is caused by warm temperature biases over the ice sheet interior in the atmospheric model, which are amplified by the downscaling method and a positive height-mass balance feedback. A similar temperature bias was pointed out by Smith et al., (2021b)

using the same model under the modern Greenland ice sheet, which produced a higher Equilibrium Line Altitude (ELA) (around 2 km high in places) compared to a high-resolution regional atmospheric model (at about 1 km high). The warm temperature bias comes from the low resolution of the atmospheric model. In reality, a very cold atmospheric layer often forms at the surface of ice sheets, especially in the interior, which induces a stable boundary layer and isolates the cold surface from the ambient warm air. However, a global climate model cannot resolve the effect of the stable boundary layer and overestimates the exchange of heat between the surrounding atmosphere and the ice sheet surface. As a result, FAMOUS overestimates the temperature in the ice sheet interior and causes a high ELA bias, which results in surface melt.

Here, we take a practical approach to mitigate the effect of the warm temperature bias in FAMOUS. This is done by modifying the height adjustment of atmospheric surface temperature to the ice tiles through the introduction of a new parameter in the model, *elevcon,* which is intended to make the parts of the ice sheet surface, towards the centre of the ice sheet, colder. Section 3.6.1 includes a description of how the *elevcon* parameter is implemented and works to affect the surface temperature and SMB during height correction, and of sensitivity experiments performed to validate the effect of different values of *elevcon* on the modern and LGM ice sheets and climates. Since the optimal value of this adjustment is uncertain, we include *elevcon* in the ensemble as a varied parameter value, between the range of 1 and 1.5 (0-50%). These values were chosen based on testing that showed that a value of 1.5 produced an equilibrium line altitude height that represents an upper limit determined by empirical data (Figure 3.14).

3.3.2 Ice dynamics in BISICLES

It has been established that ice streams exert an important control on the behaviour and geometry of an ice sheet and therefore it is crucial that in our study, the simulated location and dynamics of at least the major ice stream features, are consistent with reconstructions. Gandy et al. (2019) highlighted that the most important model ingredient necessary to successfully model ice streams is the representation of idealised subglacial hydrology. The till water layer coupled with the Coulomb sliding law described in Sect. 3.3.1 is crucial for the spontaneous generation of ice streams. However, this scheme is highly sensitive to the drainage and temperature structure of the ice sheets. Inadequate consideration of these factors can lead to a poor representation of ice streams (e.g. Sherriff-Tadano et al., 2024). Therefore, we perform a spin-up of BISICLES that results in the internal temperatures of the ice sheet being more conducive for ice stream generation over shorter integration times. We also perform sensitivity

tests varying the level of refinement of the ice streams and the rate of till water drainage to find an optimum set-up that balances computational cost with the representation of ice dynamics. These methods are described in the following sections.

3.3.2.1 Temperature spin-up

The internal temperature of ice sheets is an important factor in controlling the deformation, rheology and velocity of the ice due to the temperature dependence of the sliding law and enthalpy scheme (Blatter et al., 2010). The ice sheets start with a uniform internal temperature of 268 K and it can take tens of thousands of years for the process of cold ice advection from the interior and heat conduction from the bed to occur and reach an equilibrium, which is important for the formation of ice streams (Fyke et al., 2014; Heine and Mctigue, 1996). Thus, we perform ice sheet model only spin-ups for the LGM and the PGM to allow the ice sheet internal temperatures to reach close to equilibrium. This temperature profile is then used as the internal ice sheet temperature in the initial condition for the sensitivity tests (Sects. 3.3.2.2 and 3.3.2.3) and coupled simulations.

The spin-ups were run at 32 km resolution for 20,000 years using single surface mass balance and surface temperature fields taken from a FAMOUS-BISICLES equilibrium simulation that used climate model parameters identified to be NROY in simulations of the NAIS in Chapter 2, default ice sheet model parameters and an *elevcon* value of *1.2* (Figure 3.16). The initial ice sheet configurations were the same as used in the coupled simulations (described in Sect. 3.3.3.1). The sliding law was set to a temperature dependent Weertman sliding without till water dependent Coulomb sliding enabled since the bulk of the temperature field is not affected much by Coulomb sliding near the coast. The resulting temperature profiles are shown in Sect. 3.6.2 (Figure 3.17 and Figure 3.18).

3.3.2.2 Drain factor sensitivity tests

In their study, Sherriff-Tadano et al., (2024) used much higher values of *drain* (0.2-0.6 m yr^{-1}) than has typically been used in previous studies (0.001-0.005 m yr^{-1}; Gandy et al., 2019; Kazmierczak et al., 2022; Moreno-Parada et al., 2023). This was to prevent large till water depths leading to too large velocities across the entire ice sheet and long simulation times, as high velocities require more iterations and smaller timesteps to solve. This resulted in the till water drainage outpacing the supply and thus very small till water depths, leading to mostly Weertman sliding across the whole ice sheet.

Slow till drainage (low values of *drain*) can lead to isolated regions of fast flow, > 50 km yr^{-1}, which have a disproportionate effect on simulation time. To prevent this we introduce an

artificial drag term rising with the fourth power of ice speed and calibrated to be negligible for ice speeds below 1 km yr^{-1}. This drag factor is also used in the coupled simulations throughout the rest of this study. We then perform sensitivity tests with different values of *drain* spanning the range 0.001-0.06 m yr^{-1} but all other factors kept constant. The results of some of these tests are shown in Figure 3.19. Values of *drain* above 0.05 prevent much of the coulomb sliding at the coasts and the representation of some of the major ice streams, particularly the Hudson Strait Ice Stream, is poor. Low values usually used in ice sheet models (0.001-0.005) cause too large velocities and ice streams that remove much of the ice sheet, especially in Eurasia. Therefore, in this study, we implement a range of 0.01-0.05 to cover values just below the default till water supply rate of 0.02, to where no coulomb sliding occurs. For studies that seek to examine ice streaming of the glacial maximum ice sheets, we would recommend performing additional sensitivity tests that vary ice shelf basal melt parameterisation and geothermal heat flux, but this is beyond the scope of the present study.

3.3.2.3 Spatial resolution sensitivity tests

The base resolution of the ice sheet model is 32 km. The adaptive mesh refinement allows the areas covered by ice to be refined once to 16 km, which shows some improvement to the simulated ice streams, although the difference is only about 1.2 m yr^{-1} on average over the whole ice sheet (Figure 3.20a and 3.20b). Additional sensitivity simulations were performed refining areas of ice streaming up to 8 km and up to 4 km (Figure 3.20c and 3.20d). These tests showed that after refining to 16km, the difference in average ice velocity for any further refinement converges to zero (Figure 3.21) and the pattern of major ice stream features (Figure 3.20), the position of the marine margins and the ice volume across the NH ice sheets is not significantly changed, except across the southern area of the Eurasian ice sheet (Figure 3.1). However, computational costs are quadrupled with each level of refinement. Thus, we determine one level of refinement (16 km) to be sufficient for this study in which we are focussing more on the large-scale geometry of the ice sheet rather than the finer details of the ice streams. This is a similar conclusion to that drawn from the simulations presented by Albrecht et al., (2020) and Gandy et al., (2019), the latter further showing anything finer than 4 km does not improve the match of simulated ice streams to empirical data.

There is an increase in the velocity of up to around 3000 m yr^{-1} at the centre of some of the ice streams at the higher resolutions, which could be important during simulations of the deglaciation (Robel and Tziperman, 2016). We performed an additional simulation refining the margin of the marine section of the Eurasian ice sheet to 2 km to see if any marine processes would be captured that could not have been resolved at lower resolutions. This did not lead to

any significant difference in the ice velocity in this region compared to the 4 km simulation (Figure 3.20e), but again could be important in deglaciation simulations when MISI could be triggered (Gandy et al., 2020; Patton et al., 2015; Petrini et al., 2020; van Aalderen et al., 2024).

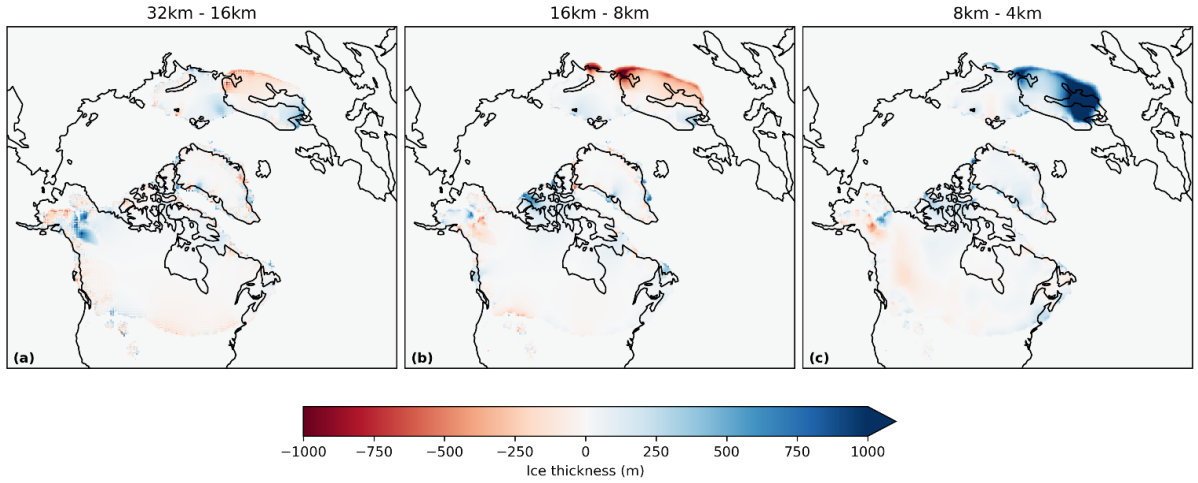

Figure 3.1: Difference in final ice sheet thickness between simulations with different levels of refinement

3.3.3 Experiment design

3.3.3.1 Boundary and initial conditions

The coupled simulations broadly follow the PMIP4 protocols for the LGM (Kageyama et al., 2017) and the PGM (Menviel et al., 2019), which prescribe greenhouse gases, orbital parameters and the Antarctic ice sheet configuration. Following the same methods in Chapter 2, we also prescribe SSTs and Sea ice from HadCM3 simulations of 140 ka and 21 ka. A description of the HadCM3 simulations, the justification for this choice of approach, and a discussion on how these SSTs may affect the result is also presented in Chapter 2. Vegetation is kept at pre-industrial distribution, which could have an effect on the results since studies have shown the importance of the albedo-vegetation feedback during glacials, particularly for the PGM (Colleoni et al., 2009b; Crucifix and Hewitt, 2005; Stone and Lunt, 2013; Willeit et al., 2024).

The interactive ice sheet model domain covers the whole NH, including the North American, Greenland and Eurasian ice sheets. The results of the work in Chapter 2 showed that the initial ice sheet model conditions used in the glacial maxima simulations overwhelmingly determined the configurations of the final ice sheets due to the ice-albedo feedback, and that the climate at the glacial maxima had an opposite impact on the difference in NAIS ice volume between the LGM and PGM to what was expected. This suggests that the evolution of the climate and the ice sheets leading up to the glacial maximum are important in determining the configurations

of the ice sheets at the glacial maximum. We, therefore, chose to initialise the LGM and PGM simulations from the respective ice sheet reconstructions available to ensure realistic ice sheet geometry for each period, accounting for the evolution of the climate and ice sheets prior to the glacial maxima. With this approach, we can examine how the differences in ice geometry and background climate between the two time periods affect the sensitivity to the model parameters that control key earth system feedbacks (e.g. ice-albedo feedback, ice-elevation feedback and climate-ice sheet interactions). The LGM orography was initiated from the GLAC-1D reconstruction (Briggs et al., 2014; Ivanovic et al., 2016; Tarasov et al., 2012; Figure 3.17a) and the PGM was initiated from a combination of a simulated NROY PGM NAIS from the ensemble in Chapter 2 (xpkyn) and a simulated PGM EIS by Pollard et al., (2023) (Figure 3.18a), and their corresponding topographies.

3.3.3.2 Ensemble design

As well as the initial ice sheet conditions, modelled ice sheet volumes and areas are also sensitive to a number of parameterisations related to climate processes, surface mass balance and ice sheet dynamics. To assess this sensitivity, we design an ensemble using maximin Latin Hypercube Sampling (Williamson, 2015; Santner et al., 2003), that consists of 120 combinations of 12 uncertain climate and ice sheet model parameters, varied over a specified range (Table 3.1). These 120 simulations are each run with the LGM and PGM initial conditions described in Sect. 3.3.3.1, resulting in 240 total simulations. Each was integrated for 500 climate years (5000 ice sheet years). Since we start from a glacial maximum configuration and spun-up internal temperatures, this is enough time for the ice sheets to (i) reach equilibrium (or close to it), and (ii) give an indication of whether the parameters are producing reasonable ice sheets and form ice streams. Each simulation took around 35 hours running on 8 cores to complete (~280 core hours).

The choice and range of parameters is adapted from several previous ensemble studies (Gandy et al., 2023; Gregoire et al., 2011; Patterson et al., 2024; Sherriff-Tadano et al., 2024). We vary three uncertain parameters related to ice sheet dynamics in BISICLES; the basal friction coefficient in the power law relation (*beta*), the till water drain factor (*drain*), and the sub-shelf melt constant (*c*). The *elevcon* parameter controls the magnitude of the height adjustment applied and the remaining parameters control the climatic conditions and ice albedo in the simulations.

Table 3.1: Parameters varied in the ensemble and the ranges sampled.

Parameter	Unit	Ensemble range	Notes
Weertman friction coefficient, *beta*	Pa $m^{-1/3}$ $a^{1/3}$	20,000 – 60,000	Represents the resistance of ice at the base to motion. The higher the value, the stronger the friction between the ice and the bedrock over which it is flowing.
Till water drain factor, *drain*	yr^{-1}	0.01 – 0.05	Controls the rate of vertical till-stored drainage and therefore water pressure in the till layer. The higher the value, the more rapidly till water is removed.
Sub-shelf melt constant, *c*	m yr^{-1} $^oC^{-1}$	1 – 50	Characterises the relationship between ocean thermal forcing and sub-shelf melt rate
Lapse rate, *tgrad*	K m^{-1}	-0.01 – -0.002	Air temperature lapse rate used during downscaling to the ice sheet surface. The more negative the number, the stronger the lapse rate effects (Smith et al., 2021b)
Sensitivity of bare ice albedo, *daice*	K^{-1}	-0.4 – 0	The sensitivity of bare ice albedo to surface air temperatures above the melt threshold (mimics darkening of the surface due to melt ponds forming in summer). The minimum value reduces the bare ice albedo to as low as 0.15 (Smith et al., 2021b)
Surface snow density threshold, *fsnow*	kg m^{-3}	350 – 800	The density threshold for snow beyond which the surface is regarded as bare ice. The higher the value, the higher the albedo for denser snow, tending to increase ice sheet albedo overall (Smith et al., 2021b)
Sensitivity to surface grain size, *av_gr*	μm^{-1}	0 – 0.01	The sensitivity of the surface snow albedo to increasing grain size. The higher the value, the more the albedo decreases over time, reducing snow albedo overall (Smith et al., 2021b)

Relative humidity threshold, *rhcrit*	Pa^{-1}	0.6 – 0.9	The threshold of relative humidity above which large-scale clouds form (Smith, 1990)
Precipitating ice fall out speed, *vf1*	$m\ s^{-1}$	1 – 2	The precipitating ice fall out speed (Heymsfield, 1977)
Cloud liquid water conversion rate, *ct*	s^{-1}	$5x10^{-5}$ – $4x10^{-4}$	Rate of conversion of cloud liquid water droplets to precipitation (Smith, 1990)
Cloud liquid water threshold, *cw*	$kg\ m^{-3}$	$1x10^{-4}$ – $2x10^{-3}$	The threshold of cloud liquid water (over land) above which precipitation forms (Smith, 1990).
Height correction, *elevcon*		1 – 1.5	Scaling factor for the height of the vertical levels read by the ice sheet model (this study)

3.3.4 Evaluating the ensemble

To evaluate the performance of the LGM ensemble members and find sets of model parameters that produce NROY ice sheet configurations, we employ an implausibility metric. This allows a robust comparison of model output to empirical evidence and previous modelling studies, taking into account their uncertainties. The implausibility metric considers constraints on LGM ice volume, ice extent and global mean air temperature (GMT) derived from studies using palaeo-records of past climate and ice sheets and numerical modelling (Table 3.2). Since the PGM is poorly constrained in these areas, we are unable to evaluate the performance of the PGM ensemble in the same way. Instead, we opt to select the PGM ensemble members that correspond to the selected LGM members to enable comparison, see whether the same parameter values produce plausible PGM ice sheets based on known configuration differences and allow us to learn more about the PGM without the restriction of uncertain constraints.

The NAIS area is evaluated based on the southern extent of the ice sheet reconstructed by Dalton et al., (2020), within ± 3 times the area of the ice lobes (Figure 3.2a). We set this envelope of uncertainty (based on ice-lobe area) to account for known common model biases, such as over-estimated Alaskan ice, and limitations such as the inability to simulate the

dynamic ice lobes (Patterson et al., 2024). Similarly, the plausible range of the EIS is considered to be within ± 3 times the area of the BIIS (Figure 3.2b) based on the reconstruction from Hughes et al., (2016). We chose to not tune to meet BIIS constraints since none of our simulations maintain ice over this area (see Sect. 3.4.1) and we do not want to compensate for/hide this limitation by over-estimating ice elsewhere. The GMT range is determined from different estimated levels of LGM cooling, and their uncertainties, relative to a pre-industrial GMT of 13.7 ± 0.1 °C (1880-1900; NOAA National Centers for Environmental Information, 2023; Sherriff-Tadano et al., 2024).

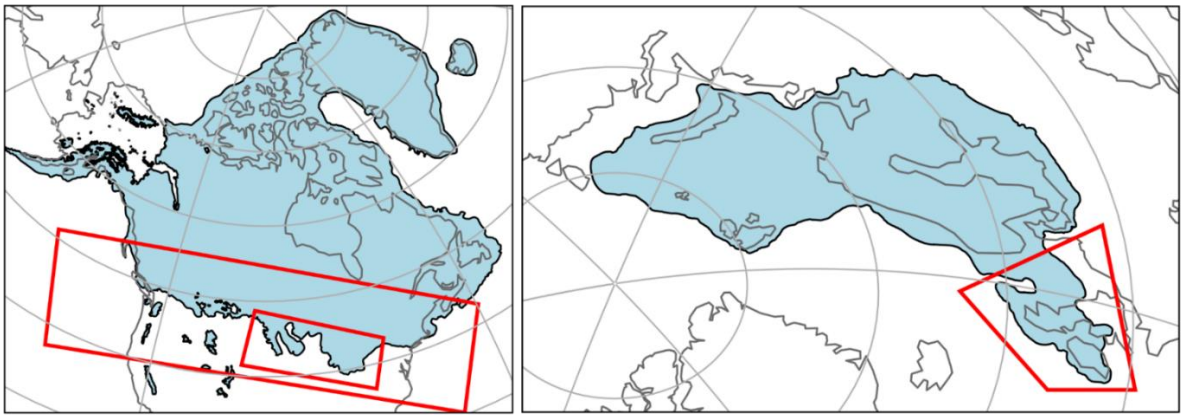

Figure 3.2: Reconstructions used in the implausibility metric. (a) North American ice sheet extent from Dalton et al., (2020); the large red box delimits the southern extent footprint used in the implausibility metric; the smaller red box indicates the area of the lobes used to calculate the range of plausible values. (b) Eurasian ice sheet extent from Hughes et al., (2016); the red box indicates the area of the BIIS used to calculate the range of plausible ice areas.

Table 3.2: The ranges of plausible values for ice sheet volume and extent (expressed in metres global mean sea level equivalent; m s.l.e.), and global mean surface air temperature (GMT; given in °C) used in our implausibility metric, and references to the published work used to derive these ranges.

Metric		Plausible range	References
North American ice sheet (NAIS)	Volume (m s.l.e.)	68 – 88	Abe-Ouchi et al., 2015; Gregoire et al., 2012; Lambeck et al., 2017; Moreno-Parada et al., 2023; Peltier et al., 2015; Simms et al., 2019; Tarasov et al., 2012
	Area (km^2)	$2.0 \times 10^6 – 7.16 \times 10^6$	Dalton et al., 2020
Eurasian ice sheet (EIS)	Volume (m s.l.e.)	13 – 23.5	Abe-Ouchi et al., 2015; Hughes et al., 2016; Lambeck et al., 2006; Patton et al., 2016; Peltier et al., 2015; Tarasov et al., 2012
	Area (km^2)	$3.83 \times 10^6 – 8.02 \times 10^6$	Hughes et al., 2016
Global Mean surface air Temperature (GMT; °C)		5.6 – 12.1	Annan et al., 2022; Annan and Hargreaves, 2013; Holden et al., 2010; Liu et al., 2023; Osman et al., 2021; Schmittner et al., 2011; Schneider von Deimling et al., 2006; Zhu et al., 2022

3.3.5 Gaussian process emulation and Sobol′ sensitivity analysis

To determine which of the model parameters had the most influence on the uncertainty in modelled ice sheet configurations, and whether this differed for each of the NH ice sheets and each glacial maxima, we perform a Sobol′ Sensitivity Analysis (Saltelli, 2002; Sobol′, 2001) on four diagnostics for each ensemble; NAIS ice volume, NAIS southern area, EIS ice volume and EIS area. This produces a first order sensitivity index which measures the contribution to the output variance by each model parameter alone; a second order index which measures the contribution from interactions between two parameters and; a total order index which is the contribution by a model parameter as a result of its first order sensitivity and all higher order interactions. An index value of 0.05 is often used as the threshold above which a parameter is considered to have an important influence on the output variance (Zhang et al., 2015).

The Sobol′ analysis requires a uniform sample of thousands of model inputs, for example, generated following Saltelli's extension of the Sobol′ sequence, which are outside of our initial

parameter sample. This would therefore require additional evaluations of the model, which would require significant additional computational resources. To this end, we train Gaussian Process (GP) emulators (Kennedy and O'Hagan, 2001; Oakley and O'Hagan, 2004) on each of the four diagnostics from the two 120 member ensembles. These emulators are then employed to evaluate the additional parameter sets generated by the Sobol′ sequence. Using this sequence and the emulators, we are able to generate and evaluate more than 200,000 samples in only a few minutes, a number which would have been computationally intractable using FAMOUS-BISICLES directly. Since we use a complex model with a large number of uncertain parameters, a sample of this size is necessary in order to increase the reliability of the Sobol′ analysis.

To evaluate the performance of our emulators and ensure their predicted output is sensible compared to the modelled output, we perform a Leave-One-Out Cross-Validation (LOOCV) on each emulator (Bastos and O'Hagan, 2009; Rougier et al., 2009). In general, leave-k-out cross-validation involves splitting the dataset of input parameters and output diagnostics into separate training sets and testing sets. The emulator is trained using the training set and then fed the input parameters of the testing set to evaluate. The values it then predicts can be compared to the actual modelled values. In the case of the LOOCV, all but one set of inputs and outputs are used as the training set and the emulator is used to predict the output left out. This process is then repeated for each of the 120 model outputs. We found that, compared to the modelled outputs, seven of the ensemble input parameter sets consistently produced poor predictions for four or more of the eight diagnostics. Therefore, to improve the quality of the emulator fit, we removed these seven inputs, re-trained the emulators, and once again performed the LOOCV. The predicted values (and their 95% credible intervals) compared to the modelled values for each emulator are shown in Sect. 3.6.4 (Figure 3.22). Overall, between 84-93% of the predicted intervals contain the true model output, which we determine is enough for the purposes of the Sobol′ analysis.

3.4 Results and discussion

3.4.1 Initial ensemble

After running the ensembles of simulations for the LGM and PGM, we obtain two sets of 120 simulations with a wide spread of NH ice sheet configurations. The ensemble mean volume of the NAIS at the LGM is 37.6 m s.l.e., with a smaller mean at the PGM of 22.8 m s.l.e.. In contrast, the LGM has a smaller mean EIS volume of 5.39 m s.l.e. compared to 12.6 m s.l.e. at the PGM. Both ensembles have a similar mean Greenland ice sheet volume of ~7 m s.l.e.. The

range in ice volume and extent across the ensembles are shown in Figure 3.3 which reveals a larger spread in NAIS volume at the LGM but a larger EIS spread at the PGM. Figure 3.3c shows that the LGM simulations tended to have more extensive ice across the Laurentide ice sheet and in the area joining the Laurentide to the Cordilleran ice sheet, but that the PGM had more extensive ice to the south and east of the EIS and over Alaska while maintaining an ice free corridor between the Laurentide and Cordilleran. Whilst these relative volumes and extents between the LGM and PGM are consistent with knowledge of the different NH ice sheet configurations at each glacial maxima, the average values are much lower than current estimates suggest. This is due to a large proportion of the ensemble members deglaciating to very low or zero ice extent (Figure 3.3a and 3.3b).

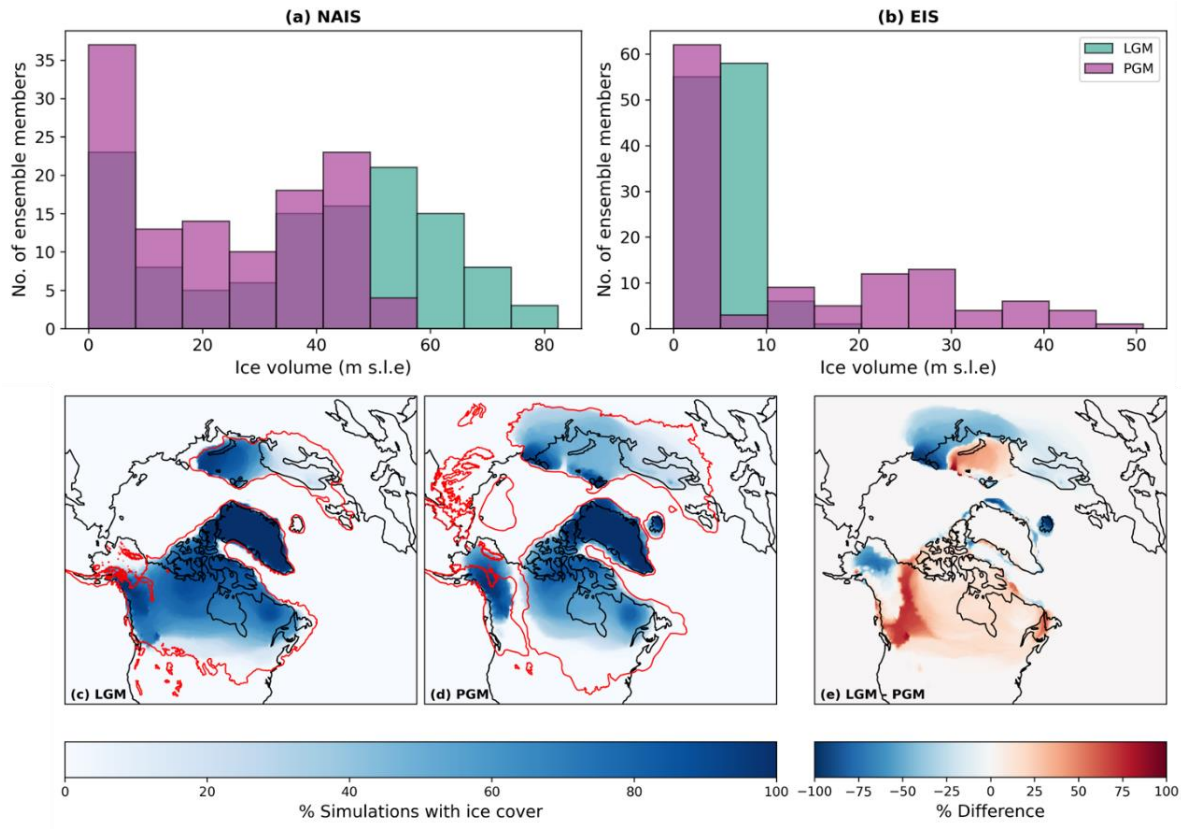

Figure 3.3: Histograms of the distribution of (a) North American and (b) Eurasian final ice volumes across the LGM and PGM ensembles and percentage of the ensemble members that had ice over areas of the domain for (a) the LGM (with the extents of Dalton et al., (2020) and Hughes et al., (2016) in red), (b) the PGM (with the Batchelor et al., (2019) extent in red), and (c) the difference between the LGM and PGM ensembles.

In particular, all simulations lack a BIIS and most display a poor match to reconstructions over Scandinavia and in the southern margin and eastern marine extent of North America. This is due to large negative SMB values over these regions (Figure 3.4) causing rapid deglaciation, with the BIIS disappearing in 600 ice sheet years or less. This is a similar result to Bradley et

al., (2024) who used a GCM to simulate the SMB across the LGM ice sheets. Their simulations showed large ablation areas across the BIIS, the southern margin of Scandinavia and the southern, Pacific and Atlantic margins of the NAIS, but low melt rates across the Barents-Kara ice sheet and Greenland. Whilst they did not use a dynamical ice sheet model, they concluded that if this SMB pattern was applied to one, it would very likely drive rapid retreat of the southern margins of both ice sheets.

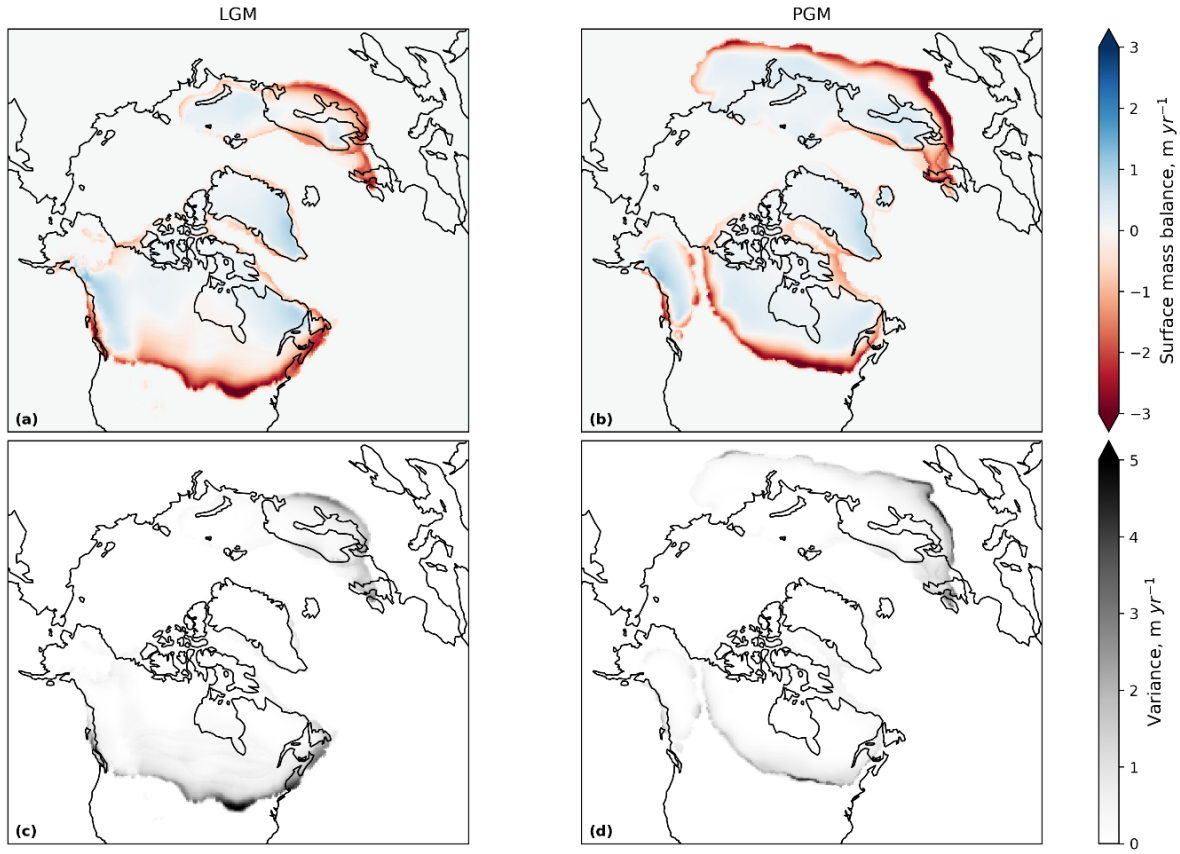

Figure 3.4: Ensemble mean surface mass balance and variance at ice sheet year 200 for (a) and (c) the LGM and (b) and (d) the PGM.

This result could reflect the asynchronous timing of the local maxima of the NH ice sheets since, for example, there is evidence that much of the NAIS reached its maximum extent at ~25 ka (Dalton et al., 2022, 2023) and the BIIS reached it maximum at ~25-23 ka before starting its retreat at ~22 ka due to a warming trend caused by a change in orbital parameters between 26–21 ka (Clark et al., 2022; Hughes et al., 2016). However, these reconstructions of the NAIS and BIIS still suggest there was extensive ice over these regions at 21 ka even if not at their maxima. In addition, Bradley et al., (2024) also performed a simulation using boundary conditions for 26 ka and obtained a similar result to 21 ka. They therefore concluded that the too negative SMBs are likely a result of biases in the simulated climate or ice sheet reconstruction, a highly non-equilibrated climate and ice sheet at the LGM, and/or the need to

retune the model for LGM climate conditions (as also shown to be necessary by Gandy et al., 2023). Indeed, many other numerical modelling studies have also found it difficult to maintain extensive ice in these regions using a range of different models, boundary conditions and model parameters (van Aalderen et al., 2023; Quiquet et al., 2021a; Scherrenberg et al., 2023b; Sherriff-Tadano et al., 2024; Ziemen et al., 2014; Zweck and Huybrechts, 2005).

In this present study, the compromise with using a coarse resolution model is that it is not able to accurately capture some of the smaller scale atmospheric circulation effects that influence precipitation and temperature patterns. This leads to biases in the modelled climate that result in some areas of the ice sheets not matching reconstructions. For example, simulations of the NAIS have grown too much ice over Alaska and the southern extents are not extensive enough (Patterson et al., 2024; Sherriff-Tadano et al., 2024; Ziemen et al., 2014). This is likely a result of an underestimation of the stationary wave effect on temperature patterns; a common feature when using low resolution atmospheric models (Abe-Ouchi et al., 2007; Ganopolski et al., 2010; Liakka et al., 2012; Roe and Lindzen, 2001).

3.4.2 Non-implausible parameter sets

We apply the implausibility metric, described in Sect. 3.3.4, to the ensemble of LGM simulations to see if there are any sets of model parameters that produce plausible ice sheets. All ensemble members have a GMT that falls within the range included in the implausibility metric due to the control in surface conditions imposed by the prescribed SSTs. The LGM simulations range from 6.34–9.20 °C and the PGM from 7.12–10.12 °C. This suggests that the SSTs used produce plausible LGM and PGM climates, causing a warmer PGM compared to the LGM, which is also in agreement with palaeo reconstructions and other dynamical models (Bintanja et al., 2005; Colleoni et al., 2016). However, due to ice extent and volume, only two LGM simulations are NROY (labelled as *NROYa* and *NROYb*). Furthermore, we acknowledge the risk that our evaluation metric may be too tightly constrained by uncertain palaeo reconstructions; ice sheet volume, in particular, is not well known. We therefore also apply the extent and volume constraints separately to explore additional plausible ice sheet configurations, especially since the volume constraint is still very uncertain and our minimum volume for the NAIS is less lenient than limits that have been used previously (e.g. Gandy et al., 2023; Sherriff-Tadano et al., 2024). This results in the selection of two more ensemble members; one that meets only the ice extent criteria (labelled as *NROY extent*) and one that meets only the ice volume criteria (labelled as *NROY volume*). All four of these NROY simulations are shown in Figure 3.5, with the corresponding four PGM simulations shown in Figure 3.6.

The volumes and extents of the NROY simulations are outlined in Table 3.3. Overall, the LGM NROY simulations show a good match to the reconstructed extents of the LGM ice sheets and the equivalent PGM simulations display a smaller NAIS and larger EIS in line with empirical evidence and previous studies. Whilst the equivalent PGM simulations show a smaller NAIS than the extent of Batchelor et al., (2019), this reconstruction represents the maximum MIS 6 extent (190-132 ka) and therefore is likely larger than the 140 ka ice sheet would have been, particularly for the NAIS. These four NROY model simulations suggest the NAIS was ~25 m s.l.e. smaller at the PGM compared to the LGM, and the EIS ~24-27 m s.l.e. larger. There are very few existing reconstructions of the PGM ice sheets and none produced using a coupled climate-ice sheet model. Our simulations perform well in comparison to these reconstructions (Figure 3.7) and thus provide a great alternative for use as boundary conditions in future climate and sea level modelling studies.

Table 3.3: Ice sheet volumes and extents at the end of the 5000 ice sheet years for the two NROY LGM simulations and the corresponding PGM simulations.

	LGM				PGM			
	NROYa	*NROYb*	*NROY extent*	*NROY volume*	*NROYa*	*NROYb*	*NROY extent*	*NROY volume*
NAIS Volume (m s.l.e.)	72.6	76.9	64.7	82.4	48.1	52.2	41.5	57.5
EIS Volume (m s.l.e.)	14.2	17.0	12.7	13.7	38.7	44.0	35.6	50.7
NAIS area (southern area) ($x10^6$ km^2)	14.2 (4.44)	13.9 (4.17)	12.4 (2.91)	13.1 (3.51)	10.9 (1.87)	10.8 (1.66)	9.31 (0.75)	10.1 (1.32)
EIS area ($x10^6$ km^2)	4.53	5.0	4.08	3.56	9.86	10.1	9.04	9.61

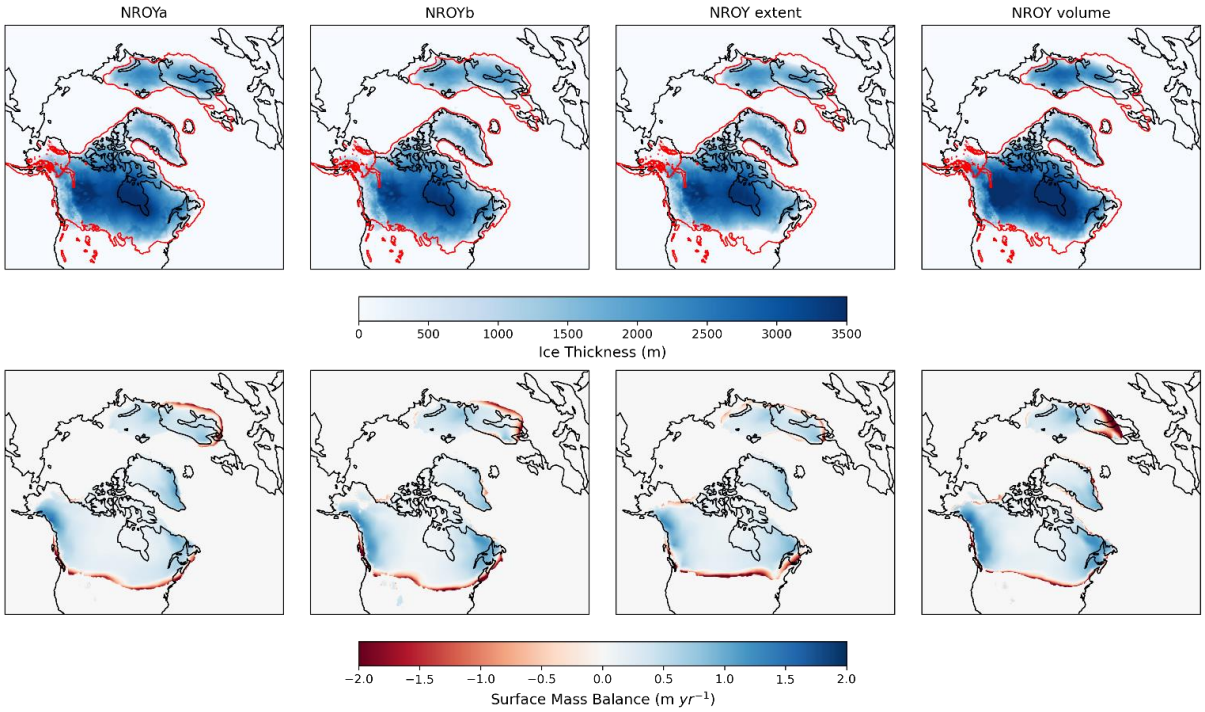

Figure 3.5: Final ice thickness and surface mass balance for the four NROY LGM simulations.

All NROY simulations still lack a BIIS, however, which suggests that biases in the climate model are the cause rather than model parameter values. Due to high rates of sub-shelf melt (~60-75 m yr^{-1}), the NROY simulations also lack ice shelves by the end of the 5000 ice sheet years, which could also have contributed to the underestimation of the eastern margin of the NAIS and the deglaciation of the BIIS (Scherrenberg et al., 2023b). However, there are not many constraints on the extent of ice shelves during the LGM or PGM since they leave few glaciological traces behind. There is some evidence that a large, thick ice shelf extended into the Arctic Ocean during the MIS 6 glaciation (Jakobsson et al., 2016; Svendsen et al., 2004) and during the last glaciation a thick ice shelf may have covered Baffin Bay (Couette et al., 2022). Similarly, the rate of sub-shelf melt is poorly constrained during past periods, however, since some studies have shown ocean driven melt to be important for the evolution of the marine based sectors of the NH ice sheets (Alvarez-Solas et al., 2019; Clark et al., 2020; Petrini et al., 2020), it may be useful to implement a more complex parameterisation or perform some additional sensitivity tests to explore this process further in future studies.

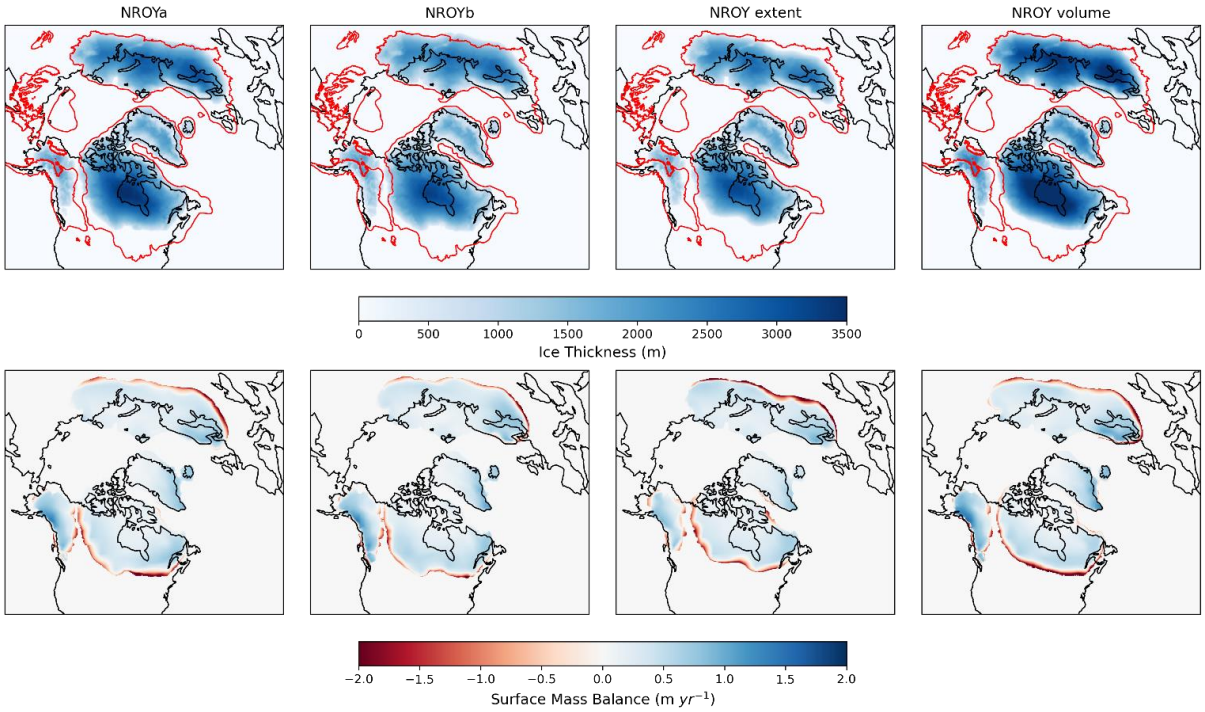

Figure 3.6: Final ice thickness and surface mass balance for the four NROY PGM simulations.

Despite difficulties in the past in obtaining a sufficient southern extent of the NAIS in lower resolution models, the *NROYa* and *NROYb* simulations do a relatively good job, only falling short of the Dalton et al., (2020) reconstruction by 3% and 9%, respectively. The two additional NROY simulations are less close to the reconstructed extent, however, and all four still fail to capture the ice lobe structures. This is because they are formed by extensions of terrestrial ice streams as a result of complex ice dynamics and subglacial processes (Jennings, 2006; Margold et al., 2018). They are also highly asynchronous, dynamic features resulting in their glacial maximum limits being very uncertain (Dalton et al., 2020; Margold et al., 2018). Therefore, it is not surprising that a relatively low resolution climate and ice sheet model with highly idealised subglacial environments is unable to resolve such features (Gandy et al., 2019; Zweck and Huybrechts, 2005).

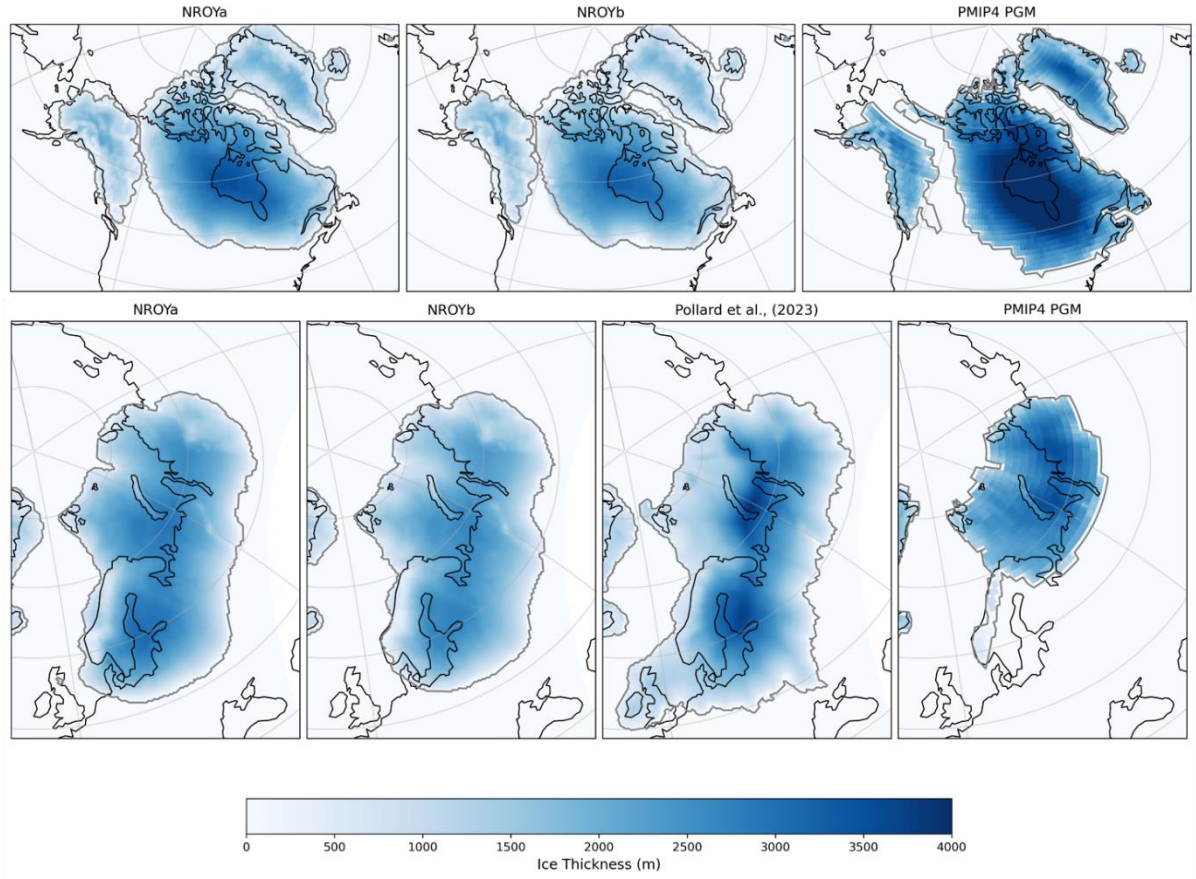

Figure 3.7: Comparison of the two NROY PGM simulations to other model reconstructions (Abe-Ouchi et al., 2013; Pollard et al., 2023).

The parameter values used in the two *NROYa* and *NROYb* simulations are in similar areas of the parameter space for all parameters except *tgrad* and *drain*, suggesting the ice sheets are fairly insensitive to these two parameters (Figure 3.23). Interestingly, Figure 3.8a and 3.8b show that, if considering the NAIS and EIS separately, there are five simulations that produce only a plausible NAIS but do not meet constraints for the EIS. Furthermore, as we have already seen, there are also simulations that produce plausible ice sheet extents but fall short on the volume and vice versa. Many of these simulations are situated in different areas of the parameters space than the two NROY simulations for most of the parameters (Figure 3.23). Figure 3.8c and 3.8d show that the *NROYa* and *NROYb* parameter sets also produce the largest PGM ice sheet extents in the ensemble but there are additional simulations that produce similar or larger volume ice sheets, which, in relation to the EIS, was not the case for the LGM. These results all suggest that both ice sheets and both time periods display different sensitivities to model parameters.

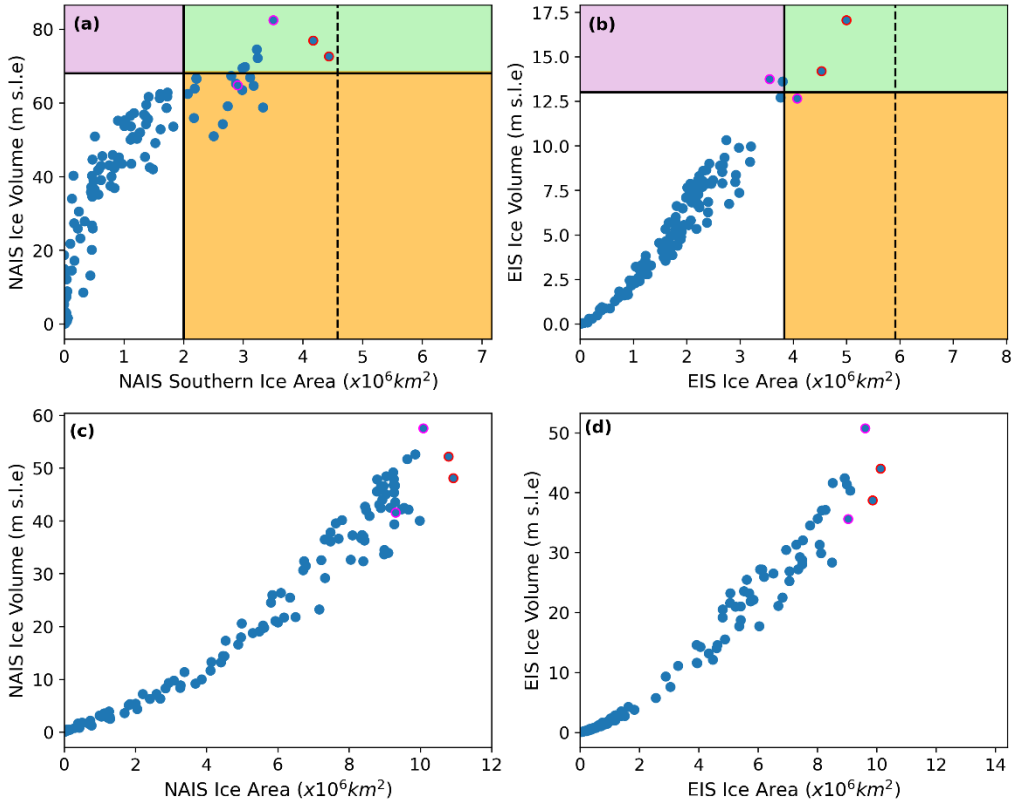

Figure 3.8: Results from the full ensembles of simulations showing (a) LGM North American ice sheet southern area versus volume and (b) LGM Eurasian ice sheet area versus volume. The solid lines show the minimum values used in the implausibility metric for area and extent and the dotted line shows the actual extent of the ice sheet reconstructions. Simulations that fall within the green box satisfy area and volume constraints for each individual ice sheet, the orange box indicates they satisfy the area constraints only and purple only the volume constraints. The points outlined in red are the two NROY simulations (i.e. fall into the green box for both ice sheets) and the points outlined in pink are the additional *NROY extent* and *NROY volume* simulations. Panels (c) and (d) show the equivalent results for the PGM ensembles without the constraints.

3.4.3 Sensitivity to parameters

To examine and quantify these different sensitivities we perform the GP emulation and Sobol′ Sensitivity analysis described in Sect. 3.3.5. Due to the performance of the emulators leading to some uncertainty in the predicted values and therefore the values of the Sobol′ indices, we are careful to not over interpret the results and only analyse the highest values and largest differences. We also use emulation to isolate the relationship between certain influential parameters and ice sheet volume in which the emulator predicts the model output across a sample of the range of one parameter whilst all other parameters are held at their midpoint values.

The first and second order sensitivity indices for the NAIS and EIS volumes for the LGM and PGM are shown in Figure 3.9a and 3.9b and the difference in sensitivities between the two ice sheets in Figure 3.9c. The analysis indicates that the ice sheets were relatively insensitive to the parameters *vf1, drain, ct, rhcrit* and *c*. The insensitivity to the value of the sub-shelf melt is unsurprising despite previous studies reporting a high sensitivity of the Antarctic and Eurasian ice sheets (Alvarez-Solas et al., 2019; Berdahl et al., 2023; Berends et al., 2023). This is because the simulations lost their ice shelves fairly soon into the model run due to either high rates of sub-shelf melt resulting from the large values of *c*, or large ablation rates as a result of other climate model parameter values.

The most influential parameters in all aspects are *fsnow* and *av_gr*, which control the albedo of the ice sheet, with larger values of *fsnow* and smaller values of *av_gr* leading to larger ice sheets. The third albedo parameter, *daice*, is also important, particularly for the NAIS, having a positive correlation with ice sheet size. However, as in the case of *NROY extent*, the value of *daice* is less important provided that *fsnow* is high and *av_gr* is low since these produce a high enough albedo to maintain an extensive ice sheet on their own (Figure 3.23). These three parameters also have important interactions with other parameters and each other. This importance of the albedo parameters is consistent with previous studies investigating the sensitivity of the NAIS to uncertain parameters (see Chapter 2 and Gandy et al., 2023; Sherriff-Tadano et al., 2024), but our detailed Sobol′ sensitivity analysis is able to not only identify the most important parameters but also quantify the importance of all the other parameters. Furthermore, the inclusion of the EIS in our analysis reveals the importance of some other parameters for the configuration of the EIS. This includes *beta*, *cw* at the LGM, and, despite the value of *tgrad* being in different areas of the parameter space for the NROY simulations, this analysis shows that the EIS is highly sensitive to this parameter, especially for the PGM. The NAIS is also sensitive to new parameters introduced in this study that were not tested in Gandy et al., (2023) or Chapter 2. This includes *beta*, and for the LGM the volume is also impacted by the value of *elevcon*.

Here we discuss some of the possible reasons these four parameters (*elevcon, cw, tgrad and beta*) could have an effect on the various ice sheets. However, further simulations and testing would need to be carried out to come to any conclusions. One reason that the LGM NAIS shows a particular sensitivity to ***elevcon*** could be related to the size of the ice sheets since it affects higher ice elevations more and, indeed, the value of the Sobol′ index for this parameter is in line with the average thickness of each ice sheet. The fact that a larger value of *elevcon* leads to a larger NAIS (Figure 3.10a) but does not impact the size of the EIS could explain why

the ensemble produced more plausible North American ice sheets at the LGM but did not perform as well for the Eurasian ice sheet (Figure 3.8). It may also explain some of the difference in NAIS size between the LGM and PGM.

Similarly, the LGM EIS being more sensitive to the value of ***cw*** than the NAIS or either PGM ice sheet could explain why there are more simulations that produced larger volume Eurasian ice sheets at the PGM than the LGM, but the NAIS behaved similarly between both periods (Figure 3.8). *Cw* has a positive correlation with EIS volume up to a value of around 0.0012 kg m^{-3} (Figure 3.10b). Any increase above this does not appear to increase the ice volume much further. This could be because lower values of *cw* cause increased precipitation due to decreasing the threshold of cloud liquid water above which precipitation forms. This has a particular effect in summer leading to higher rainfall rates over the Northern Hemisphere continents which contributes to the surface melting of the ice sheets through the flux of heat from the rain to the ice. One reason the LGM EIS is particularly susceptible to this effect could be due to its smaller size. Precipitation is not downscaled onto elevation tiles in the coupling, rather the coarse atmospheric output is applied to the ice sheet model which leads to rainfall being spread across relatively large areas of the ice sheet, therefore affecting a large proportion of the LGM EIS (Smith et al., 2021b). Another reason could be related to the change in liquid cloud cover and its effect on the energy balance. The increased precipitation leads to a decrease in the fraction of cloud cover which would allow a higher receipt of incoming shortwave radiation, thus increasing the surface melt. However, the downwelling longwave radiation may also be decreased which would have the opposite effect, decreasing the absorbed energy. Since the accumulation zone usually has a high albedo, reflecting much of the incoming solar radiation, the SMB of this area is mostly controlled by changes in the longwave fluxes. In contrast, the low albedo ablation zone is largely impacted by the shortwave radiation budget in the summer melt season. This latter process has been found to be dominant in studies of the Greenland ice sheet, with reduced cloudiness contributing to its mass loss and increasing its sensitivity to warming (Hofer et al., 2017; Izeboud et al., 2020; Mostue et al., 2024; Ryan et al., 2022). Again, due to its smaller size, a large proportion of the LGM EIS is under ablation (54% compared to around 35% for the other ice sheets in Figure 3.4), potentially explaining why it is so sensitive to changes in cloud cover.

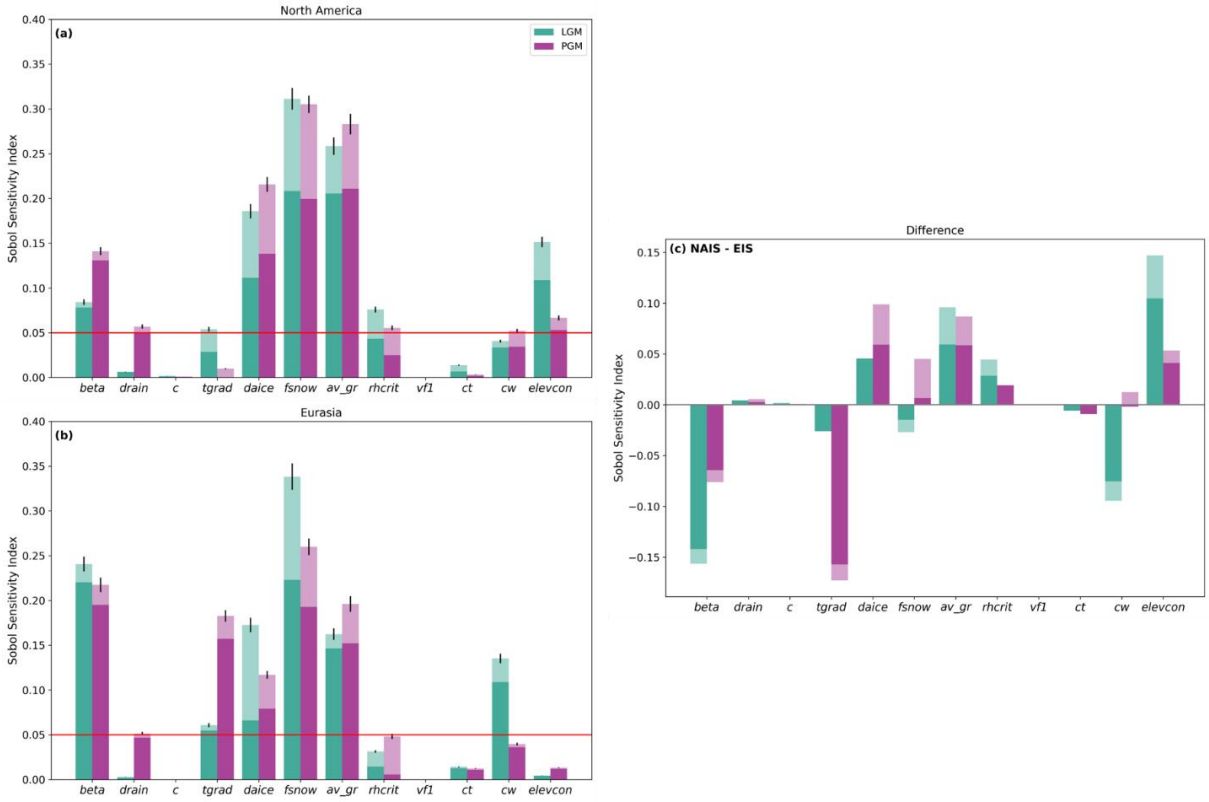

Figure 3.9: The Sobol′ sensitivity index of the ice volume for each parameter for (a) the North American ice sheet and (b) the Eurasian ice sheet. (c) The difference in sensitivity indices between the North American and Eurasian ice sheets. The darker colour represents the first order index and the lighter colour the second order index (together showing the total sensitivity). The variance of the Sobol′ indices plus the mean emulator variance is indicated by the black error bars. The red line indicates the index value of 0.05, above which the sensitivity is significant.

PGM EIS is much more sensitive to the value of ***tgrad*** than the other ice sheets. More negative values of *tgrad* cause a stronger temperature-elevation feedback, resulting in warmer temperatures at lower elevations. This is going to have the largest impact on ice sheets with larger ablation areas. Many of the simulated PGM Eurasian ice sheets collapse (Figure 3.3b) as a result of the larger ice sheet being more unstable due to the larger GIA feedback. Therefore, many of these simulations will have strong ablation over the Eurasian ice sheet that increases throughout the run, making it more sensitive to *tgrad* and the temperature-elevation feedback.

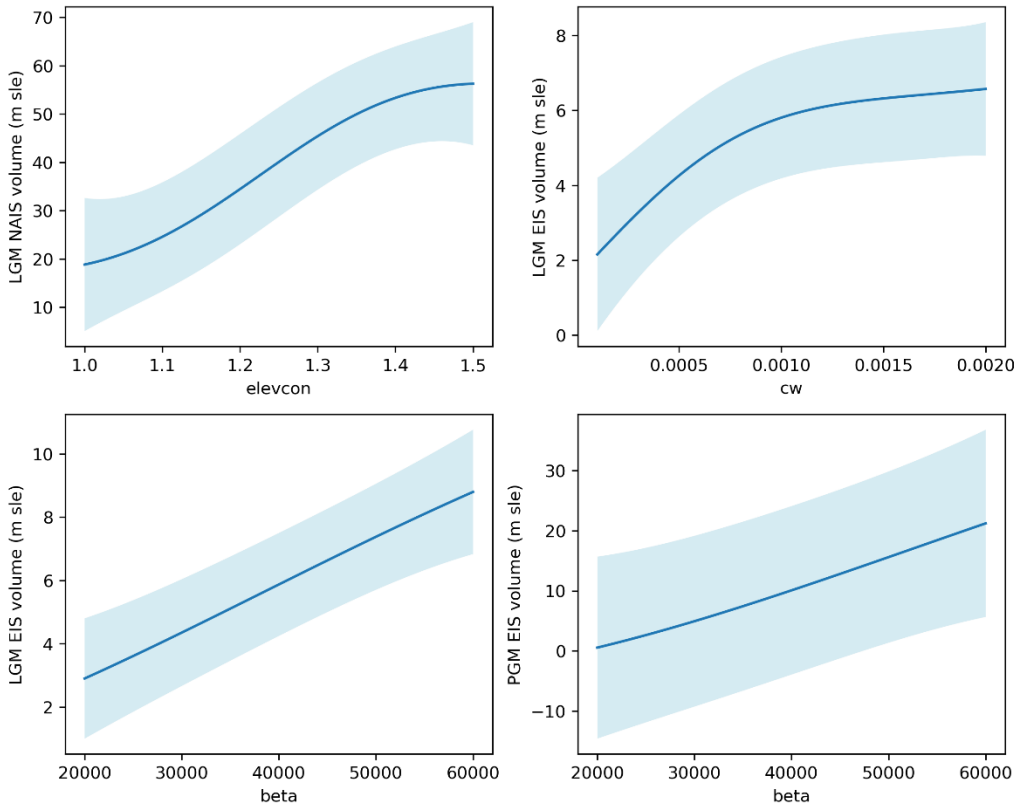

Figure 3.10: The relationship between emulated mean ice sheet volumes and (a) *elevcon* , (b) *cw* , (c) and (d) *beta* a The 95th percentiles are shown by the blue shaded region.

In addition, ***beta*** has a positive correlation to the size of the Eurasian ice sheet at both the LGM and PGM (Figure 3.10c and 3.10d) but does not have as much of an impact on the NAIS which could also explain some of the different behaviours seen between both ice sheets. *Beta* is also the only parameter that causes a large difference in the sensitivity indexes of volume and extent, with the ice volume being much more sensitive (Figure 3.11a). This could explain why the *NROY extent* simulation falls short of the volume constraints since it has a relatively low beta value (Figure 3.23). This also supports the idea that reduced basal friction results in more ice mass loss from the Eurasian ice sheet compared to North America since faster flow from the interior of the ice sheet to the more extensive marine margins causes a larger discharge of ice across the grounding line where it is calved or lost by sub-shelf melting (Figure 3.11b and 3.11c). This therefore affects the volume and thickness of the ice sheet but not so much the extent since ice already reaches the edge of the continental shelf (Blasco et al., 2021; Scherrenberg et al., 2023a; Sherriff-Tadano et al., 2024). Scherrenberg et al., (2023a) and Quiquet et al., (2021) show a similar impact of basal friction on ice sheet volume compared to extent at the LGM but also show that the thinner ice sheets, larger ablation area and increased ice velocities, caused by lower basal friction led to a faster deglaciation. Interestingly, both of the *NROYa* and *NROYb* simulations have lower values of *beta* than the five additional

simulations that produce a plausible NAIS but not EIS. This suggests that the right combination of parameters, especially in regard to the albedo parameters *fsnow*, *av_gr* and *daice*, and the interactions between parameters, can compensate for the faster flow and are thus more important for the size of Eurasia (Figure 3.23).

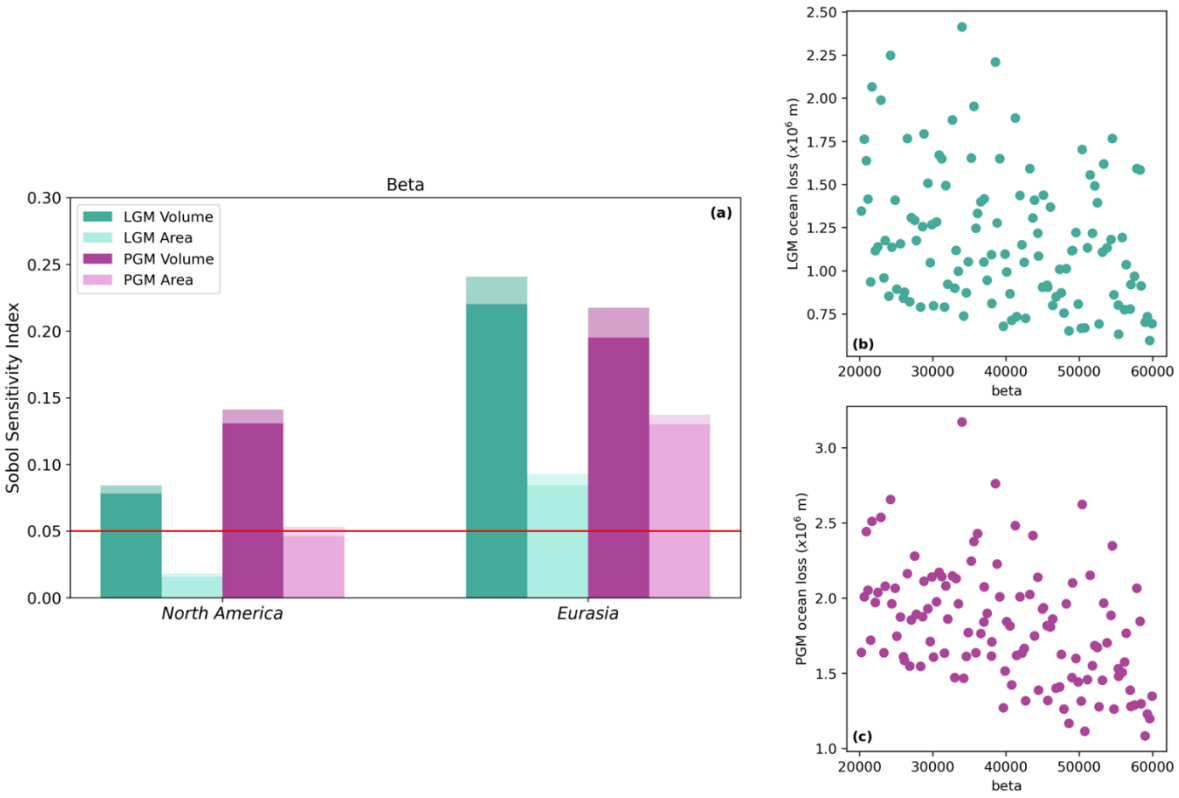

Figure 3.11: (a) Sobol′ Sensitivity Indices for the ice volume and extent at the LGM and PGM for the parameter *beta* and (b) LGM and (c) PGM total ice loss to the ocean (calving + sub-shelf melt) versus the value of *beta*.

3.4.4 Ice dynamics

The representation of ice streams in the simulations was updated from the previous FAMOUS-BISICLES simulations of the NAIS (Sherriff-Tadano et al., 2024) by performing the sensitivity tests and internal temperature spin-up detailed in Sect. 3.3.2. The velocity of areas of ice streaming in the NROY simulations range from a few hundred m yr^{-1} to 5000 m yr^{-1} which is a similar range to what has been observed on present day Antarctica and Greenland (Joughin et al., 2010; Rignot et al., 2011). We asses to what extent the modelled ice streams in the *NROYa* and *NROYb* simulations match empirical reconstructions by performing a qualitative comparison to LGM reconstructions of the Laurentide ice streams (Figure 3.12a; Margold et al., 2018) and the Eurasian ice streams (Figure 3.13a; Patton et al., 2017). For the Laurentide ice sheet, the locations of many of the ice streams show good agreement, particularly in NROYb (Figure 3.12b and 3.12c). Using the numbers and names used in Margold et al., (2018)

this includes; (1) Mackenzie Trough, (18) Amundsen Gulf, (123) Massey Sound, (129) Prince Gustaf Adolf Sea, (126) Smith Sound/Nares Strait, (22) Lancaster Sound, (23) Cumberland Sound, (24) Hudson Strait, (45) Notre Dame Channel, (133) Placentia Bay-Halibut Channel, (25) Laurentian Channel, (131) The Gully and (134) Northeast Channel IS. There are also areas of general streaming where many smaller ice streams are found (numbers 108-116 and 167-170). One major ice stream that is not very active in these simulations is (19) M'Clure Strait and there is a poor representation of ice streaming along the southern margin of the Laurentide ice sheet.

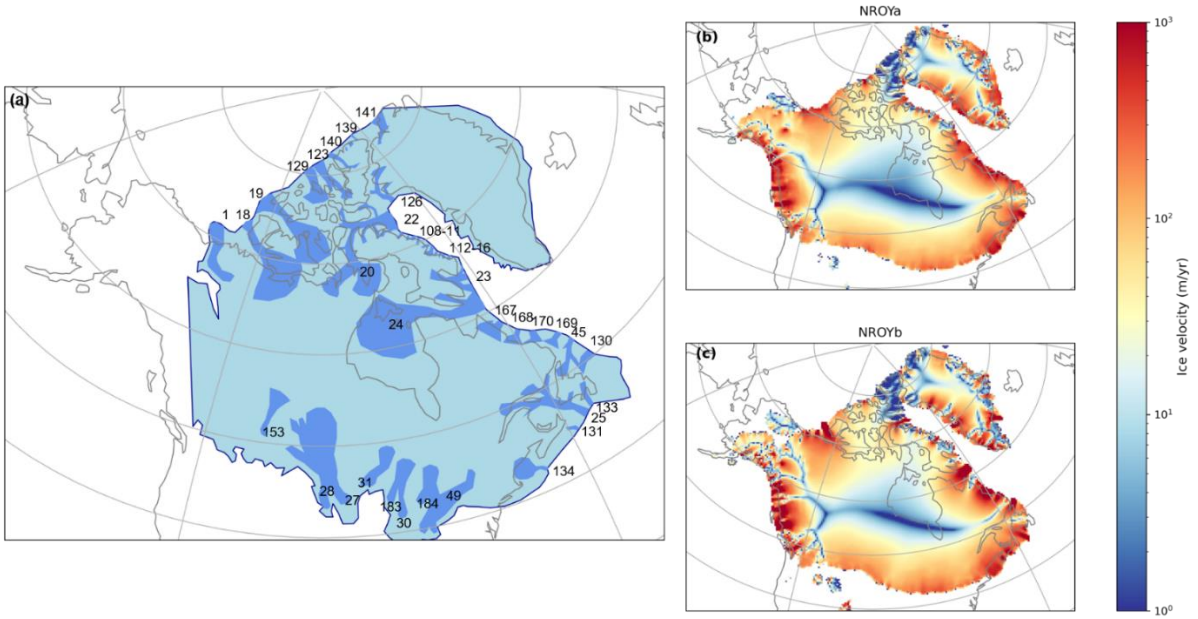

Figure 3.12: (a) Empirical reconstruction of the active LGM Laurentide ice sheet ice streams (adapted from Margold et al., (2018), and (b) NROYa and (c) NROYb ice velocities at the end of the 5000 year simulations.

The Eurasian ice sheet does not have as defined areas of ice streaming, nevertheless, some of the major ice stream features can be picked out (Figure 3.13b and 3.13c). The following numbers relate to those in Figure 3.13a and names are taken from van Aalderen et al., (2023) and Stokes and Clark, (2001). There is some streaming activity in the location of one of the major ice streams; (1) Bjørnøyrenna ice stream and (10) Svyataya Anna ice stream is relatively well represented. Some of the smaller ice streams are also modelled including; (2) Mid Norwegian, (8), (9), (11) and (12). However, other major and minor ice streams are not active in these simulations; (3) Norwegian Channel, (4) and (5) Baltic Sea, (6) Gulf of Bothnia and (7). In addition, since the BIIS is not present, neither are the ice streams in this region. Interestingly, there are active areas of ice streaming to the south of the Barents Sea that are not present in the reconstruction. This could be due to the formation of an area of ocean along the southern margin where the bedrock is below sea level, acting as a proglacial lake. This enables

the formation of ice shelves which have zero basal friction and therefore increase ice velocity (Sutherland et al., 2020).

There are no comparable reconstructions of PGM ice streaming due to difficulties in dating and the erasure of glaciological evidence following the Last Glacial advance. However, due to extent and topographic constraints on ice streaming, it is likely that ice stream location was similar across the marine margins of the ice sheets (Pollard et al., 2023). The simulated PGM NAIS velocity behaves similarly to the LGM but there is a lack of (1) Mackenzie Trough and a less pronounced (18) Amundsen Gulf as a result of the different configuration of the ice sheets in this area (i.e. the location of the ice free corridor between the Laurentide and Cordilleran ice sheets). However, there is more evidence of (19) M'Clure Strait in *NROYa* and more activity on the southern Laurentide margin (Figure 3.24). The PGM EIS velocity shows a more defined (3) Norwegian Channel ice stream and *NROYb* has a better representation of (10) Svyataya Anna, (11) and (1) Bjørnøyrenna ice stream than the LGM. There is still no streaming in the Baltic Sea but the PGM also shows activity in the South Barents Sea. There is also additional ice streaming in the Northeast where the PGM ice sheet extent further then at the LGM (Figure 3.25).

Whilst the value of *drain* does not affect the volume or area of the ice sheets (Sect. 3.4.3) it has a significant effect on the ice streaming/velocity of the simulations. The two NROY simulations display very different levels of ice streaming despite having similar configurations largely as a result of having different values of *drain*. *NROYa* has a higher value of 0.04 causing relatively quick drainage of the till water compared to *NROYb* which has a value of 0.01. Therefore, *NROYb* allows more sliding since the effective pressure is lower and thus so is the basal shear stress. The value of *drain* may become more important in simulations of deglaciations as ice streaming affects the stability of ice sheets and rate of retreat.

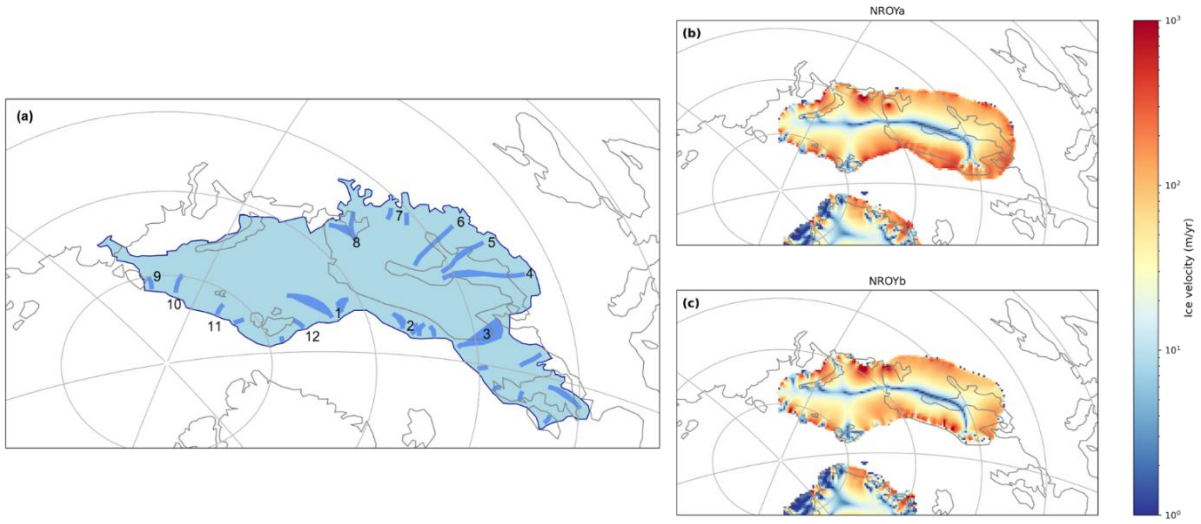

Figure 3.13: (a) Empirical reconstruction of the location of active LGM Eurasian ice sheet ice streams (adapted from Patton et al., (2017), and (b) and (c) ice velocities at the end of the 5000 year NROY simulations.

3.5 Conclusions

We ran ensembles of simulations using a coupled atmosphere-ice sheet model under LGM and PGM boundary conditions, varying uncertain climate and ice sheet model parameters. The model simulates plausible Northern Hemisphere ice sheets compared to empirical reconstructions and previous modelling studies, capturing the different configurations between the LGM and PGM. Through GP emulation and a Sobol′ sensitivity analysis, we find that the volume and extent of both the simulated Northern Hemisphere ice sheets are sensitive to the parameters that control their albedo. However, the North American ice sheet and the Eurasian ice sheet, and the two glacial maxima, display different sensitivities to certain other parameters. The size of the North American ice sheet at the LGM is sensitive to the value of the height correction parameter (*elevcon*), the size of the Eurasian ice sheet is sensitive to the value of the lapse rate parameter (*tgrad*) at the PGM and to the basal friction parameter (*beta*) at both glacial maxima. This result highlights that, as well as the use of different initial conditions for the LGM and PGM, the difference in final ice volume and extent between both periods may also be impacted by the choice of parameter values. In addition, it suggests that employing spatially varying parameter values could produce a better match to the empirical constraints of each ice sheet. Nevertheless, after applying an implausibility metric we find two sets of NROY parameter values that are plausible for both periods and both ice sheets, and we highlight an additional two simulations that we deem NROY depending on the criteria used. We also do some work to improve the representation of ice streaming in the glacial ice sheets and find that

our simulations produce a good match to empirical reconstructions of LGM ice streams, especially in simulations with lower values of till water drainage rate (*drain*).

The four NROY simulations produced in this study provide a good starting point for simulating and comparing the Last and the Penultimate deglaciations, which will be the focus of future work. However, since it has been shown in the past that models can be overtuned to certain climate conditions, it is not guaranteed that these parameter values will be conducive to the deglaciation of the ice sheets in line with empirical reconstructions and work will need to be done to test this and calibrate the model for both past and present conditions which will likely involve the use of emulators. In addition, there are some factors that were not considered or not well represented in this work that may become more important for the deglaciation. These include; the ice shelf melt parameterisation (Berends et al., 2023), the resolution at the grounding line (Gandy et al., 2021) and the representation of proglacial lakes (Sutherland et al., 2020). This study was also limited by the use of prescribed surface ocean conditions and pre-industrial vegetation and the absence of dust, all of which have been shown to initiate important feedbacks for ice sheet evolution (Ganopolski et al., 2010; Obase et al., 2021; Willeit et al., 2024). Current modelling capabilities prevented the use of a fully coupled atmosphere-ocean-ice sheet model with dynamic vegetation and dust for the large number of simulations run in this study, however as technological advances are made to enable this in the future, running similar simulations will provide useful information of the role of these other feedbacks on the evolution of the LGM and PGM ice sheets.

3.6 Appendices

3.6.1 Implementation of the *elevcon* parameter

elevcon affects the surface temperature and SMB during the height adjustment to ice sheet tiles in the following manner;

- The effective elevation of each tile is multiplied by the value of *elevcon*. A value of 1.10 (10%) means that the elevation of an 1800 m tile has been increased to 1980 m.
- Surface air temperatures and longwave radiation are downscaled to each increased elevation tile.
- Surface fluxes and SMB are calculated based on the downscaled variables and other variables from the original FAMOUS grid.

- The SMB and fluxes are then passed to the ice sheet and atmospheric models, but taken to represent the original tile elevation, not the increased elevation to which the surface temperature was actually downscaled. For example, the surface air temperature and SMB could be calculated on a 1980 m elevation tile, but they will be passed to the ice sheet and atmospheric models as outputs from an 1800 m elevation tile.

Therefore, the increase in the tile elevation is only accounted for during the downscaling of surface temperature but is not reflected when passing it to the ice sheet model or elsewhere in FAMOUS. In this way, additional cooling is applied over the ice sheet interior by *elevcon*, which can be regarded as elevation-dependent height adjustment over ice sheets. This crudely mimics the effect of the stable boundary layer in maintaining the cold surface condition in that area.

Two types of sensitivity experiments are performed with FAMOUS-BISICLES to validate the effect of *elevcon* on the modern and LGM ice sheets and climates. The first sensitivity experiment is conducted under modern climate and the Greenland ice sheet based on a control simulation performed by Lang et al. (in prep) and focuses on the effect of *elevcon* on the SMB. As shown in Smith et al., (2021b), the model simulates a mean ELA of approximately 1.8 km over the Greenland ice sheet, whereas high resolution regional atmospheric models (e.g. MAR; Fettweis et al., 2013) suggest 1.2 km, meaning that the model overestimates the ELA by 50% (Figure 3.14). Here, we applied an *elevcon* value of 50% and rerun the simulation. The inclusion of the *elevcon* adjustment strongly suppresses the negative SMB seen around the elevation of 1 km to 2 km, and the ELA drops from 1.8 km to approximately 900 m height (Figure 3.14). Given that the ELA is now underestimated compared with the high-resolution models, the value of 50% appears to be too large and can be regarded as the upper limit. However, this sensitivity experiment clarifies the substantial effect of *elevcon* on the SMB at the interior of the ice sheet. It further shows that *elevcon* can be used to explore the effect of uncertainties in the SMB at the interior of the ice sheet arising from underestimating the role of the stable boundary layer.

The second type of sensitivity experiments are performed under the LGM climate for the North American ice sheet. Here, values of 10%, 20% and 50% are tested with one of the ensemble members from Sherriff-Tadano et al., (2024) that exhibits a strong local melting of the ice sheet from parts of the interior. Results are shown in Figure 3.15. The strong local melting observed around the Hudson Bay region in the control simulation is removed in all the sensitivity

experiments. Also, depending on the magnitude of the value of *elevcon*, the negative SMB seen at the eastern part of the Rocky Mountains is reduced and pushes the ELA southwards.

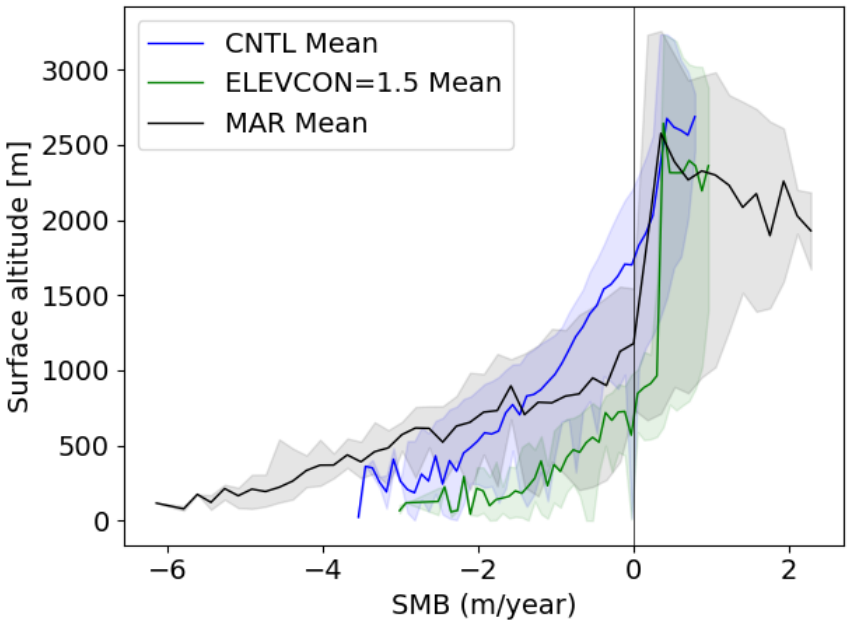

Figure 3.14: Relation of SMB and surface altitude over the Greenland ice sheet in the modern climate simulations with FAMOUS-BISICLES. The blue line (shading) shows the mean result (range) from the control experiments, and the green shows those from the sensitivity experiments that include *elevcon* with a value of 1.5 (50%). Also shown in black are the results from simulations using the MAR regional climate model (Fettweis et al., 2013).

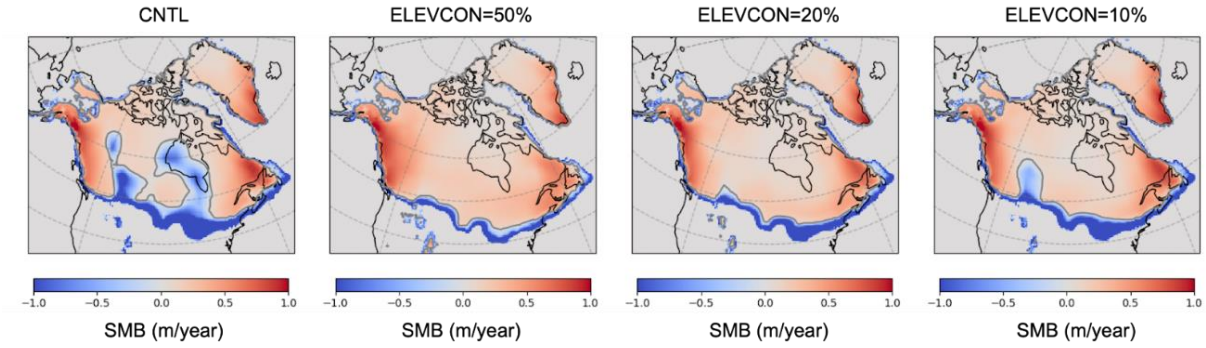

Figure 3.15: Effects of different magnitudes of *elevcon* on the spatial pattern of SMB over the North American ice sheet at the LGM. CNTL corresponds to one of the ensemble members (xppma) in Sherriff-Tadano et al. (2024).

3.6.2 BISICLES spin-up

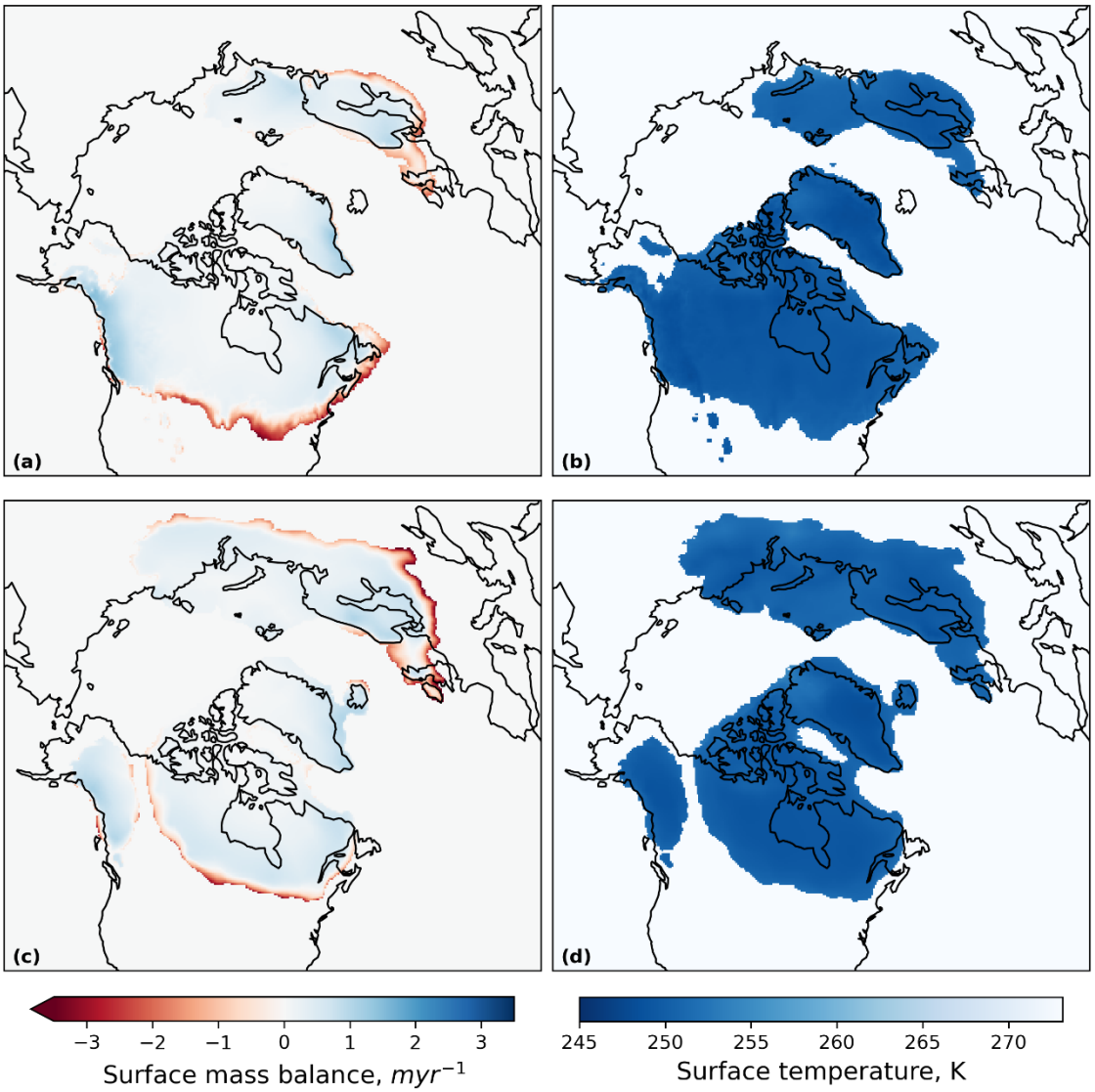

Figure 3.16: Surface mass balance and ice surface temperature fields used in the (a), (b) LGM and (c), (d) PGM spin-ups.

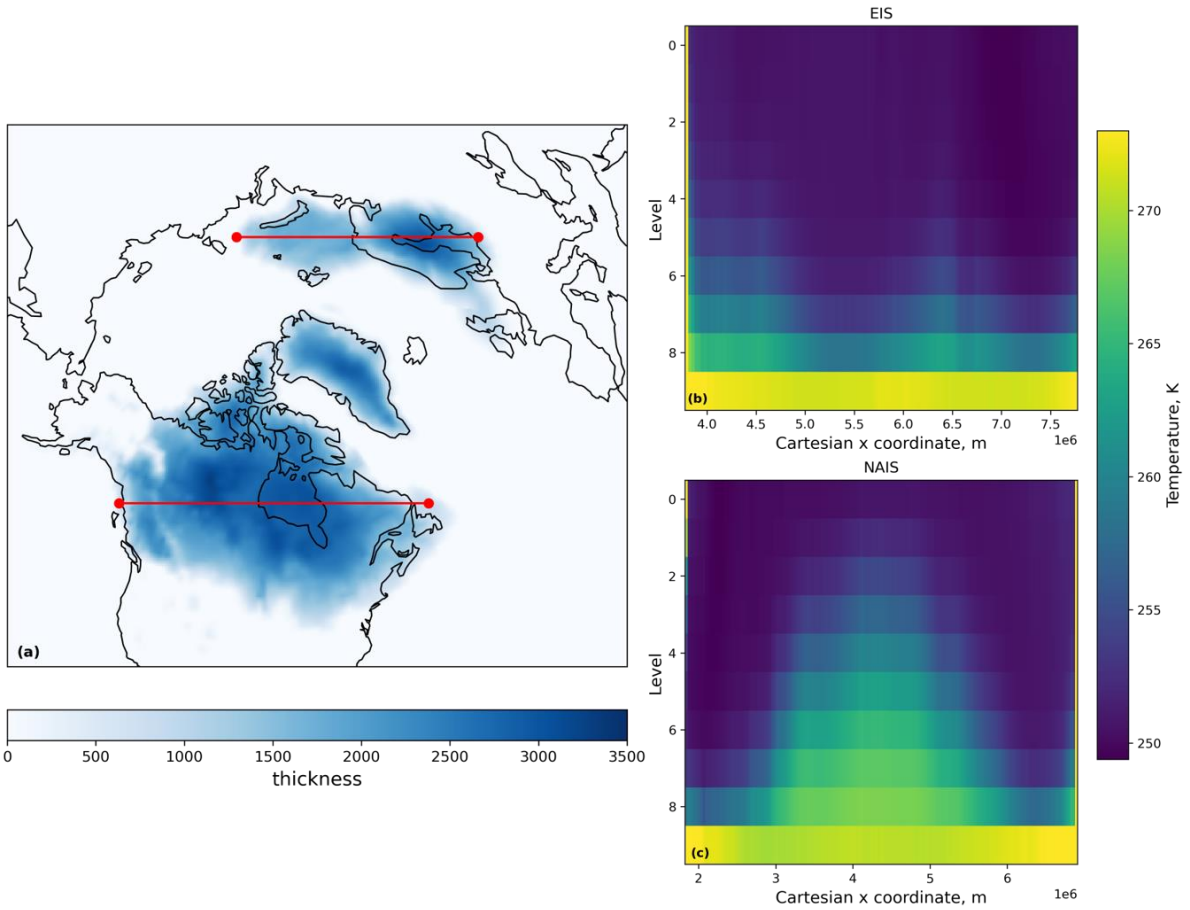

Figure 3.17: Cross section of LGM ice temperature at the end of the 20,000 year spin-up for the transects indicated by the red lines in (a), for the Eurasian ice sheet (b) and the North American ice sheet (c).

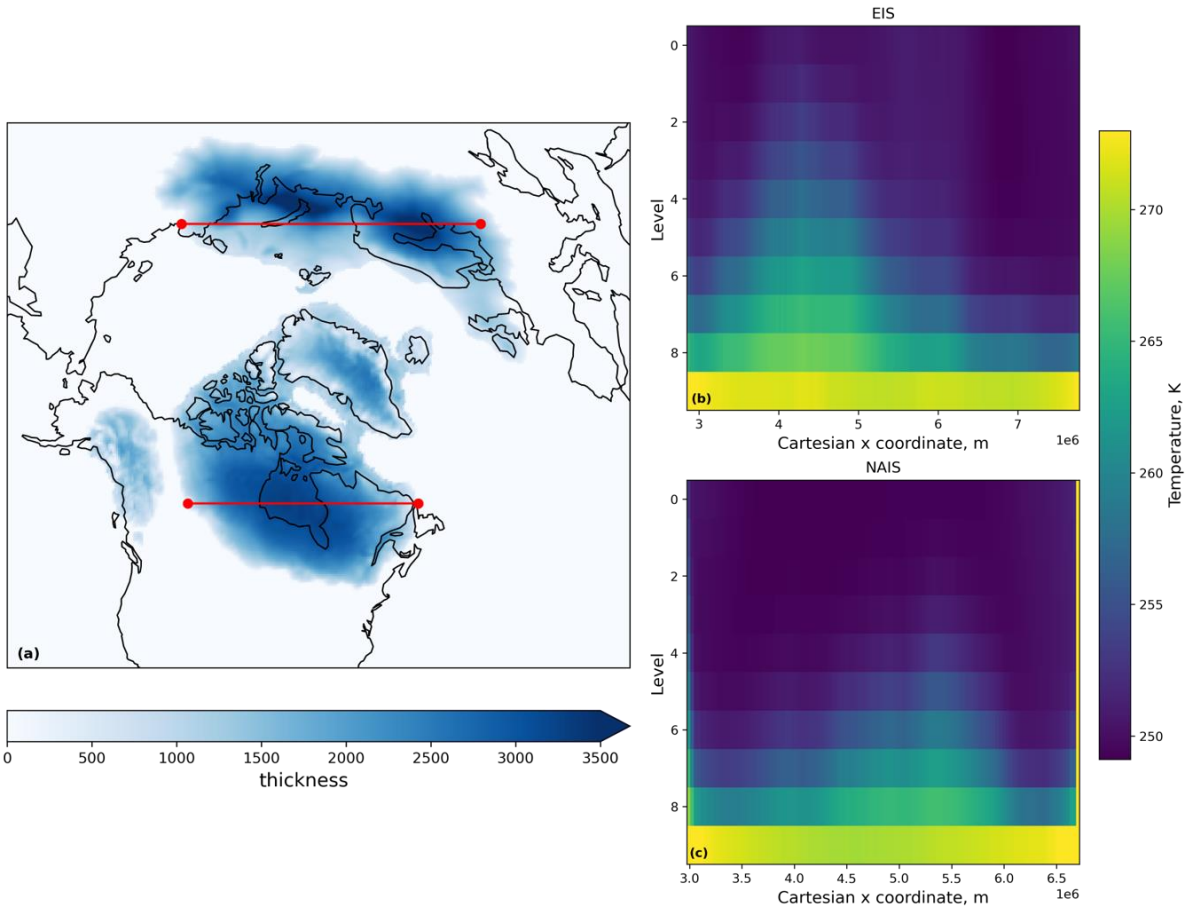

Figure 3.18: Cross section of PGM ice temperature at the end of the 20,000 year spin-up for the transects indicated by the red lines in (a), for the Eurasian ice sheet (b) and the North American ice sheet (c).

3.6.3 Sensitivity tests

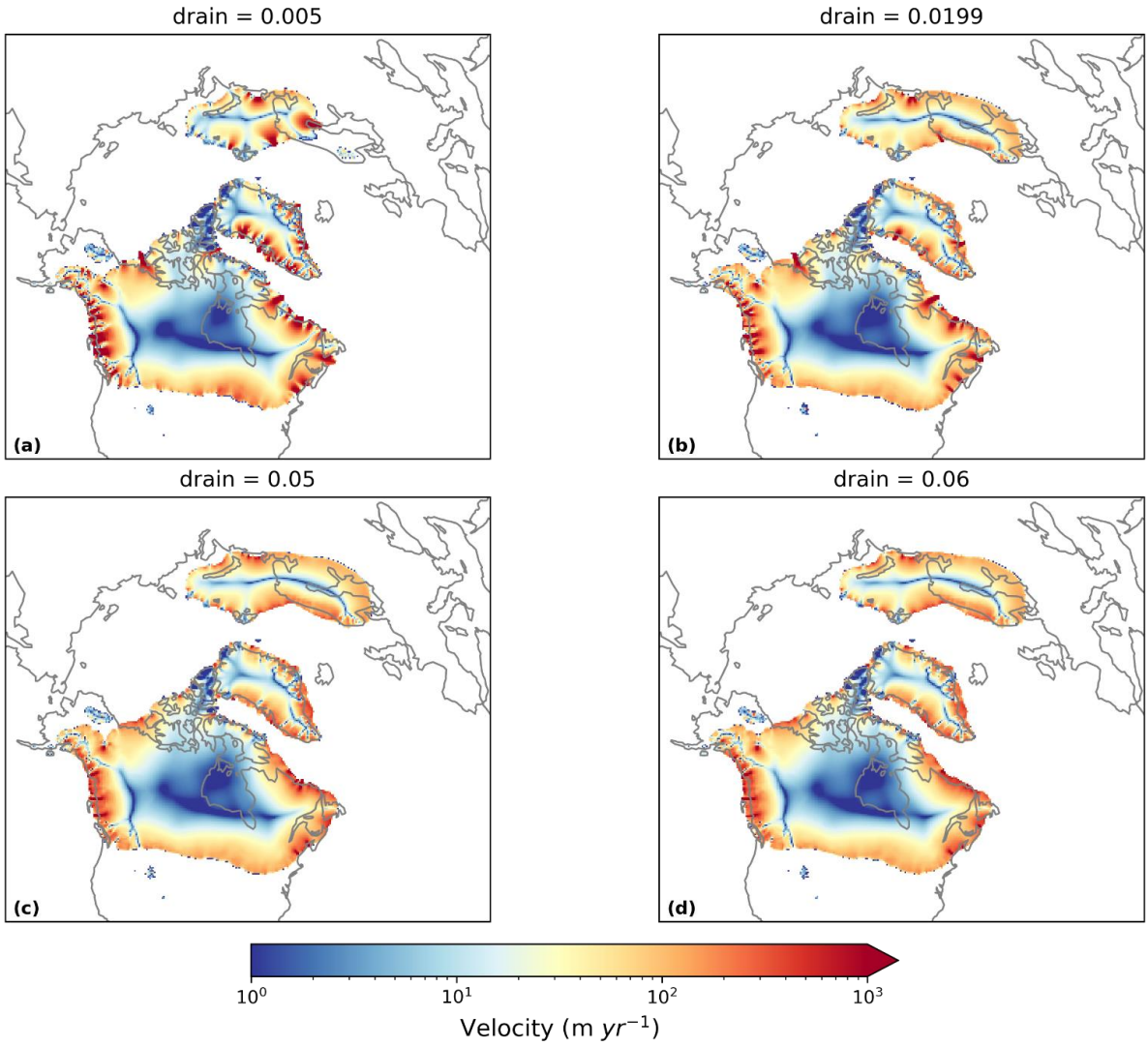

Figure 3.19: Ice velocity after 5000 ice sheet years in simulations using till water drainage rates of (a) 0.005 m yr^{-1}, (b) 0.0199 m yr^{-1}, (c) 0.05 m yr^{-1} and (d) 0.06 m yr $^{-1}$. All other parameters and initial conditions were kept the same.

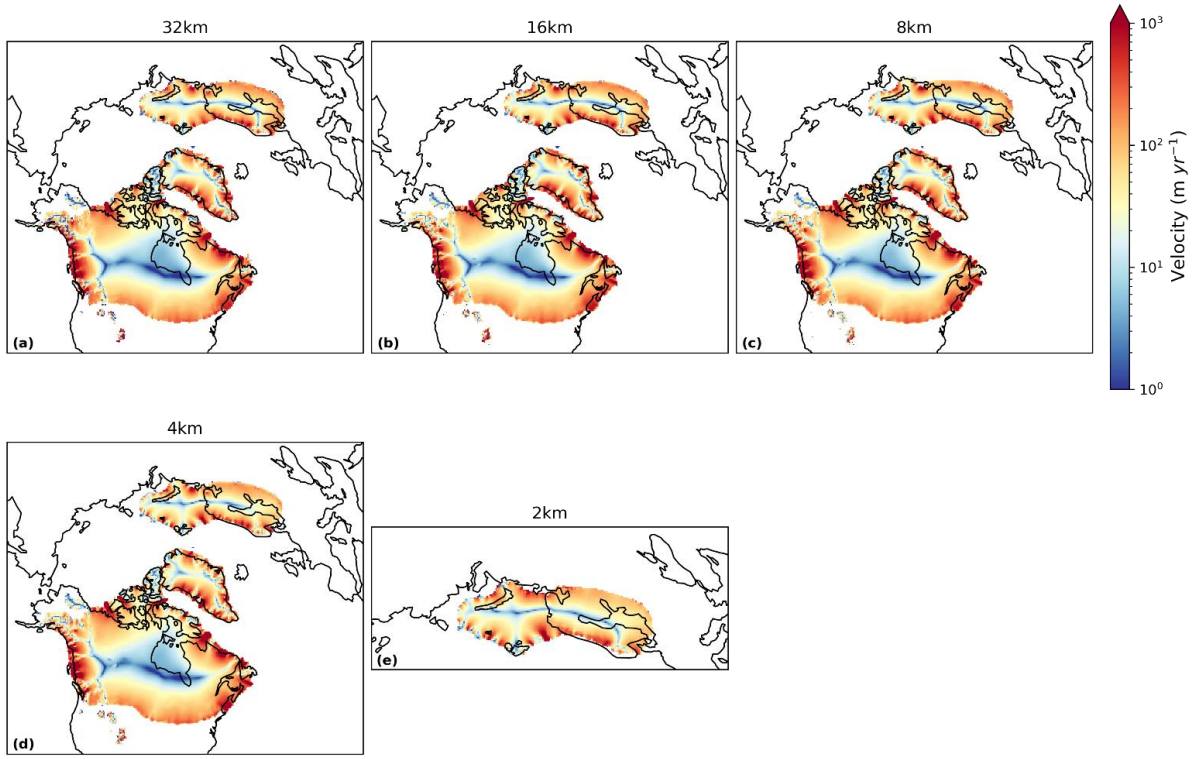

Figure 3.20: Ice velocity averaged over the 5000 year simulations using different levels of ice stream refinement. Only the marine margin was refined on panel (e).

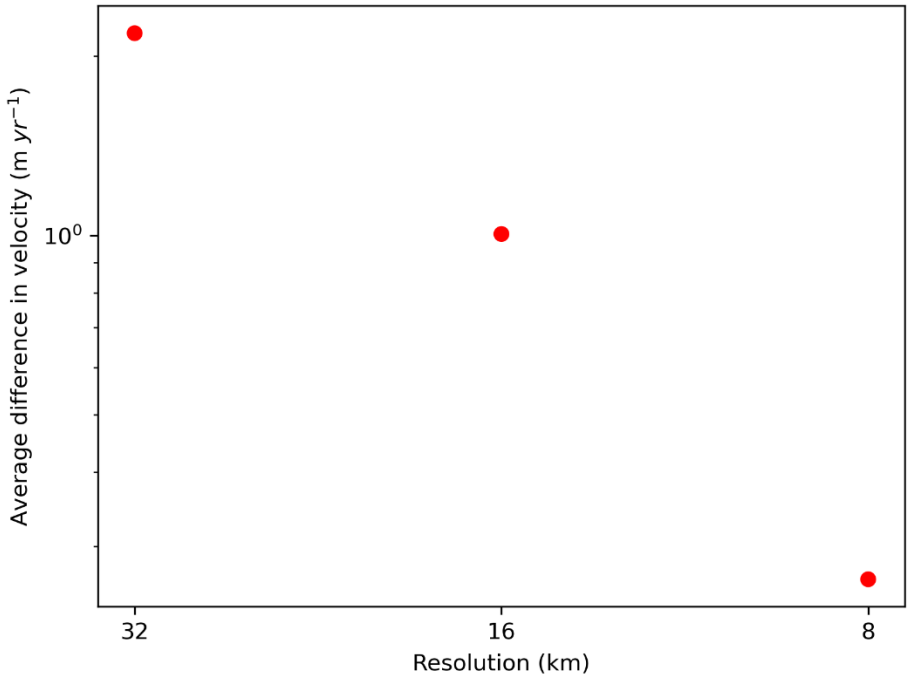

Figure 3.21: Difference in ice velocity averaged over the whole ice sheet and 5000 year simulations between the 4km resolution simulation and higher resolutions (8 km, 16 km and 32 km).

3.6.4 Leave-one-out-cross-validation (LOOCV)

Whilst a large proportion of the predicted diagnostics matched the modelled values within the 95% credible interval, the LOOCV reveals that the GP emulator struggled the most with predicting smaller ice sheet volumes and areas. This was especially the case for the PGM Eurasian ice sheet where many of the simulations collapsed due to GIA feedbacks and non-linearities in ice sheet-climate interactions. There is also one obvious outlier in all eight of the diagnostics where the emulator predicted a much higher value than what was actually modelled. This is the same parameter set (xprrk/xpruk) for each.

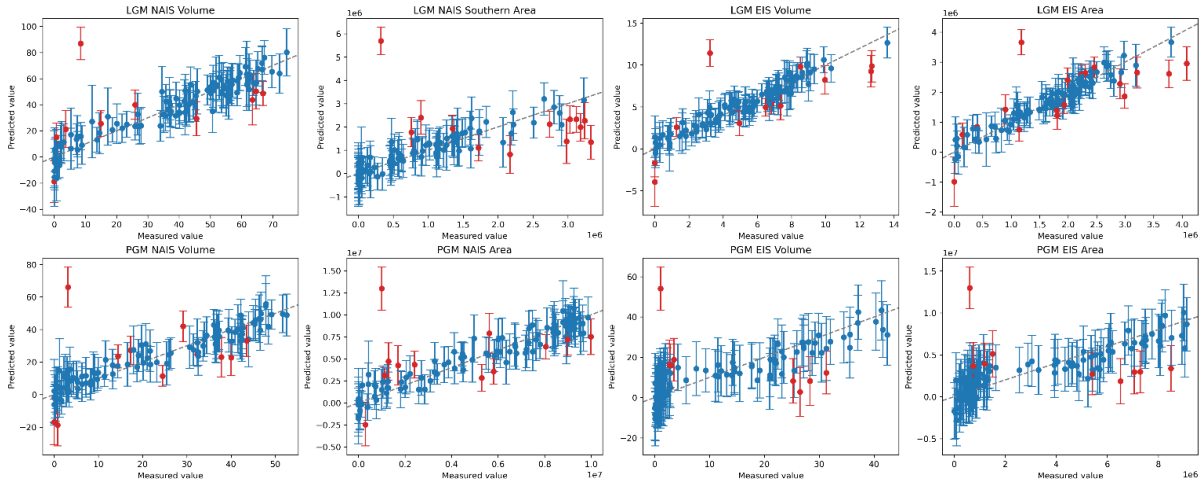

Figure 3.22: The results of the Leave-One-Out Cross Validation performed on emulators for the eight diagnostics. The points show the value produced by the numerical model against the value predicted by the emulator for the same sets of input parameters. The line through the centre is the 1:1 line and the error bars show the 95% credible interval for each point. The points for which the measured value does not fall within the error bars are highlighted in red.

3.6.5 Parameter pairs plot

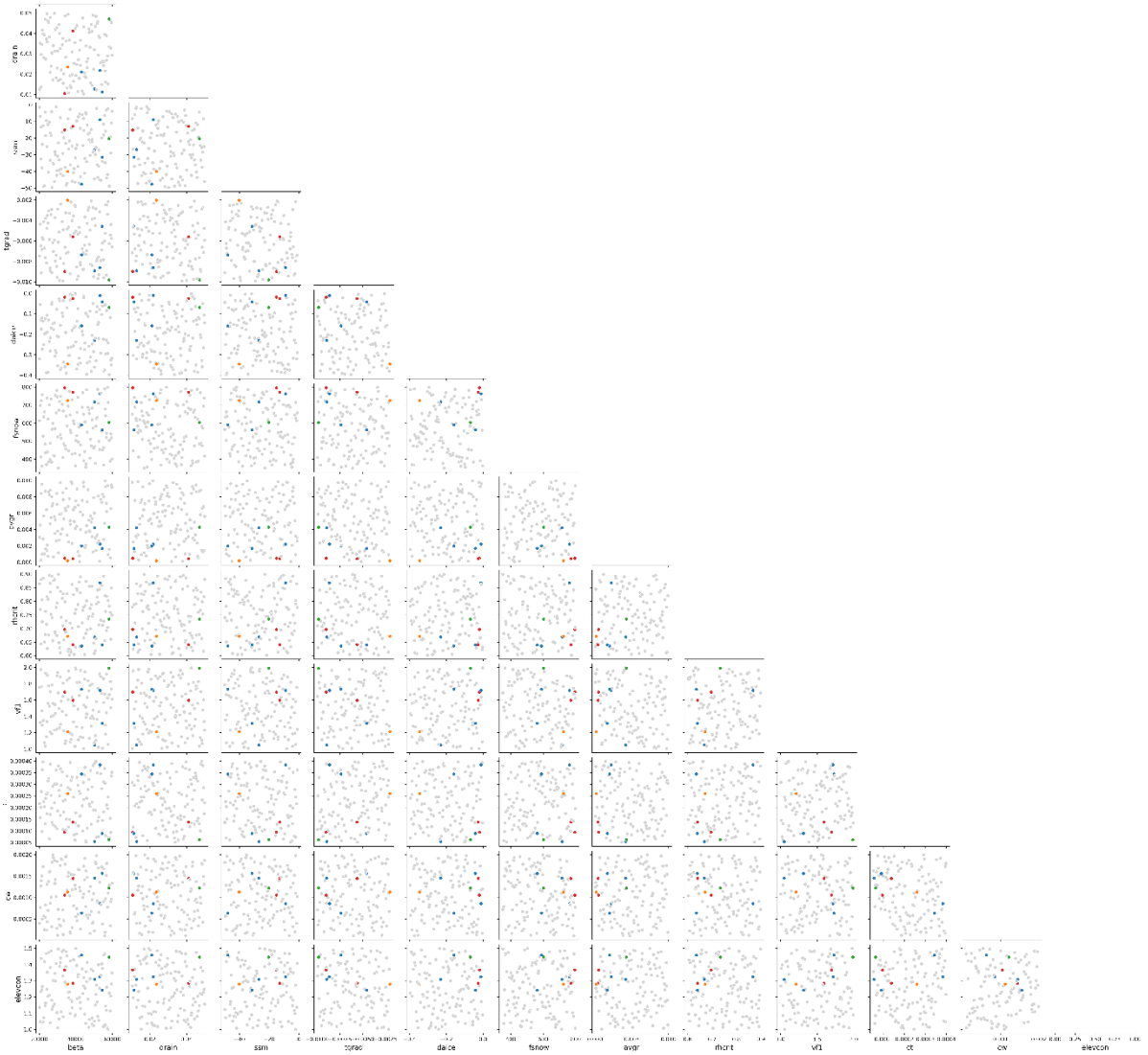

Figure 3.23: Parameter pair plot for the FAMOUS-BISICLES ensemble with the NROYa and NROYb simulations in red, NROY extent simulation in orange, NROY volume simulation in green and the four other simulations that meet the North American ice sheet constraints but not the Eurasian in blue.

3.6.6 PGM ice streams

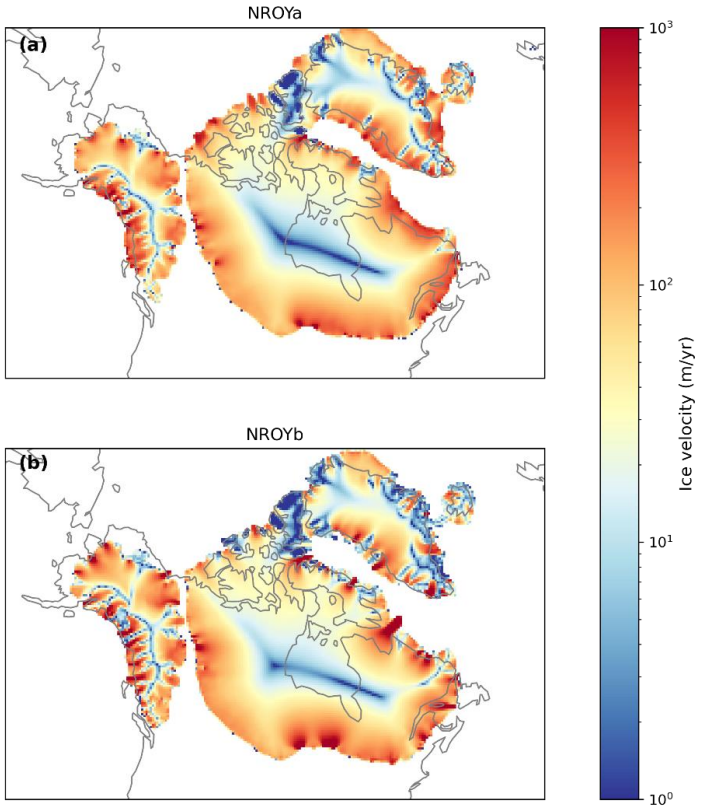

Figure 3.24: North American ice sheet ice velocity at the end of the 5000 ice sheet years for the two equivalent PGM NROY simulations.

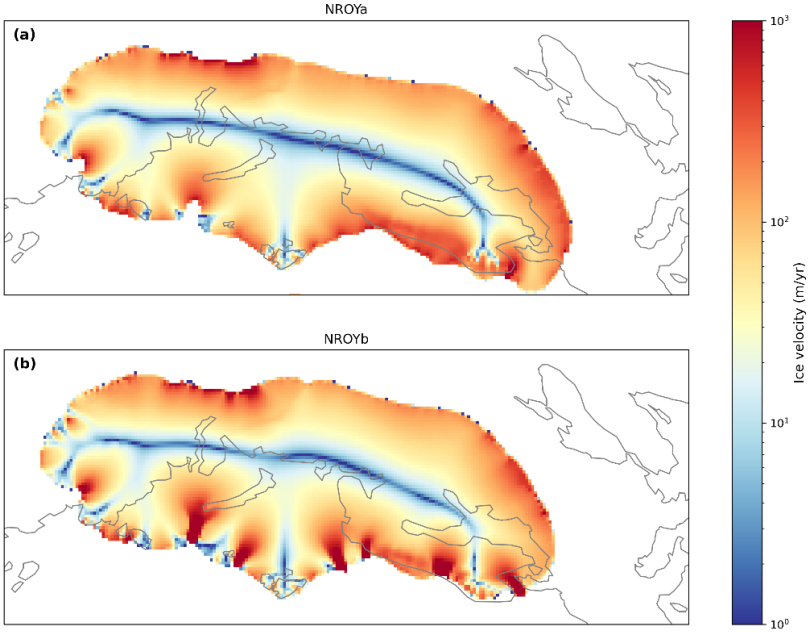

Figure 3.25: Eurasian ice sheet ice velocities at the end of the 5000 ice sheet years for the two equivalent PGM NROY simulations.

Chapter 4

4 Comparing the Last and Penultimate Deglaciations using a coupled climate-ice sheet model

4.1 Abstract

Understanding why and how the last two deglaciations differed could shed light onto the response of components of the earth system, such as ice sheets, to changes in climate forcing that are important in the context of climate change. We present results from the first simulations of the Last and Penultimate deglaciations (21-9 thousand years ago, ka, and 140-128 ka) using an atmospheric general circulation model fully coupled to an ice sheet model (FAMOUS-BISICLES) and investigate the sensitivity of the ice sheet evolutions to uncertain model parameters and individual climate forcings. We find that, under the different deglacial climate forcings and initial ice sheet states, the Northern Hemisphere ice sheets retreat at a faster rate over the Penultimate Deglaciation and result in an additional 3.3 m sea level contribution from Greenland. Global surface air temperatures are also simulated to be higher at the end of the Penultimate Deglaciation than at the end of the Last Deglaciation. The pattern of ice retreat remains similar for the North American ice sheet between the two periods, but differs for Eurasia due to different mechanisms causing ice sheet instabilities resulting from the different initial ice sheet states. Sensitivity experiments show that the rate of deglaciation is particularly sensitive to processes that impact the surface mass balance, but ice dynamics also play an important role. Sub-shelf melt rate is less significant, however it can be important where confined ice shelves are able to form. Insolation drives ice sheet retreat for both time periods, but changes in greenhouse gases and sea surface temperatures amplify the response of the ice sheets to the orbital forcing. Finally, our results demonstrate a need for tuning of coupled climate-ice sheet models under conditions of climate and ice sheet change to increase their flexibility in modelling different time periods.

4.2 Introduction

Deglaciations mark the transition from full glacial conditions to interglacial conditions and involve large shifts in the climate and ice sheets (Past Interglacials Working Group of PAGES, 2016). They are triggered by changes in the orbital configuration of the Earth causing an increase in the incoming Northern Hemisphere (NH) summer insolation (Berger, 1978; Hays et al., 1976). However, deglaciations have a large amplitude and happen relatively rapidly (~10 thousand years; kyr), compared to the long shift (~90 kyr) into glacial conditions. This contrast in speed is due to internal forcings, such as increases in greenhouse gases (GHGs), and feedbacks between components of the earth system, such as the ice sheets, solid earth and oceans (Abe-Ouchi et al., 2013; Barker and Knorr, 2021; Cheng et al., 2009; Imbrie et al., 1993). The last two deglaciations initiated under different glacial maximum ice sheet geometries and orbital configurations, and various proxy-reconstructions have suggested they differed in their amplitude, duration and sequence of events. Therefore, studying and comparing these deglaciations can provide information for how components of the earth system may respond to changes in radiative forcing in the context of future climate change (Menviel et al., 2019).

The Last Deglaciation (LDG; ~21-9 ka) occurred following the Last Glacial Maximum (LGM; ~21 ka) and since it was during the most recent glacial cycle, the evolution of the climate and ice sheets are relatively well constrained by empirical data. There is evidence of three abrupt millennial scale climate changes superimposed onto the general warming trend of the LDG; Heinrich Stadial 1 (HS1; ~18-14.7 ka), the Bølling-Allerød (BA; ~14.7-12.8 ka) and the Younger Dryas (YD; ~12.8-11.7 ka) (Ivanovic et al., 2016). During HS1 and the YD, ice core and sediment records show an abrupt cooling over Greenland and the North Atlantic followed by a slow warming over Antarctica (Alley, 2000b; Barbante et al., 2006; Buizert et al., 2015). Moving into the BA, Greenland warmed rapidly (~10 ºC; Buizert et al., 2014), coinciding (within age constraints) with a period of rapid sea level rise of more than 40 mm yr^{-1} called Meltwater Pulse 1a (MWP-1A; ~14.6-14.3 ka; Deschamps et al., 2012). This was followed by a cooling of ~1-2 °C over Antarctica known as the Antarctic Cold Reversal (ACR) (Jouzel et al., 2007; Pedro et al., 2015). Partly on this basis, these abrupt events have been linked to a change in the strength of the Atlantic Meridional Overturning Circulation (AMOC) and the transport of heat across the equator, known as the thermal bipolar seesaw, possibly triggered by the input of large amounts of freshwater into the North Atlantic due to the disintegration of the ice sheets (Böhm et al., 2015; McManus et al., 2004; Ng et al., 2018; Stocker and Johnsen,

2003). However, the exact mechanisms, timings and durations of these events are still widely debated and remain uncertain (Ivanovic et al., 2016).

Whilst there are fewer records for the Penultimate Deglaciation (PDG; ~140-127 ka), which occurred following the Penultimate Glacial Maximum (PGM; ~140 ka), the current evidence depicts a different sequence of events (Menviel et al., 2019). Notably, there was likely only one abrupt climate event during the PDG; Heinrich Stadial 11 (HS11; ~135-129 ka) (Cheng et al., 2009; Jiménez-Amat and Zahn, 2015; Martrat et al., 2014). Similar to HS1, HS11 was characterised by a weakening of the AMOC, a cooling over the NH and a gradual warming over Antarctica (Govin et al., 2015; Landais et al., 2013; Marino et al., 2015) and also coincided with a period of rapid sea level rise (Marino et al., 2015). However, HS11 started much later into the deglaciation than HS1, and lasted much longer, extending into the start of the interglacial (Böhm et al., 2015; Deaney et al., 2017; Govin et al., 2015). The reasons for these differences are still unknown, but several studies have suggested that the different glacial maxima ice sheet configurations and orbital forcing scenarios could have contributed to larger amounts of meltwater and a faster deglaciation at the PDG (Landais et al., 2013; Obase et al., 2021; Stoll et al., 2022). In addition, the Last Interglacial (LIG; ~129-116 ka) displayed different characteristics to the current Holocene interglacial (~11.7 ka to present). It was one of the warmest interglacial periods of the last 800,000 years (Masson-Delmotte et al., 2010; Pages, 2016), with global temperatures ~1-2 ºC higher than pre-industrial (Otto-Bliesner et al., 2013b; Turney and Jones, 2010). This is similar to the levels of global warming expected over the next few decades, and therefore, the LIG is of particular interest to the scientific community (Golledge et al., 2021; Intergovernmental Panel On Climate Change (IPCC), 2023a).

Last Interglacial global mean sea levels were also 1-9 m higher than present day, implying the Greenland and Antarctic ice sheets lost significant mass, but the processes that led to this retreat and the individual contributions from each ice sheet remain uncertain (Dutton et al., 2015; Dyer et al., 2021). During the LIG, the ice sheets and climate were still responding to changes that occurred during the Penultimate Deglaciation (Menviel et al., 2019). For example, it has been suggested that the longer and more persistent weak AMOC state during HS11 caused warmer Antarctic temperatures at the start of the LIG compared to the Holocene. This may have led to significant mass loss from the Antarctic ice sheet through increased subsurface ocean warming, contributing to the higher LIG sea levels (Clark et al., 2020; Marino et al., 2015; Turney et al., 2020b). Additionally, the North American ice sheet may have deglaciated at a faster rate during the PDG than the LDG causing less ice cover at the start of the LIG compared to the Holocene, which may have contributed to the warmer LIG climate through the ice-albedo feedback (Bova

et al., 2021). Hence, we need to study the evolution of these systems throughout the deglaciations in order to understand the LIG sea level highstand and thus help constrain future ice sheet response to a warming climate.

The palaeoclimate proxy record has advanced our understanding of the magnitudes and timings of earth system changes over glacial-interglacial cycles. However, it is hard to robustly extract detailed information on the processes and feedbacks that led to these changes (Harrison et al., 2016). Transient numerical simulations can be used to fill this gap and help further our understanding of the response of the earth system to changes in external forcings (e.g. insolation) and the impact on the global climate system due to the internal interactions that result from this (Ivanovic et al., 2016; Menviel et al., 2019). Researchers have performed such simulations using general circulation models (GCMs) and earth system models forced with evolving orbital parameters, GHGs and ice sheet topographies, to investigate the climate evolution over the LDG (Snoll et al., 2024) and in more recent years, over the PDG (Clark et al., 2020; Obase et al., 2021). Alternatively, the output of these transient climate simulations have been used to drive ice sheet models (ISMs) to constrain the ice sheet evolution and investigate their sensitivities to atmospheric and oceanic forcings (Clark et al., 2020; Gregoire et al., 2012, 2016; Petrini et al., 2020). However, the interactions that occur between the climate and the ice sheets impact the atmospheric and oceanic circulation and set up feedbacks such as the ice-albedo feedback and the temperature-elevation feedback (Fyke et al., 2018). These influence the ice sheet mass balance and therefore are an important contribution to the mechanisms of deglaciations (Abe-Ouchi et al., 2007; Scherrenberg et al., 2023b) but are not explicitly resolved in these standalone model simulations.

Recent technological advances have enabled the coupling of climate and ice sheet models which can capture many of the relevant feedbacks at play during deglaciations (Smith et al., 2021b). Such simulations have confirmed the role of increasing NH summer insolation as the primary trigger for the Last Deglaciation but highlighted the importance of CO_2, dust deposition and vegetation changes for modulating the timing and magnitude of ice sheet melt (Charbit et al., 2005; Ganopolski et al., 2010; Ganopolski and Brovkin, 2017; Quiquet et al., 2021a; Quiquet and Roche, 2024). However, these require integration over long timescales and at high resolutions which have a large computational cost. Therefore, many of these studies use earth system models of intermediate complexity (EMICs) such as a recent study by Quiquet and Roche, (2024), hereafter QR24, who compared EMIC-ISM simulations of the LDG and PDG. They revealed that the different orbital configurations, and resulting solar insolation forcing, caused a more rapid increase, and a higher peak, in global mean temperatures during

the PDG. This led to a quicker disintegration (by ~3 kyr) of the NH ice sheets compared to the LDG, although the patterns of retreat were similar. They also simulate the higher global mean temperatures and subsurface Southern Ocean temperatures during the LIG compatible with higher sea level and Antarctic ice sheet melt compared to the Holocene. However, these simulations both use LGM ice sheet geometries as an initial condition, whereas evidence points to a smaller North American ice sheet (NAIS) and larger Eurasian ice sheet (EIS) at the PGM (Batchelor et al., 2019; Dyke et al., 2002; Rohling et al., 2017; Svendsen et al., 2004). This will have effects on atmospheric circulation, local climate, and ice dynamics, which could impact the subsequent deglaciation. In addition, EMICs rely on simplified representations of many physical processes, which adds to the uncertainty in the results. GCMs provide a better representation of the climate since they explicitly resolve many of the relevant processes. However, uncertainty is introduced by model inputs (e.g. physical parameter values) which have been shown to impact the resulting ice sheet configurations (Chapters 2 and 3; Gandy et al., 2023; Gregoire et al., 2016; Sherriff-Tadano et al., 2024). More complex GCMs have now been coupled to an ISM (Muntjewerf et al., 2021; Smith et al., 2021b, a), including to simulate the Last Deglaciation (e.g. Ziemen et al., 2019) but, to date, no coupled GCM-ISM simulation has been performed for the Penultimate Deglaciation.

Here, we present results from transient simulations of the Last and Penultimate deglaciations using the atmospheric component of the FAMOUS GCM coupled to the BISICLES ISM (Sherriff-Tadano et al., 2024). The aim is not to perfectly reconstruct the evolution of the climate and ice sheets, but to compare the rates and patterns of deglaciation between the two periods under the different orbital and GHG forcings and initial ice sheet states. We also perform sensitivity tests to investigate the impact on the ice sheet retreat due to varying uncertain model parameters that control ice dynamics, sub-shelf melt and surface melt. In addition, we explore the roles of orbital configuration, greenhouse gases and sea surface conditions in driving the deglaciations.

4.3 Methods

4.3.1 Models

The model used in this study is FAMOUS-ice which consists of the atmospheric component of the FAMOUS GCM bi-directionally coupled to the BISICLES ISM (Sherriff-Tadano et al., 2024; Smith et al., 2021b). FAMOUS is a low resolution (7.5º x 5º) version of the HadCM3 model (Williams et al., 2013) which has enabled its use for long multi-millennial palaeo simulations and large ensembles (Gregoire et al., 2012; Gregory et al., 2012; Patterson et al.,

2024). It can be coupled to an ice sheet model through a multi-layer surface snow scheme in which the surface mass balance (SMB) is calculated on 10 vertical tiles at set elevations within each FAMOUS grid box that contains land ice. This field is then downscaled onto the finer ice sheet model grid and used by the ice sheet model to calculate changes in ice cover and surface elevation before passing this information back to FAMOUS, and so on (Smith et al., 2021b).

BISICLES is a marine ice sheet model that uses L1L2 physics and adaptive mesh refinement (AMR) making it suitable for modelling ice shelves and fast flowing ice streams efficiently (Cornford et al., 2013). The model set-up used here is mostly the same as in Chapter 3; further description can be found there and in references therein. We do, however, update the method of the sub-shelf melt rate calculation so that T_{ocn} uses subsurface (450 m) ocean temperatures instead of sea surface temperatures (SSTs), since this is around the average Barents Sea grounding line depth as used in previous studies (Clark et al., 2020; Petrini et al., 2018). The freezing point of sea water (T_f) is also calculated using the parameterisation of Beckmann and Goosse, (2003), which takes into account the salinity of the water at that depth. As in Chapter 3, the resolution over the ice sheets is 16 km. However, we refine areas of ice streaming over the Barents-Kara ice sheet (BKIS) to 2 km in order to better represent smaller scale ice stream and grounding line processes, which may be important here during deglaciation (Petrini et al., 2018). This resolution has been shown to perform almost equally to finer resolutions in this version of BISICLES, with regards to ice stream behaviour (Gandy et al., 2019), but requires computational times that are more within the constraints of this study. To reduce computational costs, we also run the simulations at 10 times acceleration such that the climate forcings are accelerated by a factor of 10 and then used to force 10 years of ice sheet integration. Thus, 12,000 years can be modelled in 1200 model years, taking ~750 core hours.

4.3.2 Experiment design

4.3.2.1 Boundary and Initial Conditions

The orbital parameters and GHGs used to force the climate model are transient following the PMIP4 deglaciation protocols (Figure 4.1; Ivanovic et al., 2016; Menviel et al., 2019). The GHGs (CO_2, N_2O and CH_4) are linearly interpolated from the datasets included in the protocols (Bereiter et al., 2015; Köhler et al., 2017; Loulergue et al., 2008; Schilt et al., 2010) and then values are selected every 10 years. The insolation is calculated from orbital parameters as per Berger, (1978). The topography over the Southern Hemisphere (including the Antarctic ice sheet) and the global land-sea mask in FAMOUS remains fixed at the glacial maximum configuration based on the reconstructions in the PMIP4 protocols (GLAC-1D from Ivanovic

et al., 2016 for the LDG, and using the ice sheet components from Abe-Ouchi et al., 2013; Briggs et al., 2014; Tarasov et al., 2012 for the PDG). Vegetation is also kept fixed at pre-industrial distributions.

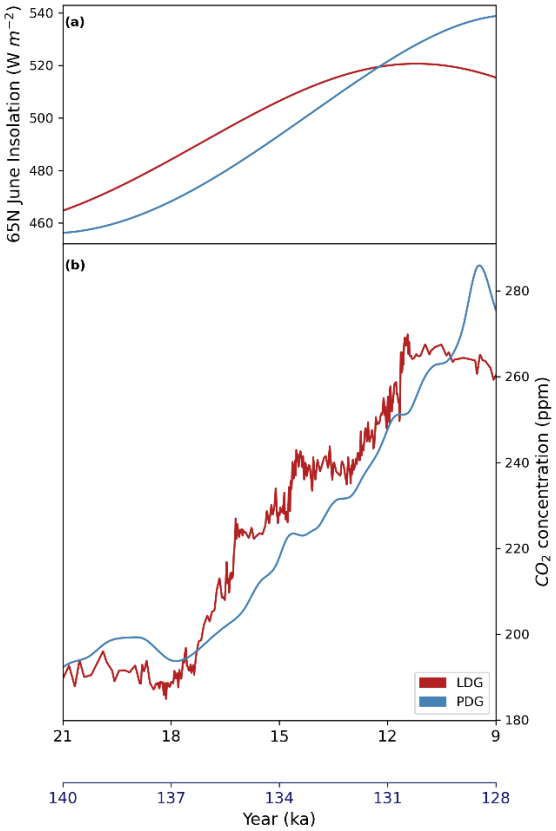

Figure 4.1: Transient (a) insolation and (b) CO_2 forcings used in the Last and Penultimate deglaciation simulations (Bereiter et al., 2015; Köhler et al., 2017; Loulergue et al., 2008; Schilt et al., 2010). Time spans 21-9 ka for the LDG (black x-axis) and 140-128 ka for the PDG (blue x-axis).

We prescribe time varying SST and sea ice fields to force the climate model, which is atmosphere-only. This forcing is taken from the multi-year monthly means from the final 100 years of HadCM3 equilibrium- type snapshot simulations spanning 140-128 ka at 4 kyr intervals for the PDG and 21-9 ka at 1 kyr intervals for the LDG (Figure 4.2a-d; see details in Armstrong et al., 2019; Huntley et al., 2023). The HadCM3 simulations were forced with corresponding orbital parameters (Berger and Loutre, 1991), GHGs (Loulergue et al., 2008; Petit et al., 1999; Spahni et al., 2005) and ice sheets (de Boer et al., 2013) for their respective time window, but note that the forcings were held constant for the full duration of each snapshot, they are not transient simulations. The annual mean subsurface temperature and salinity fields used for the ocean thermal forcing for the sub-shelf melt parameterisation were taken from the same set of simulations (Figure 4.2e). All of these fields were linearly

interpolated to create a continuous timeseries with annual timesteps for each deglaciation, and the timeseries were resampled at 10 year intervals to create our accelerated forcing.

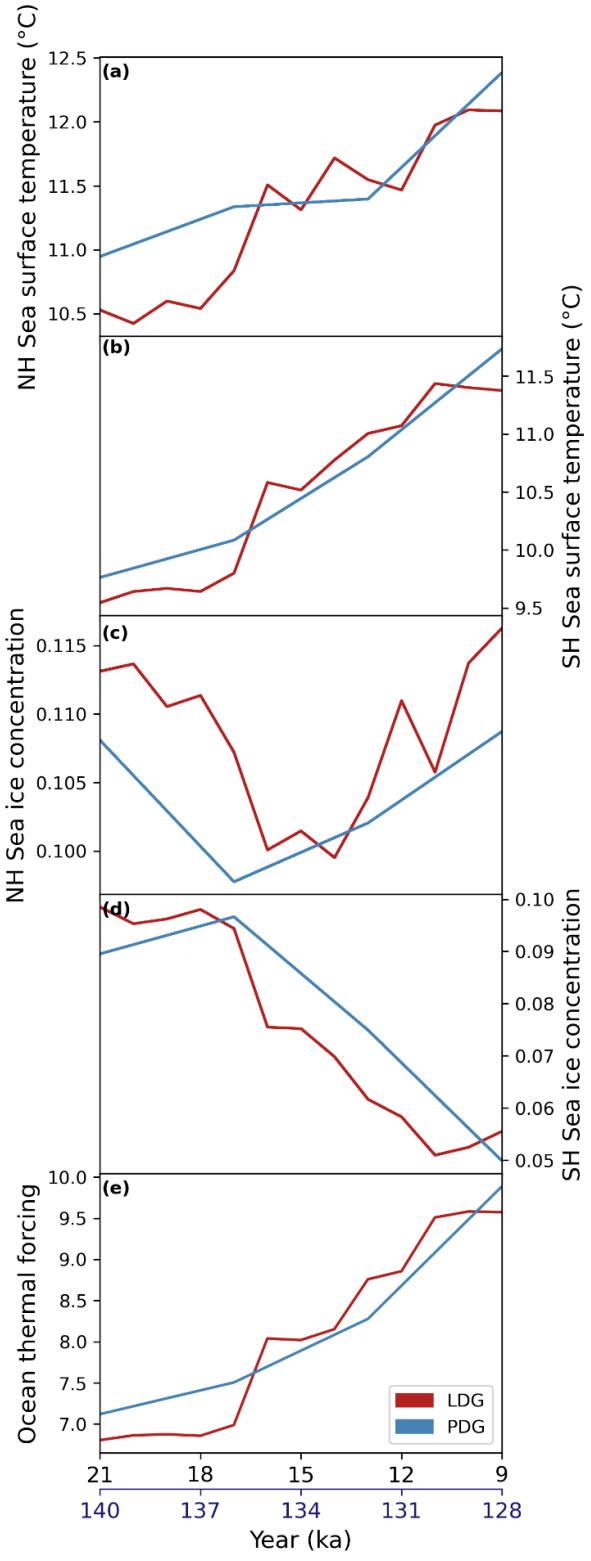

Figure 4.2: Transient forcings for the FAMOUS-ice climate and ice sheet models over the LDG and PDG, including mean (a) Northern Hemisphere and (b) Southern Hemisphere sea surface temperatures, (c) Northern Hemisphere and (d) Southern Hemisphere sea ice concentrations (0-1) and (e) sub-ocean thermal forcing.

The study in Chapter 3 employed FAMOUS-BISICLES to run perturbed parameter ensembles of simulations under constant LGM and PGM climate conditions, and initiated from model reconstructions of their distinct glacial maximum topographies, to equilibrium. Evaluation of these ensembles found four sets of parameter values that produced "Not Ruled Out Yet" (NROY) LGM and PGM NH ice sheets based on ice volume and extent constraints. We selected one of these sets of parameter values to use in our transient deglaciation experiments, which we also initiate from the glacial maxima equilibrium ice sheets produced by that combination of parameter values in that study. Two of these NROY simulations produced LGM ice sheets that fit both the volume and extent criteria. However, when testing the deglacial forcings, we found that the resulting ice sheets were too stable, especially in North America, preventing deglaciation. This could be the result of several conditions (independently, or in combination). First, the simulated maximum extent ice sheets may be too big. This seems unlikely, since the ice volumes and extents fell towards the lower end of the palaeo-constraints based on recent empirical and model data. Second, the simulated maximum extents may have been spun-up to equilibrium under constant glacial conditions for too long. In reality, it is likely that the glacial maxima climates and ice sheets were never in equilibrium. Third, the model may be unable to deglaciate from a plausible glacial maximum ice sheet due to some model bias, which may be masked in this particular climatic setting; that a single model configuration may not necessarily be sufficiently flexible to be applied across all time periods has been highlighted by previous studies (e.g. Gandy et al., 2023).

In order to find sets of parameters that produce reasonable ice sheets for both glacial maxima, deglaciation and present day conditions – i.e. a model that is sufficiently flexible as to robustly simulate climate and ice sheet change – it would be useful to perform an equivalent ensemble tuning for transient climate/ice-sheet histories; i.e. deglaciation simulations. However, to do this thoroughly would require large computational resources.

Thus, for a pragmatic approach, we here select the NROY simulation that meets the respective glacial maxima extent constraints, but falls slightly below the volume constraints (labelled *NROY extent* in Chapter 3). By implication of being smaller in volume, this ice sheet model configuration is less stable under deglacial climate change. As well as the parameter values, we take the simulated LGM ice sheet from the final year of this NROY equilibrium run performed in Chapter 3 (i.e. ice sheet year 5000), and the ice sheet from the end of the equivalent PGM simulation (see details in Sect. 4.7.1), and use these as the ice sheet model initial condition for all the LDG and PDG runs in this study (excluding LDG_{ssm} and PDG_{ssm};

see Sect. 4.3.2.2.2), respectively. This includes the spun-up ice and bedrock topography, internal temperature and velocity fields.

4.3.2.2 Sensitivity experiments

Using the described model set-up, we perform LDG and PDG simulations (Table 4.1; LDG_{ref} and PDG_{ref}). However, because the rate and pattern of deglaciation may be impacted by the uncertain model inputs, we perform additional experiments to assess the sensitivity of the simulated climate and ice sheet evolutions to some of our design choices, and the processes they influence. The result of these sensitivity tests could then be used to inform where to focus further tuning efforts in order to improve the model match to observations.

Based on the results of the ensemble in Chapter 3, we vary three uncertain model parameters; one that affects the surface mass balance (SMB) through altering the albedo of the ice (*av_gr*), one that controls the basal melt rate of floating ice (*c*) and finally, one that impacts the flow of the ice sheet (*drain*). By changing the value of each parameter one at a time, we can compare the result to the reference experiments to determine the relative importance of these three processes in the simulated deglaciations. In the following three sections, we explain the effect these parameters have on the simulations and how and why we chose to vary them.

Furthermore, to evaluate the relative impact of the climate forcings on pacing the deglaciations, we perform experiments in which we fix one climate forcing at a time to the glacial maximum value (orbit, GHGs and sea surface conditions; specifically SSTs and sea ice) whilst the rest of the forcings remain transient.

Table 4.1 details all the experiments performed in this study, their parameter values, the forcings used and how they are referred to in the text.

4.3.2.2.1 Surface mass balance parameter

Several studies have investigated the impact of uncertain climate and ice sheet model parameters on the simulated LGM and PGM ice sheets (see Chapters 2 and 3 and Gandy et al., 2023; Sherriff-Tadano et al., 2024). They all found that the parameters that change the albedo of the ice have the largest effect on the ice volume because they impact the energy balance at the surface, which can significantly alter the SMB. These parameters include; *daice*, which determines the sensitivity of the bare ice albedo to surface air temperatures above the melt threshold; *fsnow*, which sets the density threshold for snow above which the surface is regarded as bare ice; and *av_gr*, which controls the sensitivity of the surface snow albedo to increasing snow/ice grain size. While all three parameter values are important for the stability of the glacial maximum ice sheets, *daice* and *av_gr* may be more important for controlling the

deglaciation since they impact the albedo more in the ablation zone. Out of these two, the ice volume and SMB appear to be most sensitive to *av_gr* (see Chapter 3), which in the reference simulation is set towards the bottom of the range of ensemble values (0.00018). Therefore, we test the impact of increasing the value of *av_gr* to match the highest value used in a NROY simulation as found in Chapters 2 and 3 (Table 4.1; LDG_{alb} and PDG_{alb}). Increasing the value of *av_gr* acts to decrease the albedo of snow more over time and so should cause a decrease in the SMB of the ice sheets.

4.3.2.2.2 Basal mass balance parameter

As well as processes occurring at the surface, the mass balance of the ice sheets is also affected by their interactions with the ocean. The two ways that ice sheets lose mass at marine margins is through calving and sub-shelf melt, both of which are parameterised in our ice sheet model. Building on Chapter 3, we focus on the sensitivity of the ice sheet to the relationship between ocean thermal forcing and sub-shelf melt, which we explore by varying the sub-shelf melt constant, *c*. In the reference simulations, the value of *c* is high (40.2 m yr^{-1} $^{o}C^{-1}$), leading to melt rates of up to 335 m yr^{-1} across some areas of the ice shelves. This means that the simulations start and progress with almost no ice shelves present. Ice shelves could be important in controlling the deglaciation of the ice sheets since they provide a buttressing effect on the grounded ice streams, slowing the rate of discharge across the grounding line (Hanna et al., 2013). We therefore lower the value of *c* to 10 m yr^{-1} $^{o}C^{-1}$ to match the relationship between melt rate and ocean temperature found by Rignot and Jacobs, (2002) and aim to produce sub-shelf melt rates that better match those recorded in present day Antarctica (~0–43 m yr^{-1}) (Depoorter et al., 2013; Jourdain et al., 2022; Rignot et al., 2013). We first repeat the equilibrium LGM and PGM spin-ups using this new value to obtain initial ice sheets with more extensive ice shelves (see details in Sect. 4.7.1). We then start the deglaciation simulations from these spin-ups, keeping the sub-shelf melt at the lower value (Table 4.1; LDG_{ssm} and PDG_{ssm}).

4.3.2.2.3 Ice dynamics parameter

The two main parameters that impact the flow of the ice sheets are the Weertman friction coefficient, *beta*, which controls the resistance of ice at the base to motion where Weertman sliding is taking place (i.e. in the centre of the ice sheets) and the till water drain factor, *drain*, which controls the rate of till water drainage and therefore the water pressure in the till layer. Since Coulomb basal sliding depends on the effective pressure, varying *drain* has more of an impact in the fast-flowing ice streams at the margins of the ice sheets. We therefore chose to test this latter parameter since it will likely be more important for the deglaciation. In the

reference experiment, the value of *drain* is 0.0235, which is just above the till water supply rate of 0.02, meaning the drainage was just outpacing the supply of water to the till layer. We lower this to the lowest value used in the NROYs selected in Chapter 3, which is below the supply rate (Table 4.1; LDG_{drain} and PDG_{drain}). This should act to increase the depth of the till water layer and increase Coulomb sliding.

Table 4.1: List of experiments performed in this study and the parameter values and transient forcing used for each. "ALL" means that transient orbital parameters, GHGs and sea surface temperatures and sea ice were used. "NONE" means that the forcings were kept constant at glacial maximum values.

Experiment	av_gr	c	drain	Transient Forcing
LDG_{ref}	0.000176	40.2	0.0235	ALL
PDG_{ref}	0.000176	40.2	0.0235	ALL
LDG_{alb}	0.004271	40.2	0.0235	ALL
PDG_{alb}	0.004271	40.2	0.0235	ALL
LDG_{ssm}	0.000176	10.0	0.0235	ALL
PDG_{ssm}	0.000176	10.0	0.0235	ALL
LDG_{drain}	0.000176	40.2	0.0105	ALL
PDG_{drain}	0.000176	40.2	0.0105	ALL
LDG_{orbit}	0.000176	40.2	0.0235	GHG + SST
PDG_{orbit}	0.000176	40.2	0.0235	GHG + SST
LDG_{ghg}	0.000176	40.2	0.0235	ORB + SST
PDG_{ghg}	0.000176	40.2	0.0235	ORB + SST
LDG_{sst}	0.000176	40.2	0.0235	ORB + GHG
PDG_{sst}	0.000176	40.2	0.0235	ORB + GHG
LDG_{ctrl}	0.000176	40.2	0.0235	NONE
PDG_{ctrl}	0.000176	40.2	0.0235	NONE

4.4 Results

4.4.1 Reference simulations

4.4.1.1 Rate of deglaciation

Over the LDG and PDG, the NAIS and EIS lose almost all of their mass by the end of the 12,000 years of simulation, despite starting from very different ice volumes (Figure 4.3a and 4.3b). This is because the pace of the deglaciation differed between each period. During the LDG, the NAIS continues to slightly increase in volume up until around 15 ka, after which it decreases rapidly, especially between ~12 and 11 ka, until the end of the simulation at 9 ka. The PDG NAIS starts at a much lower volume (~23 m sea level equivalent (m s.l.e.) lower) and immediately starts to steadily lose mass with an increase in the rate of deglaciation around 134-131 ka (Figure 4.3a). To better compare the relative rates of deglaciation, Figure 4.4 shows the normalised ice volumes (z), calculated at every time-step (i) over each simulation by;

$$z_i = \frac{v_i - \min(v)}{\max(v) - \min(v)}, \quad (4.1)$$

where v is the actual volume. This shows that the rate of NAIS deglaciation at the LDG slightly lags that of the PDG for the majority of the deglaciation (Figure 4.4a). However, the LDG ice sheets later lose much more mass over a shorter period of time, allowing the larger LDG ice sheet to catch up to the PDG volume by 9 ka (Figure 4.3a). By the end of the simulations, when the interglacials have been reached (9 ka and 128 ka), the LDG only has 1.4 m s.l.e. more ice remaining than the PDG.

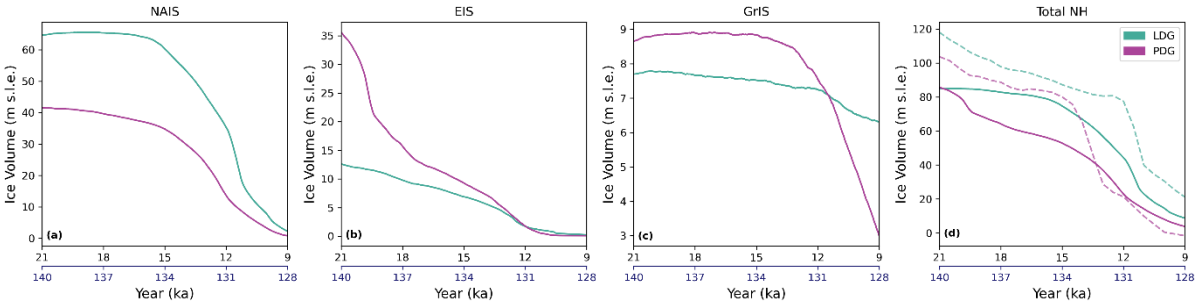

Figure 4.3: Evolution of ice volume (metres sea level equivalent) over LDG_{ref} and PDG_{ref} simulations for (a) North American ice sheet, (b) Eurasian ice sheet, (c) Greenland ice sheet, and (d) whole Northern Hemisphere with dotted lines showing ice volume evolution calculated from the sea level curve of Grant et al. (2014) and the Antarctic ice volume estimated by Briggs et al. (2014).

The EIS starts at a much lower volume at the LDG compared to the PDG (~23 m s.l.e. lower) and loses mass at a relatively constant rate over the simulation, with a slight increase ~13-12ka. On the other hand, the large PDG EIS deglaciates rapidly at the beginning of the simulation, losing over half its mass within the first 3.5 kyr (i.e. by ~136.5 ka), before slowing down until ~132.5 ka and then ending with a final rapid decrease in volume to almost zero by ~130 ka (Figure 4.3b). The normalised ice volume analysis again shows how the rate of the LDG EIS deglaciation lags that of the PDG for the entire simulation, resulting in the EIS losing all of its mass about 1 kyr sooner during the PDG, despite starting from a much larger volume (Figure 4.4b).

Greenland ice sheet (GrIS) evolution also shows significant differences between the deglaciations. Its volume during the LDG slightly increases over the first 1 kyr of the deglaciation before losing mass relatively steadily over the remaining 11 kyr, only decreasing by ~1.4 m s.l.e., with most of this taking place in the last 3 kyr of the simulation, ~12-9 ka. In contrast, the PDG starts at a higher volume and continues to slightly increase in mass for 7 kyr until ~133 ka, after which it then rapidly deglaciates, losing ~6 m s.l.e. in 5 kyr meaning it contributes 3.3 m s.l.e. more to sea level rise at the end of the PDG compared to the end of the

LDG (Figure 4.3c). As opposed to the other NH ice sheets, the rate of deglaciation of the GrIS at the PDG lags that of the LDG for the majority of the simulation (Figure 4.4c). Overall, the two deglaciations start from very similar total NH ice volumes (~85 m s.l.e.), but the PDG deglaciates at a quicker rate leading to ~5 m s.l.e. less ice than the LDG by the end of the reference simulations (Figure 4.3d). Compared to the sea level curve compiled by Grant et al. (2014), the LDG simulation displays a similar rate of deglaciation, with slow retreat of ice over the first half of the deglaciation, followed by a more rapid disintegration (Figure 4.3d). However, in our simulations, the LIG starts with 12 m s.l.e. less ice over the Northern Hemisphere than these records suggest. On the other hand, the PDG sea level data suggests a rapid decrease in ice volume ~134-132 ka compared to the more gradual decrease over the deglaciation simulated here.

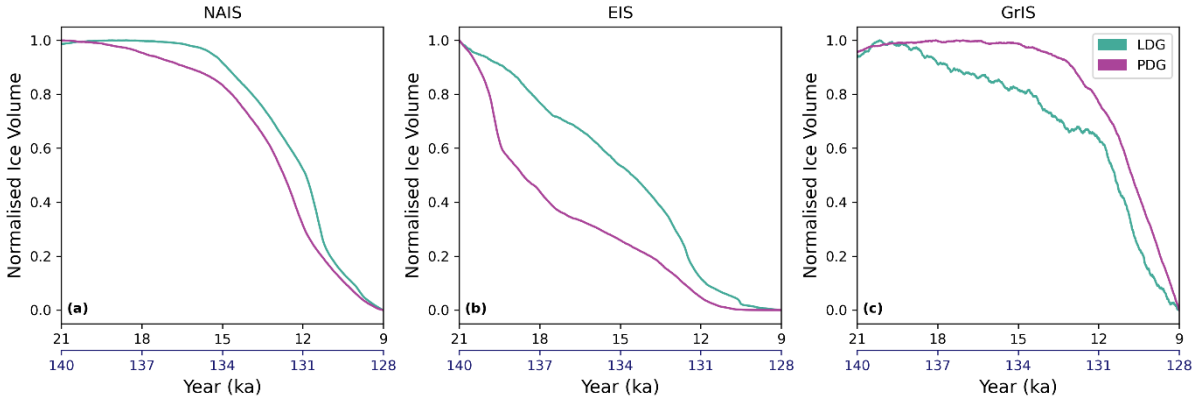

Figure 4.4: Normalised ice volume over the LDG_{ref} and PDG_{ref} simulations for (a) North American ice sheet, (b) Eurasian ice sheet, and (c) Greenland ice sheet. The x-axis shows time going from 21-9 ka for the LDG (black) and 140-128 ka for the PDG (blue).

4.4.1.2 Pattern of deglaciation

Figure 4.5 shows six snapshots of the ice sheets during the LDG simulation and Figure 4.6 compares the pattern of ice retreat at the LDG to the empirical reconstructions of ice extent by Dalton et al. (2020) and Hughes et al. (2016). Seeing where discrepancies lie can provide insight into the limitations of the model or boundary conditions. In line with the reconstructions, the NAIS slowly retreats from the southern and eastern margins until ~15 ka. However, after this, a different pattern of retreat emerges in our simulations. The empirical reconstructions depict a separation of the Laurentide and Cordilleran ice sheets from the north and south inwards, from ~16-14 ka. After this, the Laurentide and Cordilleran ice sheets continue to shrink but ice still remains over the Hudson Bay at 9 ka. In contrast, in LDG_{ref}, the ice sheet remains relatively thick over the north-west of Canada preventing a separation of the two ice sheets until ~10 ka following the retreat of a large proportion of the Laurentide ice

sheet northwards including the ice over Hudson Bay at ~12-11 ka. This occurs largely due to a huge area of ice streaming over the Bay (Figure 4.5 andFigure 4.6). Thus, by 9 ka, there is much less ice remaining over North America compared to reconstructions.

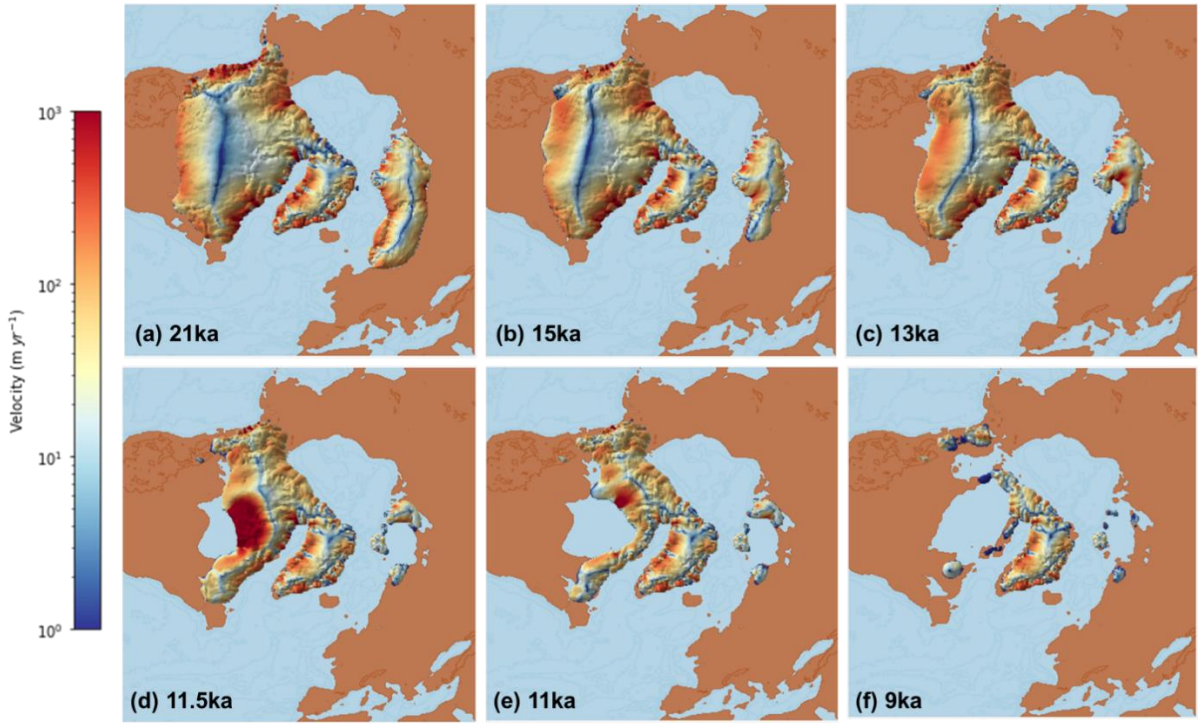

Figure 4.5: Pattern of ice retreat and velocity during LDG_{ref}

Over Eurasia, the empirical reconstructions show a slow retreat of the ice sheet until ~16 ka when a rapid retreat of the BKIS occurs causing most of the ice to disappear here by ~14 ka. Ice continues to slowly shrink over Scandinavia until, by 9 ka, there is a small amount remaining in this region over Norway and Sweden, but all the ice over the Barents-Kara Sea has melted. This is again different to our simulated pattern of retreat, where ice over Scandinavia slowly melts over the first 6 kyr, before a rapid disintegration of the BKIS occurs ~13 ka as a result of a grounding line instability initiated through a large ice stream that corresponds to the location of the major Bjørnøyrenna ice stream (Patton et al., 2017) (Figure 4.5 and Figure 4.6). This occurrence of such instability is favoured by the depressed bedrock caused by the isostatic loading of the BKIS leading to a retrograde slope. By 11 ka, the majority of the EIS has disappeared, with a much smaller area of ice remaining over Scandinavia compared to reconstructions.

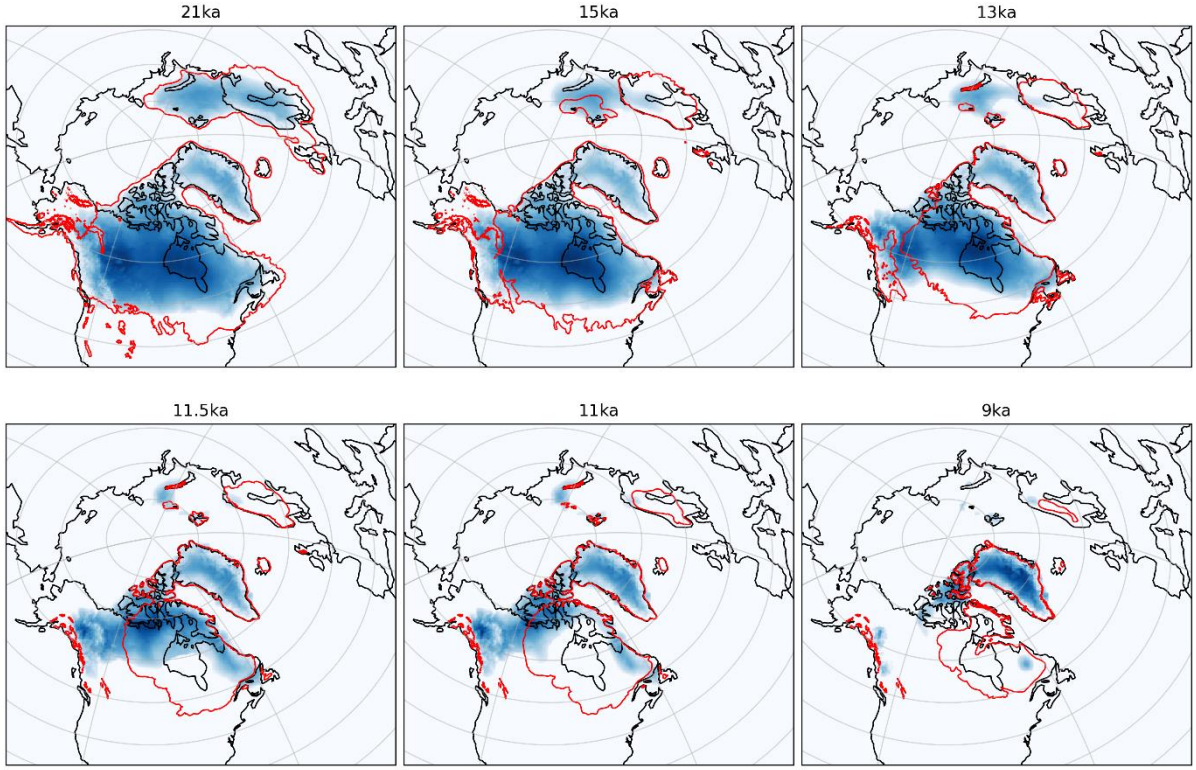

Figure 4.6: Ice thickness at selected intervals through LDG_{ref} simulation compared to the reconstruction of NAIS extent by Dalton et al. (2020) and EIS extent by Hughes et al. (2016) (in red).

Figure 4.7 shows the evolution of the PDG ice sheets at six times during the simulation. There are no equivalent empirical reconstructions for the PDG, but palaeo-records and glacial isostatic adjustment (GIA) modelling give an indication of the timings and locations of periods of major ice retreat. Similar to the LDG, the NAIS stays relatively steady over the first 6 kyr of the PDG_{ref} simulation. From around 134 ka, the NAIS begins to retreat north over the Hudson Bay, again due to the formation of a large ice stream, causing it to almost completely disappear by 128 ka, with only small patches remaining of the Cordilleran ice sheet. Speleothem and sediment records indicate a final NAIS outburst flood occurred ~129 ka suggesting the majority of the NAIS had melted by this point, in line with our simulations (Nicholl et al., 2012; Stoll et al., 2022).

By 139 ka, large areas of ice streaming have already started to form over the BKIS, within the Bjørnøyrenna ice stream as well areas further east possibly corresponding to the Svyataya Anna ice stream (van Aalderen et al., 2024), causing it to become unstable and lose significant mass in only 2 kyr by 138 ka. The ice over Scandinavia and Northern Russia then slowly starts to retreat so that by 132 ka there are only thin areas remaining over these regions and the EIS has completely disappeared by 128 ka. This is in contrast with the results of GIA modelling combined with palaeo-shoreline evidence, which suggests that a slow retreat of the entire EIS

takes place over the deglaciation with a significant area of ice still remaining over the Barents-Kara Sea at 134 ka (Lambeck et al., 2006). In addition, the large input of meltwater that would have resulted from the rapid disintegration of the BKIS seen at the beginning of the simulations, is not evident in current palaeo-records covering this period. Instead, a large shift in AMOC strength and climate conditions occurs much later at the onset of HS11 (~135 ka; Marino et al., 2015).

For both time periods, the rate and pattern of the GrIS retreat matches relatively well to palaeo-data. By the end of the LDG simulation, the Greenland ice sheet margin has retreated from the edge of the continental shelf, but still covers most of the land area. On the other hand, the PDG GrIS displays a much more significant retreat from its margins. We simulate a difference in contribution of 3.3 m s.l.e. at the end of the PDG compared to the LDG, which is higher than QR24 (2.2 m s.l.e.), but still within the range of difference reported by other studies (Quiquet et al., 2013; Rohling et al., 2019).

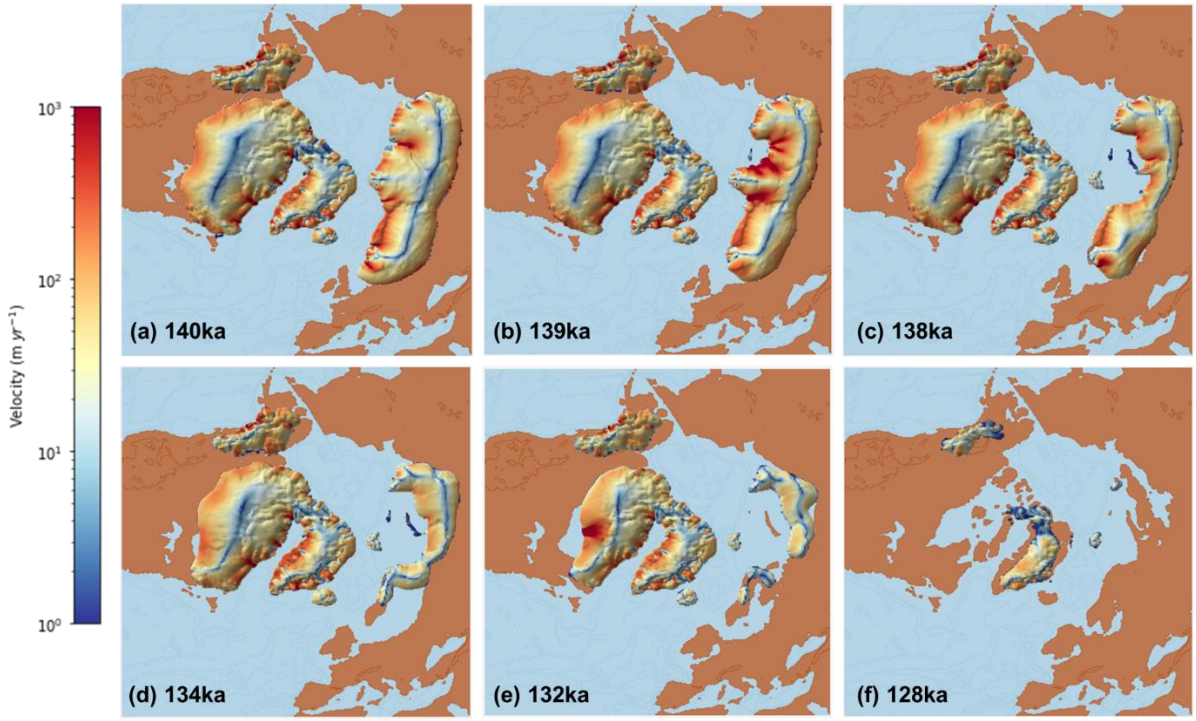

Figure 4.7: Pattern of ice retreat and velocity during PDG_{ref} (note these are different intervals to Fig. 4.5)

4.4.1.3 Comparison of simulated climates

The PDG starts with a warmer glacial maximum mean surface air temperature than the start of the LDG (~0.34 °C difference; Figure 4.8a). The spatial differences are largest over the Northern Hemisphere. The LGM is warmer over much of the Arctic and Eurasia where the ice

sheet is less extensive, but cooler over areas of the North Atlantic, North America, and Siberia (Figure 4.9a). The temperature then increases steadily over the deglaciation, with the rate of increase speeding up slightly after ~132 ka. Whilst the LDG starts with a lower global mean surface temperature, it experiences a rapid increase ~18 ka bringing it above the PDG value. This is followed by a slight cooling for ~1 kyr bringing temperature back down to the PDG level. It then starts to steadily warm up again until another relatively rapid increase in temperature occurs ~12 ka, after which the temperature then steadies (Figure 4.8a). By the final year of the simulations, the PDG is on average 2.44 °C warmer than the LDG, particularly over North America, Greenland and Antarctica (Figure 4.9b). A similar pattern of temperature change is seen for both hemispheres. However, overall the Southern Hemisphere experiences warmer temperatures (Figure 4.8b and 4.8c).

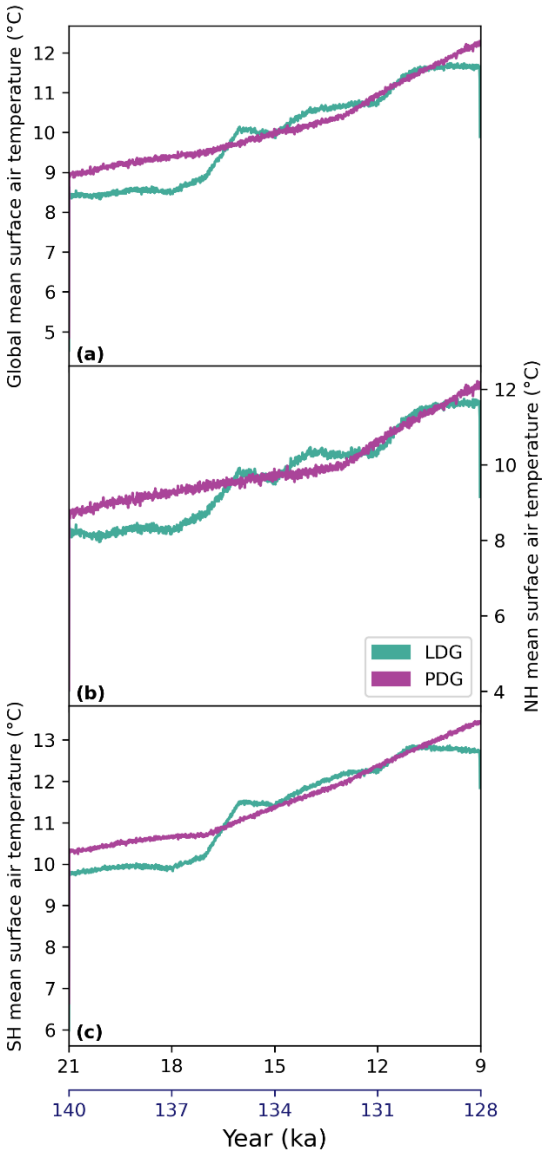

Figure 4.8: Annual mean surface air temperature evolution across (a) the globe, (b) the Northern Hemisphere, and (c) the Southern Hemisphere.

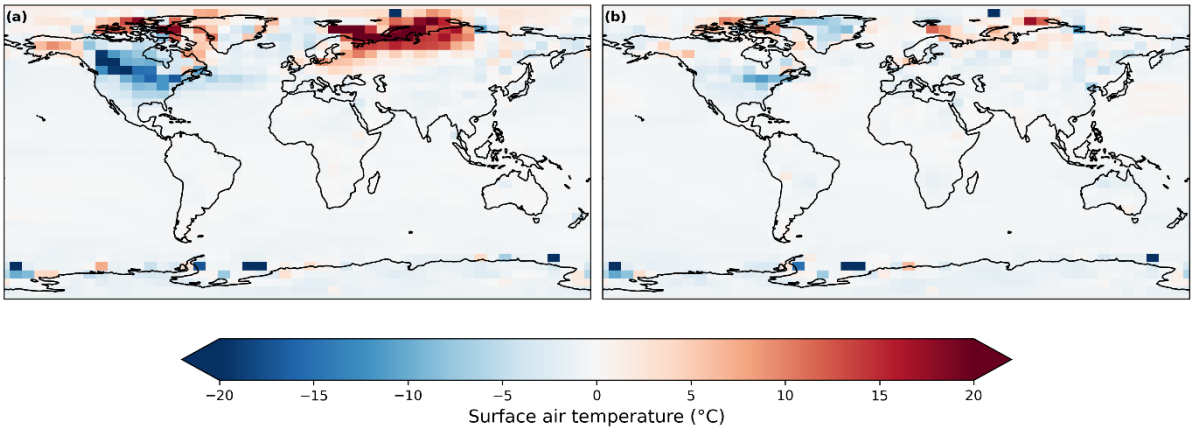

Figure 4.9: Difference in global annual surface temperature between the LDG_{ref} and PDG_{ref} averaged over (a) the first 30 years, and (b) the final 30 years of the simulations.

4.4.2 Parameter sensitivity tests

The pattern of ice retreat remains similar between the reference experiments and the sensitivity tests. Changing the values of the three selected parameters, instead impacts the rate of deglaciation to varying degrees.

Decreasing the sub-shelf melt constant (c) in the LDG_{ssm} and PDG_{ssm} simulations leads to a maximum rate of sub-shelf melt around one third of the value of the reference experiments, allowing the formation of larger areas of ice shelves especially around the time of the BKIS retreat (Figure 4.10). However, the overall influence on ice sheet retreat is small, with all LDG_{ssm} and PDG_{ssm} ice sheets ending at the same volume and configuration as the corresponding reference simulations (Figure 4.11). Digging into the detail, for the LDG NAIS and EIS, reducing the sub-shelf melt constant acts to slightly increase the rate of deglaciation, but has the opposite effect for the GrIS (Figure 4.11a-c). For the PDG, c has an even weaker impact, especially for the NAIS and GrIS, but causes a decrease in the deglaciation rate for the EIS, especially towards the start of the simulation when the large retreat over the Barents-Kara Sea takes place (Figure 4.11d-f). Therefore, the use of a smaller value of c produces a better match to empirical constraints of the PDG EIS since it delays the retreat of the BKIS.

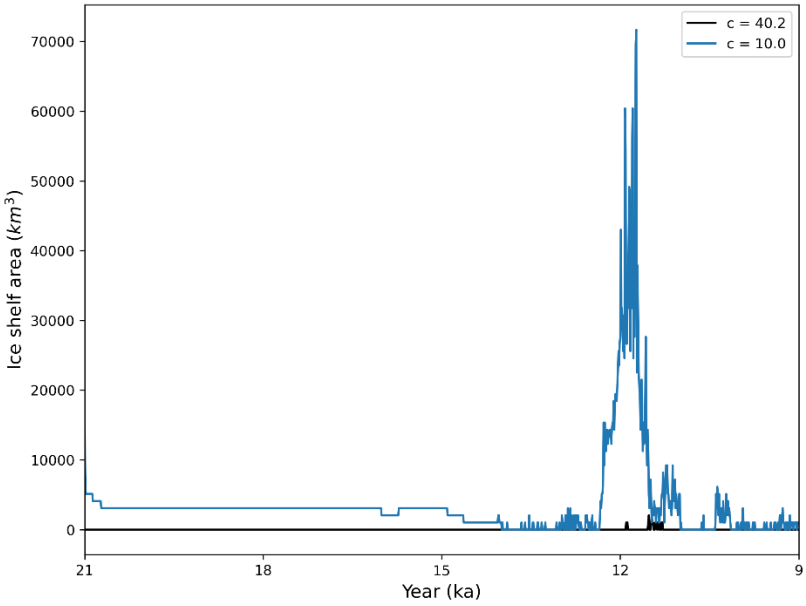

Figure 4.10: Total ice shelf area in LDG_{ref} (black) and LDG_{ssm} (blue).

Decreasing the value of the till water drainage rate (*drain*) causes an increase in the depth of the till water layer and therefore the velocity of the ice streams. This has a larger effect on the rate of deglaciation compared to the sub-shelf melt constant, with the LDG_{drain} and PDG_{drain} experiments resulting in an increased rate in all cases, except for towards the beginning of the PDG EIS deglaciation. At the end of the LDG, ~1.6 m s.l.e. less ice remains over North America and ~0.8 m s.l.e. less over Greenland when the lower *drain* value is used. Nonetheless, the PDG ends with the same ice volume as the LDG (Figure 4.11). A lower value of *drain* results in an increase in the rate of BKIS retreat at the LDG but delays its retreat at the PDG, therefore producing a better match to palaeo-data. However, it also speeds up the deglaciation of the NAIS at the LDG which is already too quick in our reference simulation compared to reconstructions.

By far the largest impact in our sensitivity simulations comes from raising the sensitivity of the surface snow albedo to increasing grain size (*av_gr*), decreasing the albedo of the ice sheet more with melt. This leads to a lower albedo, on average, across all ice sheets over the entire deglaciation, accelerating ice retreat and resulting in less ice remaining in the LDG_{alb} and PDG_{alb} experiments (Figure 4.11). The EIS and NAIS at the LDG both reach close to zero ice volume ~3 kyr sooner than the reference experiment and the GrIS rapidly loses mass after ~16 ka resulting in an ice sheet 3.5 m s.l.e. smaller than the reference (Figure 4.11a-c). Similarly, the PDG NAIS reaches close to zero ~3 kyr sooner and the EIS ~6 kyr sooner. The rate of the PDG GrIS deglaciation rapidly increases after ~134 ka resulting in less than 1 m s.l.e. of ice remaining (Figure 4.11d-f).

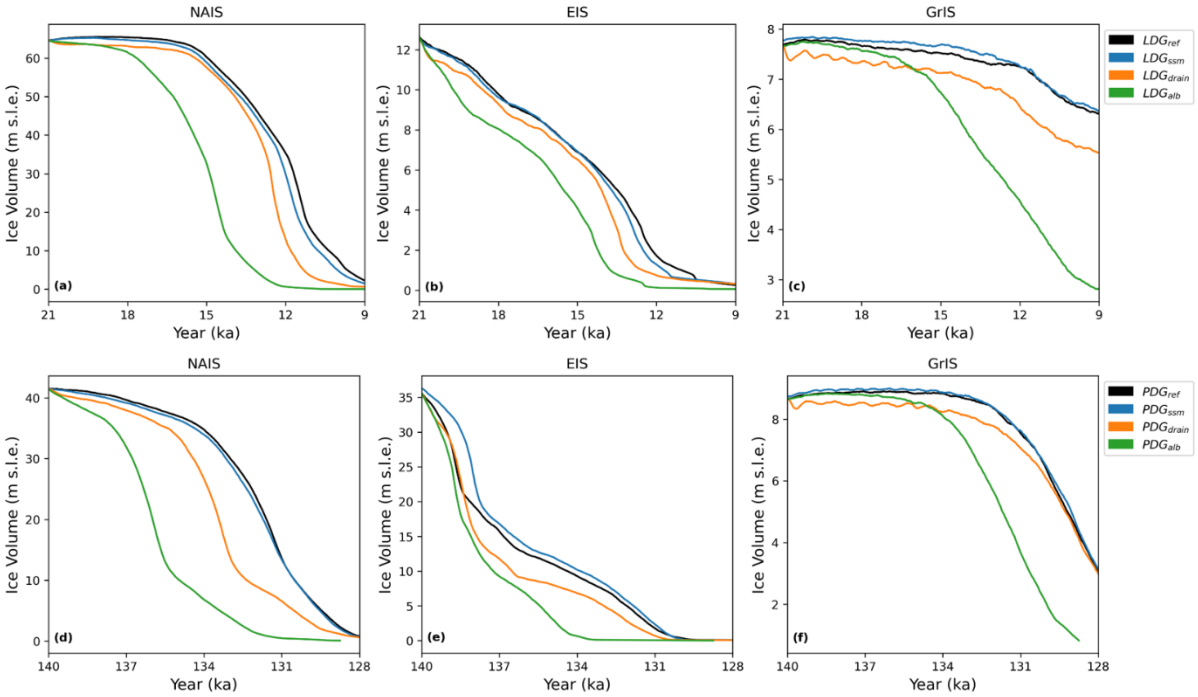

Figure 4.11: Ice volume evolution for the North American, Eurasian and Greenland ice sheets in the LDG and PDG reference experiments (black) compared to the three parameter sensitivity tests (ssm – blue, drain – orange, alb – green).

4.4.3 Forcing sensitivity tests

It is clear from our forcing sensitivity experiment that orbital configuration changes are the main driver of ice sheet retreat for both periods since fixing the parameters to their glacial maximum values in LDG_{orbit} and PDG_{orbit} prevents deglaciation (Figure 4.12). For most of the ice sheets, the LDG_{sst} and PDG_{sst} experiments, with fixed SSTs and sea ice, have the second biggest impact on the resulting deglaciation, followed by the LDG_{ghg} and PDG_{ghg} experiments with fixed GHGs, but in both cases ice sheet retreat still occurs, only at a delayed rate. Interestingly, for the PDG EIS, the collapse of the BKIS at the start of the simulations occurs under all forcing experiments, suggesting it is not triggered by external contributors, but that the simulated PGM BKIS was very close to becoming unstable (Figure 4.12e). To confirm this, we perform some additional control simulations in which the deglaciations are ran keeping all forcings constant at glacial maximum values (orbit, GHGs, SSTs/sea ice and sub-shelf melt). The results of these experiments (LDG_{ctrl} and PDG_{ctrl}) show that, even under continued glacial maximum climate conditions, the BKIS instability still occurs at the same time in the PDG simulation, before the ice volume reaches equilibrium once again (Figure 4.18). We also perform the PDG_{ctrl} simulation using a resolution of 16 km in BISICLES across the ice sheets (rather than refining the BKIS to 2 km), consistent with the set-up for the glacial maximum spin-ups that the deglaciations were initiated from (Figure 4.18e). In this case the collapse does

not occur, allowing us to conclude that the stability of the BKIS under PGM forcing changed as the resolution of the ice streams were increased. Previous studies have also shown there to be a resolution dependence of grounding line behaviour and the occurrence of marine ice sheet instabilities in ice sheet models (Cornford et al., 2016; Pattyn et al., 2013).

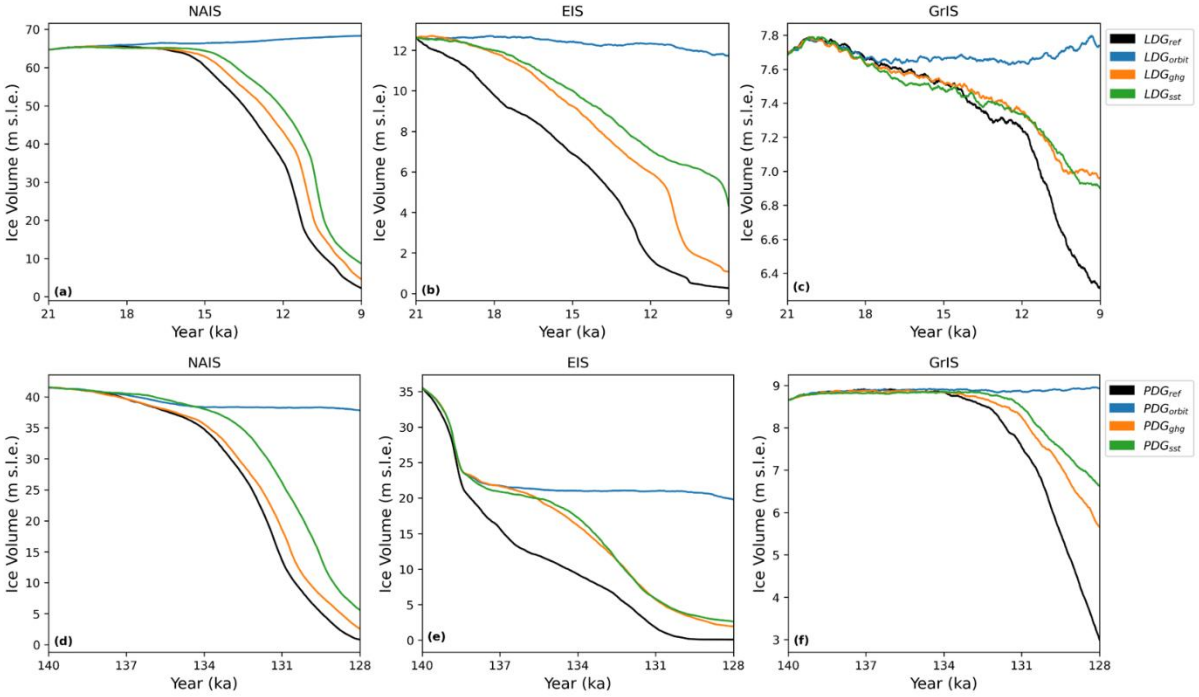

Figure 4.12: Ice volume evolution for the North American, Eurasian and Greenland ice sheets in the LDG and PDG reference experiments (black) compared to the three forcing sensitivity tests (orbit – blue, ghg – orange, sst – green).

4.5 Discussion

4.5.1 Evaluation of reference ice sheets

We find that the rate of deglaciation of the North American and Eurasian ice sheets over the PDG was quicker than the LDG, in agreement with the results of QR24, resulting in less Northern Hemisphere ice cover at the start of the Last Interglacial compared to the Holocene. Since QR24 used the same initial ice sheet configurations for both periods, this can be attributed to the different orbital and GHG forcings used. For example, the PDG experienced a more rapid increase and higher peak in NH summer insolation than the LDG, accelerating the ice retreat (Figure 4.1a). In this study, the prescribed SSTs and sea ice forcing may have also played a role. The SSTs were higher at the start of the PDG compared to the LDG (Figure 4.2a and 4.2b), contributing to elevated surface temperatures in the early stages of the PDG (Figure 4.8). The higher NH sea ice concentration at the beginning of the LDG (Figure 4.2c) could have contributed to a stronger albedo feedback, delaying warming in this region and

slowing the ice retreat. These varied retreat rates also support previous studies that suggest the different sequence of events and Last Interglacial characteristics could result from different rates of deglaciation and amounts of meltwater (Landais et al., 2013; Obase et al., 2021; Stoll et al., 2022). QR24, however, also found that these different forcings do not affect the pattern of deglaciation, but in our results the pattern of deglaciation, of the Eurasian ice sheet in particular, differs for each period. For example, during the LDG, the EIS loses mass over Scandinavia before a rapid disintegration of ice occurs over the Barents-Kara Sea, whereas it is the other way around for the PDG. In addition, our simulations display a different rate and pattern of Greenland ice sheet retreat compared to that of QR24, with the PDG lagging the LDG but producing a higher contribution to sea level overall. This suggests that the different initial ice sheet topographies at the LGM and PGM and/or prescribed ocean forcings used in this study compared to the dynamic ocean of QR24, led to a different pattern of ice sheet retreat over the LDG compared to the PDG.

The timing and pattern of NAIS and EIS ice sheet retreat differs in our simulations compared to empirical data and other empirically constrained model reconstructions, including GLAC-1D (Ivanovic et al., 2016; Tarasov et al., 2012; Tarasov and Peltier, 2002) and ICE-6G_C (VM5a) (Argus et al., 2014; Peltier et al., 2015; hereafter ICE-6G). For example, during the LDG, we simulate the separation of the Cordilleran and Laurentide ice sheets at ~10 ka which is much later than the reconstructions suggest (~16-14 ka; Dalton et al., 2020; Munyikwa et al., 2011). In addition, the final collapse of the Laurentide ice sheet over Hudson Bay occurs before this event and ~2-3 kyr too early in our simulation (Dalton et al., 2020; Ullman et al., 2016). The pattern of LDG NAIS retreat is captured better in some EMIC-ISM and stand-alone ISM simulations (Abe-Ouchi et al., 2013; Ganopolski et al., 2010; Gregoire et al., 2012; Heinemann et al., 2014; Niu et al., 2019), however others display similar results to this study (Quiquet et al., 2021a, b; Scherrenberg et al., 2023a). Nevertheless, many of these studies also simulate a later Cordilleran-Laurentide separation (e.g. 11.6 ka in Gregoire et al., 2012, 2016) or earlier final retreat (e.g. ~2 kyr early in Niu et al., 2019).

The former discrepancy could partly be a result of the ice being too thick across the Cordilleran-Laurentide saddle and north-western area of Canada. Compared to the GLAC-1D reconstruction, our ice sheet is 1-2 km thicker in this region at the LGM which suggests an overestimation of precipitation in this area. There is a known cold bias over the north-western region of Canada and Alaska in FAMOUS-ice, due to its coarse resolution, which produces excess ice growth over this area (Patterson et al., 2024; Sherriff-Tadano et al., 2024). Furthermore, precipitation is not downscaled in FAMOUS-ice which may lead to a more

widespread distribution of precipitation rather than a more realistic concentration on the slopes of ice margins (Smith et al., 2021b). Therefore, it may be the ice configuration in this area, which is impacted by the resolution of the atmospheric model, that is important for capturing this separation, rather than the complexity of the model used.

Across Eurasia, the Scandinavian ice sheet retreats too quickly in LDG_{ref}, but there is a ~2 kyr delay in the collapse of the BKIS. This timing of the BKIS ice sheet instability is more in line with the ICE-6G reconstruction, which represents the mass loss later than GLAC-1D, and with the results of Quiquet et al. (2021a). The pattern of our simulated collapse agrees relatively well with empirical reconstructions, being initiated by a retreat of the grounding line across the Bjørnøyrenna ice stream. Petrini et al. (2020) show that this instability is driven by an increase in the sub-surface ocean forcing at ~15 ka. An abrupt increase in the magnitude of our prescribed forcing occurs ~13 ka, coinciding with the start of the BKIS retreat, which could indicate a limitation in the thermal forcing parametrisation that we use. Furthermore, the ice over this region is, again, thicker in our LGM configuration and in ICE-6G compared to GLAC-1D, which could contribute to the delay of BKIS collapse. Conversely, our Scandinavian ice sheet is much thinner than both ICE-6G and GLAC-1D reconstructions, possibly explaining its faster retreat.

Compared to the modelled reconstruction used in the PMIP4 protocol (Abe-Ouchi et al., 2013; Menviel et al., 2019; Tarasov et al., 2012), our PDG_{ref} simulation also shows some differences. Again, the rate of retreat is fairly similar, with the NAIS losing most of its mass later on in the deglaciation (~132-128 ka), but the EIS volume has already decreased in size significantly by 132 ka. In the PMIP4 reconstruction, ice remains to the north of Hudson Bay at 128 ka and over the Barents-Kara Sea until ~130 ka; but we note that these modelled outputs are not necessarily more realistic than our results.

4.5.2 Causes of ice retreat

To help understand the patterns of simulated ice retreat, we examine the magnitude of total ice mass loss at the surface due to ablation and to the ocean due to sub-shelf melt and calving to see how the importance of each process varied during each deglaciation and between both time periods (Figure 4.13). The processes of retreat at play across the NAIS were similar between the LDG and PDG, hence the similar patterns of retreat were displayed between the simulations. Surface melt makes the largest contribution to mass loss for most of the deglaciation, increasing around the same time for both periods (~6 kyr in to the simulations)

following an increase in CO_2 and surface temperatures. This drives the initial melting of the southern and eastern margins around this time.

In the ice sheet model, when ice retreats and leaves behind an area of depressed bedrock at 0 m or below sea level, formed due to isostatic loading, this is treated as ocean. Therefore, the same sub-shelf melt and calving parameterisations are applied in these areas as along the marine margins. This process occurs ~8.5-10 kyr into the simulations and acts as a large proglacial lake to the south of the NAIS (Figure 4.5 and Figure 4.7). Proglacial lakes have been shown to drive rapid ice flow through promoting the formation of ice streams due to reduced friction at the ice-bed interface, changes in geometry and enhanced frontal ablation and calving. Floating ice can form on the lakes which can undergo sub-shelf melt and calving. Changes to longitudinal stresses lead to grounding line retreat which can then become unstable once it advances onto the reverse gradient bedrock, similar to processes that take place in marine terminating ice sheets (Hinck et al., 2022; Quiquet et al., 2021a, b; Sutherland et al., 2020). Thus, the majority of the NAIS ice loss towards the end of the deglaciations over Hudson Bay is facilitated by these processes as seen by the large peak in the ocean losses that occurs around this time (Figure 4.13a and 4.13d).

The magnitude of this peak is 3 times higher for the LDG, causing more of the total mass loss than surface ablation from ~12-11 ka, in line with the rapid rate of deglaciation seen during this period. This is likely due to the larger volume of ice present over North America during the LDG compared to the PDG. This mechanism of accelerated mass loss agrees with empirical evidence of the formation of Lake Agassiz along the southern margin of the Laurentide ice sheet ~13 ka (Teller and Leverington, 2004) and indeed has been modelled in other studies of the Last Deglaciation of the NAIS, which also determined these processes to be crucial in the late deglacial ice loss (Hinck et al., 2022; Matero et al., 2020; Quiquet et al., 2021b, a). Although, it is important to note that our model is not simulating Lake Agassiz, only some of the processes that occur at the ice-water boundary that have the same effect.

In reality, the freshwater of proglacial lakes has different properties to seawater, and they may sit at elevations higher than sea level, which could impact the water temperature, thermal forcing and mechanical processes and thus the rate of retreat (Benn et al., 2007; Scherrenberg et al., 2023b; Sugiyama et al., 2016). However, it is unclear what effect a more realistic parameterisation might have on our simulations since there are few constraints on the surface temperature of the lake and these characteristics could have competing impacts. For example, freshwater calving and basal melt is typically of a lower magnitude than in marine

environments (Benn et al., 2007), but water bodies at higher elevations could cause increased flotation of ice shelves and the higher density maximum of freshwater could act as a heat source, both of which act to accelerate deglaciation (Matero et al., 2020; Quiquet et al., 2021b; Scherrenberg et al., 2023a).

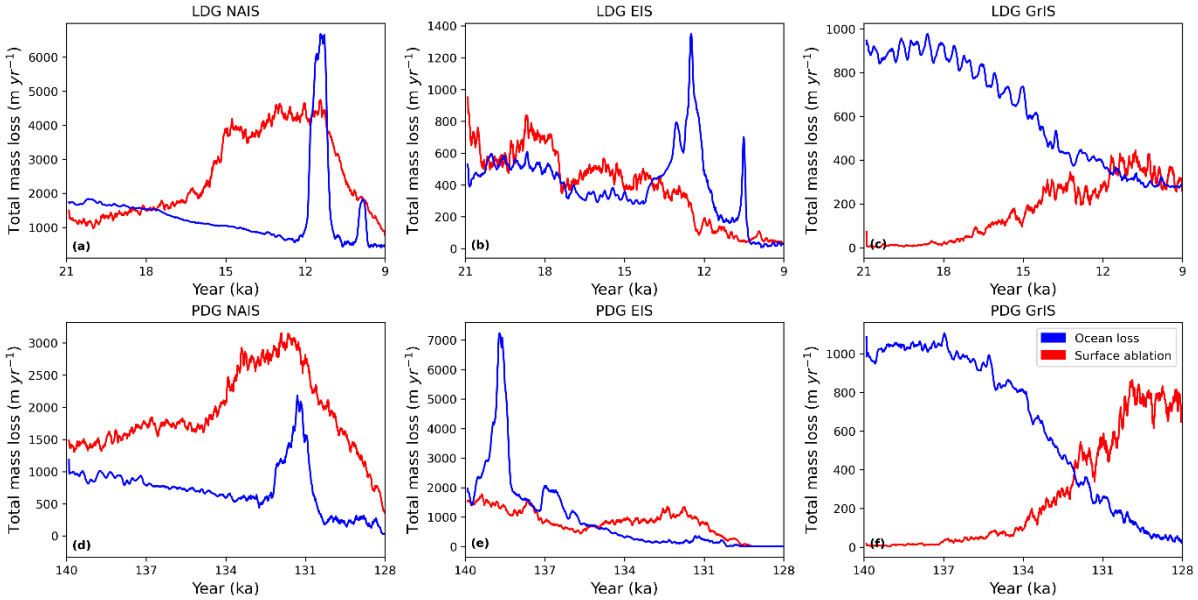

Figure 4.13: Total mass loss for each ice sheet from surface ablation (red) and ocean processes including calving and sub-shelf melt (blue) over LDG_{ref} and PDG_{ref}.

For the EIS, surface ablation is less dominant, only causing a slightly higher mass loss than oceanic processes over most of the simulation, but is still largely responsible for the gradual retreat of ice over Scandinavia (Figure 4.13b and 4.13e). Again, there are large peaks in the ocean loss (12.5 ka for the LDG and 138.5 ka for the PDG), corresponding to when the BKIS deglaciation takes place in each simulation. This shows the roles of sub-shelf melt and calving in the rapid deglaciation of this marine based ice sheet. The reason that the increased resolution triggers the BKIS collapse at the start of the deglaciation for the PDG, but not for the LDG, could be related to the presence of additional large ice streams in the initial PGM ice sheet in the region to the east of Svalbard, where the PGM EIS extends significantly further than at the LGM (Figure 4.6a). This causes a discharge of ice across the grounding line over a larger area of the marine margin forming floating ice shelves, which then undergo sub-shelf melting and calving. Increasing the ice sheet model resolution enhances these processes triggering grounding line instabilities as the ice retreats across the depressed bedrock, which is at a lower elevation than at the LDG due to the larger ice mass (Figure 4.14). Other studies have highlighted the increased sensitivity of the PGM EIS to ocean forcing and instabilities as a result of its larger size (Stoll et al., 2022).

In contrast, the only significant ice stream at the LGM is the Bjørnøyrenna ice stream to the west of Svalbard, which, in our LDG_{ref} simulation, does not start discharging significant mass until ~14-13 ka when the ocean thermal forcing displays a significant increase (Figure 4.5c). This implies that for the PDG, the main driver of retreat of the BKIS is the ice dynamics arising from the larger Eurasian ice sheet configuration that the deglaciation is initiated under, whereas for the LDG, the BKIS retreat is triggered by sub-ocean warming induced dynamical processes. This could explain why different patterns of retreat are seen in our simulations, but not in those of QR24 who initialise both deglaciations under the same LGM ice sheet states and therefore the differences in ice dynamics are not captured. That ocean temperatures trigger the Last Deglaciation of the EIS through dynamic thinning, specifically through the Bjørnøyrenna ice stream, is consistent with the findings of several previous modelling studies (Alvarez-Solas et al., 2019; Patton et al., 2017; Petrini et al., 2018, 2020).

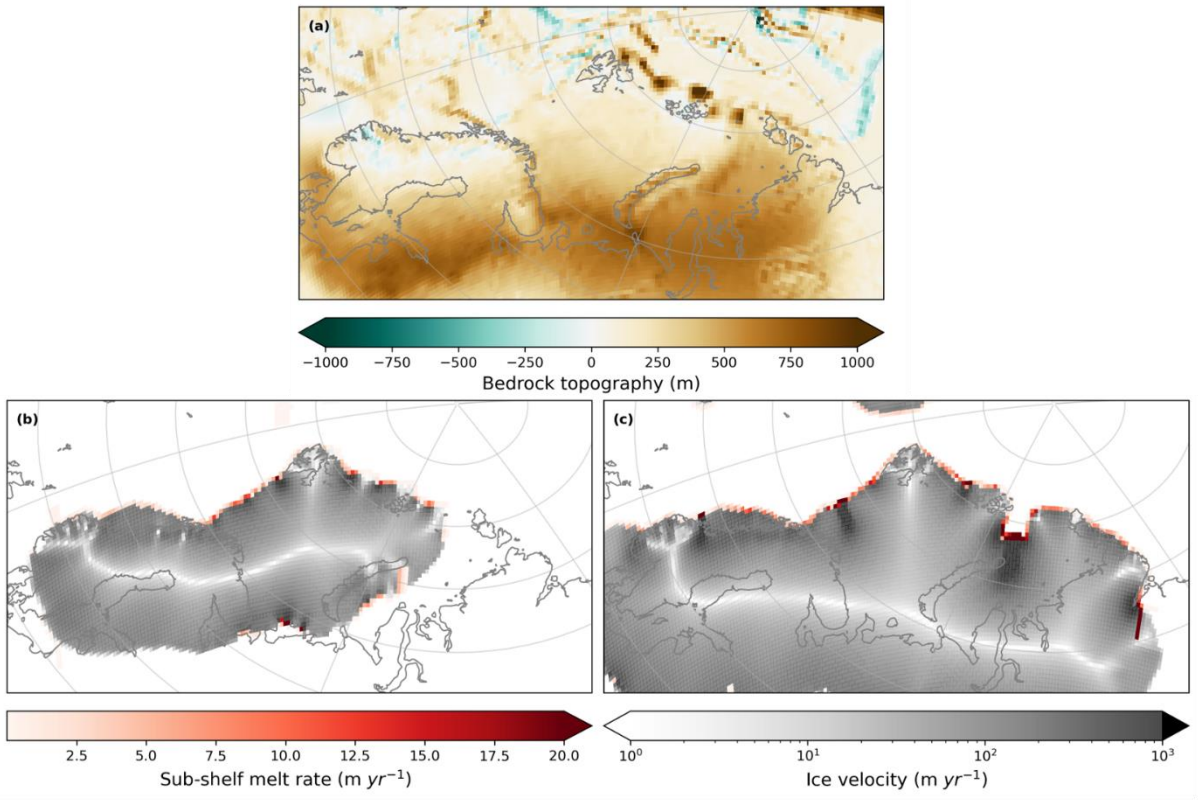

Figure 4.14: (a) Difference in bedrock height above sea level between the LDG and PDG; and ice velocity and sub-shelf melt rate at (b) LDG and (c) PDG, at 100 ice sheet years into the reference simulations.

For Greenland, ocean processes are the strongest driver of initial mass loss through its many marine based outlet glaciers, but this decreases over time as ice retreats inland (Figure 4.13c and 4.13f). The large mass loss that occurs towards the end of the deglaciations is driven by surface processes. A larger increase in ablation occurs at the PDG, leading to the bigger reduction in GrIS volume, likely due to the higher surface air temperatures that result from the

higher SSTs, insolation and GHG forcing towards the end of this period (Figure 4.1 and Figure 4.2).

4.5.3 Evaluation of reference climates

Global mean surface temperatures are 2.44 ºC warmer at the end of PDG_{ref} compared to LDG_{ref}. This is in line with proxy evidence that the LIG was warmer than the Holocene by ~1-2 ºC (Bova et al., 2021; Otto-Bliesner et al., 2013b; Turney and Jones, 2010). In addition, temperatures over Antarctica are also warmer at the end of the PDG than the LDG (~1.7 ºC), consistent with enabling an additional contribution from the Antarctic ice sheet to LIG sea level rise (Clark et al., 2020; Turney et al., 2020b). The surface air temperature patterns closely follow the prescribed SSTs for both hemispheres, with the LDG showing much more variation in the temperature change over the deglaciation compared to the PDG, which has a smoother temperature rise. This is a result of the smaller interval between the SST and sea ice forcing datasets for the LDG compared to the PDG (see Sect. 4.3.2.1), allowing shorter scale variations in SSTs to be captured. Since the HadCM3 simulations used to produce the SST data were not transient and did not include freshwater fluxes, they do not resolve the millennial scale climate changes that result from feedbacks related to the input of freshwater into the oceans (Obase et al., 2021; Snoll et al., 2024). Therefore, the simulated climate and ice sheet evolutions in this study are also not influenced by the abrupt changes caused by large variations in the strength of the AMOC (Gregoire et al., 2016; Liu et al., 2009; McManus et al., 2004). As a result, the increase in Antarctic air temperature at the start of the LIG compared to the start of the Holocene may be underestimated (Marino et al., 2015).

Since the SSTs have such a strong influence on the global mean temperatures, the use of a different SST and sea ice forcing could produce very different climates, which may impact the ice sheet evolution. For example, compared to SST fields from transient simulations of the Last Deglaciation performed by HadCM3 (Snoll et al., 2022, 2024) and CESM (iTRACE; He et al., 2021; Liu et al., 2009), the SSTs used in our study are colder on average by 2 ºC and 4.5 ºC respectively. Additionally, our methodology does not explicitly resolve feedbacks between the oceans and other components of the earth system, such as the impact of ice melting on ocean circulation, which could have a significant impact on the simulated climate and ice sheet retreat. For example, the NAIS deglaciates more rapidly than the reconstructions suggest, which may be attributed, at least in part, to the lack of meltwater flux feedbacks acting to weaken the AMOC and cool the Northern Hemisphere (e.g. during the Younger Dryas), hence

slowing down or delaying the ice retreat (Gregoire et al., 2015; Quiquet et al., 2021b; Scherrenberg et al., 2023b).

4.5.4 Parameter sensitivities

Our sensitivity tests showed that the deglaciation of the Northern Hemisphere ice sheets is much more sensitive to the parameters that affect the strength of the ice-albedo feedback and ice dynamics compared to sub-shelf melt rate. As would be expected, decreasing the sub-shelf melt forcing results in a lower contribution from ocean loss overall and enables the formation of larger areas of ice shelves (Figure 4.19). However, the impact on the rate of deglaciation is small in general and the rapid grounding line retreat at the proglacial lake boundary of the NAIS and the marine margin of the EIS still occurs around the same time even at the much lower sub-shelf melt rates. This suggests that these instabilities are not triggered by the high sub-shelf melting rates, but instead may be initiated once a threshold in surface mass balance has been reached since, in the case of the NAIS, surface ablation peaks over this region at that time, only after which the ocean processes become important. A similar conclusion is shown in previous studies that also show NAIS proglacial lake instabilities are not very sensitive to calving or sub-shelf melting (Quiquet et al., 2021b; Scherrenberg et al., 2023a). This is because decreases in the height of the ice sheet due to increased velocities at the lake boundary, subject it to high surface temperatures due to the temperature-elevation feedback, and a strongly negative SMB, which further accelerates ice flow. This thinning eventually leads to the formation of low-lying floating ice and then grounding line retreat primarily through thinning caused by further surface ablation (Hinck et al., 2022; Quiquet et al., 2021b; Scherrenberg et al., 2023b). The primary mechanism of retreat then switches to sub-shelf melt and calving once the instability is initiated. The timing of the instability is thus linked to the formation of ice shelves, which is determined by the local ice thickness, which in turn is governed by the SMB. Therefore, the early occurrence of the instability in our LDG simulations is likely due to SMB being too negative across the southern margin of the Laurentide ice sheet too early on in the deglaciation, possibly due to biases in the climate model or missing ice-ocean feedbacks.

On the other hand, the SMB remains positive across the majority of the BKIS while it retreats. In this case, insensitivity to sub-shelf melt rate could be promoted by the unconfined nature of most of the LDG ice shelves, which therefore are not exerting a buttressing effect on the grounded ice. As such, ice shelf removal does not impact the ice dynamics (van Aalderen et al., 2024; Gudmundsson, 2013).

Interestingly, the PDG EIS appears to display different behaviour and a higher sensitivity to sub-shelf melt rate, with a decreased rate of BKIS deglaciation under the reduced sub-shelf melt, particularly towards the start of deglaciation. It appears that the formation of ice shelves in front of the large PGM BKIS ice streams provides some buttressing effect on the ice streaming, slowing down the velocity (Figure 4.15) and thus the ice retreat, again showing the importance of the different ice sheet geometries for determining the patterns and drivers of deglaciation. Moreover, our study uses a simplified sub-shelf melt parameterisation in which the melt rate increases linearly with the thermal forcing, whereas several studies have determined a quadratic relationship to be more suitable (Burgard et al., 2022; Favier et al., 2019). We also do not take into account that melt rates are generally higher nearer the grounding line and depend highly on the ice shelf geometry (Beckmann and Goosse, 2003; Rignot and Jacobs, 2002), instead adopting a uniform melt rate across the ice shelves. Improving the representation of this process may result in a higher sensitivity of ice retreat to the sub-shelf melt rate.

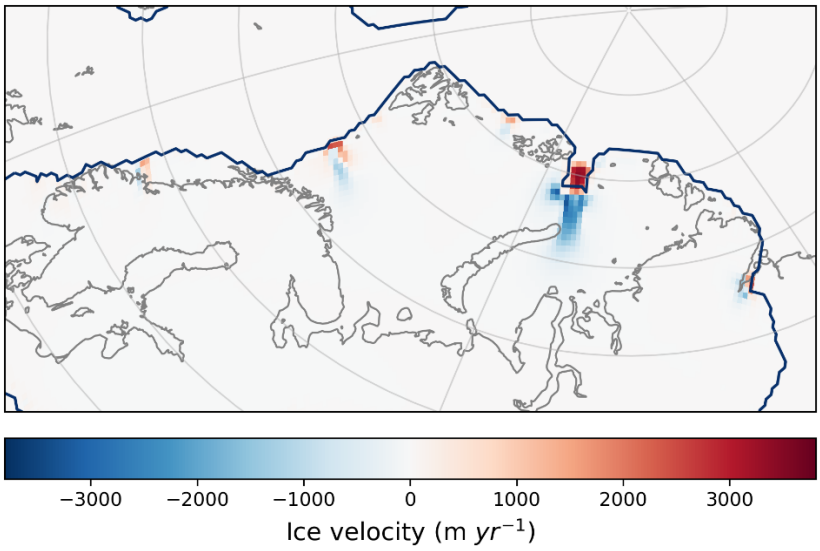

Figure 4.15: Difference in ice velocity between the PDG_{ssm} and PDG_{ref} simulations at ice sheet year 100. The blue contour shows the ice sheet extent in PDG_{ref} at this time.

In general, decreasing the rate of till water drainage causes an increase in the magnitude of ocean loss and an earlier deglaciation (Figure 4.20). This is because the Coulomb sliding at the edges of the ice sheet increases resulting in faster ice streaming which decreases ice thickness and transports more ice towards the ablation area and marine/proglacial lake margins. Again, the opposite effect is seen at the beginning of the PDG, where reducing the value of *drain* results in a slower retreat of the BKIS and a slightly later peak in ocean loss. This is because initially, the faster velocity allows more ice to be transported out of the large BKIS ice streams

where more extensive, confined ice shelves then form, providing a buttressing effect on interior ice, which in turn slows down the ice flow, until subsurface ocean or surface air temperatures increase enough to remove the shelves quicker than they can form.

Increasing the value of *av_gr* had the biggest impact on the rate and pattern of deglaciation. It acted to increase the magnitude of surface ablation across all ice sheets leading to a faster deglaciation and smaller interglacial ice sheet (Figure 4.21). It also caused the peak in NAIS ocean loss to occur earlier, evidencing the role of SMB on triggering proglacial lake instabilities. The peak in ocean loss also occurs earlier for the LGM EIS, which suggests that the instabilities that occur here are also sensitive to SMB. The lower albedo causes a negative SMB across the BKIS margin in LDG_{alb}, further accelerating the ocean-driven grounding line retreat. On the other hand, the timing of marine ice sheet retreat remains the same for the PDG since it is mostly driven by dynamical and ocean-based processes.

The sensitivity of the timing of ice loss to model parameters could imply that some of the discrepancies between the simulated ice retreat and empirical reconstructions could be minimised by tuning the model to meet constraints over the deglaciation; i.e. a period of climate and ice sheet change. For example, lowering the till water drainage rate could improve the modelled rate of deglaciation of the EIS during both periods since it acts to accelerate the collapse of the BKIS during the LDG, but delays it during the PDG, producing a better match to observations. However, this would also cause a faster retreat of the NAIS which would not be desirable. Therefore, tuning may need to be carried out individually for each ice sheet and non-uniform parameter values applied across the Northern Hemisphere. In addition, finding parameters that produce plausible glacial maximum ice sheets and a realistic deglaciation could be challenging since the higher albedos of the two glacial maximum NROY simulations failed to deglaciate at all in North America. Nevertheless, this could be worked towards by running ensembles of transient simulations, then training and employing emulators to evaluate several iterative waves of parameter sets, covering much more of the parameter space, whilst remaining computationally feasible. Failing the finding of any overlap of parameter space, improvements to the model physics and parameterisations will need to be investigated further. Alternatively, applying temporally evolving parameter values could be another solution that could be explored in future work.

4.5.5 Forcing sensitivities

The results of the fixed forcing experiments show the changing orbital configuration, and the resulting increase in incoming insolation, throughout the deglaciations, is the primary driver of

ice sheet retreat over both periods. Greenhouse gas and sea surface changes have a lesser impact on the ice volume, amplifying the response of the earth system to the insolation changes, but fixing their values does not act to prevent deglaciation or the triggering of ice sheet instabilities. This is in agreement with the Milankovitch theory and other modelling studies that have shown insolation to be the main trigger of deglaciations, with CO_2 and other factors such as vegetation and ocean conditions, playing a secondary role (Charbit et al., 2005; Ganopolski and Brovkin, 2017; Gregoire et al., 2015; Hays et al., 1976; Quiquet and Roche, 2024). The fact that the BKIS collapses at the start of the PDG even under the fixed forcings further highlights the role of the ice stream dynamics and ice shelf processes in causing this instability, rather than any climate trigger, suggesting that the glacial maximum ice sheet used in these simulations was close to its tipping point and very sensitive to changes in resolution that triggered mechanisms of collapse.

4.5.6 Limitations and future work

To avoid the inconsistencies caused by the change in ice sheet model grid resolution between the glacial maximum spin-ups and subsequent deglaciation simulations, future studies could take several different approaches. For example, the transient experiments could be run at a lower resolution, however this may mean that grounding line processes are inadequately captured. Alternatively, a second spin-up phase could be carried out at the higher resolution or the use of higher resolution topography could be beneficial across all stages. Further work will be needed to find an appropriate balance between process representation and computational expense.

As well as a simplified representation of proglacial lake and marine sub-shelf melt in our simulations and the use of prescribed ocean conditions, we identify some other design choices that could have impacted the results. Firstly, in the climate model, the land-sea mask remains fixed to the LGM and PGM configuration throughout the duration of the simulations. In reality, as the ice sheets retreat during deglaciations, the volume of the ocean increases and the crust rebounds due to GIA. This changes the coastlines, causing areas that were once land to be flooded by water (creating new ocean), and areas that were once submerged to become new land. The change in the area of different surface types can impact the albedo and therefore the climate locally and globally. For example, Bouttes et al. (2023) showed that changes in albedo due to an increase in the area of the ocean, and therefore sea ice, during deglaciation, cause cooler temperatures, especially over Greenland. However, in their study the ice sheets were not interactive and so the effect of the Greenland cooling on ice sheet evolution was not verified.

Performing an additional sensitivity test in which the land-sea mask is manually updated at various stages of deglaciation would be useful in future work.

We also keep vegetation at fixed pre-industrial coverage, but several studies have highlighted the role of vegetation dynamics in amplifying orbital forcing, and thus mean global temperature change, during glacial-interglacial cycles due to the vegetation-snow albedo feedback (Horton et al., 2010; Quiquet and Roche, 2024; Willeit et al., 2024). The use of a glacial vegetation field (compared to present day) has been shown to cause a decrease in annual mean surface temperature at the LGM, especially over Eurasia, which may delay the deglaciation in our simulations (Crucifix and Hewitt, 2005; Jiang, 2008).

In addition, whilst BISICLES accounts for the GIA of bedrock topography, it does not include the global and local sea level change due to the gravitational pull of the ice sheets or changing ice sheet volume (e.g. Gomez et al., 2013). Sea level rise or fall in the vicinity of the grounding line can facilitate or delay its retreat, and therefore be another factor contributing to marine ice sheet instabilities (Han et al., 2021). Thus, as the ice sheets retreat, the gravitational force they exert on the ocean reduces and local sea level falls which may slow grounding line retreat. This could delay the early collapse of the BKIS or Laurentide ice sheet seen in our results. An increase in global mean sea level can also amplify ice sheet sensitivity to sub-shelf melt, which could have the opposite effect (Petrini et al., 2020).

4.6 Conclusions

This paper has produced one of the first transient simulations of the Penultimate Deglaciation using an atmospheric general circulation model coupled to an ice sheet model, which is contrasted with an equivalent Last Deglaciation simulation. We have shown that, in agreement with previous studies and empirical evidence, the Northern Hemisphere ice sheets deglaciated at a faster rate, and ended with a lower ice volume overall during the PDG compared to the LDG. In addition, we simulate a higher contribution from the GrIS to sea level rise and higher Antarctic surface air temperatures at the end of the PDG, which is also in line with the suggested contribution of the GrIS and Antarctic ice sheet to the LIG sea level highstand.

For both periods, the orbital configuration is the main driver of deglaciation, with greenhouse gases and sea surface conditions playing a secondary role, acting to amplify the response of the ice sheets to insolation changes.

The rate of deglaciation is largely impacted by the albedo of the ice sheet through its influence on the surface mass balance, and to a lesser extent by the rate of till water drainage, which

impacts the ice velocity. The simulations show only a small sensitivity to the rate of sub-shelf melt.

Grounding line instabilities occur in the NAIS and EIS for both periods and cause significant rapid ice retreat, but are triggered by different mechanisms and are therefore sensitive to different forcings. The formation of an area of ocean, acting as a large proglacial lake, along the southern margin of the Laurentide ice sheet around the same time for both the LDG and PDG, leads to an instability as the grounding line retreats across the depressed bedrock. This is facilitated by the increased velocities and formation of low-lying ice shelves which are subjected to high negative SMB. This process therefore shows sensitivities to the SMB (*av_gr*) and dynamics (*drain*) parameters. On the other hand, the EIS displays a marine ice sheet instability in the BKIS, which occurs at different times in the simulations and which we suggest is due to the different glacial maximum ice sheet configurations and resulting dynamics. The larger PDG EIS produces a more depressed bedrock than at the LGM, and the PGM ice sheet has more active ice streams, which form areas of confined ice shelves that undergo sub-shelf melt and calving, enabling an increase in resolution to trigger grounding line retreat in these simulations even under glacial maximum climate conditions. However, the LDG EIS ice stream dynamics only become significant in the retreat once the sub-ocean forcing is high enough, with negative SMB causing further acceleration. Therefore, the NAIS and LDG EIS retreat is sensitive to parameters that control the SMB (*av_gr*) and dynamics (*drain*), whereas the PDG EIS is more sensitive to the sub-shelf melt (*c*) and the dynamics parameter (*drain*), however a decrease in the latter results in a delay in the occurrence of the instability in contrast to an acceleration during the LDG.

Another major finding of this study is the need to tune model parameters to fit constraints across all stages of glacial-interglacial periods, which could be done through transient ensemble simulations or emulation. This may require looser constraints on what is considered a "good fit" under current model capabilities or the application of spatially and/or temporally varying parameter values.

4.7 Appendices

4.7.1 Glacial maximum spin-ups

Figure 4.16 shows the timeseries of NH ice volume for the LGM and PGM glacial maximum equilibrium simulation referred to as *NROY extent* in Chapter 3. The parameter values used in these simulations are used in all the experiments performed in this study (excluding where one parameter value is changed in the sensitivity tests described in Sect. 4.3.2.2). In addition, the

ice sheet state from the final year of these runs is used as the initial condition for the deglaciation simulations.

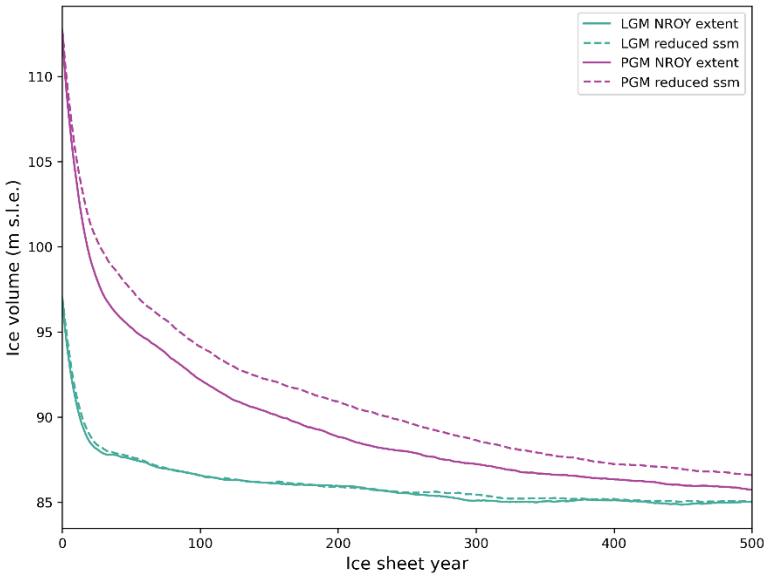

Figure 4.16: Glacial maximum spin-up ice volume evolution for the LGM and PGM *NROY extent* simulations and the same simulations but with a reduced sub-shelf melt constant.

The exceptions are experiments LDG_{ssm} and PDG_{ssm}, which were initiated from the end of 500-year glacial maximum spin-ups that were performed using exactly the same parameters as the reference experiments except for the value of the sub-shelf melt constant, *c*, which was lowered to a value of 10. The timeseries of ice volume for these spin-ups are also shown in Figure 4.16. This had a very small impact on the overall ice sheet volume at the LGM, but a slightly larger impact at the PGM where it produced ~3.8 m s.l.e. more ice. Figure 4.17 shows the spatial difference in ice thickness between the glacial maxima ice sheet used in the reference experiments and the end of the 500 climate-year (5,000 ice sheet-year) glacial maxima spin-ups, using the lower sub-shelf melt constant. The lower parameter value forms thicker ice across the BKIS, Southern Greenland and Eastern Laurentide ice sheets, but causes thinner ice over Northern Greenland, parts of the Innuitian ice sheet and over Scandinavia at the LGM.

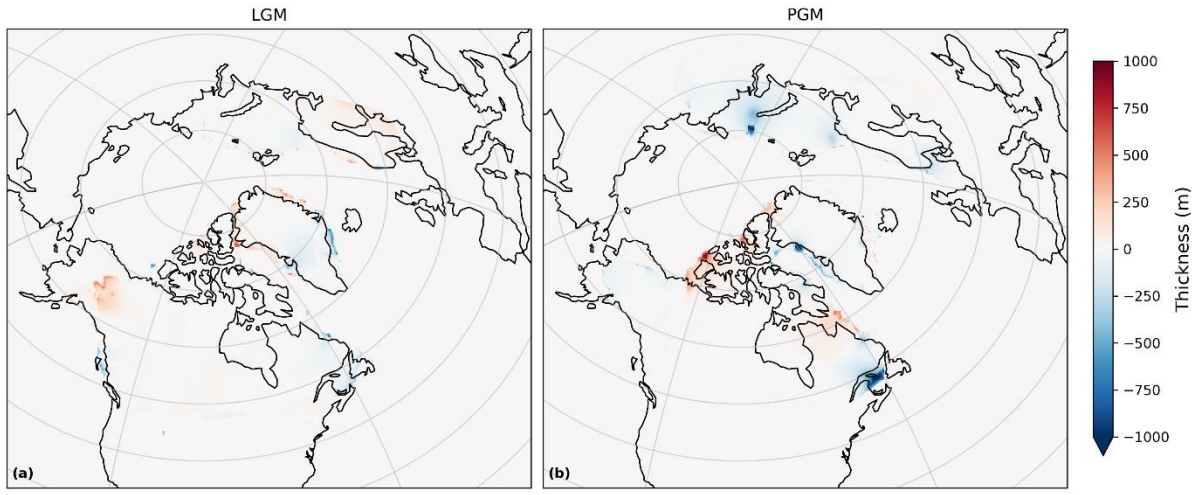

Figure 4.17: Difference in ice thickness between the initial ice sheets used in (a) LDG_{ref} and LDG_{ssm} and (b) PDG_{ref} and PDG_{ssm}.

4.7.2 Control experiments

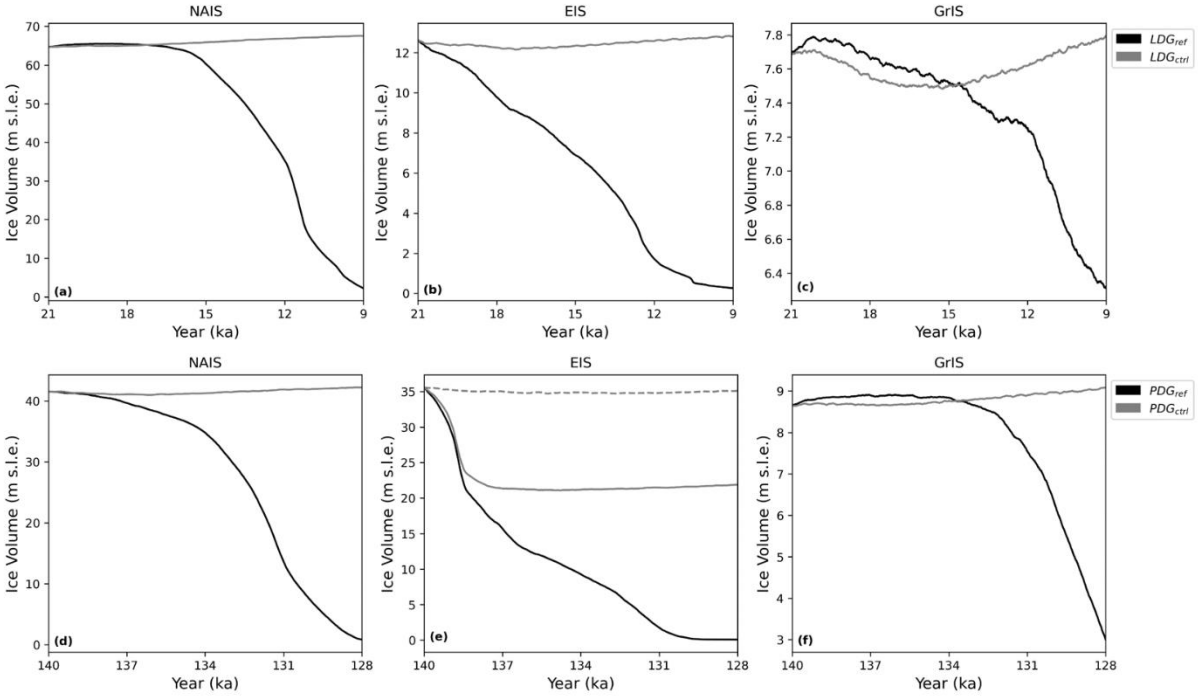

Figure 4.18: Ice volume evolution for the North American, Eurasian and Greenland ice sheets over the LDG_{ref} and PDG_{ref} experiments (black) compared to the LDG_{ctrl} and PDG_{ctrl} experiments (grey). The Eurasian ice sheet volume evolution for the PDGctrl experiment with reduced resolution is shown by the dashed grey line in panel (e).

4.7.3 Surface ablation and ocean loss in the parameter sensitivity experiments

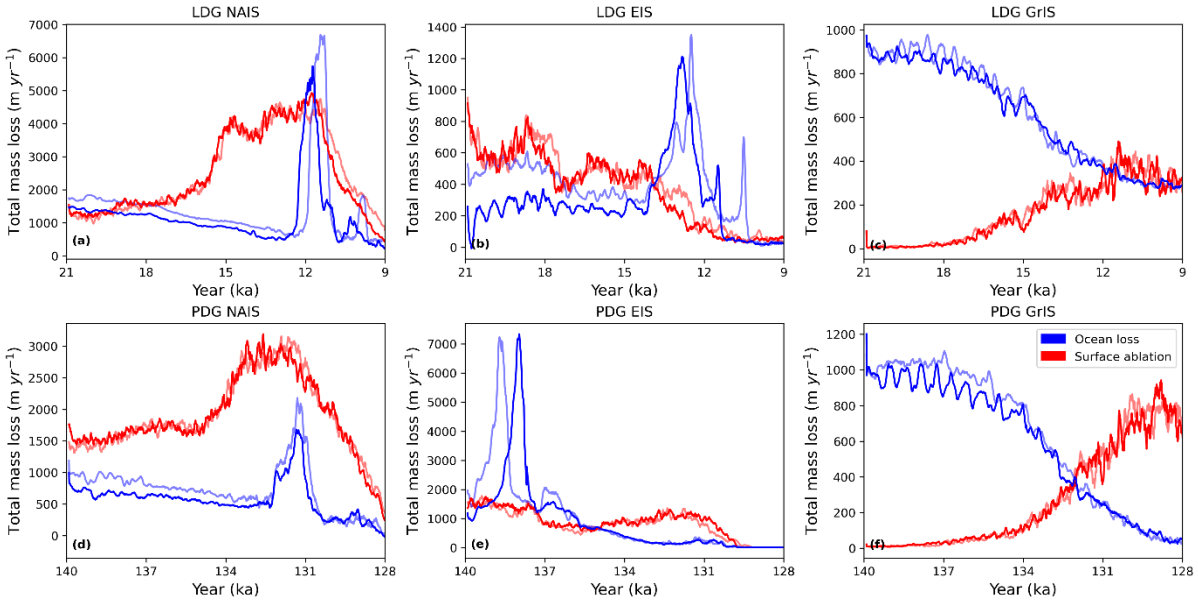

Figure 4.19: Total mass loss for each ice sheet from surface ablation (red) and ocean processes including calving and sub-shelf melt (blue) over LDG_{ssm} and PDG_{ssm} (solid colour) and LDG_{ref} and PDG_{ref} (lighter colour).

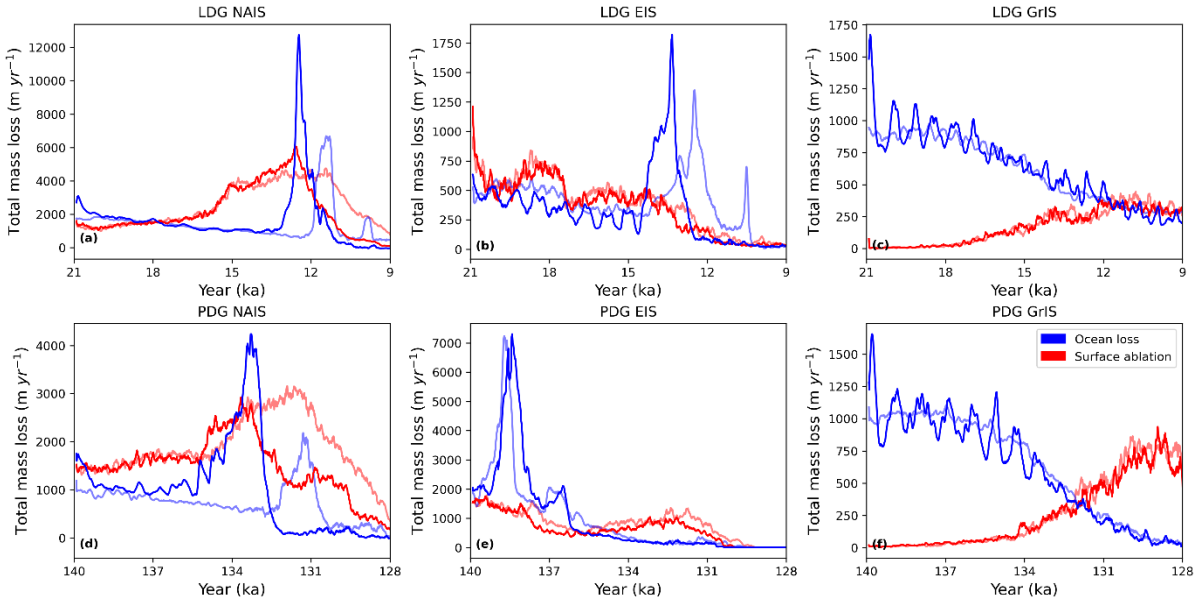

Figure 4.20: Total mass loss for each ice sheet from surface ablation (red) and ocean processes including calving and sub-shelf melt (blue) over LDG_{drain} and PDG_{drain} (solid colour) and LDG_{ref} and PDG_{ref} (lighter colour).

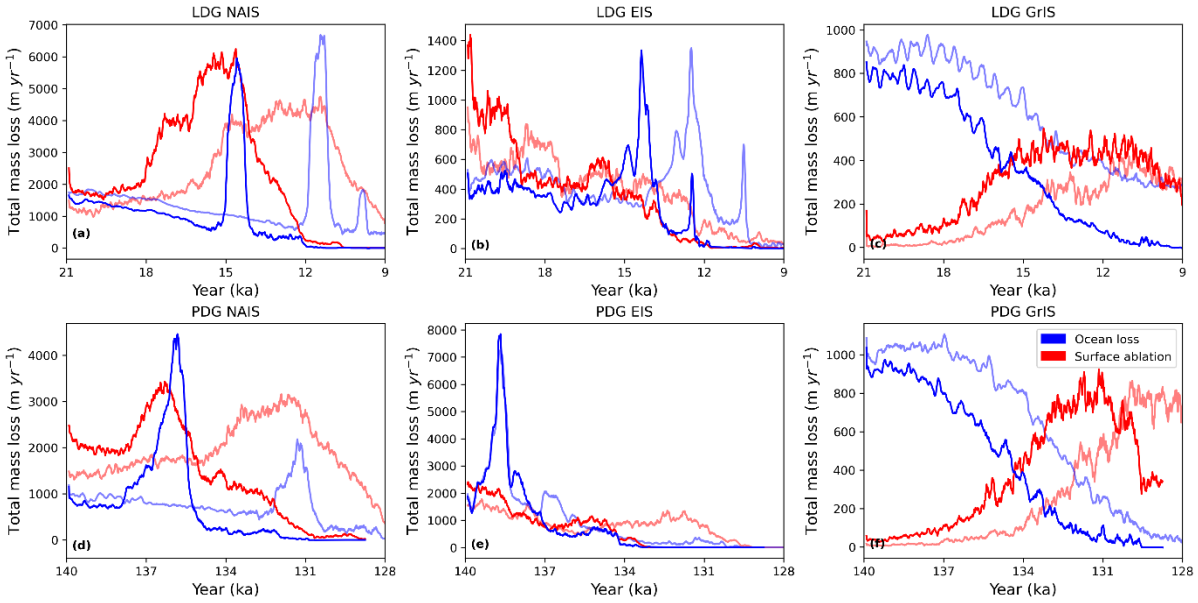

Figure 4.21: Total mass loss for each ice sheet from surface ablation (red) and ocean processes, including calving and sub-shelf melt (blue) over LDG_{alb} and PDG_{alb} (solid colour) and LDG_{ref} and PDG_{ref} (lighter colour).

Chapter 5

5 Discussion and conclusions

5.1 Review of aims and research questions

The overall aim of this thesis is to investigate and compare the ice sheet and climate evolutions over the Last and Penultimate deglaciations. This was broken down into four research questions (**RQs; Chapter 1**) which were addressed by fulfilling four objectives (**OBJs;** Table 5.1) through the use of numerical climate and ice sheet models, model-data comparison techniques, uncertainty quantification and sensitivity analysis (**Chapters 2-4**). This section answers the RQs based on the work presented in this thesis (**Chapters 2-4**):

> **RQ1**. Why did the configuration of the Northern Hemisphere ice sheets differ during the Last Glacial Maximum and Penultimate Glacial Maximum?
>
> **RQ2**. Which climatological and glaciological processes and feedbacks are important when simulating glacial periods?
>
> **RQ3**. What are the similarities and differences between the last two deglaciations due to the different transient climate forcings (orbit, greenhouse gases, sea surface conditions) and initial ice sheet states?
>
> **RQ4**. What were the main drivers of ice sheet retreat during the last two deglaciations?

Table 5.1: Research objectives and the relevant thesis chapters in which they are addressed.

Objective	**Chapter(s)**
OBJ1. Develop implausibility metrics to constrain the model output and find simulations that produce plausible LGM and PGM Northern Hemisphere ice sheets	2, 3
OBJ2. Assess the uncertainty in the simulated ice sheets that arises from model parameter and boundary condition uncertainties	2, 3, 4
OBJ3. Determine the sensitivity of the individual ice sheet evolutions to model parameters	2, 3, 4

OBJ4. Evaluate the importance of different drivers in the deglaciations through sensitivity tests	4

5.1.1 RQ1. Why did the configuration of the Northern Hemisphere ice sheets differ during the Last Glacial Maximum and Penultimate Glacial Maximum?

There is evidence that the configuration of the Northern Hemisphere (NH) ice sheets differed between the Last Glacial Maximum (LGM) and Penultimate Glacial Maximum (PGM), despite similar greenhouse gas (GHG) concentrations and global average insolation. Reconstructions indicate the Eurasian ice sheet (EIS) was smaller during the LGM, while the North American ice sheet (NAIS) was larger (Batchelor et al., 2019). These differences likely influenced deglaciation pathways by affecting the initial climate state, glacial isostatic adjustments and meltwater inputs. However, the reasons for these disparities remain unclear and cannot be fully deduced from empirical evidence alone, requiring numerical modelling for deeper insights. **Chapter 2** explores these differences in relation to the NAIS using coupled climate-ice sheet ensemble simulations. Initialising the Glimmer ice sheet model with an 18.2 ka ice sheet topography for both glacial maxima should allow the effects of variations in orbital, GHG, and sea surface forcings on ice sheet configurations to be examined. The study aimed to identify the sensitivity of surface mass balance (SMB) to the different glacial maxima climate states and whether these forcings resulted in configurations aligning with empirical evidence. In order to achieve this, objective 1 (**OBJ1**) first needed to be met to tune FAMOUS-Glimmer and see whether it was capable of simulating a plausible LGM NAIS which could then be used in the subsequent analysis and comparison to the equivalent PGM simulation. An evaluation of the LGM ensemble revealed six parameter sets producing plausible ice sheets (73.9–97.1 m s.l.e.), while the same parameters generated smaller PGM ice sheets (53.4–83.4 m s.l.e.), consistent with the limited empirical evidence and other modelling studies.

A limitation arose in the coupling between the FAMOUS and Glimmer models, where FAMOUS did not adjust ice-covered grid cells to match unglaciated areas in Glimmer. As a result, initial ice extents (but not topography) mirrored the predefined conditions in FAMOUS from the PMIP4 protocols, with higher albedo over the LGM Laurentide-Cordilleran saddle region compared to the PGM. This prompted additional sensitivity simulations and factorial decomposition to separate the roles of climate forcing (orbit, GHGs and SSTs/sea ice) and initial ice cover on the resulting ice sheet volumes. Results showed that the PGM climate alone

would yield a larger NAIS than the LGM climate, thus differences in initial ice cover, driven by ice-albedo feedbacks, explained the distinct configurations. These findings suggest the varying climate trajectories leading to each glacial maximum were the key to the different ice sheet sizes as the ice sheets were likely not in equilibrium with the prevailing climate during the maxima, owing to their long response timescales (Ziemen et al., 2014). Transient simulations of glacial build-up are needed to further understand the processes involved and answer RQ1. This result also highlights the sensitivity of simulated ice sheets to the initial condition and therefore the need for better empirical constraints on the reconstructions used, or a quantification of the resulting uncertainty through the use of multiple reconstructions as initial conditions.

5.1.2 RQ2. Which climatological and glaciological processes and feedbacks are important when simulating glacial periods?

Accurately simulating glacial ice sheets at their maximum extent and during deglaciation requires a comprehensive representation of key glaciological and climatological processes and interactions. These include basal sliding, grounding line dynamics, glacial isostatic adjustment (GIA), and SMB influences such as temperature and precipitation changes. However, significant uncertainties surround these processes, their roles in ice sheet evolution, and their optimal parameterisations in models. Notably, models that perform well for present day ice sheets may not be directly applicable to other regions or time periods (Gandy et al., 2023). Objectives 2 (**OBJ2**) and 3 (**OBJ3**) focus on assessing these uncertainties and the sensitivities of simulated ice sheets to model parameters. Through large ensemble analyses and sensitivity tests across **Chapters 2-4**, my research identifies which processes are critical to accurately modelling ice sheet extent and volume.

The ice-albedo feedback is identified as a crucial factor influencing SMB and, consequently, ice sheet growth and stability. Albedo directly impacts the amount of incoming solar radiation reflected, which regulates surface temperatures and the potential for ice sheet growth. **Chapter 2** demonstrates that simulations of the LGM starting with a larger ice coverage exhibited higher albedos. This reflected more solar radiation, cooled the climate, and supported further ice growth. Conversely, simulations initialised with the smaller PGM ice sheet under LGM climate conditions failed to grow to LGM size, underlining the sensitivity of ice sheets to initial albedo condition.

Moreover, **Chapters 2** and **3** perform large perturbed parameter ensembles and sensitivity analyses to quantify the impact of uncertain model parameters, revealing the dominance of

albedo related parameters (*daice*, *fsnow*, av_gr) in controlling the ice sheet volume and extent. High values of *daice* (bare ice albedo sensitivity) and f*snow* (snow albedo density threshold) and low values of *av_gr* (snow albedo sensitivity to grain size), increase the albedo of the ice sheets. Simulations achieving realistic LGM ice sheet configurations, presented in Chapter 2, consistently displayed albedos exceeding 0.69 across North America and Greenland. The balance among these three parameters is thus essential for maintaining large ice sheets during glacial maxima. The use of emulation in Chapter 3 enabled the parameter sensitivities to be more clearly quantified through a Sobol′ sensitivity analysis. These three parameters displayed relatively high first order and second order sensitivity indices confirming their significant individual influence on ice sheet volume as well as the importance of their interactions with other parameters.

Similarly to Sherriff-Tadano et al., (2024), the results from these chapters suggest that the sensitivity to *daice* diminishes if *fsnow* is sufficiently high and *av_gr* sufficiently low, at least in the case of North America. Nevertheless, to maintain the large enough ice sheets over both North America and Eurasia in the two "Not Ruled Out Yet" (NROY) simulations in Chapter 3, extreme values of all three parameters were needed, indicating complex interactions between parameters that differ for each ice sheet and thus need careful tuning to achieve plausible ice sheets.

Chapter 4 focuses on the deglaciation phase, showing the interplay between SMB, ocean losses and ice dynamics during ice sheet retreat. Firstly, the ice sheets from the two NROY simulations from Chapter 3 were too stable and failed to deglaciate under the transient deglacial climate forcings, particularly over North America. This suggests that the extreme values of albedo parameters needed to maintain the glacial maximum Eurasian ice sheet, caused too strong of an ice-albedo feedback, and positive SMB, over the NAIS. On the other hand, using a set of parameters that had a lower albedo and thus produced ice sheets that fell just below ice volume constraints, enabled ice retreat.

Sensitivity tests also showed how sensitive the timing of this retreat is to the value of *av_gr*. Increasing it to a value that still produced a plausible glacial maximum ice sheet in Chapter 3, led to a faster deglaciation during both periods (by ~3000 years) and extensive Greenland ice sheet loss due to widespread ablation. Lower albedo conditions intensifies surface melting highlighting the importance of maintaining sufficiently high albedo during deglaciation simulations to avoid unrealistic retreat scenarios. This result also underscores the fact that there may not be one area of the parameter space that produces realistic ice sheets across the different

time periods and regions. Work needs to be done to tune model parameters across periods of ice sheet change, potentially requiring looser constraints on what is considered "good enough" under current model capabilities or employing spatially and/or temporally varying parameter values.

Albedo had a greater impact on ice retreat than sub-shelf melting or ice streaming, underscoring the dominance of SMB in determining ice sheet stability. Despite this, interactions between SMB and ice dynamics remain critical. For example, SMB can influence the rate of ice streaming and trigger or accelerate instabilities, demonstrating a cascading effect on deglaciation processes (van Aalderen et al., 2024; Hinck et al., 2022).

While SMB processes dominate overall ice sheet evolution, ice dynamics parameters play a secondary but significant role, particularly in controlling ice thickness and retreat rates. Chapter 2 reveals that lower values of the *basal sliding* parameter used by Glimmer reduces ice velocities, promoting a larger volume and thicker NAIS through reducing the amount of ice transported to ablation areas. Similarly, lower values of *beta* (Weertman sliding) used in BISICLES in Chapter 3 had the same effect on the NH ice sheets. The marine-based EIS was particularly sensitive to this parameter due to the importance of calving and sub-shelf melt on controlling its mass. Thus, the magnitude of the sliding parameter determines how much ice is transported, and subsequently lost, to these marine margins. The *drain* parameter, controlling Coulomb sliding, influenced ice stream formation but had minimal impact on glacial maximum ice sheet volume and extent. Chapter 4 revealed that lower *drain* values led to faster, more pronounced ice streaming, accelerating retreat by transporting ice to ablation zones and marine margins. However, when confined ice shelves are able to form, lower *drain* values led to more extensive ice shelves that enhanced buttressing, slowing ice loss. These results show that different phases of ice sheet evolution are sensitive to different aspects of ice dynamics. During glacial maxima, accurately representing basal sliding across the entire ice sheet is crucial for simulating realistic volumes. On the other hand, during deglaciation, ice streaming dynamics become important, with marine terminating ice sheets, such as Eurasia and Greenland, being particularly sensitive to these processes.

This work underscores the complexity of ice sheet modelling, highlighting the need for careful calibration of SMB-related parameters, particularly albedo, across all stages of the glacial-interglacial cycle and all ice sheets. While this research takes important steps towards finding a unified parameter space and identifies key sensitivities, the findings suggest that additional large-ensemble simulations are required to refine parameters further and enhance model

reliability. The dominance of SMB processes over ice dynamics in determining ice sheet configuration, also suggests that future models should prioritise the accurate representation of surface processes while incorporating sufficient ice dynamics to address its role in the deglaciations.

5.1.3 RQ3. What are the similarities and differences between the last two deglaciations due to the different transient climate forcings (orbit, GHGs, sea surface conditions) and initial ice sheet states?

There is evidence that the last two deglaciations differed in their climate trajectories and ice sheet evolutions which led to characteristically different interglacials (Menviel et al., 2019). A recent coupled model experiment by Quiquet and Roche (2024), reveals faster NH ice sheet disintegration during the PDG, compared to the LDG, due to higher peak global temperatures and stronger orbital forcing. However, their study has limitations in its use of an earth system model of intermediate complexity (EMIC) that uses a simplified approximation of the atmospheric equations (quasi-geostrophic model; iLOVECLIM) and less realistic representations of key surface mass balance and albedo processes (Quiquet and Roche, 2024). In addition, they initialise the LDG and PDG simulations from the same LGM ice sheet geometries, neglecting any impacts resulting from the different glacial maximum ice sheet configurations, for example; ice-albedo feedbacks.

Chapter 4 presents a series of transient simulations that aim to improve on this previous approach and address objectives 3 (**OBJ3**) and 4 (**OBJ4**), and in doing so, highlight similarities and differences between climates and ice sheets of the last two deglaciations. These simulations were driven by distinct transient climate forcings and initiated under their respective glacial maximum ice sheet configurations. These are also the first transient simulations of the Penultimate Deglaciation performed with a general circulation model (GCM) coupled to an ice sheet model (ISM), providing valuable insights into the interactions between the climate and the ice sheets underpinning ice sheet retreat during this period. Compared to an EMIC, the FAMOUS GCM uses a more complex atmosphere model (based on the primitive equations) and updated calculations of SMB and snow and ice albedo, which this study has shown to be particularly important for NH ice sheet evolution (see RQ2; Sect. 5.1.2). In addition, the L1L2 physics used in BISICLES ISM is of a higher order than the hybrid SIA-SSA model, GRISLI, used in the study by Quiquet and Roche (2024) (Pattyn et al., 2013). Therefore, the simulated ice stream location and dynamics is likely less dependent on the spatial resolution in BISICLES (Hindmarsh, 2009). We also impose a higher resolution of 16 km over the ice sheets, refined

down to 2 km over the marine margins of the EIS, compared to the 40 km resolution used in GRISLI, which may help certain areas of ice streaming be more accurately represented (Gandy et al., 2019).

Sensitivity tests holding individual climate forcing components constant at glacial maximum levels, while allowing others to evolve, reveal similar mechanisms driving deglaciation during both periods. These will be discussed further in Sect. 5.1.4. Both deglaciations were marked by rapid ice sheet retreat with episodes of accelerated ice loss linked to instabilities in the NH ice sheets. However, a faster rate of deglaciation was seen during the PDG compared to the LDG aligning with previous studies (Quiquet and Roche, 2024; Stoll et al., 2022) and can, in part, be attributed to differences in the timing and magnitude of insolation, GHG concentrations and SST and sea ice changes. For example, the PDG experienced a more rapid increase and higher peak in NH summer insolation than the LDG, accelerating the ice retreat. In addition, the SST values used in these simulations were higher at the start of the PDG compared to the LDG, contributing to elevated surface temperatures in the early stages of the PDG. The sea ice concentration was also higher in the NH at the beginning of the LDG simulations which would have contributed to a stronger albedo feedback, delaying warming in this region and slowing the ice retreat.

Despite differences in initial configurations, the NAIS followed a similar pattern of retreat during both deglaciations. Over the first ~6000 years, the southern and eastern margins retreated gradually, followed by a large instability leading to a rapid Laurentide ice sheet collapse within a few thousand years. However, the timing of this instability in the simulations occurs earlier than suggested by reconstructions, pointing to potential discrepancies in modelled processes. In addition, the LDG simulations lacked the characteristic separation of the Cordilleran and Laurentide ice sheets at ~16-14 ka, as documented by empirical reconstructions and modelling studies (Dalton et al., 2020; Gregoire et al., 2012), which could be a result of model biases leading to too thick ice in this region or missing or simplified processes.

On the other hand, the EIS displayed distinct retreat patterns due to differences in initial configurations and dynamics. During the PDG, the Barents-Kara ice sheet (BKIS) collapsed rapidly at the onset, driven by dynamic instabilities. This contributed significantly to the faster overall deglaciation rate of the PDG. In contrast, during the LDG, the BKIS did not collapse until ~8000 years into the simulation, resulting in a smaller amount of mass loss due to its smaller size. The rapid collapse of the BKIS in all PDG forcing scenarios, including full PGM

conditions, suggests it likely stemmed from ice dynamic processes, rather than surface processes, resulting from its larger size and more prevalent ice streams. Further tests showed that the BKIS became unstable as the ice stream resolution was increased between the glacial maximum spin-ups and deglaciation simulation, enhancing these dynamic processes of retreat (i.e. ice velocity) and triggering grounding line instabilities. There are no empirical reconstructions of the Eurasian ice sheet deglaciation during this time period and so the reality of this event is uncertain. It has been suggested that the larger PGM EIS would have been more sensitive to instabilities due to its isostatic loading (Stoll et al., 2022) but there is an absence of abrupt climate changes in empirical records that correspond to the timing of this simulated instability. This suggests that our equilibrium spin-up integration was too long or that refinements are needed to GIA processes, ice streaming, or topography in our model to produce a more stable marine ice sheet.

The simulated surface temperatures lacked abrupt climate changes observed in proxy records, such as Heinrich Stadial 1 and Heinrich Stadial 11. These abrupt events are closely tied to variations in the strength of the Atlantic Meridional Overturning Circulation due to meltwater input (McManus et al., 2004). However, the use of prescribed SSTs in these simulations, and the omission of critical ice-ocean feedbacks, prevented accurate representation of these mechanisms. This limitation likely affected the evolution of the ice sheets in the model and contributed to discrepancies between the simulated ice sheet retreat and geological reconstructions. To explore the differences between the two deglaciations further, particularly regarding mechanisms involving ocean circulation changes, future studies could use transient SST forcings from simulations that account for freshwater feedbacks or employ a fully coupled atmosphere-ocean-ice sheet model.

The end states of the two deglaciation simulations align with known differences between the Last Interglacial and Holocene periods (Capron et al., 2017b; Otto-Bliesner et al., 2013b). At the end of the PDG simulation, marking the onset of the Last Interglacial, global temperatures were approximately 2.4 ºC higher, with Antarctic temperatures ~2 ºC warmer, conducive to greater Antarctic ice sheet loss (Marino et al., 2015). There was also more extensive NH ice sheet retreat (~5 m s.l.e.), especially in Greenland. This excess ice loss corresponds to the higher sea levels observed during the LIG compared to the Holocene, aligning the simulations with proxy evidence (Dutton and Lambeck, 2012).

Overall, the results of these transient GCM-ISM (FAMOUS-BISICLES) simulations displayed many similarities to the EMIC-ISM (iLOVECLIM-GRISLI) simulations of Quiquet and Roche

(2024), especially in regard to the rate of deglaciation and pattern of NAIS ice retreat. This could be because, although FAMOUS has a much more complex representation of atmospheric processes, its low resolution, required to run these multi-millennial simulations, prevents many of these processes from being resolved. Therefore, the gap between the EMIC and GCM used in these studies is not actually that large, and since the retreat of the NAIS is primarily driven by surface processes simulated by these models, they result in similar ice sheet evolutions.

The main difference seen is in the processes occurring over the marine section of the Eurasian ice sheet, particularly the simulation of the grounding line instability across the Bjørnøyrenna Ice Stream, which my simulations are able to capture but is missing from those by Quiquet and Roche (2024). This could be because the retreat in this region depends more on ice sheet dynamics and the basal melt rate which are governed by the ISM. The two models used in these studies, GRISLI and BISICLES, display more significant differences, with BISICLES using more complex physics and a higher resolution than GRISLI. It is therefore able to simulate ice streaming to a higher accuracy (Pattyn et al., 2013). This comparison suggests that, in future simulations, it may be adequate to use the more computationally efficient EMIC, which also has the added benefit of additional components such as a vegetation and ocean model, but that a more complex ISM is still beneficial for simulating marine ice sheet evolution and ice stream dynamics. In order to reap the benefit that a GCM has over an EMIC, higher resolutions will need to be used, which may become possible as technological advances continue to be made.

In conclusion, the last two deglaciations share similarities in their underlying mechanisms, in that they were both triggered by an increase in insolation and the occurrence of grounding line instabilities accelerated ice sheet retreat. However, they differ significantly in timing, regional dynamics, and the magnitude of changes due to differences in climate forcing and initial ice sheet states. The different climate evolution over the PDG and larger PGM Eurasian ice sheet led to a faster deglaciation compared to the LDG. These differences influenced the pace and character of warming, ice sheet retreat, and sea-level rise, resulting in warmer global temperatures and higher sea levels at the start of the Last Interglacial compared to the Holocene.

5.1.4 RQ4. What are the main drivers of ice sheet retreat during the last two deglaciations?

Research question 3 (**RQ3**) describes the similarities and differences between the retreat of the NH ice sheets in simulations of the Last and Penultimate deglaciations. Through sensitivity tests and analysis of the mass balance of the ice sheets, **Chapter 4** aims to explain these characteristics and answer research question 4 (**RQ4**), thus further contributing to objectives 3

(**OBJ3**) and 4 (**OBJ4**). Sensitivity tests examining the three main climate forcings revealed that both deglaciations were driven by similar mechanisms. Without a transient orbital forcing, the ice sheets were not able to deglaciate showing that insolation changes have a primary role in initiating ice retreat, in agreement with the Milankovitch theory and previous studies (Berger, 1980; Charbit et al., 2005; Ganopolski and Brovkin, 2017; Hays et al., 1976; Heinemann et al., 2014; Quiquet and Roche, 2024). Whilst deglaciation occurred under glacial maximum GHG and SST levels, the magnitude of ice sheet change was reduced. This demonstrates that GHGs and SSTs amplify the ice sheets response to orbital forcing. Among these factors, SST changes had the second largest influence on ice volume, except for the PDG Eurasian ice sheet and LDG Greenland ice sheet, where GHGs had an equally significant impact. This distinction is likely due to the smaller role of surface processes in marine-based ice sheet retreat, which is more influenced by oceanic processes than by SST-driven air temperature changes. This result agrees with the conclusion of other studies which show insolation as the main driver of deglaciation with secondary roles from CO_2, as well as other factors such as dust deposition, vegetation changes and ocean circulation, in modulating the timing and magnitude of retreat (Charbit et al., 2005; Ganopolski and Brovkin, 2017; Gregoire et al., 2015; Quiquet and Roche, 2024).

While insolation increases are necessary to drive deglaciation and can partly explain varying retreat rates, they alone cannot account for observed patterns and instabilities. Analysis of the relative contributions to ice loss from surface ablation compared to ocean losses, due to sub-shelf melt and calving, give more insight into which processes were responsible. Surface melt drove most NAIS losses during the LDG and PDG. Grounding line instabilities over Hudson Bay arose once ice retreated and allowed the formation of areas of ocean in the regions depressed below sea level, acting as large proglacial lakes. The geometry of the ice sheet became unstable over the reversed gradient bedrock and sub-shelf melt and calving facilitated rapid mass loss as ice shelves developed. This instability is sensitive to the value of the albedo parameter *av_gr*, with lower albedos triggering earlier, and larger magnitudes of, surface melt, accelerating grounding line retreat and the resulting instabilities. It is also sensitive to the value of the *drain* parameter, with lower values increasing the velocity of ice streaming, causing thinner ice sheets and increasing the flux of ice across the grounding line, accelerating ocean-driven loss and overall deglaciation.

The EIS exhibited more equal contributions from surface ablation and ocean losses due to its extensive marine margins. Scandinavian ice sheet retreat was primarily surface-driven, with ocean losses peaking during grounding line instabilities in the BKIS, facilitated by the

depressed bedrock, which led to its rapid retreat. For the LDG, these instabilities were driven sub-ocean warming induced dynamics and accelerated by surface ablation, and were thus influenced by albedo and basal sliding parameters, but were less sensitive to sub-shelf melt rates, highlighting the importance of surface processes and dynamics in the mechanism of retreat. During the PDG, EIS instability occurred even under constant PGM climate forcings and is triggered by an increase in ice sheet model grid resolution amplifying the dynamic processes leading to grounding line retreat. It is mostly affected by the sub-shelf melt parameter with smaller sub-shelf melt values delaying collapse due to enabling the formation of confined ice shelves which provided buttressing. This underscores the importance of dynamic and oceanic processes over climate triggers in the PDG simulation, but also the role topography can play in delaying or accelerating deglaciation if it is conducive to the formation of confined ice shelves. In addition, the resolution dependence of the BKIS collapse under PGM forcing, emphasises the need to carefully consider the level of refinement implemented at marine margins in equilibrium and deglaciation simulations. For the Greenland ice sheet during both periods, ocean-driven losses are significant throughout most of the retreat due to the extensive presence of marine outlet glaciers. However, surface ablation becomes increasingly important over time, eventually emerging as the primary driver of retreat towards the later stages. Ablation was thus largely responsible for the greater mass loss at the end of the PDG compared to the LDG. Therefore, the Greenland deglaciation is mostly impacted by the albedo parameter.

My findings demonstrate that while insolation initiates deglaciation, the rates and patterns of retreat depend heavily on the interplay of surface, ocean, and dynamic processes, influenced by regional characteristics and sensitivities, such as ice sheet geometry and the relative contributions of SMB versus marine processes. This interplay highlights the critical role of feedback mechanisms, where localised instabilities, such as proglacial lake or marine grounding line retreat, can amplify deglaciation rates. Additionally, parameter sensitivities like albedo and drainage rate, and resolution dependencies, demonstrate that small variations in surface or dynamic properties can significantly alter ice sheet behaviour, underscoring the need for accurate parameterisation in ice sheet models. Collectively, these findings contribute to a nuanced understanding of the drivers of NH ice sheet retreat, emphasising the importance of integrating regional dynamics with global climate forcings to predict future ice sheet responses under changing climate conditions.

5.2 Limitations and future work

As highlighted throughout this thesis, there are many challenges in the numerical modelling of palaeoclimate and ice sheets related to limitations in computational resources, availability and reliability of observational constraints and our knowledge of important processes. The methodological choices made in this work have attempted to address some of these challenges whilst also remaining within the scope of this study. Thus, the results presented are not without their limitations and future model and data developments may improve on the reliability of the simulated deglaciations.

5.2.1 Initial ice sheet states

The initial ice sheet configurations used in simulations significantly influence the outcomes, yet there remain substantial uncertainties in the volume and distribution of NH ice sheets, particularly during the PGM. Model reconstructions of these ice sheets vary widely depending on the techniques and models employed, which has considerable implications for simulated climate and ice dynamics due to effects on atmospheric circulation, GIA, and albedo (Bouttes et al., 2023; Izumi et al., 2023). Further work could be undertaken adopting varied ice sheet configurations, as suggested in the PMIP4 protocols (Ivanovic et al., 2016; Kageyama et al., 2017), which could provide valuable comparisons of simulated regional and global climates and help address uncertainties tied to reconstruction-dependent variability. The ensembles of simulations carried out for this thesis have provided a large range of LGM and PGM NH ice sheet topographies that could be used for this purpose.

Due to computational constraints, the glacial maximum simulations in this thesis were spun up to equilibrium before initiating deglaciation simulations from these stable ice sheets. However, since ice sheets were likely never in equilibrium with the climate, transient simulations covering both ice sheet build-up and retreat phases could yield more realistic representations of their extent and reduce reliance on static reconstructions.

Finally, in this thesis, the Antarctic ice sheet geometry was fixed to its glacial maximum state as prescribed by PMIP4 protocols, excluding its potential interactions with global climate and NH ice sheet evolution. For example, a reduction in its surface elevation could further amplify the increase in surface temperatures simulated over this region. However, this topographic change may also lead to a cooling over the rest of the globe due to changes in surface air pressure (Huang et al., 2023; Tewari et al., 2021). Future simulations incorporating a dynamically evolving Antarctic ice sheet could reveal its role in shaping climate and ice sheet responses during deglaciation.

5.2.2 Climate forcing

This study advanced previous research by utilising a coupled climate-ice sheet model, which minimizes uncertainties associated with climate forcings. However, computational constraints limited the model's scope, as only the atmospheric component of the FAMOUS GCM was used. Ocean conditions were prescribed, preventing dynamic interactions between the climate, ice sheets, and oceans. This limitation means that critical feedbacks involving meltwater forcing and changes in ocean circulation were not explicitly modelled (Obase et al., 2021; Romé et al., 2022). Consequently, abrupt climate changes that may have impacted ice sheet evolution and played a significant role in interglacial sea level rise were absent (Gregoire et al., 2016; Marino et al., 2015). In addition, since the global mean temperatures are highly influenced by the SST forcing, any biases in the fields used could impact the resulting ice sheet evolutions. For example, the HadCM3 model used to produce the SSTs prescribed in Chapters 3 and 4 show a cold bias, with respect to observations and other PMIP models, of up to 4 ºC in the global LGM ocean cooling (Kageyama et al., 2021). Modelling studies have shown that prescribing cooler SSTs, and more extensive sea ice cover, results in a cooling over the North Atlantic which induces a more positive SMB over the Eurasian ice sheet due to increased precipitation (Colleoni et al., 2011). Future research should aim to use fully coupled atmosphere-ocean-ice sheet models, incorporating freshwater forcing to capture these essential processes. However, this may introduce additional biases in the simulated climate from the atmosphere-ocean interactions (Dentith et al., 2019; Wang et al., 2014), which may be amplified by the low resolution model, and so work would need to be done to tune the ocean model and minimise these biases.

Moreover, this thesis has discussed the importance of several factors—vegetation, dust deposition, proglacial lakes, and land-sea mask feedbacks—which were either fixed, simplified, or omitted. Sensitivity tests incorporating glacial maximum vegetation or a dynamic vegetation model (e.g. Meissner et al., 2003), dust deposition effects (e.g. Ganopolski et al., 2010), a proglacial lake model (e.g. Hinck et al., 2022) and updated land-sea mask (Bouttes et al., 2023) would thus provide useful insights into the importance of these interactions during deglaciations. Nevertheless, increasing the complexity of models may not necessarily provide more answers and may increase the uncertainty in the results due to the additional parameterisations. Therefore, it would be advisable to only add in these components if striving to answer specific questions on these processes.

5.2.3 Modelling limitations

5.2.3.1 Climate model

The large ensembles of simulations presented in this thesis have enabled the successful tuning of FAMOUS-ice to produce plausible NH ice sheet configurations within known model structural uncertainties. However, persistent discrepancies remain between the modelled ice sheets and reconstructions, which, as well as stemming from running simulations to equilibrium or missing feedbacks, may also be caused by deficiencies in the atmospheric model.

FAMOUS's low resolution facilitates coupled simulations over multi-millennial timescales and supports the execution of large ensembles within the computational and temporal constraints of this research. Nevertheless, this low resolution inadequately captures finer-scale atmospheric processes that influence temperature and precipitation patterns, introducing biases in the simulated climate that affect ice sheet topography. For instance, it has been shown that Atmosphere GCM (AGCM) simulations using horizontal resolutions close to that of FAMOUS (~5.6º), produce lower and smoother topographies, larger southern ablation zones, increased cloudiness and a poor representation of planetary stationary wave effects, compared to resolutions of ~3.8º or higher (Dong and Valdes, 2000; Löfverström et al., 2016; Lofverstrom and Liakka, 2018). These factors can result in substantially warmer summer temperatures over all NH ice sheets, and reduced precipitation over the southwestern parts of the ice sheets. Since the Eurasian ice sheet is particularly sensitive to temperature changes (Abe-Ouchi et al., 2013), this climatology results in the ice sheet model being unable to reproduce the reconstructed western extent of the LGM EIS (Lofverstrom and Liakka, 2018). Therefore, the large negative SMB over Eurasia seen in the simulations presented in this thesis, contributing to the unrealistic loss of ice over the British-Irish ice sheet and Scandinavia, may partly be a result of the horizontal resolution used. Similarly, the position of the southern margin of the ice sheets and magnitude of the warm temperature anomaly over northwestern North America has been shown to be dependent on feedbacks between ice sheets and temperatures induced by changes in stationary waves (Liakka et al., 2012; Löfverström et al., 2014; Roe and Lindzen, 2001). Thus, the insufficient southern and eastern margins of the Laurentide ice sheet and the excessive ice growth over Alaska, seen in our simulations, is also partly an artefact of resolution. Ziemen et al. (2014) note that increasing the resolution of their AGCM from 3.75º to 1.9º reduces the cold bias over Alaska. However, many of these features also depend on the response of clouds (Gregory et al., 2012), which were able to be evaluated in the ensembles performed in this thesis showcasing a strength of FAMOUS-ice.

Another limitation is the warm temperature bias over the NAIS interior, caused by the model's inability to resolve the stable boundary layer (Sherriff-Tadano et al., 2024). This bias is exacerbated by downscaling methods and the positive height–mass balance feedback from coupling with the ice sheet model, resulting in unrealistic interior melting. Future research should thus prioritise refining atmospheric processes and downscaling methods to enhance model accuracy. To address these issues in this thesis, the *elevcon* tuning parameter was included in Chapters 3 and 4 to produce a better fit to observations and ensure a sufficiently large NAIS, particularly for the LGM. However, as *elevcon* lacks a direct physical basis, its optimal value may vary across different ice sheets and periods. Other possible adjustments could be tested to compensate for the poorly resolved topography such as implementing higher or rougher topography in the atmospheric dynamics and drag schemes.

Precipitation is not currently downscaled onto the ice sheet surface, leading to a broader precipitation distribution rather than concentration on ice sheet slopes and margins (Smith et al., 2021b). This limitation likely contributes to underestimation of accumulation in critical areas such as the southern NAIS or excess accumulation in areas such as the Cordilleran-Laurentide saddle region, possibly hindering the separation of the Laurentide and Cordilleran ice sheets during the LDG simulations. Machine learning from higher resolution AGCM simulations could be a useful way to address some of these problems.

5.2.3.2 Ice sheet model

Two different ice sheet models were used in this thesis to simulate the same glacial maximum periods, Glimmer and BISICLES. They differ in their spatial resolutions and parameterisations of critical ice sheet processes (e.g. basal sliding, GIA and sub-shelf melting). For example, BISICLES has more advanced physics for representing ice streaming and marine-based dynamics (Cornford et al., 2013; Gandy et al., 2019), making it better suited to modelling the Eurasian ice sheet but it has a tendency towards simulating smaller PGM North American ice sheet volumes, with 37% of the FAMOUS-BISICLES PGM ensemble being < 10 m s.l.e. (whereas the lower end of volume estimates is ~39 m s.l.e.), compared to 21% in FAMOUS-Glimmer (Figure 5.1). This could be due to these differences in dynamics influencing ice distribution and feedbacks. Glimmer's more simple physics (Rutt et al., 2009) may produce thicker ice margins and larger volumes due to its limited representation of ice stream processes, which in turn limits the positive temperature-elevation feedbacks initiated by the lower elevation areas of ice streaming.

The divergence in results highlights how differences in model design and parameterisations can significantly influence outcomes, and models that are worse performing in certain scenarios are not necessarily the worse models. These discrepancies underscore the sensitivity of ice sheet models to their underlying assumptions and emphasise the need for caution when interpreting or comparing their results. This limitation also suggests that the parameterisation of key processes, such as ice stream dynamics and basal sliding, requires further refinement to achieve more consistent and realistic simulations across models.

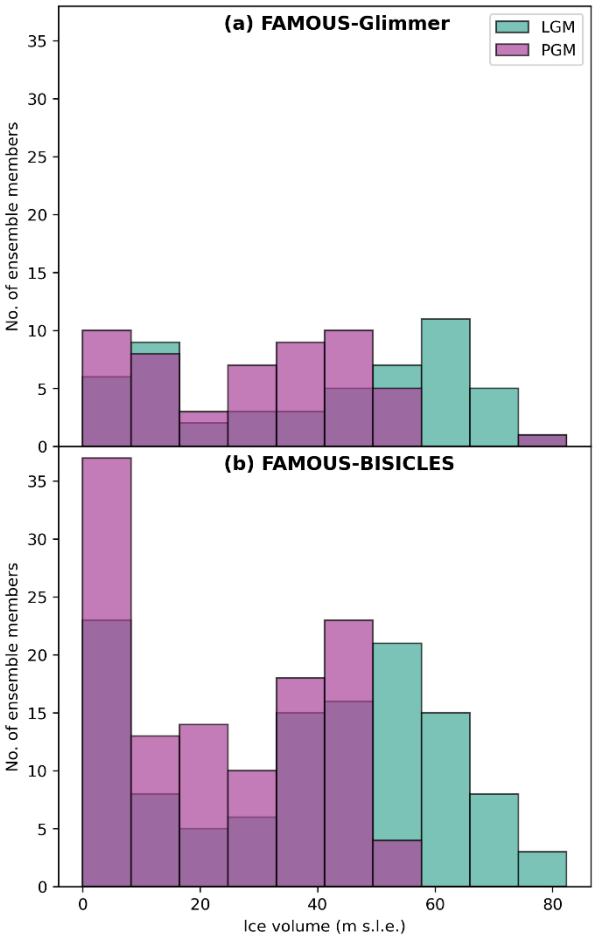

Figure 5.1: Distribution of LGM and PGM North American ice sheet volumes across (a) the FAMOUS-Glimmer ensemble in Chapter 2, and (b) the FAMOUS-BISICLES ensemble in Chapter 3.

The simplifications in representing ice streaming, sub-shelf melt and proglacial lakes in the ice sheet models are just a few of several areas that could benefit from refinement in future work. A spatially uniform geothermal heat flux was used in this study to simplify its representation (~95 mWm^{-2}). The magnitude of this flux influences basal water availability and, consequently, ice sheet stability and thickness over long timescales (Smith-Johnsen et al., 2020), in a similar way to the other basal sliding parameters (e.g. *drain*) examined in this study. However, geothermal heat flux varies significantly across North America and Eurasia, and using spatially

distributed values could improve the model fit to reconstructions. Previous research has shown that incorporating realistic heat flux distributions significantly impacts basal meltwater production, potentially improving ice stream representations where topographic controls are limited (Gandy et al., 2019; Näslund et al., 2005). For example, implementing higher values measured to the west of North America could facilitate the Laurentide-Cordilleran separation and the lower values over Hudson Bay and Scandinavia could delay the ice retreat in these regions (Blackwell and Richards, 2004; Näslund et al., 2005).

There are also uncertainties related to the resolutions used to simulate certain processes in the ice sheet models. In Chapter 3, the ice sheets were modelled at 16 km resolution, sufficient only for capturing large-scale geometry (Sherriff-Tadano et al., 2024). In Chapter 4, the resolution of the areas of ice streaming across the marine-based section of the Eurasian ice sheet was refined to 2 km, given the importance of ice streaming and grounding line dynamics during ice retreat (Petrini et al., 2018). This resolution was chosen because simulations using the updated basal sliding scheme in BISICLES showed that 2 km resolution produced ice stream generation that was a good match to empirical data, but also quantitatively and qualitatively similar to simulations performed at 1 km resolution (Gandy et al., 2019).

Whilst this level of refinement captured grounding line instabilities in this area, some studies suggest even finer resolutions (<1 km) are required to accurately resolve grounding line behaviour in some regions (Cornford et al., 2015; Pattyn et al., 2013). Therefore, the response may be underestimated and further refinement may yield different results regarding the timing and magnitude of these instabilities. On the other hand, high-resolution bedrock topography (~1–2 km) can better capture narrow features that control ice stream formation and improve the modelling of ice dynamics in coastal areas (Castleman et al., 2022; Durand et al., 2011). Consequently, even if the grounding lines were simulated at a higher resolution, this may not improve the simulation of ice dynamics if the bedrock remains at the base resolution of 32 km. However, computational costs quadruple with each level of refinement, making it impractical to apply such resolutions across large temporal and spatial scales. Future studies could address this by focusing on specific regions, such as individual ice streams, run at <1 km resolution, nested within a larger domain, to refine understanding of grounding line sensitivity to climate forcings and their role in the deglaciations.

Processes and feedbacks related to GIA, which account for the Earth's response to the loading and unloading of ice sheets over time, may also be important for simulating the deglaciation of the NH ice sheets. The simulations in Chapters 3 and 4 accounted for bedrock height changes

due to ice sheet loading but did not incorporate the effects of global and local sea level changes driven by variations in ice volume and gravitational pull exerted by the ice sheets. For instance, bedrock rebound and reduced gravitational attraction resulting from marine ice sheet mass loss can stabilize or slow grounding line retreat through reducing local water depths, as demonstrated in previous studies (van Calcar et al., 2023; Gomez et al., 2010). Including these sea-level feedbacks could mitigate rapid collapses observed in the results of Chapter 4, such as the early disintegration of the BKIS during the PDG and the Laurentide ice sheet over Hudson Bay (Han et al., 2021). However, the lack of detailed bathymetry data and uncertainties in upper mantle viscosity remain significant barriers to accurately quantifying the strength of these feedbacks.

5.2.4 Techniques

The work presented in this thesis heavily relies on model-data comparisons to validate the ability of ice sheet models to meet constraints on ice sheet extent and volume. However, this process is inherently dependent on the accuracy and availability of empirical data and model reconstructions. While the extent of LGM ice sheets is relatively well-established, uncertainties remain due to measurement and dating limitations as well as the interpretation of proxy data. Recent reconstructions of the NAIS and EIS (Dalton et al., 2023; Hughes et al., 2016) attempt to address these issues by providing minimum, maximum, and "best guess" estimates of ice sheet extents. However, volume reconstructions, which rely more heavily on indirect evidence and numerical modelling, remain subject to even greater uncertainty, resulting in a wide range of reported values (e.g. Rohling et al., 2017). Beyond reconstruction uncertainties, structural model discrepancies, including known biases in the models, create additional challenges in achieving precise matches to observations.

This study introduces an implausibility metric to account for some sources of uncertainty, such as representation of ice lobe dynamics, determining what level of error is tolerable while still considering the results plausible. However, this metric, whilst fully transparent, is based on subjective judgments by the authors rather than on statistical measures. Moreover, the use of single-value constraints for volume and area introduces the risk that a simulated ice sheet might meet overall plausibility criteria for volume while having an unrealistic spatial distribution of ice.

Several more sophisticated methods and tools have been developed that enable a more systematic, spatially detailed assessment of model accuracy based on its match to mapped features such as moraine positions and flowsets (Ely et al., 2021). For example; The Automated

Proximity and Conformity Analysis (APCA) tool (Li et al., 2008; Napieralski et al., 2006) and The Automated Flow Direction Analysis (AFDA) tool (Li et al., 2007). However, these tools also rely on a set of thresholds determined by human-judgement to be acceptable and the extent to which a model is able to reproduce these specific features will vary depending on resolution and representation of physics, such as basal sliding (Ely et al., 2021).

Due to the lack of robust empirical data for the extent and configuration of the ice sheets during the Penultimate Glacial Cycle, I did not attempt to constrain the model for this period through the same methods. Instead, the results of the LGM model-data comparison are used to rule out the equivalent PGM simulations which are then assessed to be plausible based on known general comparisons in ice sheet sizes between the two periods. In this way we test whether model parameters that produce a plausible LGM ice sheet can also produce a plausible PGM ice sheet, and from this we can learn more about the extent and volume of the PGM ice sheets. As a result, these tools that compare more specific features of ice sheet shape and dynamics may be less suitable for constraining periods for which they do not represent, and thus the use of more general metrics, based on a combination of empirical and model data, may remain the best suited technique in the context of this thesis (Edwards et al., 2019; Williamson et al., 2013). In addition, the course resolutions of the models used meant the simulated ice sheets lacked sufficient detail in the margin positions and flow fields to enable comparison to specific mapped features.

Nevertheless, the application of implausibility metrics in Chapters 2 and 3 indicates that only a small proportion of simulations can be considered plausible and large areas of the parameter space remain "Not Ruled Out Yet" (NROY). Whilst the 120 simulations carried out in Chapter 3 follows the general rule of 10 runs per dimension of the parameter space (Loeppky et al., 2009), it has been shown that employing emulators to evaluate additional waves of thousands of sets of parameter values, combined with history matching, is an effective, and computationally attainable, technique for refining the parameter space further to reduce biases in climate models (Li et al., 2019; Williamson et al., 2013, 2015). To this end, further developing the Gaussian Process emulators trained to predict the key ice sheet metrics (volume and extent) for the Sobol′ analysis in Chapter 3, could be a valuable next step in achieving this.

My results have shown that parameter sets producing NROY ice sheets at their glacial maximum can be unsuitable for simulating realistic deglaciation scenarios (Chapter 4). This underscores the limitation of applying a single model configuration across different time periods. Running ensembles of transient deglaciation simulations could help identify parameter

sets that yield "good enough" ice sheet behaviour across various temporal stages and periods of ice sheet change. Interestingly, there is very little overlap (if any) between the NROY parameter space identified in this study and that by Sherriff-Tadano et al., (2024) for the LGM NAIS, and that determined for simulations of the present-day Greenland ice sheet (Figure 5.2; Lang et al., in prep). This is largely a result of the parameters *daice* and *av_gr*, and modern Greenland favouring lower ice albedo compared to the LGM NAIS. Improvements to model treatment of albedo, refinements to the implausibility metric or expanding transient ensemble runs to include present-day and even future ice sheet conditions could help pinpoint parameter spaces that perform well across all periods, thus producing a more flexible model better able to robustly simulate change. Alternatively, work to employ transiently evolving parameter values could also be a potential solution. Statistical emulation and advanced machine learning may provide a practical way to perform ensembles of multi-millennia ice sheet evolution, overcoming the computational demands of the physical simulator (in this case FAMOUS-ice).

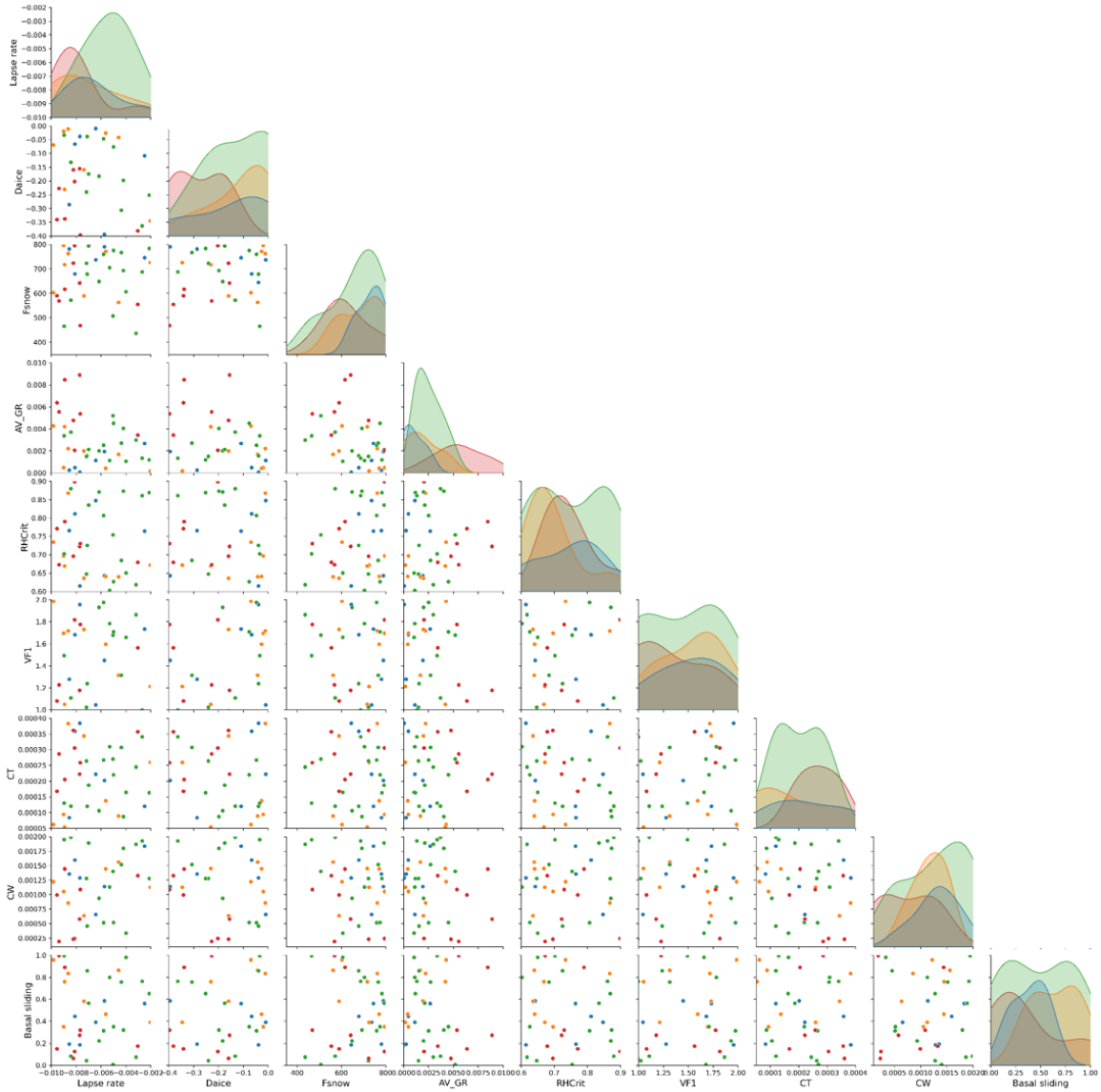

Figure 5.2: Parameter pair plot for the NROY simulations from the FAMOUS-Glimmer ensemble (Chapter 2; blue), FAMOUS-BISICLES ensemble (including the NAIS only NROYs, Chapter 3; orange), LGM NAIS ensemble (Sherriff-Tadano et al., 2024; green) and modern Greenland ensemble (Lang et al., in prep; red).

5.3 Conclusions

In summary, this thesis has successfully tuned a coupled climate-ice sheet model to simulate the Northern Hemisphere ice sheets at the LGM and PGM producing a series of plausible, physically consistent glacial maximum ice sheet initial conditions. This has enabled the first coupled GCM-ISM transient simulations of the Penultimate Deglaciation to be performed and compared to the Last Deglaciation, providing valuable insight into the climate-ice sheet interactions that occurred during both periods.

The use of a low resolution GCM enabled the quantification of the uncertainty in simulated ice sheet volumes due to uncertain model parameters through large ensembles and sensitivity

analyses, and model-data comparison techniques were employed through implausibility metrics to evaluate the performance of the model.

Whilst both deglaciations were driven by changes in the insolation and amplified by greenhouse gas and sea surface temperature changes, the climate forcings and initial conditions of the Penultimate Deglaciation produced a faster disintegration of the NH ice sheets than those of the Last Deglaciation. The simulations show the importance of grounding line instabilities in the retreat of the NAIS during both periods, which could arise due to the formation of proglacial lakes. These instabilities are sensitive to the surface mass balance and ice stream velocity. Marine ice sheet instabilities are responsible for much of the EIS retreat, however for the LDG, these are not very sensitive to marine processes and instead are controlled by surface ablation and ice dynamics. On the other hand, the larger PGM ice sheet is particularly unstable and more sensitive to the rate of sub-shelf melt due to the formation of confined ice shelves. Overall, the results of several sensitivity analyses throughout this thesis revealed the dominance of the ice-albedo feedback in determining the size of the simulated ice sheets and thus careful consideration of the initial ice sheet conditions and model parameters that control the ice sheet albedo is needed when modelling glacial-interglacial cycles. In addition, the representation of ice dynamics in the ice sheet model becomes important for modelling marine ice sheets and controlling the rate of ice retreat during deglaciations.

Another underlying conclusion of this work is that it is unrealistic to assume the climate and ice sheets were in equilibrium at any stage of the glacial-interglacial cycle and doing so may prevent the accurate representation of the maximum extent of the ice sheets at a particular time. Equilibrium simulations of the NAIS under PGM climate conditions produced a larger volume of ice compared to the LGM, contrary to constraint data, suggesting that the glacial maximum ice sheet configuration was likely determined by the climate evolution prior to this point in time. In addition, some model-data discrepancies displayed in the simulations, like the excess ice growth over Alaska, may also be a result of this assumption. Therefore, performing transient simulations of the build-up and decay of the NH ice sheets would be more useful and may help produce a better match to empirical data.

Finally, the ensembles performed in this thesis were able to find sets of model parameters that produced plausible equilibrium NH ice sheets during both the LGM and PGM, however, these parameters and resulting ice sheet configurations were not the most suitable for simulating the deglaciation. Moreover, comparison to the parameter space that produces a plausible modern day Greenland ice sheet does not display any overlap with the LGM NAIS. This result

underscores the need to constrain the model over transient simulations or multiple time periods to find areas of the parameter space that work for all scenarios and increase the reliability of the model for projecting future ice sheet and climate changes. This will likely require a less stringent view on what is a “plausible” ice sheet and the use of emulators to efficiently and feasibly evaluate many sets of parameters over several waves of ensembles.

Bibliography

Abe-Ouchi, A., Segawa, T., and Saito, F.: Climatic Conditions for modelling the Northern Hemisphere ice sheets throughout the ice age cycle, Clim. Past, 3, 423–438, https://doi.org/10.5194/cp-3-423-2007, 2007.

Abe-Ouchi, A., Saito, F., Kawamura, K., Raymo, M. E., Okuno, J., Takahashi, K., and Blatter, H.: Insolation-driven 100,000-year glacial cycles and hysteresis of ice-sheet volume, Nature, 500, 190–193, https://doi.org/10.1038/nature12374, 2013.

Abe-Ouchi, A., Saito, F., Kageyama, M., Braconnot, P., Harrison, S. P., Lambeck, K., Otto-Bliesner, B. L., Peltier, W. R., Tarasov, L., Peterschmitt, J.-Y., and Takahashi, K.: Ice-sheet configuration in the CMIP5/PMIP3 Last Glacial Maximum experiments, Geosci. Model Dev., 8, 3621–3637, https://doi.org/10.5194/gmd-8-3621-2015, 2015.

Albrecht, T., Winkelmann, R., and Levermann, A.: Glacial-cycle simulations of the Antarctic Ice Sheet with the Parallel Ice Sheet Model (PISM) – Part 1: Boundary conditions and climatic forcing, The Cryosphere, 14, 599–632, https://doi.org/10.5194/tc-14-599-2020, 2020.

Alder, J. R. and Hostetler, S. W.: Applying the Community Ice Sheet Model to evaluate PMIP3 LGM climatologies over the North American ice sheets, Clim. Dyn., 53, 2807–2824, https://doi.org/10.1007/s00382-019-04663-x, 2019.

Allen, J. R. M., Forrest, M., Hickler, T., Singarayer, J. S., Valdes, P. J., and Huntley, B.: Global vegetation patterns of the past 140,000 years, J. Biogeogr., 47, 2073–2090, https://doi.org/10.1111/jbi.13930, 2020.

Alley, R. B.: Ice-core evidence of abrupt climate changes, Proc. Natl. Acad. Sci., 97, 1331–1334, https://doi.org/10.1073/pnas.97.4.1331, 2000a.

Alley, R. B.: The Younger Dryas cold interval as viewed from central Greenland, Quat. Sci. Rev., 19, 213–226, https://doi.org/10.1016/S0277-3791(99)00062-1, 2000b.

Alley, R. B., Andrews, J. T., Brigham-Grette, J., Clarke, G. K. C., Cuffey, K. M., Fitzpatrick, J. J., Funder, S., Marshall, S. J., Miller, G. H., Mitrovica, J. X., Muhs, D. R., Otto-Bliesner,

B. L., Polyak, L., and White, J. W. C.: History of the Greenland Ice Sheet: paleoclimatic insights, Quat. Sci. Rev., 29, 1728–1756, https://doi.org/10.1016/j.quascirev.2010.02.007, 2010.

Alvarez-Solas, J., Charbit, S., Ritz, C., Paillard, D., Ramstein, G., and Dumas, C.: Links between ocean temperature and iceberg discharge during Heinrich events, Nat. Geosci., 3, 122–126, https://doi.org/10.1038/ngeo752, 2010.

Alvarez-Solas, J., Banderas, R., Robinson, A., and Montoya, M.: Ocean-driven millennial-scale variability of the Eurasian ice sheet during the last glacial period simulated with a hybrid ice-sheet–shelf model, Clim. Past, 15, 957–979, https://doi.org/10.5194/cp-15-957-2019, 2019.

An, S.-I., Moon, J.-Y., Dijkstra, H. A., Yang, Y.-M., and Song, H.: Antarctic meltwater reduces the Atlantic meridional overturning circulation through oceanic freshwater transport and atmospheric teleconnections, Commun. Earth Environ., 5, 1–9, https://doi.org/10.1038/s43247-024-01670-7, 2024.

Andersen, K. K., Azuma, N., Barnola, J.-M., Bigler, M., Biscaye, P., Caillon, N., Chappellaz, J., Clausen, H. B., Dahl-Jensen, D., Fischer, H., Flückiger, J., Fritzsche, D., Fujii, Y., Goto-Azuma, K., Grønvold, K., Gundestrup, N. S., Hansson, M., Huber, C., Hvidberg, C. S., Johnsen, S. J., Jonsell, U., Jouzel, J., Kipfstuhl, S., Landais, A., Leuenberger, M., Lorrain, R., Masson-Delmotte, V., Miller, H., Motoyama, H., Narita, H., Popp, T., Rasmussen, S. O., Raynaud, D., Rothlisberger, R., Ruth, U., Samyn, D., Schwander, J., Shoji, H., Siggard-Andersen, M.-L., Steffensen, J. P., Stocker, T., Sveinbjörnsdóttir, A. E., Svensson, A., Takata, M., Tison, J.-L., Thorsteinsson, Th., Watanabe, O., Wilhelms, F., White, J. W. C., and North Greenland Ice Core Project members: High-resolution record of Northern Hemisphere climate extending into the last interglacial period, Nature, 431, 147–151, https://doi.org/10.1038/nature02805, 2004.

Anderson, P., Bermike, O., Bigelow, N., Brigham-Grette, J., Duvall, M., Edwards, M. E., Frechette, B., Funder, S., Johnsen, S., Knies, J., Koerner, R., Lozhkin, A., Marshall, S., Matthiessen, J., Macdonald, G., Miller, G., Montoya, M., Muhs, D., Otto-Bliesner, B., Overpeck, J., Reeh, N., Sejrup, H., Spielhagen, R., Turner, C., and Velichko, A.: Last Interglacial Arctic warmth confirms polar amplification of climate change, Quat. Sci. Rev., 25, 1383–1400, https://doi.org/10.1016/j.quascirev.2006.01.033, 2006.

Andreassen, K. and Winsborrow, M.: Signature of ice streaming in Bjørnøyrenna, Polar North Atlantic, through the Pleistocene and implications for ice-stream dynamics, Ann. Glaciol., 50, 17–26, https://doi.org/10.3189/172756409789624238, 2009.

Annan, J. D. and Hargreaves, J. C.: A new global reconstruction of temperature changes at the Last Glacial Maximum, Clim. Past, 9, 367–376, https://doi.org/10.5194/cp-9-367-2013, 2013.

Annan, J. D., Hargreaves, J. C., and Mauritsen, T.: A new global surface temperature reconstruction for the Last Glacial Maximum, Clim. Past, 18, 1883–1896, https://doi.org/10.5194/cp-18-1883-2022, 2022.

Argus, D. F., Peltier, W. R., Drummond, R., and Moore, A. W.: The Antarctica component of postglacial rebound model ICE-6G_C (VM5a) based on GPS positioning, exposure age dating of ice thicknesses, and relative sea level histories, Geophys. J. Int., 198, 537–563, https://doi.org/10.1093/gji/ggu140, 2014.

Armstrong, E., Hopcroft, P. O., and Valdes, P. J.: A simulated Northern Hemisphere terrestrial climate dataset for the past 60,000 years, Sci. Data, 6, 265, https://doi.org/10.1038/s41597-019-0277-1, 2019.

Astfalck, L., Williamson, D., Gandy, N., Gregoire, L., and Ivanovic, R.: Coexchangeable Process Modeling for Uncertainty Quantification in Joint Climate Reconstruction, J. Am. Stat. Assoc., 119, 1751–1764, https://doi.org/10.1080/01621459.2024.2325705, 2024.

Augustin, L., Barbante, C., Barnes, P. R. F., Marc Barnola, J., Bigler, M., Castellano, E., Cattani, O., Chappellaz, J., Dahl-Jensen, D., Delmonte, B., Dreyfus, G., Durand, G., Falourd, S., Fischer, H., Flückiger, J., Hansson, M. E., Huybrechts, P., Jugie, G., Johnsen, S. J., Jouzel, J., Kaufmann, P., Kipfstuhl, J., Lambert, F., Lipenkov, V. Y., Littot, G. C., Longinelli, A., Lorrain, R., Maggi, V., Masson-Delmotte, V., Miller, H., Mulvaney, R., Oerlemans, J., Oerter, H., Orombelli, G., Parrenin, F., Peel, D. A., Petit, J.-R., Raynaud, D., Ritz, C., Ruth, U., Schwander, J., Siegenthaler, U., Souchez, R., Stauffer, B., Peder Steffensen, J., Stenni, B., Stocker, T. F., Tabacco, I. E., Udisti, R., van de Wal, R. S. W., van den Broeke, M., Weiss, J., Wilhelms, F., Winther, J.-G., Wolff, E. W., Zucchelli, M., EPICA community members, and EPICA community members (participants are listed alphabetically): Eight glacial cycles from an Antarctic ice core, Nature, 429, 623–628, https://doi.org/10.1038/nature02599, 2004.

Austermann, J., Mitrovica, J. X., Latychev, K., and Milne, G. A.: Barbados-based estimate of ice volume at Last Glacial Maximum affected by subducted plate, Nat. Geosci., 6, 553–557, https://doi.org/10.1038/ngeo1859, 2013.

Bakker, P., Schmittner, A., Lenaerts, J. T. M., Abe-Ouchi, A., Bi, D., van den Broeke, M. R., Chan, W.-L., Hu, A., Beadling, R. L., Marsland, S. J., Mernild, S. H., Saenko, O. A., Swingedouw, D., Sullivan, A., and Yin, J.: Fate of the Atlantic Meridional Overturning Circulation: Strong decline under continued warming and Greenland melting, Geophys. Res. Lett., 43, 12,252-12,260, https://doi.org/10.1002/2016GL070457, 2016.

Bakker, P., Rogozhina, I., Merkel, U., and Prange, M.: Hypersensitivity of glacial summer temperatures in Siberia, Clim. Past, 16, 371–386, https://doi.org/10.5194/cp-16-371-2020, 2020.

Bamber, J. L., Oppenheimer, M., Kopp, R. E., Aspinall, W. P., and Cooke, R. M.: Ice Sheet and Climate Processes Driving the Uncertainty in Projections of Future Sea Level Rise: Findings From a Structured Expert Judgement Approach, Earths Future, 10, e2022EF002772, https://doi.org/10.1029/2022EF002772, 2022.

Barbante, C., Barnola, J.-M., Becagli, S., Beer, J., Bigler, M., Boutron, C., Blunier, T., Castellano, E., Cattani, O., Chappellaz, J., Dahl-Jensen, D., Debret, M., Delmonte, B., Dick, D., Falourd, S., Faria, S., Federer, U., Fischer, H., Freitag, J., Frenzel, A., Fritzsche, D., Fundel, F., Gabrielli, P., Gaspari, V., Gersonde, R., Graf, W., Grigoriev, D., Hamann, I., Hansson, M., Hoffmann, G., Hutterli, M. A., Huybrechts, P., Isaksson, E., Johnsen, S., Jouzel, J., Kaczmarska, M., Karlin, T., Kaufmann, P., Kipfstuhl, S., Kohno, M., Lambert, F., Lambrecht, A., Lambrecht, A., Landais, A., Lawer, G., Leuenberger, M., Littot, G., Loulergue, L., Lüthi, D., Maggi, V., Marino, F., Masson-Delmotte, V., Meyer, H., Miller, H., Mulvaney, R., Narcisi, B., Oerlemans, J., Oerter, H., Parrenin, F., Petit, J.-R., Raisbeck, G., Raynaud, D., Röthlisberger, R., Ruth, U., Rybak, O., Severi, M., Schmitt, J., Schwander, J., Siegenthaler, U., Siggaard-Andersen, M.-L., Spahni, R., Steffensen, J. P., Stenni, B., Stocker, T. F., Tison, J.-L., Traversi, R., Udisti, R., Valero-Delgado, F., van den Broeke, M. R., van de Wal, R. S. W., Wagenbach, D., Wegner, A., Weiler, K., Wilhelms, F., Winther, J.-G., Wolff, E., and EPICA Community Members: One-to-one coupling of glacial climate variability in Greenland and Antarctica, Nature, 444, 195–198, https://doi.org/10.1038/nature05301, 2006.

Barker, S. and Knorr, G.: Millennial scale feedbacks determine the shape and rapidity of glacial termination, Nat. Commun., 12, 2273, https://doi.org/10.1038/s41467-021-22388-6, 2021.

Barker, S., Chen, J., Gong, X., Jonkers, L., Knorr, G., and Thornalley, D.: Icebergs not the trigger for North Atlantic cold events, Nature, 520, 333–336, https://doi.org/10.1038/nature14330, 2015.

Bar-Or, R., Erlick, C., and Gildor, H.: The role of dust in glacial–interglacial cycles, Quat. Sci. Rev., 27, 201–208, https://doi.org/10.1016/j.quascirev.2007.10.015, 2008.

Bartlein, P. J., Harrison, S. P., Brewer, S., Connor, S., Davis, B. A. S., Gajewski, K., Guiot, J., Harrison-Prentice, T. I., Henderson, A., Peyron, O., Prentice, I. C., Scholze, M., Seppä, H., Shuman, B., Sugita, S., Thompson, R. S., Viau, A. E., Williams, J., and Wu, H.: Pollen-based continental climate reconstructions at 6 and 21 ka: a global synthesis, Clim. Dyn., 37, 775–802, https://doi.org/10.1007/s00382-010-0904-1, 2011.

Bastos, L. S. and O'Hagan, A.: Diagnostics for Gaussian Process Emulators, Technometrics, 51, 425–438, https://doi.org/10.1198/TECH.2009.08019, 2009.

Batchelor, C. L., Margold, M., Krapp, M., Murton, D. K., Dalton, A. S., Gibbard, P. L., Stokes, C. R., Murton, J. B., and Manica, A.: The configuration of Northern Hemisphere ice sheets through the Quaternary, Nat. Commun., 10, 3713, https://doi.org/10.1038/s41467-019-11601-2, 2019.

Beckmann, A. and Goosse, H.: A parameterization of ice shelf–ocean interaction for climate models, Ocean Model., 5, 157–170, https://doi.org/10.1016/S1463-5003(02)00019-7, 2003.

Beghin, P., Charbit, S., Dumas, C., Kageyama, M., Roche, D. M., and Ritz, C.: Interdependence of the growth of the Northern Hemisphere ice sheets during the last glaciation: the role of atmospheric circulation, Clim. Past, 10, 345–358, https://doi.org/10.5194/cp-10-345-2014, 2014.

Beghin, P., Charbit, S., Dumas, C., Kageyama, M., and Ritz, C.: How might the North American ice sheet influence the northwestern Eurasian climate?, Clim. Past, 11, 1467–1490, https://doi.org/10.5194/cp-11-1467-2015, 2015.

Benn, D. I., Warren, C. R., and Mottram, R. H.: Calving processes and the dynamics of calving glaciers, Earth-Sci. Rev., 82, 143–179, https://doi.org/10.1016/j.earscirev.2007.02.002, 2007.

Benn, D. I., Cowton, T., Todd, J., and Luckman, A.: Glacier Calving in Greenland, Curr. Clim. Change Rep., 3, 282–290, https://doi.org/10.1007/s40641-017-0070-1, 2017.

Bentley, M. J., Ó Cofaigh, C., Anderson, J. B., Conway, H., Davies, B., Graham, A. G. C., Hillenbrand, C.-D., Hodgson, D. A., Jamieson, S. S. R., Larter, R. D., Mackintosh, A., Smith, J. A., Verleyen, E., Ackert, R. P., Bart, P. J., Berg, S., Brunstein, D., Canals, M., Colhoun, E. A., Crosta, X., Dickens, W. A., Domack, E., Dowdeswell, J. A., Dunbar, R., Ehrmann, W., Evans, J., Favier, V., Fink, D., Fogwill, C. J., Glasser, N. F., Gohl, K., Golledge, N. R., Goodwin, I., Gore, D. B., Greenwood, S. L., Hall, B. L., Hall, K., Hedding, D. W., Hein, A. S., Hocking, E. P., Jakobsson, M., Johnson, J. S., Jomelli, V., Jones, R. S., Klages, J. P., Kristoffersen, Y., Kuhn, G., Leventer, A., Licht, K., Lilly, K., Lindow, J., Livingstone, S. J., Massé, G., McGlone, M. S., McKay, R. M., Melles, M., Miura, H., Mulvaney, R., Nel, W., Nitsche, F. O., O'Brien, P. E., Post, A. L., Roberts, S. J., Saunders, K. M., Selkirk, P. M., Simms, A. R., Spiegel, C., Stolldorf, T. D., Sugden, D. E., van der Putten, N., van Ommen, T., Verfaillie, D., Vyverman, W., Wagner, B., White, D. A., Witus, A. E., and Zwartz, D.: A community-based geological reconstruction of Antarctic Ice Sheet deglaciation since the Last Glacial Maximum, Quat. Sci. Rev., 100, 1–9, https://doi.org/10.1016/j.quascirev.2014.06.025, 2014.

Berdahl, M., Leguy, G., Lipscomb, W. H., Urban, N. M., and Hoffman, M. J.: Exploring ice sheet model sensitivity to ocean thermal forcing and basal sliding using the Community Ice Sheet Model (CISM), The Cryosphere, 17, 1513–1543, https://doi.org/10.5194/tc-17-1513-2023, 2023.

Bereiter, B., Eggleston, S., Schmitt, J., Nehrbass-Ahles, C., Stocker, T. F., Fischer, H., Kipfstuhl, S., and Chappellaz, J.: Revision of the EPICA Dome C CO2 record from 800 to 600 kyr before present, Geophys. Res. Lett., 42, 542–549, https://doi.org/10.1002/2014GL061957, 2015.

Berends, C. J., de Boer, B., and van de Wal, R. S. W.: Reconstructing the evolution of ice sheets, sea level, and atmospheric CO_2 during the past 3.6 million years, Clim. Past, 17, 361–377, https://doi.org/10.5194/cp-17-361-2021, 2021.

Berends, C. J., Stap, L. B., and Wal, R. S. W. van de: Strong impact of sub-shelf melt parameterisation on ice-sheet retreat in idealised and realistic Antarctic topography, J. Glaciol., 69, 1434–1448, https://doi.org/10.1017/jog.2023.33, 2023.

Berger, A.: Long-Term Variations of Daily Insolation and Quaternary Climatic Changes, J. Atmospheric Sci., 35, 2362–2367, https://doi.org/10.1175/1520-0469(1978)035<2362:LTVODI>2.0.CO;2, 1978.

Berger, A.: The Milankovitch astronomical theory of paleoclimates: A modern review, Vistas Astron., 24, 103–122, https://doi.org/10.1016/0083-6656(80)90026-4, 1980.

Berger, A. and Loutre, M. F.: Insolation values for the climate of the last 10 million years, Quat. Sci. Rev., 10, 297–317, https://doi.org/10.1016/0277-3791(91)90033-Q, 1991.

Bintanja, R., van de Wal, R. S. W., and Oerlemans, J.: Modelled atmospheric temperatures and global sea levels over the past million years, Nature, 437, 125–128, https://doi.org/10.1038/nature03975, 2005.

Blackwell, D.D. and Richards, M.: Geothermal Map of North America, AAPG Map, scale 1:6,500,000, Product Code 423, 2004.

Blasco, J., Alvarez-Solas, J., Robinson, A., and Montoya, M.: Exploring the impact of atmospheric forcing and basal drag on the Antarctic Ice Sheet under Last Glacial Maximum conditions, The Cryosphere, 15, 215–231, https://doi.org/10.5194/tc-15-215-2021, 2021.

Blatter, H.: Velocity and stress fields in grounded glaciers: a simple algorithm for including deviatoric stress gradients, J. Glaciol., 41, 333–344, https://doi.org/10.3189/S002214300001621X, 1995.

Blatter, H., Greve, R., and Abe-Ouchi, A.: A short history of the thermomechanical theory and modeling of glaciers and ice sheets, J. Glaciol., 56, 1087–1094, https://doi.org/10.3189/002214311796406059, 2010.

Blatter, H., Greve, R., and Abe-Ouchi, A.: Present State and Prospects of Ice Sheet and Glacier Modelling, Surv. Geophys., 32, 555–583, https://doi.org/10.1007/s10712-011-9128-0, 2011.

Blunier, T. and Brook, E. J.: Timing of Millennial-Scale Climate Change in Antarctica and Greenland During the Last Glacial Period, Science, 291, 109–112, https://doi.org/10.1126/science.291.5501.109, 2001.

Blunier, T., Chappellaz, J., Schwander, J., Dällenbach, A., Stauffer, B., Stocker, T. F., Raynaud, D., Jouzel, J., Clausen, H. B., Hammer, C. U., and Johnsen, S. J.: Asynchrony of Antarctic and Greenland climate change during the last glacial period, Nature, 394, 739–743, https://doi.org/10.1038/29447, 1998.

de Boer, B., van de Wal, R. S. W., Lourens, L. J., Bintanja, R., and Reerink, T. J.: A continuous simulation of global ice volume over the past 1 million years with 3-D ice-sheet models, Clim. Dyn., 41, 1365–1384, https://doi.org/10.1007/s00382-012-1562-2, 2013.

Böhm, E., Lippold, J., Gutjahr, M., Frank, M., Blaser, P., Antz, B., Fohlmeister, J., Frank, N., Andersen, M. B., and Deininger, M.: Strong and deep Atlantic meridional overturning circulation during the last glacial cycle, Nature, 517, 73–76, https://doi.org/10.1038/nature14059, 2015.

Bonelli, S., Charbit, S., Kageyama, M., Woillez, M.-N., Ramstein, G., Dumas, C., and Quiquet, A.: Investigating the evolution of major Northern Hemisphere ice sheets during the last glacial-interglacial cycle, Clim. Past, 5, 329–345, https://doi.org/10.5194/cp-5-329-2009, 2009.

Bouttes, N., Lhardy, F., Quiquet, A., Paillard, D., Goosse, H., and Roche, D. M.: Deglacial climate changes as forced by different ice sheet reconstructions, Clim. Past, 19, 1027–1042, https://doi.org/10.5194/cp-19-1027-2023, 2023.

Bova, S., Rosenthal, Y., Liu, Z., Godad, S. P., and Yan, M.: Seasonal origin of the thermal maxima at the Holocene and the last interglacial, Nature, 589, 548–553, https://doi.org/10.1038/s41586-020-03155-x, 2021.

Box, J. E., Fettweis, X., Stroeve, J. C., Tedesco, M., Hall, D. K., and Steffen, K.: Greenland ice sheet albedo feedback: thermodynamics and atmospheric drivers, The Cryosphere, 6, 821–839, https://doi.org/10.5194/tc-6-821-2012, 2012.

Braconnot, P., Harrison, S. P., Kageyama, M., Bartlein, P. J., Masson-Delmotte, V., Abe-Ouchi, A., Otto-Bliesner, B., and Zhao, Y.: Evaluation of climate models using

palaeoclimatic data, Nat. Clim. Change, 2, 417–424, https://doi.org/10.1038/nclimate1456, 2012.

Bradley, S. L., Reerink, T. J., van de Wal, R. S. W., and Helsen, M. M.: Simulation of the Greenland Ice Sheet over two glacial–interglacial cycles: investigating a sub-ice- shelf melt parameterization and relative sea level forcing in an ice-sheet–ice-shelf model, Clim. Past, 14, 619–635, https://doi.org/10.5194/cp-14-619-2018, 2018.

Bradley, S. L., Sellevold, R., Petrini, M., Vizcaino, M., Georgiou, S., Zhu, J., Otto-Bliesner, B. L., and Lofverstrom, M.: Surface mass balance and climate of the Last Glacial Maximum Northern Hemisphere ice sheets: simulations with CESM2.1, Clim. Past, 20, 211–235, https://doi.org/10.5194/cp-20-211-2024, 2024.

Briggs, R., Pollard, D., and Tarasov, L.: A glacial systems model configured for large ensemble analysis of Antarctic deglaciation, The Cryosphere, 7, 1949–1970, https://doi.org/10.5194/tc-7-1949-2013, 2013.

Briggs, R. D., Pollard, D., and Tarasov, L.: A data-constrained large ensemble analysis of Antarctic evolution since the Eemian, Quat. Sci. Rev., 103, 91–115, https://doi.org/10.1016/j.quascirev.2014.09.003, 2014.

Broecker, W. S.: Massive iceberg discharges as triggers for global climate change, Nature, 372, 421–424, https://doi.org/10.1038/372421a0, 1994.

Broecker, W. S.: Paleocean circulation during the Last Deglaciation: A bipolar seesaw?, Paleoceanography, 13, 119–121, https://doi.org/10.1029/97PA03707, 1998.

Broecker, W. S. and van Donk, J.: Insolation changes, ice volumes, and the O18 record in deep-sea cores, Rev. Geophys., 8, 169–198, https://doi.org/10.1029/RG008i001p00169, 1970.

Budyko, M. I.: The effect of solar radiation variations on the climate of the Earth, Tellus, 21, 611–619, https://doi.org/10.1111/j.2153-3490.1969.tb00466.x, 1969.

Bueler, E. and Brown, J.: Shallow shelf approximation as a “sliding law” in a thermomechanically coupled ice sheet model, J. Geophys. Res. Earth Surf., 114, https://doi.org/10.1029/2008JF001179, 2009.

Bueler, E. and van Pelt, W.: Mass-conserving subglacial hydrology in the Parallel Ice Sheet Model version 0.6, Geosci. Model Dev., 8, 1613–1635, https://doi.org/10.5194/gmd-8-1613-2015, 2015.

Buizert, C., Gkinis, V., Severinghaus, J. P., He, F., Lecavalier, B. S., Kindler, P., Leuenberger, M., Carlson, A. E., Vinther, B., Masson-Delmotte, V., White, J. W. C., Liu, Z., Otto-Bliesner, B., and Brook, E. J.: Greenland temperature response to climate forcing during the last deglaciation, Science, 345, 1177–1180, https://doi.org/10.1126/science.1254961, 2014.

Buizert, C., Adrian, B., Ahn, J., Albert, M., Alley, R. B., Baggenstos, D., Bauska, T. K., Bay, R. C., Bencivengo, B. B., Bentley, C. R., Brook, E. J., Chellman, N. J., Clow, G. D., Cole-Dai, J., Conway, H., Cravens, E., Cuffey, K. M., Dunbar, N. W., Edwards, J. S., Fegyveresi, J. M., Ferris, D. G., Fitzpatrick, J. J., Fudge, T. J., Gibson, C. J., Gkinis, V., Goetz, J. J., Gregory, S., Hargreaves, G. M., Iverson, N., Johnson, J. A., Jones, T. R., Kalk, M. L., Kippenhan, M. J., Koffman, B. G., Kreutz, K., Kuhl, T. W., Lebar, D. A., Lee, J. E., Marcott, S. A., Markle, B. R., Maselli, O. J., McConnell, J. R., McGwire, K. C., Mitchell, L. E., Mortensen, N. B., Neff, P. D., Nishiizumi, K., Nunn, R. M., Orsi, A. J., Pasteris, D. R., Pedro, J. B., Pettit, E. C., Buford Price, P., Priscu, J. C., Rhodes, R. H., Rosen, J. L., Schauer, A. J., Schoenemann, S. W., Sendelbach, P. J., Severinghaus, J. P., Shturmakov, A. J., Sigl, M., Slawny, K. R., Souney, J. M., Sowers, T. A., Spencer, M. K., Steig, E. J., Taylor, K. C., Twickler, M. S., Vaughn, B. H., Voigt, D. E., Waddington, E. D., Welten, K. C., Wendricks, A. W., White, J. W. C., Winstrup, M., Wong, G. J., Woodruff, T. E., and WAIS Divide Project Members: Precise interpolar phasing of abrupt climate change during the last ice age, Nature, 520, 661–665, https://doi.org/10.1038/nature14401, 2015.

Burgard, C., Jourdain, N. C., Reese, R., Jenkins, A., and Mathiot, P.: An assessment of basal melt parameterisations for Antarctic ice shelves, The Cryosphere, 16, 4931–4975, https://doi.org/10.5194/tc-16-4931-2022, 2022.

Capron, E., Govin, A., Feng, R., Otto-Bliesner, B. L., and Wolff, E. W.: Critical evaluation of climate syntheses to benchmark CMIP6/PMIP4 127 ka Last Interglacial simulations in the high-latitude regions, Quat. Sci. Rev., 168, 137–150, https://doi.org/10.1016/j.quascirev.2017.04.019, 2017a.

Capron, É., Govin, A., and Stone, E. J.: Recent advances on the dynamical representation and our understanding of the warmer-than-present last interglacial climate, Quat. Rev. Assoc. Fr. Pour Létude Quat., 185–193, https://doi.org/10.4000/quaternaire.8029, 2017b.

Carlson, A. E.: Why there was not a Younger Dryas-like event during the Penultimate Deglaciation, Quat. Sci. Rev., 27, 882–887, https://doi.org/10.1016/j.quascirev.2008.02.004, 2008.

Carrivick, J. L. and Tweed, F. S.: Proglacial lakes: character, behaviour and geological importance, Quat. Sci. Rev., 78, 34–52, https://doi.org/10.1016/j.quascirev.2013.07.028, 2013.

Castleman, B. A., Schlegel, N.-J., Caron, L., Larour, E., and Khazendar, A.: Derivation of bedrock topography measurement requirements for the reduction of uncertainty in ice-sheet model projections of Thwaites Glacier, The Cryosphere, 16, 761–778, https://doi.org/10.5194/tc-16-761-2022, 2022.

Chandler, D. and Langebroek, P.: Southern Ocean sea surface temperature synthesis: Part 2. Penultimate glacial and last interglacial, Quat. Sci. Rev., 271, 107190, https://doi.org/10.1016/j.quascirev.2021.107190, 2021.

Charbit, S., Kageyama, M., Roche, D., Ritz, C., and Ramstein, G.: Investigating the mechanisms leading to the deglaciation of past continental northern hemisphere ice sheets with the CLIMBER–GREMLINS coupled model, Glob. Planet. Change, 48, 253–273, https://doi.org/10.1016/j.gloplacha.2005.01.002, 2005.

Charbit, S., Ritz, C., Philippon, G., Peyaud, V., and Kageyama, M.: Numerical reconstructions of the Northern Hemisphere ice sheets through the last glacial-interglacial cycle, Clim. Past, 3, 15–37, https://doi.org/10.5194/cp-3-15-2007, 2007.

Cheng, H., Edwards, R. L., Broecker, W. S., Denton, G. H., Kong, X., Wang, Y., Zhang, R., and Wang, X.: Ice Age Terminations, Science, 326, 248–252, https://doi.org/10.1126/science.1177840, 2009.

Clark, C. D., Hughes, A. L. C., Greenwood, S. L., Jordan, C., and Sejrup, H. P.: Pattern and timing of retreat of the last British-Irish Ice Sheet, Quat. Sci. Rev., 44, 112–146, https://doi.org/10.1016/j.quascirev.2010.07.019, 2012a.

Clark, C. D., Ely, J. C., Hindmarsh, R. C. A., Bradley, S., Ignéczi, A., Fabel, D., Ó Cofaigh, C., Chiverrell, R. C., Scourse, J., Benetti, S., Bradwell, T., Evans, D. J. A., Roberts, D. H., Burke, M., Callard, S. L., Medialdea, A., Saher, M., Small, D., Smedley, R. K., Gasson, E., Gregoire, L., Gandy, N., Hughes, A. L. C., Ballantyne, C., Bateman, M. D., Bigg, G. R.,

Doole, J., Dove, D., Duller, G. A. T., Jenkins, G. T. H., Livingstone, S. L., McCarron, S., Moreton, S., Pollard, D., Praeg, D., Sejrup, H. P., Van Landeghem, K. J. J., and Wilson, P.: Growth and retreat of the last British–Irish Ice Sheet, 31 000 to 15 000 years ago: the BRITICE-CHRONO reconstruction, Boreas, 51, 699–758, https://doi.org/10.1111/bor.12594, 2022.

Clark, P. U. and Mix, A. C.: Ice sheets and sea level of the Last Glacial Maximum, Quat. Sci. Rev., 21, 1–7, https://doi.org/10.1016/S0277-3791(01)00118-4, 2002.

Clark, P. U., Dyke, A. S., Shakun, J. D., Carlson, A. E., Clark, J., Wohlfarth, B., Mitrovica, J. X., Hostetler, S. W., and McCabe, A. M.: The Last Glacial Maximum, Science, 325, 710–714, https://doi.org/10.1126/science.1172873, 2009.

Clark, P. U., Shakun, J. D., Baker, P. A., Bartlein, P. J., Brewer, S., Brook, E., Carlson, A. E., Cheng, H., Kaufman, D. S., Liu, Z., Marchitto, T. M., Mix, A. C., Morrill, C., Otto-Bliesner, B. L., Pahnke, K., Russell, J. M., Whitlock, C., Adkins, J. F., Blois, J. L., Clark, J., Colman, S. M., Curry, W. B., Flower, B. P., He, F., Johnson, T. C., Lynch-Stieglitz, J., Markgraf, V., McManus, J., Mitrovica, J. X., Moreno, P. I., and Williams, J. W.: Global climate evolution during the last deglaciation, Proc. Natl. Acad. Sci., 109, E1134–E1142, https://doi.org/10.1073/pnas.1116619109, 2012b.

Clark, P. U., He, F., Golledge, N. R., Mitrovica, J. X., Dutton, A., Hoffman, J. S., and Dendy, S.: Oceanic forcing of penultimate deglacial and last interglacial sea-level rise, Nature, 577, 660–664, https://doi.org/10.1038/s41586-020-1931-7, 2020.

Claussen, M., Mysak, L., Weaver, A., Crucifix, M., Fichefet, T., Loutre, M.-F., Weber, S., Alcamo, J., Alexeev, V., Berger, A., Calov, R., Ganopolski, A., Goosse, H., Lohmann, G., Lunkeit, F., Mokhov, I., Petoukhov, V., Stone, P., and Wang, Z.: Earth system models of intermediate complexity: closing the gap in the spectrum of climate system models, Clim. Dyn., 18, 579–586, https://doi.org/10.1007/s00382-001-0200-1, 2002.

Colleoni, F. and Liakka, J.: Transient simulations of the Eurasian ice sheet during the Saalian glacial cycle, SKB TR-19-17, 2020.

Colleoni, F., Krinner, G., Jakobsson, M., Peyaud, V., and Ritz, C.: Influence of regional parameters on the surface mass balance of the Eurasian ice sheet during the peak Saalian (140 kya), Glob. Planet. Change, 68, 132–148, https://doi.org/10.1016/j.gloplacha.2009.03.021, 2009a.

Colleoni, F., Krinner, G., and Jakobsson, M.: Sensitivity of the Late Saalian (140 kyrs BP) and LGM (21 kyrs BP) Eurasian ice sheet surface mass balance to vegetation feedbacks, Geophys. Res. Lett., 36, https://doi.org/10.1029/2009GL037200, 2009b.

Colleoni, F., Liakka, J., Krinner, G., Jakobsson, M., Masina, S., and Peyaud, V.: The sensitivity of the Late Saalian (140 ka) and LGM (21 ka) Eurasian ice sheets to sea surface conditions, Clim. Dyn., 37, 531–553, https://doi.org/10.1007/s00382-010-0870-7, 2011.

Colleoni, F., Wekerle, C., Näslund, J.-O., Brandefelt, J., and Masina, S.: Constraint on the penultimate glacial maximum Northern Hemisphere ice topography (≈140 kyrs BP), Quat. Sci. Rev., 137, 97–112, https://doi.org/10.1016/j.quascirev.2016.01.024, 2016.

Cornford, S. L., Martin, D. F., Graves, D. T., Ranken, D. F., Le Brocq, A. M., Gladstone, R. M., Payne, A. J., Ng, E. G., and Lipscomb, W. H.: Adaptive mesh, finite volume modeling of marine ice sheets, J. Comput. Phys., 232, 529–549, https://doi.org/10.1016/j.jcp.2012.08.037, 2013.

Cornford, S. L., Martin, D. F., Payne, A. J., Ng, E. G., Le Brocq, A. M., Gladstone, R. M., Edwards, T. L., Shannon, S. R., Agosta, C., van den Broeke, M. R., Hellmer, H. H., Krinner, G., Ligtenberg, S. R. M., Timmermann, R., and Vaughan, D. G.: Century-scale simulations of the response of the West Antarctic Ice Sheet to a warming climate, The Cryosphere, 9, 1579–1600, https://doi.org/10.5194/tc-9-1579-2015, 2015.

Cornford, S. L., Martin, D. F., Lee, V., Payne, A. J., and Ng, E. G.: Adaptive mesh refinement versus subgrid friction interpolation in simulations of Antarctic ice dynamics, Ann. Glaciol., 57, 1–9, https://doi.org/10.1017/aog.2016.13, 2016.

Couette, P.-O., Lajeunesse, P., Ghienne, J.-F., Dorschel, B., Gebhardt, C., Hebbeln, D., and Brouard, E.: Evidence for an extensive ice shelf in northern Baffin Bay during the Last Glacial Maximum, Commun. Earth Environ., 3, 1–12, https://doi.org/10.1038/s43247-022-00559-7, 2022.

Crucifix, M. and Hewitt, C. D.: Impact of vegetation changes on the dynamics of the atmosphere at the Last Glacial Maximum, Clim. Dyn., 25, 447–459, https://doi.org/10.1007/s00382-005-0013-8, 2005.

Crucifix, M. and Loutre, F. M.: Transient simulations over the last interglacial period (126–115 kyr BP): feedback and forcing analysis, Clim. Dyn., 19, 417–433, https://doi.org/10.1007/s00382-002-0234-z, 2002.

Dahl-Jensen, D., Albert, M. R., Aldahan, A., Azuma, N., Balslev-Clausen, D., Baumgartner, M., Berggren, A.-M., Bigler, M., Binder, T., Blunier, T., Bourgeois, J. C., Brook, E. J., Buchardt, S. L., Buizert, C., Capron, E., Chappellaz, J., Chung, J., Clausen, H. B., Cvijanovic, I., Davies, S. M., Ditlevsen, P., Eicher, O., Fischer, H., Fisher, D. A., Fleet, L. G., Gfeller, G., Gkinis, V., Gogineni, S., Goto-Azuma, K., Grinsted, A., Gudlaugsdottir, H., Guillevic, M., Hansen, S. B., Hansson, M., Hirabayashi, M., Hong, S., Hur, S. D., Huybrechts, P., Hvidberg, C. S., Iizuka, Y., Jenk, T., Johnsen, S. J., Jones, T. R., Jouzel, J., Karlsson, N. B., Kawamura, K., Keegan, K., Kettner, E., Kipfstuhl, S., Kjær, H. A., Koutnik, M., Kuramoto, T., Köhler, P., Laepple, T., Landais, A., Langen, P. L., Larsen, L. B., Leuenberger, D., Leuenberger, M., Leuschen, C., Li, J., Lipenkov, V., Martinerie, P., Maselli, O. J., Masson-Delmotte, V., McConnell, J. R., Miller, H., Mini, O., Miyamoto, A., Montagnat-Rentier, M., Mulvaney, R., Muscheler, R., Orsi, A. J., Paden, J., Panton, C., Pattyn, F., Petit, J.-R., Pol, K., Popp, T., Possnert, G., Prié, F., Prokopiou, M., Quiquet, A., Rasmussen, S. O., Raynaud, D., Ren, J., Reutenauer, C., Ritz, C., Röckmann, T., Rosen, J. L., Rubino, M., Rybak, O., Samyn, D., Sapart, C. J., Schilt, A., Schmidt, A. M. Z., Schwander, J., Schüpbach, S., Seierstad, I., et al.: Eemian interglacial reconstructed from a Greenland folded ice core, Nature, 493, 489–494, https://doi.org/10.1038/nature11789, 2013.

Dalton, A. S., Margold, M., Stokes, C. R., Tarasov, L., Dyke, A. S., Adams, R. S., Allard, S., Arends, H. E., Atkinson, N., Attig, J. W., Barnett, P. J., Barnett, R. L., Batterson, M., Bernatchez, P., Borns, H. W., Breckenridge, A., Briner, J. P., Brouard, E., Campbell, J. E., Carlson, A. E., Clague, J. J., Curry, B. B., Daigneault, R.-A., Dubé-Loubert, H., Easterbrook, D. J., Franzi, D. A., Friedrich, H. G., Funder, S., Gauthier, M. S., Gowan, A. S., Harris, K. L., Hétu, B., Hooyer, T. S., Jennings, C. E., Johnson, M. D., Kehew, A. E., Kelley, S. E., Kerr, D., King, E. L., Kjeldsen, K. K., Knaeble, A. R., Lajeunesse, P., Lakeman, T. R., Lamothe, M., Larson, P., Lavoie, M., Loope, H. M., Lowell, T. V., Lusardi, B. A., Manz, L., McMartin, I., Nixon, F. C., Occhietti, S., Parkhill, M. A., Piper, D. J. W., Pronk, A. G., Richard, P. J. H., Ridge, J. C., Ross, M., Roy, M., Seaman, A., Shaw, J., Stea, R. R., Teller, J. T., Thompson, W. B., Thorleifson, L. H., Utting, D. J., Veillette, J. J., Ward, B. C., Weddle, T. K., and Wright, H. E.: An updated radiocarbon-based ice margin

chronology for the last deglaciation of the North American Ice Sheet Complex, Quat. Sci. Rev., 234, 106223, https://doi.org/10.1016/j.quascirev.2020.106223, 2020.

Dalton, A. S., Stokes, C. R., and Batchelor, C. L.: Evolution of the Laurentide and Innuitian ice sheets prior to the Last Glacial Maximum (115 ka to 25 ka), Earth-Sci. Rev., 224, 103875, https://doi.org/10.1016/j.earscirev.2021.103875, 2022.

Dalton, A. S., Dulfer, H. E., Margold, M., Heyman, J., Clague, J. J., Froese, D. G., Gauthier, M. S., Hughes, A. L. C., Jennings, C. E., Norris, S. L., and Stoker, B. J.: Deglaciation of the north American ice sheet complex in calendar years based on a comprehensive database of chronological data: NADI-1, Quat. Sci. Rev., 321, 108345, https://doi.org/10.1016/j.quascirev.2023.108345, 2023.

Dansgaard, W., Johnsen, S. J., Clausen, H. B., Dahl-Jensen, D., Gundestrup, N. S., Hammer, C. U., Hvidberg, C. S., Steffensen, J. P., Sveinbjörnsdottir, A. E., Jouzel, J., and Bond, G.: Evidence for general instability of past climate from a 250-kyr ice-core record, Nature, 364, 218–220, https://doi.org/10.1038/364218a0, 1993.

Davies-Barnard, T., Ridgwell, A., Singarayer, J., and Valdes, P.: Quantifying the influence of the terrestrial biosphere on glacial–interglacial climate dynamics, Clim. Past, 13, 1381–1401, https://doi.org/10.5194/cp-13-1381-2017, 2017.

Davini, P., von Hardenberg, J., Filippi, L., and Provenzale, A.: Impact of Greenland orography on the Atlantic Meridional Overturning Circulation, Geophys. Res. Lett., 42, 871–879, https://doi.org/10.1002/2014GL062668, 2015.

Deaney, E. L., Barker, S., and van de Flierdt, T.: Timing and nature of AMOC recovery across Termination 2 and magnitude of deglacial CO2 change, Nat. Commun., 8, 14595, https://doi.org/10.1038/ncomms14595, 2017.

DeConto, R. M. and Pollard, D.: Contribution of Antarctica to past and future sea-level rise, Nature, 531, 591–597, https://doi.org/10.1038/nature17145, 2016.

Delmonte, B., Basile-Doelsch, I., Petit, J.-R., Maggi, V., Revel-Rolland, M., Michard, A., Jagoutz, E., and Grousset, F.: Comparing the Epica and Vostok dust records during the last 220,000 years: stratigraphical correlation and provenance in glacial periods, Earth-Sci. Rev., 66, 63–87, https://doi.org/10.1016/j.earscirev.2003.10.004, 2004.

Dentith, J. E., Ivanovic, R. F., Gregoire, L. J., Tindall, J. C., and Smith, R. S.: Ocean circulation drifts in multi-millennial climate simulations: the role of salinity corrections and climate feedbacks, Clim. Dyn., 52, 1761–1781, https://doi.org/10.1007/s00382-018-4243-y, 2019.

Dentith, J. E., Ivanovic, R. F., Gregoire, L. J., Tindall, J. C., and Robinson, L. F.: Simulating stable carbon isotopes in the ocean component of the FAMOUS general circulation model with MOSES1 (XOAVI), Geosci. Model Dev., 13, 3529–3552, https://doi.org/10.5194/gmd-13-3529-2020, 2020.

Denton, G. H., Anderson, R. F., Toggweiler, J. R., Edwards, R. L., Schaefer, J. M., and Putnam, A. E.: The Last Glacial Termination, Science, 328, 1652–1656, https://doi.org/10.1126/science.1184119, 2010.

Depoorter, M. A., Bamber, J. L., Griggs, J. A., Lenaerts, J. T. M., Ligtenberg, S. R. M., van den Broeke, M. R., and Moholdt, G.: Calving fluxes and basal melt rates of Antarctic ice shelves, Nature, 502, 89–92, https://doi.org/10.1038/nature12567, 2013.

Deschamps, P., Durand, N., Bard, E., Hamelin, B., Camoin, G., Thomas, A. L., Henderson, G. M., Okuno, J., and Yokoyama, Y.: Ice-sheet collapse and sea-level rise at the Bølling warming 14,600 years ago, Nature, 483, 559–564, https://doi.org/10.1038/nature10902, 2012.

Dong, B. and Valdes, P. J.: Climates at the Last Glacial Maximum: Influence of Model Horizontal Resolution, 2000.

Drew, M. and Tarasov, L.: Surging of a Hudson Strait-scale ice stream: subglacial hydrology matters but the process details mostly do not, The Cryosphere, 17, 5391–5415, https://doi.org/10.5194/tc-17-5391-2023, 2023.

Drysdale, R., Couchoud, I., Zanchetta, G., Isola, I., Regattieri, E., Hellstrom, J., Govin, A., Tzedakis, P. C., Ireland, T., Corrick, E., Greig, A., Wong, H., Piccini, L., Holden, P., and Woodhead, J.: Magnesium in subaqueous speleothems as a potential palaeotemperature proxy, Nat. Commun., 11, 5027, https://doi.org/10.1038/s41467-020-18083-7, 2020.

Dupont, T. K. and Alley, R. B.: Assessment of the importance of ice-shelf buttressing to ice-sheet flow, Geophys. Res. Lett., 32, https://doi.org/10.1029/2004GL022024, 2005.

Durand, G., Gagliardini, O., Favier, L., Zwinger, T., and le Meur, E.: Impact of bedrock description on modeling ice sheet dynamics, Geophys. Res. Lett., 38, https://doi.org/10.1029/2011GL048892, 2011.

Dutton, A. and Barlow, N.: What do we know about Last Interglacial sea level?, Past Glob. Chang. Mag., 27, https://doi.org/10.22498/pages.27.1.6, 2019.

Dutton, A. and Lambeck, K.: Ice Volume and Sea Level During the Last Interglacial, Science, 337, 216–219, https://doi.org/10.1126/science.1205749, 2012.

Dutton, A., Carlson, A. E., Long, A. J., Milne, G. A., Clark, P. U., DeConto, R., Horton, B. P., Rahmstorf, S., and Raymo, M. E.: Sea-level rise due to polar ice-sheet mass loss during past warm periods, Science, 349, aaa4019, https://doi.org/10.1126/science.aaa4019, 2015.

Dyer, B., Austermann, J., D'Andrea, W. J., Creel, R. C., Sandstrom, M. R., Cashman, M., Rovere, A., and Raymo, M. E.: Sea-level trends across The Bahamas constrain peak last interglacial ice melt, Proc. Natl. Acad. Sci., 118, e2026839118, https://doi.org/10.1073/pnas.2026839118, 2021.

Dyke, A. S., Andrews, J. T., Clark, P. U., England, J. H., Miller, G. H., Shaw, J., and Veillette, J. J.: The Laurentide and Innuitian ice sheets during the Last Glacial Maximum, Quat. Sci. Rev., 21, 9–31, https://doi.org/10.1016/S0277-3791(01)00095-6, 2002.

Edwards, P. N.: History of climate modeling, WIREs Clim. Change, 2, 128–139, https://doi.org/10.1002/wcc.95, 2011.

Edwards, T. L., Brandon, M. A., Durand, G., Edwards, N. R., Golledge, N. R., Holden, P. B., Nias, I. J., Payne, A. J., Ritz, C., and Wernecke, A.: Revisiting Antarctic ice loss due to marine ice-cliff instability, Nature, 566, 58–64, https://doi.org/10.1038/s41586-019-0901-4, 2019.

Edwards, T. L., Nowicki, S., Marzeion, B., Hock, R., Goelzer, H., Seroussi, H., Jourdain, N. C., Slater, D. A., Turner, F. E., Smith, C. J., McKenna, C. M., Simon, E., Abe-Ouchi, A., Gregory, J. M., Larour, E., Lipscomb, W. H., Payne, A. J., Shepherd, A., Agosta, C., Alexander, P., Albrecht, T., Anderson, B., Asay-Davis, X., Aschwanden, A., Barthel, A., Bliss, A., Calov, R., Chambers, C., Champollion, N., Choi, Y., Cullather, R., Cuzzone, J., Dumas, C., Felikson, D., Fettweis, X., Fujita, K., Galton-Fenzi, B. K., Gladstone, R., Golledge, N. R., Greve, R., Hattermann, T., Hoffman, M. J., Humbert, A., Huss, M.,

Huybrechts, P., Immerzeel, W., Kleiner, T., Kraaijenbrink, P., Le clec'h, S., Lee, V., Leguy, G. R., Little, C. M., Lowry, D. P., Malles, J.-H., Martin, D. F., Maussion, F., Morlighem, M., O'Neill, J. F., Nias, I., Pattyn, F., Pelle, T., Price, S. F., Quiquet, A., Radić, V., Reese, R., Rounce, D. R., Rückamp, M., Sakai, A., Shafer, C., Schlegel, N.-J., Shannon, S., Smith, R. S., Straneo, F., Sun, S., Tarasov, L., Trusel, L. D., Van Breedam, J., van de Wal, R., van den Broeke, M., Winkelmann, R., Zekollari, H., Zhao, C., Zhang, T., and Zwinger, T.: Projected land ice contributions to twenty-first-century sea level rise, Nature, 593, 74–82, https://doi.org/10.1038/s41586-021-03302-y, 2021.

Ehlers, J., Gibbard, P. L., and Hughes, P. D.: Chapter 4 - Quaternary Glaciations and Chronology, in: Past Glacial Environments (Second Edition), edited by: Menzies, J. and van der Meer, J. J. M., Elsevier, 77–101, https://doi.org/10.1016/B978-0-08-100524-8.00003-8, 2018.

Ely, J. C., Clark, C. D., Hindmarsh, R. C. A., Hughes, A. L. C., Greenwood, S. L., Bradley, S. L., Gasson, E., Gregoire, L., Gandy, N., Stokes, C. R., and Small, D.: Recent progress on combining geomorphological and geochronological data with ice sheet modelling, demonstrated using the last British–Irish Ice Sheet, J. Quat. Sci., 36, 946–960, https://doi.org/10.1002/jqs.3098, 2021.

Essery, R. L. H., Best, M. J., Betts, R. A., Cox, P. M., and Taylor, C. M.: Explicit Representation of Subgrid Heterogeneity in a GCM Land Surface Scheme, J. Hydrometeorol., 4, 530–543, https://doi.org/10.1175/1525-7541(2003)004<0530:EROSHI>2.0.CO;2, 2003.

Favier, L., Jourdain, N. C., Jenkins, A., Merino, N., Durand, G., Gagliardini, O., Gillet-Chaulet, F., and Mathiot, P.: Assessment of sub-shelf melting parameterisations using the ocean–ice-sheet coupled model NEMO(v3.6)–Elmer/Ice(v8.3), Geosci. Model Dev., 12, 2255–2283, https://doi.org/10.5194/gmd-12-2255-2019, 2019.

Fettweis, X., Franco, B., Tedesco, M., van Angelen, J. H., Lenaerts, J. T. M., van den Broeke, M. R., and Gallée, H.: Estimating the Greenland ice sheet surface mass balance contribution to future sea level rise using the regional atmospheric climate model MAR, The Cryosphere, 7, 469–489, https://doi.org/10.5194/tc-7-469-2013, 2013.

Fischer, H., Meissner, K. J., Mix, A. C., Abram, N. J., Austermann, J., Brovkin, V., Capron, E., Colombaroli, D., Daniau, A.-L., Dyez, K. A., Felis, T., Finkelstein, S. A., Jaccard, S. L.,

McClymont, E. L., Rovere, A., Sutter, J., Wolff, E. W., Affolter, S., Bakker, P., Ballesteros-Cánovas, J. A., Barbante, C., Caley, T., Carlson, A. E., Churakova (Sidorova), O., Cortese, G., Cumming, B. F., Davis, B. A. S., de Vernal, A., Emile-Geay, J., Fritz, S. C., Gierz, P., Gottschalk, J., Holloway, M. D., Joos, F., Kucera, M., Loutre, M.-F., Lunt, D. J., Marcisz, K., Marlon, J. R., Martinez, P., Masson-Delmotte, V., Nehrbass-Ahles, C., Otto-Bliesner, B. L., Raible, C. C., Risebrobakken, B., Sánchez Goñi, M. F., Arrigo, J. S., Sarnthein, M., Sjolte, J., Stocker, T. F., Velasquez Alvárez, P. A., Tinner, W., Valdes, P. J., Vogel, H., Wanner, H., Yan, Q., Yu, Z., Ziegler, M., and Zhou, L.: Palaeoclimate constraints on the impact of 2 °C anthropogenic warming and beyond, Nat. Geosci., 11, 474–485, https://doi.org/10.1038/s41561-018-0146-0, 2018.

Fyke, J., Sergienko, O., Löfverström, M., Price, S., and Lenaerts, J. T. M.: An Overview of Interactions and Feedbacks Between Ice Sheets and the Earth System, Rev. Geophys., 56, 361–408, https://doi.org/10.1029/2018RG000600, 2018.

Fyke, J. G., Weaver, A. J., Pollard, D., Eby, M., Carter, L., and Mackintosh, A.: A new coupled ice sheet/climate model: description and sensitivity to model physics under Eemian, Last Glacial Maximum, late Holocene and modern climate conditions, Geosci. Model Dev., 4, 117–136, https://doi.org/10.5194/gmd-4-117-2011, 2011.

Fyke, J. G., Sacks, W. J., and Lipscomb, W. H.: A technique for generating consistent ice sheet initial conditions for coupled ice sheet/climate models, Geosci. Model Dev., 7, 1183–1195, https://doi.org/10.5194/gmd-7-1183-2014, 2014.

Gandy, N., Gregoire, L. J., Ely, J. C., Clark, C. D., Hodgson, D. M., Lee, V., Bradwell, T., and Ivanovic, R. F.: Marine ice sheet instability and ice shelf buttressing of the Minch Ice Stream, northwest Scotland, The Cryosphere, 12, 3635–3651, https://doi.org/10.5194/tc-12-3635-2018, 2018.

Gandy, N., Gregoire, L. J., Ely, J. C., Cornford, S. L., Clark, C. D., and Hodgson, D. M.: Exploring the ingredients required to successfully model the placement, generation, and evolution of ice streams in the British-Irish Ice Sheet, Quat. Sci. Rev., 223, 105915, https://doi.org/10.1016/j.quascirev.2019.105915, 2019.

Gandy, N., Gregoire, L. J., Ely, J. C., Cornford, S. L., Clark, C. D., and Hodgson, D. M.: Collapse of the Last Eurasian Ice Sheet in the North Sea Modulated by Combined Processes

of Ice Flow, Surface Melt, and Marine Ice Sheet Instabilities, J. Geophys. Res. Earth Surf., 126, e2020JF005755, https://doi.org/10.1029/2020JF005755, 2021.

Gandy, N., Astfalck, L. C., Gregoire, L. J., Ivanovic, R. F., Patterson, V. L., Sherriff-Tadano, S., Smith, R. S., Williamson, D., and Rigby, R.: De-Tuning Albedo Parameters in a Coupled Climate Ice Sheet Model to Simulate the North American Ice Sheet at the Last Glacial Maximum, J. Geophys. Res. Earth Surf., 128, e2023JF007250, https://doi.org/10.1029/2023JF007250, 2023.

Ganopolski, A. and Brovkin, V.: Simulation of climate, ice sheets and CO_2 evolution during the last four glacial cycles with an Earth system model of intermediate complexity, Clim. Past, 13, 1695–1716, https://doi.org/10.5194/cp-13-1695-2017, 2017.

Ganopolski, A., Calov, R., and Claussen, M.: Simulation of the last glacial cycle with a coupled climate ice-sheet model of intermediate complexity, Clim. Past, 6, 229–244, https://doi.org/10.5194/cp-6-229-2010, 2010.

Gardner, P., Lord, C., and Barthorpe, R. J.: Bayesian history matching for structural dynamics applications, Mech. Syst. Signal Process., 143, 106828, https://doi.org/10.1016/j.ymssp.2020.106828, 2020.

Gasson, E. G. W., DeConto, R. M., Pollard, D., and Clark, C. D.: Numerical simulations of a kilometre-thick Arctic ice shelf consistent with ice grounding observations, Nat. Commun., 9, 1510, https://doi.org/10.1038/s41467-018-03707-w, 2018.

Gilford, D. M., Ashe, E. L., DeConto, R. M., Kopp, R. E., Pollard, D., and Rovere, A.: Could the Last Interglacial Constrain Projections of Future Antarctic Ice Mass Loss and Sea-Level Rise?, J. Geophys. Res. Earth Surf., 125, e2019JF005418, https://doi.org/10.1029/2019JF005418, 2020.

Golledge, N. R., Keller, E. D., Gomez, N., Naughten, K. A., Bernales, J., Trusel, L. D., and Edwards, T. L.: Global environmental consequences of twenty-first-century ice-sheet melt, Nature, 566, 65–72, https://doi.org/10.1038/s41586-019-0889-9, 2019.

Golledge, N. R., Clark, P. U., He, F., Dutton, A., Turney, C. S. M., Fogwill, C. J., Naish, T. R., Levy, R. H., McKay, R. M., Lowry, D. P., Bertler, N. a. N., Dunbar, G. B., and Carlson, A. E.: Retreat of the Antarctic Ice Sheet During the Last Interglaciation and Implications for

Future Change, Geophys. Res. Lett., 48, e2021GL094513, https://doi.org/10.1029/2021GL094513, 2021.

Gomez, N., Mitrovica, J. X., Huybers, P., and Clark, P. U.: Sea level as a stabilizing factor for marine-ice-sheet grounding lines, Nat. Geosci., 3, 850–853, https://doi.org/10.1038/ngeo1012, 2010.

Gomez, N., Pollard, D., and Mitrovica, J. X.: A 3-D coupled ice sheet – sea level model applied to Antarctica through the last 40 ky, Earth Planet. Sci. Lett., 384, 88–99, https://doi.org/10.1016/j.epsl.2013.09.042, 2013.

Gomez, N., Pollard, D., and Holland, D.: Sea-level feedback lowers projections of future Antarctic Ice-Sheet mass loss, Nat. Commun., 6, 8798, https://doi.org/10.1038/ncomms9798, 2015.

Gordon, C., Cooper, C., Senior, C. A., Banks, H., Gregory, J. M., Johns, T. C., Mitchell, J. F. B., and Wood, R. A.: The simulation of SST, sea ice extents and ocean heat transports in a version of the Hadley Centre coupled model without flux adjustments, Clim. Dyn., 16, 147–168, https://doi.org/10.1007/s003820050010, 2000.

Govin, A., Capron, E., Tzedakis, P. C., Verheyden, S., Ghaleb, B., Hillaire-Marcel, C., St-Onge, G., Stoner, J. S., Bassinot, F., Bazin, L., Blunier, T., Combourieu-Nebout, N., El Ouahabi, A., Genty, D., Gersonde, R., Jimenez-Amat, P., Landais, A., Martrat, B., Masson-Delmotte, V., Parrenin, F., Seidenkrantz, M.-S., Veres, D., Waelbroeck, C., and Zahn, R.: Sequence of events from the onset to the demise of the Last Interglacial: Evaluating strengths and limitations of chronologies used in climatic archives, Quat. Sci. Rev., 129, 1–36, https://doi.org/10.1016/j.quascirev.2015.09.018, 2015.

Gowan, E. J., Zhang, X., Khosravi, S., Rovere, A., Stocchi, P., Hughes, A. L. C., Gyllencreutz, R., Mangerud, J., Svendsen, J.-I., and Lohmann, G.: A new global ice sheet reconstruction for the past 80 000 years, Nat. Commun., 12, 1199, https://doi.org/10.1038/s41467-021-21469-w, 2021.

Grant, K. M., Rohling, E. J., Ramsey, C. B., Cheng, H., Edwards, R. L., Florindo, F., Heslop, D., Marra, F., Roberts, A. P., Tamisiea, M. E., and Williams, F.: Sea-level variability over five glacial cycles, Nat. Commun., 5, 5076, https://doi.org/10.1038/ncomms6076, 2014.

Gregoire, L. J., Valdes, P. J., Payne, A. J., and Kahana, R.: Optimal tuning of a GCM using modern and glacial constraints, Clim. Dyn., 37, 705–719, https://doi.org/10.1007/s00382-010-0934-8, 2011.

Gregoire, L. J., Payne, A. J., and Valdes, P. J.: Deglacial rapid sea level rises caused by ice-sheet saddle collapses, Nature, 487, 219–222, https://doi.org/10.1038/nature11257, 2012.

Gregoire, L. J., Valdes, P. J., and Payne, A. J.: The relative contribution of orbital forcing and greenhouse gases to the North American deglaciation, Geophys. Res. Lett., 42, 9970–9979, https://doi.org/10.1002/2015GL066005, 2015.

Gregoire, L. J., Otto-Bliesner, B., Valdes, P. J., and Ivanovic, R.: Abrupt Bølling warming and ice saddle collapse contributions to the Meltwater Pulse 1a rapid sea level rise, Geophys. Res. Lett., 43, 9130–9137, https://doi.org/10.1002/2016GL070356, 2016.

Gregoire, L. J., Ivanovic, R. F., Maycock, A. C., Valdes, P. J., and Stevenson, S.: Holocene lowering of the Laurentide ice sheet affects North Atlantic gyre circulation and climate, Clim. Dyn., 51, 3797–3813, https://doi.org/10.1007/s00382-018-4111-9, 2018.

Gregory, J. M., Browne, O. J. H., Payne, A. J., Ridley, J. K., and Rutt, I. C.: Modelling large-scale ice-sheet–climate interactions following glacial inception, Clim. Past, 8, 1565–1580, https://doi.org/10.5194/cp-8-1565-2012, 2012.

Gregory, J. M., George, S. E., and Smith, R. S.: Large and irreversible future decline of the Greenland ice sheet, The Cryosphere, 14, 4299–4322, https://doi.org/10.5194/tc-14-4299-2020, 2020.

Gudmundsson, G. H.: Ice-shelf buttressing and the stability of marine ice sheets, The Cryosphere, 7, 647–655, https://doi.org/10.5194/tc-7-647-2013, 2013.

Gudmundsson, G. H., Paolo, F. S., Adusumilli, S., and Fricker, H. A.: Instantaneous Antarctic ice sheet mass loss driven by thinning ice shelves, Geophys. Res. Lett., 46, 13903–13909, https://doi.org/10.1029/2019GL085027, 2019.

Han, H. K., Gomez, N., Pollard, D., and DeConto, R.: Modeling Northern Hemispheric Ice Sheet Dynamics, Sea Level Change, and Solid Earth Deformation Through the Last Glacial Cycle, J. Geophys. Res. Earth Surf., 126, e2020JF006040, https://doi.org/10.1029/2020JF006040, 2021.

Hanna, E., Navarro, F. J., Pattyn, F., Domingues, C. M., Fettweis, X., Ivins, E. R., Nicholls, R. J., Ritz, C., Smith, B., Tulaczyk, S., Whitehouse, P. L., and Zwally, H. J.: Ice-sheet mass balance and climate change, Nature, 498, 51–59, https://doi.org/10.1038/nature12238, 2013.

Harrison, S. P., Bartlein, P. J., Izumi, K., Li, G., Annan, J., Hargreaves, J., Braconnot, P., and Kageyama, M.: Evaluation of CMIP5 palaeo-simulations to improve climate projections, Nat. Clim. Change, 5, 735–743, https://doi.org/10.1038/nclimate2649, 2015.

Harrison, S. P., Bartlein, P. J., and Prentice, I. C.: What have we learnt from palaeoclimate simulations?, J. Quat. Sci., 31, 363–385, https://doi.org/10.1002/jqs.2842, 2016.

Hays, J. D., Imbrie, J., and Shackleton, N. J.: Variations in the Earth's Orbit: Pacemaker of the Ice Ages, Science, 194, 1121–1132, https://doi.org/10.1126/science.194.4270.1121, 1976.

Haywood, A. M., Valdes, P. J., Aze, T., Barlow, N., Burke, A., Dolan, A. M., von der Heydt, A. S., Hill, D. J., Jamieson, S. S. R., Otto-Bliesner, B. L., Salzmann, U., Saupe, E., and Voss, J.: What can Palaeoclimate Modelling do for you?, Earth Syst. Environ., 3, 1–18, https://doi.org/10.1007/s41748-019-00093-1, 2019.

He, C., Liu, Z., Otto-Bliesner, B. L., Brady, E. C., Zhu, C., Tomas, R., Clark, P. U., Zhu, J., Jahn, A., Gu, S., Zhang, J., Nusbaumer, J., Noone, D., Cheng, H., Wang, Y., Yan, M., and Bao, Y.: Hydroclimate footprint of pan-Asian monsoon water isotope during the last deglaciation, Sci. Adv., 7, eabe2611, https://doi.org/10.1126/sciadv.abe2611, 2021.

He, F., Shakun, J. D., Clark, P. U., Carlson, A. E., Liu, Z., Otto-Bliesner, B. L., and Kutzbach, J. E.: Northern Hemisphere forcing of Southern Hemisphere climate during the last deglaciation, Nature, 494, 81–85, https://doi.org/10.1038/nature11822, 2013.

Heine, J. T. and Mctigue, D. F.: A case for cold-based continental ice sheets — a transient thermal model, J. Glaciol., 42, 37–42, https://doi.org/10.3189/S0022143000030513, 1996.

Heinemann, M., Timmermann, A., Elison Timm, O., Saito, F., and Abe-Ouchi, A.: Deglacial ice sheet meltdown: orbital pacemaking and CO_2 effects, Clim. Past, 10, 1567–1579, https://doi.org/10.5194/cp-10-1567-2014, 2014.

Heinrich, H.: Origin and consequences of cyclic ice rafting in the Northeast Atlantic Ocean during the past 130,000 years, Quat. Res., 29, 142–152, https://doi.org/10.1016/0033-5894(88)90057-9, 1988.

Hemming, S. R.: Heinrich events: Massive late Pleistocene detritus layers of the North Atlantic and their global climate imprint, Rev. Geophys., 42, https://doi.org/10.1029/2003RG000128, 2004.

Hewitt, I. J.: Subglacial Plumes, Annu. Rev. Fluid Mech., 52, 145–169, https://doi.org/10.1146/annurev-fluid-010719-060252, 2020.

Heymsfield, A. J.: Precipitation Development in Stratiform Ice Clouds: A Microphysical and Dynamical Study, 1977.

Hinck, S., Gowan, E. J., Zhang, X., and Lohmann, G.: PISM-LakeCC: Implementing an adaptive proglacial lake boundary in an ice sheet model, The Cryosphere, 16, 941–965, https://doi.org/10.5194/tc-16-941-2022, 2022.

Hindmarsh, R. C. A.: Consistent generation of ice-streams via thermo-viscous instabilities modulated by membrane stresses, Geophys. Res. Lett., 36, https://doi.org/10.1029/2008GL036877, 2009.

Hofer, D., Raible, C. C., Dehnert, A., and Kuhlemann, J.: The impact of different glacial boundary conditions on atmospheric dynamics and precipitation in the North Atlantic region, Clim. Past, 8, 935–949, https://doi.org/10.5194/cp-8-935-2012, 2012.

Hofer, S., Tedstone, A. J., Fettweis, X., and Bamber, J. L.: Decreasing cloud cover drives the recent mass loss on the Greenland Ice Sheet, Sci. Adv., 3, e1700584, https://doi.org/10.1126/sciadv.1700584, 2017.

Hoffman, J. S., Clark, P. U., Parnell, A. C., and He, F.: Regional and global sea-surface temperatures during the last interglaciation, Science, 355, 276–279, https://doi.org/10.1126/science.aai8464, 2017.

Hoffman, M. and Price, S.: Feedbacks between coupled subglacial hydrology and glacier dynamics, J. Geophys. Res. Earth Surf., 119, 414–436, https://doi.org/10.1002/2013JF002943, 2014.

Holden, P. B., Edwards, N. R., Oliver, K. I. C., Lenton, T. M., and Wilkinson, R. D.: A probabilistic calibration of climate sensitivity and terrestrial carbon change in GENIE-1, Clim. Dyn., 35, 785–806, https://doi.org/10.1007/s00382-009-0630-8, 2010.

Holland, P. R., Jenkins, A., and Holland, D. M.: The Response of Ice Shelf Basal Melting to Variations in Ocean Temperature, J. Clim., 21, 2558–2572, https://doi.org/10.1175/2007JCLI1909.1, 2008.

Hopcroft, P. O., Valdes, P. J., and Ingram, W.: Using the Mid-Holocene "Greening" of the Sahara to Narrow Acceptable Ranges on Climate Model Parameters, Geophys. Res. Lett., 48, e2020GL092043, https://doi.org/10.1029/2020GL092043, 2021.

Horton, D. E., Poulsen, C. J., and Pollard, D.: Influence of high-latitude vegetation feedbacks on late Palaeozoic glacial cycles, Nat. Geosci., 3, 572–577, https://doi.org/10.1038/ngeo922, 2010.

Hostetler, S. W., Bartlein, P. J., Clark, P. U., Small, E. E., and Solomon, A. M.: Simulated influences of Lake Agassiz on the climate of central North America 11,000 years ago, Nature, 405, 334–337, https://doi.org/10.1038/35012581, 2000.

Huang, X., Yang, S., Haywood, A., Tindall, J., Jiang, D., Wang, Y., Sun, M., and Zhang, S.: How changing the height of the Antarctic ice sheet affects global climate: a mid-Pliocene case study, Clim. Past, 19, 731–745, https://doi.org/10.5194/cp-19-731-2023, 2023.

Hubbard, A., Bradwell, T., Golledge, N., Hall, A., Patton, H., Sugden, D., Cooper, R., and Stoker, M.: Dynamic cycles, ice streams and their impact on the extent, chronology and deglaciation of the British–Irish ice sheet, Quat. Sci. Rev., 28, 758–776, https://doi.org/10.1016/j.quascirev.2008.12.026, 2009.

Hughes, A. L. C., Gyllencreutz, R., Lohne, Ø. S., Mangerud, J., and Svendsen, J. I.: The last Eurasian ice sheets – a chronological database and time-slice reconstruction, DATED-1, Boreas, 45, 1–45, https://doi.org/10.1111/bor.12142, 2016.

Hughes, P. D. and Gibbard, P. L.: Global glacier dynamics during 100 ka Pleistocene glacial cycles, Quat. Res., 90, 222–243, https://doi.org/10.1017/qua.2018.37, 2018.

Hughes, P. D., Gibbard, P. L., and Ehlers, J.: Timing of glaciation during the last glacial cycle: evaluating the concept of a global 'Last Glacial Maximum' (LGM), Earth-Sci. Rev., 125, 171–198, https://doi.org/10.1016/j.earscirev.2013.07.003, 2013.

Huntley, B., Allen, J. R. M., Forrest, M., Hickler, T., Ohlemüller, R., Singarayer, J. S., and Valdes, P. J.: Global biome patterns of the Middle and Late Pleistocene, J. Biogeogr., 50, 1352–1372, https://doi.org/10.1111/jbi.14619, 2023.

Huybers, P.: Early Pleistocene Glacial Cycles and the Integrated Summer Insolation Forcing, Science, 313, 508–511, https://doi.org/10.1126/science.1125249, 2006.

Imbrie, J., Berger, A., Boyle, E. A., Clemens, S. C., Duffy, A., Howard, W. R., Kukla, G., Kutzbach, J., Martinson, D. G., McIntyre, A., Mix, A. C., Molfino, B., Morley, J. J., Peterson, L. C., Pisias, N. G., Prell, W. L., Raymo, M. E., Shackleton, N. J., and Toggweiler, J. R.: On the structure and origin of major glaciation cycles 2. The 100,000-year cycle, Paleoceanography, 8, 699–735, https://doi.org/10.1029/93PA02751, 1993.

Intergovernmental Panel on Climate Change (IPCC) (Ed.): Evaluation of Climate Models, in: Climate Change 2013 – The Physical Science Basis: Working Group I Contribution to the Fifth Assessment Report of the Intergovernmental Panel on Climate Change, Cambridge University Press, Cambridge, 741–866, https://doi.org/10.1017/CBO9781107415324.020, 2014.

Intergovernmental Panel on Climate Change (IPCC): Climate Change 2021 – The Physical Science Basis: Working Group I Contribution to the Sixth Assessment Report of the Intergovernmental Panel on Climate Change, 1st ed., Cambridge University Press, https://doi.org/10.1017/9781009157896, 2023a.

Intergovernmental Panel on Climate Change (IPCC) (Ed.): Future Global Climate: Scenario-based Projections and Near-term Information, in: Climate Change 2021 – The Physical Science Basis: Working Group I Contribution to the Sixth Assessment Report of the Intergovernmental Panel on Climate Change, Cambridge University Press, Cambridge, 553–672, https://doi.org/10.1017/9781009157896.006, 2023b.

Intergovernmental Panel on Climate Change (IPCC) (Ed.): Ocean, Cryosphere and Sea Level Change, in: Climate Change 2021 – The Physical Science Basis: Working Group I Contribution to the Sixth Assessment Report of the Intergovernmental Panel on Climate

Change, Cambridge University Press, Cambridge, 1211–1362, https://doi.org/10.1017/9781009157896.011, 2023c.

Ivanovic, R. F., Gregoire, L. J., Kageyama, M., Roche, D. M., Valdes, P. J., Burke, A., Drummond, R., Peltier, W. R., and Tarasov, L.: Transient climate simulations of the deglaciation 21–9 thousand years before present (version 1) – PMIP4 Core experiment design and boundary conditions, Geosci. Model Dev., 9, 2563–2587, https://doi.org/10.5194/gmd-9-2563-2016, 2016.

Ivanovic, R. F., Gregoire, L. J., Wickert, A. D., Valdes, P. J., and Burke, A.: Collapse of the North American ice saddle 14,500 years ago caused widespread cooling and reduced ocean overturning circulation, Geophys. Res. Lett., 44, 383–392, https://doi.org/10.1002/2016GL071849, 2017.

Izeboud, M., Lhermitte, S., Van Tricht, K., Lenaerts, J. T. M., Van Lipzig, N. P. M., and Wever, N.: The Spatiotemporal Variability of Cloud Radiative Effects on the Greenland Ice Sheet Surface Mass Balance, Geophys. Res. Lett., 47, e2020GL087315, https://doi.org/10.1029/2020GL087315, 2020.

Izumi, K., Valdes, P., Ivanovic, R., and Gregoire, L.: Impacts of the PMIP4 ice sheets on Northern Hemisphere climate during the last glacial period, Clim. Dyn., 60, 2481–2499, https://doi.org/10.1007/s00382-022-06456-1, 2023.

Jakobsson, M., Björck, S., Alm, G., Andrén, T., Lindeberg, G., and Svensson, N.-O.: Reconstructing the Younger Dryas ice dammed lake in the Baltic Basin: Bathymetry, area and volume, Glob. Planet. Change, 57, 355–370, https://doi.org/10.1016/j.gloplacha.2007.01.006, 2007.

Jakobsson, M., Nilsson, J., O'Regan, M., Backman, J., Löwemark, L., Dowdeswell, J. A., Mayer, L., Polyak, L., Colleoni, F., Anderson, L. G., Björk, G., Darby, D., Eriksson, B., Hanslik, D., Hell, B., Marcussen, C., Sellén, E., and Wallin, Å.: An Arctic Ocean ice shelf during MIS 6 constrained by new geophysical and geological data, Quat. Sci. Rev., 29, 3505–3517, https://doi.org/10.1016/j.quascirev.2010.03.015, 2010.

Jakobsson, M., Nilsson, J., Anderson, L., Backman, J., Björk, G., Cronin, T. M., Kirchner, N., Koshurnikov, A., Mayer, L., Noormets, R., O'Regan, M., Stranne, C., Ananiev, R., Barrientos Macho, N., Cherniykh, D., Coxall, H., Eriksson, B., Flodén, T., Gemery, L., Gustafsson, Ö., Jerram, K., Johansson, C., Khortov, A., Mohammad, R., and Semiletov, I.:

Evidence for an ice shelf covering the central Arctic Ocean during the penultimate glaciation, Nat. Commun., 7, 10365, https://doi.org/10.1038/ncomms10365, 2016.

Jenkins, A., Dutrieux, P., Jacobs, S. S., McPhail, S. D., Perrett, J. R., Webb, A. T., and White, D.: Observations beneath Pine Island Glacier in West Antarctica and implications for its retreat, Nat. Geosci., 3, 468–472, https://doi.org/10.1038/ngeo890, 2010.

Jennings, C. E.: Terrestrial ice streams—a view from the lobe, Geomorphology, 75, 100–124, https://doi.org/10.1016/j.geomorph.2005.05.016, 2006.

Jiang, D.: Vegetation and soil feedbacks at the Last Glacial Maximum, Palaeogeogr. Palaeoclimatol. Palaeoecol., 268, 39–46, https://doi.org/10.1016/j.palaeo.2008.07.023, 2008.

Jiménez-Amat, P. and Zahn, R.: Offset timing of climate oscillations during the last two glacial-interglacial transitions connected with large-scale freshwater perturbation, Paleoceanography, 30, 768–788, https://doi.org/10.1002/2014PA002710, 2015.

Jonkers, L., Bothe, O., and Kucera, M.: Preface: Advances in paleoclimate data synthesis and analysis of associated uncertainty: towards data–model integration to understand the climate, Clim. Past, 17, 2577–2581, https://doi.org/10.5194/cp-17-2577-2021, 2021.

Joughin, I., Smith, B. E., Howat, I. M., Scambos, T., and Moon, T.: Greenland flow variability from ice-sheet-wide velocity mapping, J. Glaciol., 56, 415–430, https://doi.org/10.3189/002214310792447734, 2010.

Joughin, I., Alley, R. B., and Holland, D. M.: Ice-Sheet Response to Oceanic Forcing, Science, 338, 1172–1176, https://doi.org/10.1126/science.1226481, 2012.

Joughin, I., Smith, B. E., and Medley, B.: Marine Ice Sheet Collapse Potentially Under Way for the Thwaites Glacier Basin, West Antarctica, Science, 344, 735–738, https://doi.org/10.1126/science.1249055, 2014.

Jourdain, N. C., Mathiot, P., Burgard, C., Caillet, J., and Kittel, C.: Ice Shelf Basal Melt Rates in the Amundsen Sea at the End of the 21st Century, Geophys. Res. Lett., 49, e2022GL100629, https://doi.org/10.1029/2022GL100629, 2022.

Jouzel, J., Masson-Delmotte, V., Cattani, O., Dreyfus, G., Falourd, S., Hoffmann, G., Minster, B., Nouet, J., Barnola, J. M., Chappellaz, J., Fischer, H., Gallet, J. C., Johnsen, S.,

Leuenberger, M., Loulergue, L., Luethi, D., Oerter, H., Parrenin, F., Raisbeck, G., Raynaud, D., Schilt, A., Schwander, J., Selmo, E., Souchez, R., Spahni, R., Stauffer, B., Steffensen, J. P., Stenni, B., Stocker, T. F., Tison, J. L., Werner, M., and Wolff, E. W.: Orbital and Millennial Antarctic Climate Variability over the Past 800,000 Years, Science, 317, 793–796, https://doi.org/10.1126/science.1141038, 2007a.

Jouzel, J., Stiévenard, M., Johnsen, S. J., Landais, A., Masson-Delmotte, V., Sveinbjornsdottir, A., Vimeux, F., von Grafenstein, U., and White, J. W. C.: The GRIP deuterium-excess record, Quat. Sci. Rev., 26, 1–17, https://doi.org/10.1016/j.quascirev.2006.07.015, 2007b.

Kachuck, S. B., Martin, D. F., Bassis, J. N., and Price, S. F.: Rapid Viscoelastic Deformation Slows Marine Ice Sheet Instability at Pine Island Glacier, Geophys. Res. Lett., 47, e2019GL086446, https://doi.org/10.1029/2019GL086446, 2020.

Kageyama, M. and Valdes, P. J.: Impact of the North American ice-sheet orography on the Last Glacial Maximum eddies and snowfall, Geophys. Res. Lett., 27, 1515–1518, https://doi.org/10.1029/1999GL011274, 2000.

Kageyama, M., Valdes, P. J., Ramstein, G., Hewitt, C., and Wyputta, U.: Northern Hemisphere Storm Tracks in Present Day and Last Glacial Maximum Climate Simulations: A Comparison of the European PMIP Models, J. Clim., 12, 742–760, https://doi.org/10.1175/1520-0442(1999)012<0742:NHSTIP>2.0.CO;2, 1999.

Kageyama, M., Charbit, S., Ritz, C., Khodri, M., and Ramstein, G.: Quantifying ice-sheet feedbacks during the last glacial inception, Geophys. Res. Lett., 31, https://doi.org/10.1029/2004GL021339, 2004.

Kageyama, M., Albani, S., Braconnot, P., Harrison, S. P., Hopcroft, P. O., Ivanovic, R. F., Lambert, F., Marti, O., Peltier, W. R., Peterschmitt, J.-Y., Roche, D. M., Tarasov, L., Zhang, X., Brady, E. C., Haywood, A. M., LeGrande, A. N., Lunt, D. J., Mahowald, N. M., Mikolajewicz, U., Nisancioglu, K. H., Otto-Bliesner, B. L., Renssen, H., Tomas, R. A., Zhang, Q., Abe-Ouchi, A., Bartlein, P. J., Cao, J., Li, Q., Lohmann, G., Ohgaito, R., Shi, X., Volodin, E., Yoshida, K., Zhang, X., and Zheng, W.: The PMIP4 contribution to CMIP6 – Part 4: Scientific objectives and experimental design of the PMIP4-CMIP6 Last Glacial Maximum experiments and PMIP4 sensitivity experiments, Geosci. Model Dev., 10, 4035–4055, https://doi.org/10.5194/gmd-10-4035-2017, 2017.

Kageyama, M., Harrison, S. P., Kapsch, M.-L., Lofverstrom, M., Lora, J. M., Mikolajewicz, U., Sherriff-Tadano, S., Vadsaria, T., Abe-Ouchi, A., Bouttes, N., Chandan, D., Gregoire, L. J., Ivanovic, R. F., Izumi, K., LeGrande, A. N., Lhardy, F., Lohmann, G., Morozova, P. A., Ohgaito, R., Paul, A., Peltier, W. R., Poulsen, C. J., Quiquet, A., Roche, D. M., Shi, X., Tierney, J. E., Valdes, P. J., Volodin, E., and Zhu, J.: The PMIP4 Last Glacial Maximum experiments: preliminary results and comparison with the PMIP3 simulations, Clim. Past, 17, 1065–1089, https://doi.org/10.5194/cp-17-1065-2021, 2021.

Kapsch, M.-L., Mikolajewicz, U., Ziemen, F., and Schannwell, C.: Ocean Response in Transient Simulations of the Last Deglaciation Dominated by Underlying Ice-Sheet Reconstruction and Method of Meltwater Distribution, Geophys. Res. Lett., 49, e2021GL096767, https://doi.org/10.1029/2021GL096767, 2022.

Kazmierczak, E., Sun, S., Coulon, V., and Pattyn, F.: Subglacial hydrology modulates basal sliding response of the Antarctic ice sheet to climate forcing, The Cryosphere, 16, 4537–4552, https://doi.org/10.5194/tc-16-4537-2022, 2022.

Kennedy, M. C. and O'Hagan, A.: Bayesian Calibration of Computer Models, J. R. Stat. Soc. Ser. B Stat. Methodol., 63, 425–464, https://doi.org/10.1111/1467-9868.00294, 2001.

Kirchner, N., Ahlkrona, J., Gowan, E. J., Lötstedt, P., Lea, J. M., Noormets, R., von Sydow, L., Dowdeswell, J. A., and Benham, T.: Shallow ice approximation, second order shallow ice approximation, and full Stokes models: A discussion of their roles in palaeo-ice sheet modelling and development, Quat. Sci. Rev., 147, 136–147, https://doi.org/10.1016/j.quascirev.2016.01.032, 2016.

Kleman, J. and Borgström, I.: Reconstruction of Palaeo-Ice Sheets: The Use of Geomorphological Data, Earth Surf. Process. Landf., 21, 893–909, https://doi.org/10.1002/(SICI)1096-9837(199610)21:10<893::AID-ESP620>3.0.CO;2-U, 1996.

Kleman, J., Hättestrand, C., Stroeven, A. P., Jansson, K. N., De Angelis, H., and Borgström, I.: Reconstruction of Palaeo-Ice Sheets - Inversion of their Glacial Geomorphological Record, in: Glacier Science and Environmental Change, John Wiley & Sons, Ltd, 192–198, https://doi.org/10.1002/9780470750636.ch38, 2006.

Knies, J., Kleiber, H.-P., Matthiessen, J., Müller, C., and Nowaczyk, N.: Marine ice-rafted debris records constrain maximum extent of Saalian and Weichselian ice-sheets along the

northern Eurasian margin, Glob. Planet. Change, 31, 45–64, https://doi.org/10.1016/S0921-8181(01)00112-6, 2001.

Köhler, P., Nehrbass-Ahles, C., Schmitt, J., Stocker, T. F., and Fischer, H.: A 156 kyr smoothed history of the atmospheric greenhouse gases CO_2, CH_4, and N_2O and their radiative forcing, Earth Syst. Sci. Data, 9, 363–387, https://doi.org/10.5194/essd-9-363-2017, 2017.

Konrad, H., Sasgen, I., Pollard, D., and Klemann, V.: Potential of the solid-Earth response for limiting long-term West Antarctic Ice Sheet retreat in a warming climate, Earth Planet. Sci. Lett., 432, 254–264, https://doi.org/10.1016/j.epsl.2015.10.008, 2015.

Kopp, R. E., Simons, F. J., Mitrovica, J. X., Maloof, A. C., and Oppenheimer, M.: Probabilistic assessment of sea level during the last interglacial stage, Nature, 462, 863–867, https://doi.org/10.1038/nature08686, 2009.

Kopp, R. E., DeConto, R. M., Bader, D. A., Hay, C. C., Horton, R. M., Kulp, S., Oppenheimer, M., Pollard, D., and Strauss, B. H.: Evolving Understanding of Antarctic Ice-Sheet Physics and Ambiguity in Probabilistic Sea-Level Projections, Earths Future, 5, 1217–1233, https://doi.org/10.1002/2017EF000663, 2017.

Krinner, G., Mangerud, J., Jakobsson, M., Crucifix, M., Ritz, C., and Svendsen, J. I.: Enhanced ice sheet growth in Eurasia owing to adjacent ice-dammed lakes, Nature, 427, 429–432, https://doi.org/10.1038/nature02233, 2004.

Krinner, G., Boucher, O., and Balkanski, Y.: Ice-free glacial northern Asia due to dust deposition on snow, Clim. Dyn., 27, 613–625, https://doi.org/10.1007/s00382-006-0159-z, 2006.

Krinner, G., Diekmann, B., Colleoni, F., and Stauch, G.: Global, regional and local scale factors determining glaciation extent in Eastern Siberia over the last 140,000 years, Quat. Sci. Rev., 30, 821–831, https://doi.org/10.1016/j.quascirev.2011.01.001, 2011.

Lambeck, K., Purcell, A., Funder, S., KJæR, K. H., Larsen, E., and Moller, P.: Constraints on the Late Saalian to early Middle Weichselian ice sheet of Eurasia from field data and rebound modelling, Boreas, 35, 539–575, https://doi.org/10.1080/03009480600781875, 2006.

Lambeck, K., Rouby, H., Purcell, A., Sun, Y., and Sambridge, M.: Sea level and global ice volumes from the Last Glacial Maximum to the Holocene, Proc. Natl. Acad. Sci., 111, 15296–15303, https://doi.org/10.1073/pnas.1411762111, 2014.

Lambeck, K., Purcell, A., and Zhao, S.: The North American Late Wisconsin ice sheet and mantle viscosity from glacial rebound analyses, Quat. Sci. Rev., 158, 172–210, https://doi.org/10.1016/j.quascirev.2016.11.033, 2017.

Lambert, F., Delmonte, B., Petit, J. R., Bigler, M., Kaufmann, P. R., Hutterli, M. A., Stocker, T. F., Ruth, U., Steffensen, J. P., and Maggi, V.: Dust-climate couplings over the past 800,000 years from the EPICA Dome C ice core, Nature, 452, 616–619, https://doi.org/10.1038/nature06763, 2008.

Landais, A., Dreyfus, G., Capron, E., Jouzel, J., Masson-Delmotte, V., Roche, D. M., Prié, F., Caillon, N., Chappellaz, J., Leuenberger, M., Lourantou, A., Parrenin, F., Raynaud, D., and Teste, G.: Two-phase change in CO2, Antarctic temperature and global climate during Termination II, Nat. Geosci., 6, 1062–1065, https://doi.org/10.1038/ngeo1985, 2013.

Landais, A., Masson-Delmotte, V., Capron, E., Langebroek, P. M., Bakker, P., Stone, E. J., Merz, N., Raible, C. C., Fischer, H., Orsi, A., Prié, F., Vinther, B., and Dahl-Jensen, D.: How warm was Greenland during the last interglacial period?, Clim. Past, 12, 1933–1948, https://doi.org/10.5194/cp-12-1933-2016, 2016.

Le clec'h, S., Charbit, S., Quiquet, A., Fettweis, X., Dumas, C., Kageyama, M., Wyard, C., and Ritz, C.: Assessment of the Greenland ice sheet–atmosphere feedbacks for the next century with a regional atmospheric model coupled to an ice sheet model, The Cryosphere, 13, 373–395, https://doi.org/10.5194/tc-13-373-2019, 2019.

Lecavalier, B. S., Milne, G. A., Simpson, M. J. R., Wake, L., Huybrechts, P., Tarasov, L., Kjeldsen, K. K., Funder, S., Long, A. J., Woodroffe, S., Dyke, A. S., and Larsen, N. K.: A model of Greenland ice sheet deglaciation constrained by observations of relative sea level and ice extent, Quat. Sci. Rev., 102, 54–84, https://doi.org/10.1016/j.quascirev.2014.07.018, 2014.

Lee, V., Cornford, S. L., and Payne, A. J.: Initialization of an ice-sheet model for present-day Greenland, Ann. Glaciol., 56, 129–140, https://doi.org/10.3189/2015AoG70A121, 2015.

Levermann, A. and Winkelmann, R.: A simple equation for the melt elevation feedback of ice sheets, The Cryosphere, 10, 1799–1807, https://doi.org/10.5194/tc-10-1799-2016, 2016.

Li, D., DeConto, R. M., and Pollard, D.: Climate model differences contribute deep uncertainty in future Antarctic ice loss, Sci. Adv., 9, eadd7082, https://doi.org/10.1126/sciadv.add7082, 2023a.

Li, Q., Marshall, J., Rye, C. D., Romanou, A., Rind, D., and Kelley, M.: Global Climate Impacts of Greenland and Antarctic Meltwater: A Comparative Study, https://doi.org/10.1175/JCLI-D-22-0433.1, 2023b.

Li, S., Rupp, D. E., Hawkins, L., Mote, P. W., McNeall, D., Sparrow, S. N., Wallom, D. C. H., Betts, R. A., and Wettstein, J. J.: Reducing climate model biases by exploring parameter space with large ensembles of climate model simulations and statistical emulation, Geosci. Model Dev., 12, 3017–3043, https://doi.org/10.5194/gmd-12-3017-2019, 2019.

Li, Y., Napieralski, J., Harbor, J., and Hubbard, A.: Identifying patterns of correspondence between modeled flow directions and field evidence: An automated flow direction analysis, Comput. Geosci., 33, 141–150, https://doi.org/10.1016/j.cageo.2006.06.016, 2007.

Li, Y., Napieralski, J., and Harbor, J.: A revised automated proximity and conformity analysis method to compare predicted and observed spatial boundaries of geologic phenomena, Comput. Geosci., 34, 1806–1814, https://doi.org/10.1016/j.cageo.2008.01.003, 2008.

Liakka, J. and Lofverstrom, M.: Arctic warming induced by the Laurentide Ice Sheet topography, Clim. Past, 14, 887–900, https://doi.org/10.5194/cp-14-887-2018, 2018.

Liakka, J. and Nilsson, J.: The impact of topographically forced stationary waves on local ice-sheet climate, J. Glaciol., 56, 534–544, https://doi.org/10.3189/002214310792447824, 2010.

Liakka, J., Nilsson, J., and Löfverström, M.: Interactions between stationary waves and ice sheets: linear versus nonlinear atmospheric response, Clim. Dyn., 38, 1249–1262, https://doi.org/10.1007/s00382-011-1004-6, 2012.

Liakka, J., Löfverström, M., and Colleoni, F.: The impact of the North American glacial topography on the evolution of the Eurasian ice sheet over the last glacial cycle, Clim. Past, 12, 1225–1241, https://doi.org/10.5194/cp-12-1225-2016, 2016.

Lin, Y., Hibbert, F. D., Whitehouse, P. L., Woodroffe, S. A., Purcell, A., Shennan, I., and Bradley, S. L.: A reconciled solution of Meltwater Pulse 1A sources using sea-level fingerprinting, Nat. Commun., 12, 2015, https://doi.org/10.1038/s41467-021-21990-y, 2021.

Lisiecki, L. E.: Links between eccentricity forcing and the 100,000-year glacial cycle, Nat. Geosci., 3, 349–352, https://doi.org/10.1038/ngeo828, 2010.

Lisiecki, L. E. and Raymo, M. E.: A Pliocene-Pleistocene stack of 57 globally distributed benthic δ18O records, Paleoceanography, 20, https://doi.org/10.1029/2004PA001071, 2005.

Liu, Y., Moore, J. C., Cheng, X., Gladstone, R. M., Bassis, J. N., Liu, H., Wen, J., and Hui, F.: Ocean-driven thinning enhances iceberg calving and retreat of Antarctic ice shelves, Proc. Natl. Acad. Sci., 112, 3263–3268, https://doi.org/10.1073/pnas.1415137112, 2015.

Liu, Z., Otto-Bliesner, B. L., He, F., Brady, E. C., Tomas, R., Clark, P. U., Carlson, A. E., Lynch-Stieglitz, J., Curry, W., Brook, E., Erickson, D., Jacob, R., Kutzbach, J., and Cheng, J.: Transient Simulation of Last Deglaciation with a New Mechanism for Bølling-Allerød Warming, Science, 325, 310–314, https://doi.org/10.1126/science.1171041, 2009.

Liu, Z., Bao, Y., Thompson, L. G., Mosley-Thompson, E., Tabor, C., Zhang, G. J., Yan, M., Lofverstrom, M., Montanez, I., and Oster, J.: Tropical mountain ice core δ18O: A Goldilocks indicator for global temperature change, Sci. Adv., 9, eadi6725, https://doi.org/10.1126/sciadv.adi6725, 2023.

Loeppky, J. L., Sacks, J., and Welch, W. J.: Choosing the Sample Size of a Computer Experiment: A Practical Guide, Technometrics, 51, 366–376, https://doi.org/10.1198/TECH.2009.08040, 2009.

Lofverstrom, M. and Liakka, J.: The influence of atmospheric grid resolution in a climate model-forced ice sheet simulation, The Cryosphere, 12, 1499–1510, https://doi.org/10.5194/tc-12-1499-2018, 2018.

Löfverström, M. and Lora, J. M.: Abrupt regime shifts in the North Atlantic atmospheric circulation over the last deglaciation, Geophys. Res. Lett., 44, 8047–8055, https://doi.org/10.1002/2017GL074274, 2017.

Löfverström, M., Caballero, R., Nilsson, J., and Kleman, J.: Evolution of the large-scale atmospheric circulation in response to changing ice sheets over the last glacial cycle, Clim. Past, 10, 1453–1471, https://doi.org/10.5194/cp-10-1453-2014, 2014.

Löfverström, M., Caballero, R., Nilsson, J., and Messori, G.: Stationary Wave Reflection as a Mechanism for Zonalizing the Atlantic Winter Jet at the LGM, https://doi.org/10.1175/JAS-D-15-0295.1, 2016.

Loulergue, L., Schilt, A., Spahni, R., Masson-Delmotte, V., Blunier, T., Lemieux, B., Barnola, J.-M., Raynaud, D., Stocker, T. F., and Chappellaz, J.: Orbital and millennial-scale features of atmospheric CH4 over the past 800,000 years, Nature, 453, 383–386, https://doi.org/10.1038/nature06950, 2008.

Lunt, D. J., Haywood, A. M., Schmidt, G. A., Salzmann, U., Valdes, P. J., Dowsett, H. J., and Loptson, C. A.: On the causes of mid-Pliocene warmth and polar amplification, Earth Planet. Sci. Lett., 321–322, 128–138, https://doi.org/10.1016/j.epsl.2011.12.042, 2012.

Lüthi, D., Le Floch, M., Bereiter, B., Blunier, T., Barnola, J.-M., Siegenthaler, U., Raynaud, D., Jouzel, J., Fischer, H., Kawamura, K., and Stocker, T. F.: High-resolution carbon dioxide concentration record 650,000–800,000 years before present, Nature, 453, 379–382, https://doi.org/10.1038/nature06949, 2008.

Mackintosh, A. N., Verleyen, E., O'Brien, P. E., White, D. A., Jones, R. S., McKay, R., Dunbar, R., Gore, D. B., Fink, D., Post, A. L., Miura, H., Leventer, A., Goodwin, I., Hodgson, D. A., Lilly, K., Crosta, X., Golledge, N. R., Wagner, B., Berg, S., van Ommen, T., Zwartz, D., Roberts, S. J., Vyverman, W., and Masse, G.: Retreat history of the East Antarctic Ice Sheet since the Last Glacial Maximum, Quat. Sci. Rev., 100, 10–30, https://doi.org/10.1016/j.quascirev.2013.07.024, 2014.

Manabe, S. and Broccoli, A. J.: The influence of continental ice sheets on the climate of an ice age, J. Geophys. Res. Atmospheres, 90, 2167–2190, https://doi.org/10.1029/JD090iD01p02167, 1985.

Marcott, S. A., Clark, P. U., Padman, L., Klinkhammer, G. P., Springer, S. R., Liu, Z., Otto-Bliesner, B. L., Carlson, A. E., Ungerer, A., Padman, J., He, F., Cheng, J., and Schmittner, A.: Ice-shelf collapse from subsurface warming as a trigger for Heinrich events, Proc. Natl. Acad. Sci. U. S. A., 108, 13415–13419, https://doi.org/10.1073/pnas.1104772108, 2011.

Marcott, S. A., Bauska, T. K., Buizert, C., Steig, E. J., Rosen, J. L., Cuffey, K. M., Fudge, T. J., Severinghaus, J. P., Ahn, J., Kalk, M. L., McConnell, J. R., Sowers, T., Taylor, K. C., White, J. W. C., and Brook, E. J.: Centennial-scale changes in the global carbon cycle during the last deglaciation, Nature, 514, 616–619, https://doi.org/10.1038/nature13799, 2014.

Margari, V., Skinner, L. C., Hodell, D. A., Martrat, B., Toucanne, S., Grimalt, J. O., Gibbard, P. L., Lunkka, J. P., and Tzedakis, P. C.: Land-ocean changes on orbital and millennial time scales and the penultimate glaciation, Geology, 42, 183–186, https://doi.org/10.1130/G35070.1, 2014.

Margold, M., Stokes, C. R., and Clark, C. D.: Reconciling records of ice streaming and ice margin retreat to produce a palaeogeographic reconstruction of the deglaciation of the Laurentide Ice Sheet, Quat. Sci. Rev., 189, 1–30, https://doi.org/10.1016/j.quascirev.2018.03.013, 2018.

Marino, G., Rohling, E. J., Rodríguez-Sanz, L., Grant, K. M., Heslop, D., Roberts, A. P., Stanford, J. D., and Yu, J.: Bipolar seesaw control on last interglacial sea level, Nature, 522, 197–201, https://doi.org/10.1038/nature14499, 2015.

Marshall, S. J. and Clark, P. U.: Basal temperature evolution of North American ice sheets and implications for the 100-kyr cycle, Geophys. Res. Lett., 29, 67-1-67–4, https://doi.org/10.1029/2002GL015192, 2002.

Marshall, S. J., James, T. S., and Clarke, G. K. C.: North American Ice Sheet reconstructions at the Last Glacial Maximum, Quat. Sci. Rev., 21, 175–192, https://doi.org/10.1016/S0277-3791(01)00089-0, 2002.

Marsiat, I. and Valdes, P. J.: Sensitivity of the Northern Hemisphere climate of the Last Glacial Maximum to sea surface temperatures, Clim. Dyn., 17, 233–248, https://doi.org/10.1007/s003820000108, 2001.

Martin, M. A., Winkelmann, R., Haseloff, M., Albrecht, T., Bueler, E., Khroulev, C., and Levermann, A.: The Potsdam Parallel Ice Sheet Model (PISM-PIK) – Part 2: Dynamic equilibrium simulation of the Antarctic ice sheet, The Cryosphere, 5, 727–740, https://doi.org/10.5194/tc-5-727-2011, 2011.

Martrat, B., Jimenez-Amat, P., Zahn, R., and Grimalt, J. O.: Similarities and dissimilarities between the last two deglaciations and interglaciations in the North Atlantic region, Quat. Sci. Rev., 99, 122–134, https://doi.org/10.1016/j.quascirev.2014.06.016, 2014.

Masson-Delmotte, V., Stenni, B., Pol, K., Braconnot, P., Cattani, O., Falourd, S., Kageyama, M., Jouzel, J., Landais, A., Minster, B., Barnola, J. M., Chappellaz, J., Krinner, G., Johnsen, S., Röthlisberger, R., Hansen, J., Mikolajewicz, U., and Otto-Bliesner, B.: EPICA Dome C record of glacial and interglacial intensities, Quat. Sci. Rev., 29, 113–128, https://doi.org/10.1016/j.quascirev.2009.09.030, 2010.

Masson-Delmotte, V., Schulz, M., Abe-Ouchi, A., Beer, J., Ganopolski, A., Fidel, J., Rouco, G., Jansen, E., Lambeck, K., Luterbacher, J., Naish, T., Ramesh, R., Rojas, M., Shao, X., Anchukaitis, K., Arblaster, J., Bartlein, P. J., Benito, G., Clark, P., Comiso, J. C., Crowley, T., Deckker, P. D., de Vernal, A., Delmonte, B., DiNezio, P., Dowsett, H. J., Edwards, R. L., Fischer, H., Fleitmann, D., Foster, G., Fröhlich, C., Hall, A., Hargreaves, J., Haywood, A., Hollis, C., Krinner, G., Landais, A., Li, C., Lunt, D., Mahowald, N., McGregor, S., Meehl, G., Mitrovica, J. X., Moberg, A., Mudelsee, M., Muhs, D. R., Mulitza, S., Müller, S., Overland, J., Parrenin, F., Pearson, P., Robock, A., Rohling, E., Salzmann, U., Savarino, J., Sedláček, J., Shindell, D., Smerdon, J., Solomina, O., Tarasov, P., Vinther, B., Waelbroeck, C., Wolf, D., Yokoyama, Y., Yoshimori, M., Zachos, J., Zwartz, D., Gupta, A. K., Rahimzadeh, F., Raynaud, D., and Wanner, H.: Information from Paleoclimate Archives, 2013.

Matero, I. S. O., Gregoire, L. J., and Ivanovic, R. F.: Simulating the Early Holocene demise of the Laurentide Ice Sheet with BISICLES (public trunk revision 3298), Geosci. Model Dev., 13, 4555–4577, https://doi.org/10.5194/gmd-13-4555-2020, 2020.

McGuffie, K. and Henderson-Sellers, A.: A Climate Modelling Primer, John Wiley & Sons, 302 pp., 2005.

McKay, M. D.: Latin hypercube sampling as a tool in uncertainty analysis of computer models, in: Proceedings of the 24th conference on Winter simulation - WSC '92, the 24th conference, Arlington, Virginia, United States, 557–564, https://doi.org/10.1145/167293.167637, 1992.

McKay, N. P., Overpeck, J. T., and Otto-Bliesner, B. L.: The role of ocean thermal expansion in Last Interglacial sea level rise, Geophys. Res. Lett., 38, https://doi.org/10.1029/2011GL048280, 2011.

McManus, J. F., Oppo, D. W., and Cullen, J. L.: A 0.5-Million-Year Record of Millennial-Scale Climate Variability in the North Atlantic, Science, 283, 971–975, https://doi.org/10.1126/science.283.5404.971, 1999.

McManus, J. F., Francois, R., Gherardi, J.-M., Keigwin, L. D., and Brown-Leger, S.: Collapse and rapid resumption of Atlantic meridional circulation linked to deglacial climate changes, Nature, 428, 834–837, https://doi.org/10.1038/nature02494, 2004.

Meehl, G. A., Senior, C. A., Eyring, V., Flato, G., Lamarque, J.-F., Stouffer, R. J., Taylor, K. E., and Schlund, M.: Context for interpreting equilibrium climate sensitivity and transient climate response from the CMIP6 Earth system models, Sci. Adv., 6, eaba1981, https://doi.org/10.1126/sciadv.aba1981, 2020.

Meissner, K. J., Weaver, A. J., Matthews, H. D., and Cox, P. M.: The role of land surface dynamics in glacial inception: a study with the UVic Earth System Model, Clim. Dyn., 21, 515–537, https://doi.org/10.1007/s00382-003-0352-2, 2003.

Menviel, L., Timmermann, A., Timm, O. E., and Mouchet, A.: Deconstructing the Last Glacial termination: the role of millennial and orbital-scale forcings, Quat. Sci. Rev., 30, 1155–1172, https://doi.org/10.1016/j.quascirev.2011.02.005, 2011.

Menviel, L., Capron, E., Govin, A., Dutton, A., Tarasov, L., Abe-Ouchi, A., Drysdale, R. N., Gibbard, P. L., Gregoire, L., He, F., Ivanovic, R. F., Kageyama, M., Kawamura, K., Landais, A., Otto-Bliesner, B. L., Oyabu, I., Tzedakis, P. C., Wolff, E., and Zhang, X.: The penultimate deglaciation: protocol for Paleoclimate Modelling Intercomparison Project (PMIP) phase 4 transient numerical simulations between 140 and 127 ka, version 1.0, Geosci. Model Dev., 12, 3649–3685, https://doi.org/10.5194/gmd-12-3649-2019, 2019.

Merz, N., Raible, C. C., and Woollings, T.: North Atlantic Eddy-Driven Jet in Interglacial and Glacial Winter Climates, J. Clim., 28, 3977–3997, https://doi.org/10.1175/JCLI-D-14-00525.1, 2015.

Milne, G. A., Mitrovica, J. X., and Schrag, D. P.: Estimating past continental ice volume from sea-level data, Quat. Sci. Rev., 21, 361–376, https://doi.org/10.1016/S0277-3791(01)00108-1, 2002.

Moreno-Parada, D., Alvarez-Solas, J., Blasco, J., Montoya, M., and Robinson, A.: Simulating the Laurentide Ice Sheet of the Last Glacial Maximum, The Cryosphere, 17, 2139–2156, https://doi.org/10.5194/tc-17-2139-2023, 2023.

Mostue, I. A., Hofer, S., Storelvmo, T., and Fettweis, X.: Cloud- and ice-albedo feedbacks drive greater Greenland Ice Sheet sensitivity to warming in CMIP6 than in CMIP5, The Cryosphere, 18, 475–488, https://doi.org/10.5194/tc-18-475-2024, 2024.

Muntjewerf, L., Sacks, W. J., Lofverstrom, M., Fyke, J., Lipscomb, W. H., Ernani da Silva, C., Vizcaino, M., Thayer-Calder, K., Lenaerts, J. T. M., and Sellevold, R.: Description and Demonstration of the Coupled Community Earth System Model v2 – Community Ice Sheet Model v2 (CESM2-CISM2), J. Adv. Model. Earth Syst., 13, e2020MS002356, https://doi.org/10.1029/2020MS002356, 2021.

Munyikwa, K., Feathers, J. K., Rittenour, T. M., and Shrimpton, H. K.: Constraining the Late Wisconsinan retreat of the Laurentide ice sheet from western Canada using luminescence ages from postglacial aeolian dunes, Quat. Geochronol., 6, 407–422, https://doi.org/10.1016/j.quageo.2011.03.010, 2011.

Naafs, B. D. A., Hefter, J., Acton, G., Haug, G. H., Martínez-Garcia, A., Pancost, R., and Stein, R.: Strengthening of North American dust sources during the late Pliocene (2.7 Ma), Earth Planet. Sci. Lett., 317–318, 8–19, https://doi.org/10.1016/j.epsl.2011.11.026, 2012a.

Naafs, B. D. A., Hefter, J., Acton, G., Haug, G. H., Martínez-Garcia, A., Pancost, R., and Stein, R.: Strengthening of North American dust sources during the late Pliocene (2.7 Ma), Earth Planet. Sci. Lett., 317–318, 8–19, https://doi.org/10.1016/j.epsl.2011.11.026, 2012b.

Naafs, B. D. A., Hefter, J., and Stein, R.: Millennial-scale ice rafting events and Hudson Strait Heinrich(-like) Events during the late Pliocene and Pleistocene: a review, Quat. Sci. Rev., 80, 1–28, https://doi.org/10.1016/j.quascirev.2013.08.014, 2013.

Napieralski, J., Li, Y., and Harbor, J.: Comparing predicted and observed spatial boundaries of geologic phenomena: Automated Proximity and Conformity Analysis applied to ice sheet

reconstructions, Comput. Geosci., 32, 124–134, https://doi.org/10.1016/j.cageo.2005.05.011, 2006.

Näslund, J.-O., Jansson, P., Fastook, J. L., Johnson, J., and Andersson, L.: Detailed spatially distributed geothermal heat-flow data for modeling of basal temperatures and meltwater production beneath the Fennoscandian ice sheet, Ann. Glaciol., 40, 95–101, https://doi.org/10.3189/172756405781813582, 2005.

Ng, H. C., Robinson, L. F., McManus, J. F., Mohamed, K. J., Jacobel, A. W., Ivanovic, R. F., Gregoire, L. J., and Chen, T.: Coherent deglacial changes in western Atlantic Ocean circulation, Nat. Commun., 9, 2947, https://doi.org/10.1038/s41467-018-05312-3, 2018.

Nias, I. J., Cornford, S. L., and Payne, A. J.: New Mass-Conserving Bedrock Topography for Pine Island Glacier Impacts Simulated Decadal Rates of Mass Loss, Geophys. Res. Lett., 45, 3173–3181, https://doi.org/10.1002/2017GL076493, 2018.

Nicholl, J. A. L., Hodell, D. A., Naafs, B. D. A., Hillaire-Marcel, C., Channell, J. E. T., and Romero, O. E.: A Laurentide outburst flooding event during the last interglacial period, Nat. Geosci., 5, 901–904, https://doi.org/10.1038/ngeo1622, 2012.

Niessen, F., Hong, J. K., Hegewald, A., Matthiessen, J., Stein, R., Kim, H., Kim, S., Jensen, L., Jokat, W., Nam, S.-I., and Kang, S.-H.: Repeated Pleistocene glaciation of the East Siberian continental margin, Nat. Geosci., 6, 842–846, https://doi.org/10.1038/ngeo1904, 2013.

Niu, L., Lohmann, G., Hinck, S., Gowan, E. J., and Krebs-Kanzow, U.: The sensitivity of Northern Hemisphere ice sheets to atmospheric forcing during the last glacial cycle using PMIP3 models, J. Glaciol., 65, 645–661, https://doi.org/10.1017/jog.2019.42, 2019.

Niu, L., Lohmann, G., Gierz, P., Gowan, E. J., and Knorr, G.: Coupled climate-ice sheet modelling of MIS-13 reveals a sensitive Cordilleran Ice Sheet, Glob. Planet. Change, 200, 103474, https://doi.org/10.1016/j.gloplacha.2021.103474, 2021.

Norris, S. L., Garcia-Castellanos, D., Jansen, J. D., Carling, P. A., Margold, M., Woywitka, R. J., and Froese, D. G.: Catastrophic Drainage From the Northwestern Outlet of Glacial Lake Agassiz During the Younger Dryas, Geophys. Res. Lett., 48, e2021GL093919, https://doi.org/10.1029/2021GL093919, 2021.

Nowicki, S. and Seroussi, H.: Projections of Future Sea Level Contributions from the Greenland and Antarctic Ice Sheets: Challenges Beyond Dynamical Ice Sheet Modeling, Oceanography, 31, 109–117, https://doi.org/10.5670/oceanog.2018.216, 2018.

Oakley, J. E. and O'Hagan, A.: Probabilistic Sensitivity Analysis of Complex Models: A Bayesian Approach, J. R. Stat. Soc. Ser. B Stat. Methodol., 66, 751–769, https://doi.org/10.1111/j.1467-9868.2004.05304.x, 2004.

Obase, T., Abe-Ouchi, A., and Saito, F.: Abrupt climate changes in the last two deglaciations simulated with different Northern ice sheet discharge and insolation, Sci. Rep., 11, 22359, https://doi.org/10.1038/s41598-021-01651-2, 2021.

Obrochta, S. P., Crowley, T. J., Channell, J. E. T., Hodell, D. A., Baker, P. A., Seki, A., and Yokoyama, Y.: Climate variability and ice-sheet dynamics during the last three glaciations, Earth Planet. Sci. Lett., 406, 198–212, https://doi.org/10.1016/j.epsl.2014.09.004, 2014.

Oppo, D. W., McManus, J. F., and Cullen, J. L.: Evolution and demise of the Last Interglacial warmth in the subpolar North Atlantic, Quat. Sci. Rev., 25, 3268–3277, https://doi.org/10.1016/j.quascirev.2006.07.006, 2006.

Osman, M. B., Tierney, J. E., Zhu, J., Tardif, R., Hakim, G. J., King, J., and Poulsen, C. J.: Globally resolved surface temperatures since the Last Glacial Maximum, Nature, 599, 239–244, https://doi.org/10.1038/s41586-021-03984-4, 2021.

Otto-Bliesner, B. L., Rosenbloom, N., Stone, E. J., McKay, N. P., Lunt, D. J., Brady, E. C., and Overpeck, J. T.: How warm was the last interglacial? New model–data comparisons, Philos. Trans. R. Soc. Math. Phys. Eng. Sci., 371, 20130097, https://doi.org/10.1098/rsta.2013.0097, 2013a.

Otto-Bliesner, B. L., Rosenbloom, N., Stone, E. J., McKay, N. P., Lunt, D. J., Brady, E. C., and Overpeck, J. T.: How warm was the last interglacial? New model–data comparisons, Philos. Trans. R. Soc. Math. Phys. Eng. Sci., 371, 20130097, https://doi.org/10.1098/rsta.2013.0097, 2013b.

Pages, P. I. W. G. of: Interglacials of the last 800,000 years, Rev. Geophys., 54, 162–219, https://doi.org/10.1002/2015RG000482, 2016.

Parizek, B. R. and Alley, R. B.: Implications of increased Greenland surface melt under global-warming scenarios: ice-sheet simulations, Quat. Sci. Rev., 23, 1013–1027, https://doi.org/10.1016/j.quascirev.2003.12.024, 2004.

Parker, R. L., Foster, G. L., Gutjahr, M., Wilson, P. A., Littler, K. L., Cooper, M. J., Michalik, A., Milton, J. A., Crocket, K. C., and Bailey, I.: Laurentide Ice Sheet extent over the last 130 thousand years traced by the Pb isotope signature of weathering inputs to the Labrador Sea, Quat. Sci. Rev., 287, 107564, https://doi.org/10.1016/j.quascirev.2022.107564, 2022.

Patterson, V. L., Gregoire, L. J., Ivanovic, R., Gandy, N., Owen, J., Smith, R. S., Pollard, O. G., and Astfalck, L. C.: Contrasting the Penultimate and Last Glacial Maxima (140 and 21 ka BP) using coupled climate-ice sheet modelling, Clim. Past Discuss., 1–37, https://doi.org/10.5194/cp-2024-10, 2024.

Patton, H., Andreassen, K., Bjarnadóttir, L. R., Dowdeswell, J. A., Winsborrow, M. C. M., Noormets, R., Polyak, L., Auriac, A., and Hubbard, A.: Geophysical constraints on the dynamics and retreat of the Barents Sea ice sheet as a paleobenchmark for models of marine ice sheet deglaciation, Rev. Geophys., 53, 1051–1098, https://doi.org/10.1002/2015RG000495, 2015.

Patton, H., Hubbard, A., Andreassen, K., Winsborrow, M., and Stroeven, A. P.: The build-up, configuration, and dynamical sensitivity of the Eurasian ice-sheet complex to Late Weichselian climatic and oceanic forcing, Quat. Sci. Rev., 153, 97–121, https://doi.org/10.1016/j.quascirev.2016.10.009, 2016.

Patton, H., Hubbard, A., Andreassen, K., Auriac, A., Whitehouse, P. L., Stroeven, A. P., Shackleton, C., Winsborrow, M., Heyman, J., and Hall, A. M.: Deglaciation of the Eurasian ice sheet complex, Quat. Sci. Rev., 169, 148–172, https://doi.org/10.1016/j.quascirev.2017.05.019, 2017.

Pattyn, F.: A new three-dimensional higher-order thermomechanical ice sheet model: Basic sensitivity, ice stream development, and ice flow across subglacial lakes, J. Geophys. Res. Solid Earth, 108, https://doi.org/10.1029/2002JB002329, 2003.

Pattyn, F., Schoof, C., Perichon, L., Hindmarsh, R. C. A., Bueler, E., de Fleurian, B., Durand, G., Gagliardini, O., Gladstone, R., Goldberg, D., Gudmundsson, G. H., Huybrechts, P., Lee, V., Nick, F. M., Payne, A. J., Pollard, D., Rybak, O., Saito, F., and Vieli, A.: Results of the

Marine Ice Sheet Model Intercomparison Project, MISMIP, The Cryosphere, 6, 573–588, https://doi.org/10.5194/tc-6-573-2012, 2012.

Pattyn, F., Perichon, L., Durand, G., Favier, L., Gagliardini, O., Hindmarsh, R. C. A., Zwinger, T., Albrecht, T., Cornford, S., Docquier, D., Fürst, J. J., Goldberg, D., Gudmundsson, G. H., Humbert, A., Hütten, M., Huybrechts, P., Jouvet, G., Kleiner, T., Larour, E., Martin, D., Morlighem, M., Payne, A. J., Pollard, D., Rückamp, M., Rybak, O., Seroussi, H., Thoma, M., and Wilkens, N.: Grounding-line migration in plan-view marine ice-sheet models: results of the ice2sea MISMIP3d intercomparison, J. Glaciol., 59, 410–422, https://doi.org/10.3189/2013JoG12J129, 2013.

Pattyn, F., Favier, L., Sun, S., and Durand, G.: Progress in Numerical Modeling of Antarctic Ice-Sheet Dynamics, Curr. Clim. Change Rep., 3, 174–184, https://doi.org/10.1007/s40641-017-0069-7, 2017.

Pattyn, F., Ritz, C., Hanna, E., Asay-Davis, X., DeConto, R., Durand, G., Favier, L., Fettweis, X., Goelzer, H., Golledge, N. R., Kuipers Munneke, P., Lenaerts, J. T. M., Nowicki, S., Payne, A. J., Robinson, A., Seroussi, H., Trusel, L. D., and van den Broeke, M.: The Greenland and Antarctic ice sheets under 1.5 °C global warming, Nat. Clim. Change, 8, 1053–1061, https://doi.org/10.1038/s41558-018-0305-8, 2018.

Paul, A., Mulitza, S., Stein, R., and Werner, M.: Glacial Ocean Map (GLOMAP), https://doi.org/10.1594/PANGAEA.923262, 2020.

Paul, A., Mulitza, S., Stein, R., and Werner, M.: A global climatology of the ocean surface during the Last Glacial Maximum mapped on a regular grid (GLOMAP), Clim. Past, 17, 805–824, https://doi.org/10.5194/cp-17-805-2021, 2021.

Pelt, W. J. J. V. and Oerlemans, J.: Numerical simulations of cyclic behaviour in the Parallel Ice Sheet Model (PISM), J. Glaciol., 58, 347–360, https://doi.org/10.3189/2012JoG11J217, 2012.

Peltier, W. R., Argus, D. F., and Drummond, R.: Space geodesy constrains ice age terminal deglaciation: The global ICE-6G_C (VM5a) model, J. Geophys. Res. Solid Earth, 120, 450–487, https://doi.org/10.1002/2014JB011176, 2015.

Petit, J. R., Jouzel, J., Raynaud, D., Barkov, N. I., Barnola, J.-M., Basile, I., Bender, M., Chappellaz, J., Davis, M., Delaygue, G., Delmotte, M., Kotlyakov, V. M., Legrand, M.,

Lipenkov, V. Y., Lorius, C., PÉpin, L., Ritz, C., Saltzman, E., and Stievenard, M.: Climate and atmospheric history of the past 420,000 years from the Vostok ice core, Antarctica, Nature, 399, 429–436, https://doi.org/10.1038/20859, 1999.

Petoukhov, V., Claussen, M., Berger, A., Crucifix, M., Eby, M., Eliseev, A. V., Fichefet, T., Ganopolski, A., Goosse, H., Kamenkovich, I., Mokhov, I. I., Montoya, M., Mysak, L. A., Sokolov, A., Stone, P., Wang, Z., and Weaver, A. J.: EMIC Intercomparison Project (EMIP–CO2): comparative analysis of EMIC simulations of climate, and of equilibrium and transient responses to atmospheric CO2 doubling, Clim. Dyn., 25, 363–385, https://doi.org/10.1007/s00382-005-0042-3, 2005.

Petrini, M., Colleoni, F., Kirchner, N., Hughes, A. L. C., Camerlenghi, A., Rebesco, M., Lucchi, R. G., Forte, E., Colucci, R. R., and Noormets, R.: Interplay of grounding-line dynamics and sub-shelf melting during retreat of the Bjørnøyrenna Ice Stream, Sci. Rep., 8, 7196, https://doi.org/10.1038/s41598-018-25664-6, 2018.

Petrini, M., Colleoni, F., Kirchner, N., Hughes, A. L. C., Camerlenghi, A., Rebesco, M., Lucchi, R. G., Forte, E., Colucci, R. R., Noormets, R., and Mangerud, J.: Simulated last deglaciation of the Barents Sea Ice Sheet primarily driven by oceanic conditions, Quat. Sci. Rev., 238, 106314, https://doi.org/10.1016/j.quascirev.2020.106314, 2020.

Peyaud, V.: Rôle de la dynamique des calottes glaciaires dans les grands changements climatiques des périodes glaciaires-interglaciaires., PhD Thesis, Université Joseph-Fourier - Grenoble I, 2006.

Pittard, M. L., Whitehouse, P. L., Bentley, M. J., and Small, D.: An ensemble of Antarctic deglacial simulations constrained by geological observations, Quat. Sci. Rev., 298, 107800, https://doi.org/10.1016/j.quascirev.2022.107800, 2022.

Pollard, D.: A retrospective look at coupled ice sheet–climate modeling, Clim. Change, 100, 173–194, https://doi.org/10.1007/s10584-010-9830-9, 2010.

Pollard, D. and DeConto, R. M.: Description of a hybrid ice sheet-shelf model, and application to Antarctica, Geosci. Model Dev., 5, 1273–1295, https://doi.org/10.5194/gmd-5-1273-2012, 2012.

Pollard, D., Chang, W., Haran, M., Applegate, P., and DeConto, R.: Large ensemble modeling of the last deglacial retreat of the West Antarctic Ice Sheet: comparison of simple and

advanced statistical techniques, Geosci. Model Dev., 9, 1697–1723, https://doi.org/10.5194/gmd-9-1697-2016, 2016.

Pollard, O. G., Barlow, N. L. M., Gregoire, L. J., Gomez, N., Cartelle, V., Ely, J. C., and Astfalck, L. C.: Quantifying the uncertainty in the Eurasian ice-sheet geometry at the Penultimate Glacial Maximum (Marine Isotope Stage 6), The Cryosphere, 17, 4751–4777, https://doi.org/10.5194/tc-17-4751-2023, 2023.

Pope, V. D., Gallani, M. L., Rowntree, P. R., and Stratton, R. A.: The impact of new physical parametrizations in the Hadley Centre climate model: HadAM3, Clim. Dyn., 16, 123–146, https://doi.org/10.1007/s003820050009, 2000.

Pritchard, M. S., Bush, A. B. G., and Marshall, S. J.: Neglecting ice-atmosphere interactions underestimates ice sheet melt in millennial-scale deglaciation simulations, Geophys. Res. Lett., 35, 2007GL031738, https://doi.org/10.1029/2007GL031738, 2008.

Pukelsheim, F.: The Three Sigma Rule, Am. Stat., 48, 88–91, https://doi.org/10.1080/00031305.1994.10476030, 1994.

Quiquet, A. and Roche, D. M.: Investigating similarities and differences of the penultimate and last glacial terminations with a coupled ice sheet–climate model, Clim. Past, 20, 1365–1385, https://doi.org/10.5194/cp-20-1365-2024, 2024.

Quiquet, A., Ritz, C., Punge, H. J., and Salas y Mélia, D.: Greenland ice sheet contribution to sea level rise during the last interglacial period: a modelling study driven and constrained by ice core data, Clim. Past, 9, 353–366, https://doi.org/10.5194/cp-9-353-2013, 2013.

Quiquet, A., Roche, D. M., Dumas, C., Bouttes, N., and Lhardy, F.: Climate and ice sheet evolutions from the last glacial maximum to the pre-industrial period with an ice-sheet–climate coupled model, Clim. Past, 17, 2179–2199, https://doi.org/10.5194/cp-17-2179-2021, 2021a.

Quiquet, A., Dumas, C., Paillard, D., Ramstein, G., Ritz, C., and Roche, D. M.: Deglacial Ice Sheet Instabilities Induced by Proglacial Lakes, Geophys. Res. Lett., 48, e2020GL092141, https://doi.org/10.1029/2020GL092141, 2021b.

Rabineau, M., Berné, S., Olivet, J.-L., Aslanian, D., Guillocheau, F., and Joseph, P.: Paleo sea levels reconsidered from direct observation of paleoshoreline position during Glacial

Maxima (for the last 500,000 yr), Earth Planet. Sci. Lett., 252, 119–137, https://doi.org/10.1016/j.epsl.2006.09.033, 2006.

Rahmstorf, S., Box, J. E., Feulner, G., Mann, M. E., Robinson, A., Rutherford, S., and Schaffernicht, E. J.: Exceptional twentieth-century slowdown in Atlantic Ocean overturning circulation, Nat. Clim. Change, 5, 475–480, https://doi.org/10.1038/nclimate2554, 2015.

Reed, B., Green, J. A. M., Jenkins, A., and Gudmundsson, G. H.: Recent irreversible retreat phase of Pine Island Glacier, Nat. Clim. Change, 14, 75–81, https://doi.org/10.1038/s41558-023-01887-y, 2024.

Rignot, E. and Jacobs, S. S.: Rapid Bottom Melting Widespread near Antarctic Ice Sheet Grounding Lines, Science, 296, 2020–2023, https://doi.org/10.1126/science.1070942, 2002.

Rignot, E., Mouginot, J., and Scheuchl, B.: Ice Flow of the Antarctic Ice Sheet, Science, 333, 1427–1430, https://doi.org/10.1126/science.1208336, 2011.

Rignot, E., Jacobs, S., Mouginot, J., and Scheuchl, B.: Ice-Shelf Melting Around Antarctica, Science, 341, 266–270, https://doi.org/10.1126/science.1235798, 2013.

Rignot, E., Mouginot, J., Scheuchl, B., van den Broeke, M., van Wessem, M. J., and Morlighem, M.: Four decades of Antarctic Ice Sheet mass balance from 1979–2017, Proc. Natl. Acad. Sci., 116, 1095–1103, https://doi.org/10.1073/pnas.1812883116, 2019.

Robel, A. A. and Tziperman, E.: The role of ice stream dynamics in deglaciation, J. Geophys. Res. Earth Surf., 121, 1540–1554, https://doi.org/10.1002/2016JF003937, 2016.

Roberts, D. H., Long, A. J., Schnabel, C., Davies, B. J., Xu, S., Simpson, M. J. R., and Huybrechts, P.: Ice sheet extent and early deglacial history of the southwestern sector of the Greenland Ice Sheet, Quat. Sci. Rev., 28, 2760–2773, https://doi.org/10.1016/j.quascirev.2009.07.002, 2009.

Roberts, W. H. G., Valdes, P. J., and Payne, A. J.: Topography's crucial role in Heinrich Events, Proc. Natl. Acad. Sci., 111, 16688–16693, https://doi.org/10.1073/pnas.1414882111, 2014.

Roe, G. H. and Lindzen, R. S.: The Mutual Interaction between Continental-Scale Ice Sheets and Atmospheric Stationary Waves, J. Clim., 14, 1450–1465, https://doi.org/10.1175/1520-0442(2001)014<1450:TMIBCS>2.0.CO;2, 2001.

Rohling, E. J., Hibbert, F. D., Williams, F. H., Grant, K. M., Marino, G., Foster, G. L., Hennekam, R., de Lange, G. J., Roberts, A. P., Yu, J., Webster, J. M., and Yokoyama, Y.: Differences between the last two glacial maxima and implications for ice-sheet, δ18O, and sea-level reconstructions, Quat. Sci. Rev., 176, 1–28, https://doi.org/10.1016/j.quascirev.2017.09.009, 2017.

Rohling, E. J., Hibbert, F. D., Grant, K. M., Galaasen, E. V., Irvalı, N., Kleiven, H. F., Marino, G., Ninnemann, U., Roberts, A. P., Rosenthal, Y., Schulz, H., Williams, F. H., and Yu, J.: Asynchronous Antarctic and Greenland ice-volume contributions to the last interglacial sea-level highstand, Nat. Commun., 10, 5040, https://doi.org/10.1038/s41467-019-12874-3, 2019.

Romé, Y. M., Ivanovic, R. F., Gregoire, L. J., Sherriff-Tadano, S., and Valdes, P. J.: Millennial-Scale Climate Oscillations Triggered by Deglacial Meltwater Discharge in Last Glacial Maximum Simulations, Paleoceanogr. Paleoclimatology, 37, e2022PA004451, https://doi.org/10.1029/2022PA004451, 2022.

Rougier, J., Maute, A., Guillas, S., and Richmond, A. D.: Expert Knowledge and Multivariate Emulation: The Thermosphere-lonosphere Electrodynamics General Circulation Model (TIE-GCM), Technometrics, 51, 414–424, 2009.

Rutt, I. C., Hagdorn, M., Hulton, N. R. J., and Payne, A. J.: The Glimmer community ice sheet model, J. Geophys. Res. Earth Surf., 114, https://doi.org/10.1029/2008JF001015, 2009.

Ryan, J. C., Smith, L. C., Cooley, S. W., Pearson, B., Wever, N., Keenan, E., and Lenaerts, J. T. M.: Decreasing surface albedo signifies a growing importance of clouds for Greenland Ice Sheet meltwater production, Nat. Commun., 13, 4205, https://doi.org/10.1038/s41467-022-31434-w, 2022.

Saltelli, A.: Making best use of model evaluations to compute sensitivity indices, Comput. Phys. Commun., 145, 280–297, https://doi.org/10.1016/S0010-4655(02)00280-1, 2002.

Scherrenberg, M., Berends, C., and Van De Wal, R.: Late Pleistocene glacial terminations accelerated by proglacial lakes, https://doi.org/10.5194/cp-2023-42, 3 July 2023a.

Scherrenberg, M. D. W., Berends, C. J., Stap, L. B., and van de Wal, R. S. W.: Modelling feedbacks between the Northern Hemisphere ice sheets and climate during the last glacial cycle, Clim. Past, 19, 399–418, https://doi.org/10.5194/cp-19-399-2023, 2023b.

Schilt, A., Baumgartner, M., Schwander, J., Buiron, D., Capron, E., Chappellaz, J., Loulergue, L., Schüpbach, S., Spahni, R., Fischer, H., and Stocker, T. F.: Atmospheric nitrous oxide during the last 140,000 years, Earth Planet. Sci. Lett., 300, 33–43, https://doi.org/10.1016/j.epsl.2010.09.027, 2010.

Schmidt, G. A., Annan, J. D., Bartlein, P. J., Cook, B. I., Guilyardi, E., Hargreaves, J. C., Harrison, S. P., Kageyama, M., LeGrande, A. N., Konecky, B., Lovejoy, S., Mann, M. E., Masson-Delmotte, V., Risi, C., Thompson, D., Timmermann, A., Tremblay, L.-B., and Yiou, P.: Using palaeo-climate comparisons to constrain future projections in CMIP5, Clim. Past, 10, 221–250, https://doi.org/10.5194/cp-10-221-2014, 2014a.

Schmidt, P., Lund, B., Näslund, J.-O., and Fastook, J.: Comparing a thermo-mechanical Weichselian Ice Sheet reconstruction to reconstructions based on the sea level equation: aspects of ice configurations and glacial isostatic adjustment, Solid Earth, 5, 371–388, https://doi.org/10.5194/se-5-371-2014, 2014b.

Schmittner, A., Urban, N. M., Shakun, J. D., Mahowald, N. M., Clark, P. U., Bartlein, P. J., Mix, A. C., and Rosell-Melé, A.: Climate Sensitivity Estimated from Temperature Reconstructions of the Last Glacial Maximum, Science, 334, 1385–1388, https://doi.org/10.1126/science.1203513, 2011.

Schneider von Deimling, T., Ganopolski, A., Held, H., and Rahmstorf, S.: How cold was the Last Glacial Maximum?, Geophys. Res. Lett., 33, https://doi.org/10.1029/2006GL026484, 2006.

Schoof, C.: A variational approach to ice stream flow, J. Fluid Mech., 556, 227–251, https://doi.org/10.1017/S0022112006009591, 2006.

Schoof, C.: Ice sheet grounding line dynamics: Steady states, stability, and hysteresis, J. Geophys. Res.: Earth Surface, 112, https://doi.org/10.1029/2006JF000664, 2007.

Schoof, C. and Hindmarsh, R. C. A.: Thin-Film Flows with Wall Slip: An Asymptotic Analysis of Higher Order Glacier Flow Models, Q. J. Mech. Appl. Math., 63, 73–114, https://doi.org/10.1093/qjmam/hbp025, 2010.

Sejrup, H. P., Nygård, A., Hall, A. M., and Haflidason, H.: Middle and Late Weichselian (Devensian) glaciation history of south-western Norway, North Sea and eastern UK, Quat. Sci. Rev., 28, 370–380, https://doi.org/10.1016/j.quascirev.2008.10.019, 2009.

Sejrup, H. P., Hjelstuen, B. O., Patton, H., Esteves, M., Winsborrow, M., Rasmussen, T. L., Andreassen, K., and Hubbard, A.: The role of ocean and atmospheric dynamics in the marine-based collapse of the last Eurasian Ice Sheet, Commun. Earth Environ., 3, 1–10, https://doi.org/10.1038/s43247-022-00447-0, 2022.

Sellevold, R., van Kampenhout, L., Lenaerts, J. T. M., Noël, B., Lipscomb, W. H., and Vizcaino, M.: Surface mass balance downscaling through elevation classes in an Earth system model: application to the Greenland ice sheet, The Cryosphere, 13, 3193–3208, https://doi.org/10.5194/tc-13-3193-2019, 2019.

Shackleton, S., Baggenstos, D., Menking, J. A., Dyonisius, M. N., Bereiter, B., Bauska, T. K., Rhodes, R. H., Brook, E. J., Petrenko, V. V., McConnell, J. R., Kellerhals, T., Häberli, M., Schmitt, J., Fischer, H., and Severinghaus, J. P.: Global ocean heat content in the Last Interglacial, Nat. Geosci., 13, 77–81, https://doi.org/10.1038/s41561-019-0498-0, 2020.

Shakun, J. D., Lea, D. W., Lisiecki, L. E., and Raymo, M. E.: An 800-kyr record of global surface ocean δ18O and implications for ice volume-temperature coupling, Earth Planet. Sci. Lett., 426, 58–68, https://doi.org/10.1016/j.epsl.2015.05.042, 2015.

Sherriff-Tadano, S., Abe-Ouchi, A., Yoshimori, M., Oka, A., and Chan, W.-L.: Influence of glacial ice sheets on the Atlantic meridional overturning circulation through surface wind change, Clim. Dyn., 50, 2881–2903, https://doi.org/10.1007/s00382-017-3780-0, 2018.

Sherriff-Tadano, S., Abe-Ouchi, A., and Oka, A.: Impact of mid-glacial ice sheets on deep ocean circulation and global climate, Clim. Past, 17, 95–110, https://doi.org/10.5194/cp-17-95-2021, 2021.

Sherriff-Tadano, S., Ivanovic, R., Gregoire, L., Lang, C., Gandy, N., Gregory, J., Edwards, T. L., Pollard, O., and Smith, R. S.: Large-ensemble simulations of the North American and Greenland ice sheets at the Last Glacial Maximum with a coupled atmospheric general circulation–ice sheet model, Clim. Past, 20, 1489–1512, https://doi.org/10.5194/cp-20-1489-2024, 2024.

Shi, Y., Gong, W., Duan, Q., Charles, J., Xiao, C., and Wang, H.: How parameter specification of an Earth system model of intermediate complexity influences its climate simulations, Prog. Earth Planet. Sci., 6, 46, https://doi.org/10.1186/s40645-019-0294-x, 2019.

Simms, A. R., Lisiecki, L., Gebbie, G., Whitehouse, P. L., and Clark, J. F.: Balancing the last glacial maximum (LGM) sea-level budget, Quat. Sci. Rev., 205, 143–153, https://doi.org/10.1016/j.quascirev.2018.12.018, 2019.

Smith, R. N. B.: A scheme for predicting layer clouds and their water content in a general circulation model, Q. J. R. Meteorol. Soc., 116, 435–460, https://doi.org/10.1002/qj.49711649210, 1990.

Smith, R. S. and Gregory, J.: The last glacial cycle: transient simulations with an AOGCM, Clim. Dyn., 38, 1545–1559, https://doi.org/10.1007/s00382-011-1283-y, 2012.

Smith, R. S., Gregory, J. M., and Osprey, A.: A description of the FAMOUS (version XDBUA) climate model and control run, Geosci. Model Dev., 1, 53–68, https://doi.org/10.5194/gmd-1-53-2008, 2008.

Smith, R. S., Mathiot, P., Siahaan, A., Lee, V., Cornford, S. L., Gregory, J. M., Payne, A. J., Jenkins, A., Holland, P. R., Ridley, J. K., and Jones, C. G.: Coupling the U.K. Earth System Model to Dynamic Models of the Greenland and Antarctic Ice Sheets, J. Adv. Model. Earth Syst., 13, e2021MS002520, https://doi.org/10.1029/2021MS002520, 2021a.

Smith, R. S., George, S., and Gregory, J. M.: FAMOUS version xotzt (FAMOUS-ice): a general circulation model (GCM) capable of energy- and water-conserving coupling to an ice sheet model, Geosci. Model Dev., 14, 5769–5787, https://doi.org/10.5194/gmd-14-5769-2021, 2021b.

Smith-Johnsen, S., Schlegel, N.-J., de Fleurian, B., and Nisancioglu, K. H.: Sensitivity of the Northeast Greenland Ice Stream to Geothermal Heat, J. Geophys. Res. Earth Surf., 125, e2019JF005252, https://doi.org/10.1029/2019JF005252, 2020.

Snoll, B., Ivanovic, R. F., Valdes, P. J., Maycock, A. C., and Gregoire, L. J.: Effect of orographic gravity wave drag on Northern Hemisphere climate in transient simulations of the last deglaciation, Clim. Dyn., 59, 2067–2079, https://doi.org/10.1007/s00382-022-06196-2, 2022.

Snoll, B., Ivanovic, R., Gregoire, L., Sherriff-Tadano, S., Menviel, L., Obase, T., Abe-Ouchi, A., Bouttes, N., He, C., He, F., Kapsch, M., Mikolajewicz, U., Muglia, J., and Valdes, P.: A multi-model assessment of the early last deglaciation (PMIP4 LDv1): a meltwater perspective, Clim. Past, 20, 789–815, https://doi.org/10.5194/cp-20-789-2024, 2024.

Sobol′, I. M.: Global sensitivity indices for nonlinear mathematical models and their Monte Carlo estimates, Math. Comput. Simul., 55, 271–280, https://doi.org/10.1016/S0378-4754(00)00270-6, 2001.

Spahni, R., Chappellaz, J., Stocker, T. F., Loulergue, L., Hausammann, G., Kawamura, K., Flückiger, J., Schwander, J., Raynaud, D., Masson-Delmotte, V., and Jouzel, J.: Atmospheric Methane and Nitrous Oxide of the Late Pleistocene from Antarctic Ice Cores, Science, 310, 1317–1321, https://doi.org/10.1126/science.1120132, 2005.

Stap, L. B., van de Wal, R. S. W., de Boer, B., Bintanja, R., and Lourens, L. J.: Interaction of ice sheets and climate during the past 800 000 years, Clim. Past, 10, 2135–2152, https://doi.org/10.5194/cp-10-2135-2014, 2014.

Stein, R., Fahl, K., Gierz, P., Niessen, F., and Lohmann, G.: Arctic Ocean sea ice cover during the penultimate glacial and the last interglacial, Nat. Commun., 8, 373, https://doi.org/10.1038/s41467-017-00552-1, 2017.

Stirling, C. H., Esat, T. M., Lambeck, K., and McCulloch, M. T.: Timing and duration of the Last Interglacial: evidence for a restricted interval of widespread coral reef growth, Earth Planet. Sci. Lett., 160, 745–762, https://doi.org/10.1016/S0012-821X(98)00125-3, 1998.

Stocker, T. F. and Johnsen, S. J.: A minimum thermodynamic model for the bipolar seesaw, Paleoceanography, 18, https://doi.org/10.1029/2003PA000920, 2003.

Stokes, C. R. and Clark, C. D.: Palaeo-ice streams, Quat. Sci. Rev., 20, 1437–1457, https://doi.org/10.1016/S0277-3791(01)00003-8, 2001.

Stokes, C. R., Tarasov, L., Blomdin, R., Cronin, T. M., Fisher, T. G., Gyllencreutz, R., Hättestrand, C., Heyman, J., Hindmarsh, R. C. A., Hughes, A. L. C., Jakobsson, M., Kirchner, N., Livingstone, S. J., Margold, M., Murton, J. B., Noormets, R., Peltier, W. R., Peteet, D. M., Piper, D. J. W., Preusser, F., Renssen, H., Roberts, D. H., Roche, D. M., Saint-Ange, F., Stroeven, A. P., and Teller, J. T.: On the reconstruction of palaeo-ice sheets:

Recent advances and future challenges, Quat. Sci. Rev., 125, 15–49, https://doi.org/10.1016/j.quascirev.2015.07.016, 2015.

Stoll, H. M., Cacho, I., Gasson, E., Sliwinski, J., Kost, O., Moreno, A., Iglesias, M., Torner, J., Perez-Mejias, C., Haghipour, N., Cheng, H., and Edwards, R. L.: Rapid northern hemisphere ice sheet melting during the penultimate deglaciation, Nat. Commun., 13, 3819, https://doi.org/10.1038/s41467-022-31619-3, 2022.

Stone, E. J. and Lunt, D. J.: The role of vegetation feedbacks on Greenland glaciation, Clim. Dyn., 40, 2671–2686, https://doi.org/10.1007/s00382-012-1390-4, 2013.

Stone, E. J., Lunt, D. J., Annan, J. D., and Hargreaves, J. C.: Quantification of the Greenland ice sheet contribution to Last Interglacial sea level rise, Clim. Past, 9, 621–639, https://doi.org/10.5194/cp-9-621-2013, 2013.

Sugiyama, S., Minowa, M., Sakakibara, D., Skvarca, P., Sawagaki, T., Ohashi, Y., Naito, N., and Chikita, K.: Thermal structure of proglacial lakes in Patagonia, J. Geophys. Res. Earth Surf., 121, 2270–2286, https://doi.org/10.1002/2016JF004084, 2016.

Sutherland, J. L., Carrivick, J. L., Gandy, N., Shulmeister, J., Quincey, D. J., and Cornford, S. L.: Proglacial Lakes Control Glacier Geometry and Behavior During Recession, Geophys. Res. Lett., 47, e2020GL088865, https://doi.org/10.1029/2020GL088865, 2020.

Svendsen, J. I., Alexanderson, H., Astakhov, V. I., Demidov, I., Dowdeswell, J. A., Funder, S., Gataullin, V., Henriksen, M., Hjort, C., Houmark-Nielsen, M., Hubberten, H. W., Ingólfsson, Ó., Jakobsson, M., Kjær, K. H., Larsen, E., Lokrantz, H., Lunkka, J. P., Lyså, A., Mangerud, J., Matiouchkov, A., Murray, A., Möller, P., Niessen, F., Nikolskaya, O., Polyak, L., Saarnisto, M., Siegert, C., Siegert, M. J., Spielhagen, R. F., and Stein, R.: Late Quaternary ice sheet history of northern Eurasia, Quat. Sci. Rev., 23, 1229–1271, https://doi.org/10.1016/j.quascirev.2003.12.008, 2004.

Tarasov, L. and Peltier, W. R.: Greenland glacial history and local geodynamic consequences, Geophys. J. Int., 150, 198–229, https://doi.org/10.1046/j.1365-246X.2002.01702.x, 2002.

Tarasov, L. and Peltier, W. R.: A geophysically constrained large ensemble analysis of the deglacial history of the North American ice-sheet complex, Quat. Sci. Rev., 23, 359–388, https://doi.org/10.1016/j.quascirev.2003.08.004, 2004.

Tarasov, L., Dyke, A. S., Neal, R. M., and Peltier, W. R.: A data-calibrated distribution of deglacial chronologies for the North American ice complex from glaciological modeling, Earth Planet. Sci. Lett., 315–316, 30–40, https://doi.org/10.1016/j.epsl.2011.09.010, 2012.

Tedesco, M., Fettweis, X., van den Broeke, M. R., van de Wal, R. S. W., Smeets, C. J. P. P., van de Berg, W. J., Serreze, M. C., and Box, J. E.: The role of albedo and accumulation in the 2010 melting record in Greenland, Environ. Res. Lett., 6, 014005, https://doi.org/10.1088/1748-9326/6/1/014005, 2011.

Teller, J. T. and Leverington, D. W.: Glacial Lake Agassiz: A 5000 yr history of change and its relationship to the δ18O record of Greenland, GSA Bull., 116, 729–742, https://doi.org/10.1130/B25316.1, 2004.

Tewari, K., Mishra, S. K., Dewan, A., Dogra, G., and Ozawa, H.: Influence of the height of Antarctic ice sheet on its climate, Polar Sci., 28, 100642, https://doi.org/10.1016/j.polar.2021.100642, 2021.

Tierney, J. E., Zhu, J., King, J., Malevich, S. B., Hakim, G. J., and Poulsen, C. J.: Glacial cooling and climate sensitivity revisited, Nature, 584, 569–573, https://doi.org/10.1038/s41586-020-2617-x, 2020a.

Tierney, J. E., Zhu, J., King, J., Malevich, S. B., Hakim, G., and Poulsen, C.: Last Glacial Maximum SST proxy collection and data assimilation, https://doi.org/10.1594/PANGAEA.920596, 2020b.

Timmermann, A., Knies, J., Timm, O. E., Abe-Ouchi, A., and Friedrich, T.: Promotion of glacial ice sheet buildup 60–115 kyr B.P. by precessionally paced Northern Hemispheric meltwater pulses, Paleoceanography, 25, https://doi.org/10.1029/2010PA001933, 2010.

Truffer, M. and Motyka, R. J.: Where glaciers meet water: Subaqueous melt and its relevance to glaciers in various settings, Rev. Geophys., 54, 220–239, https://doi.org/10.1002/2015RG000494, 2016.

Tsai, V. C., Stewart, A. L., and Thompson, A. F.: Marine ice-sheet profiles and stability under Coulomb basal conditions, J. Glaciol., 61, 205–215, https://doi.org/10.3189/2015JoG14J221, 2015.

Turney, C. S. M. and Jones, R. T.: Does the Agulhas Current amplify global temperatures during super-interglacials?, J. Quat. Sci., 25, 839–843, https://doi.org/10.1002/jqs.1423, 2010.

Turney, C. S. M., Jones, R. T., McKay, N. P., van Sebille, E., Thomas, Z. A., Hillenbrand, C.-D., and Fogwill, C. J.: A global mean sea surface temperature dataset for the Last Interglacial (129–116 ka) and contribution of thermal expansion to sea level change, Earth Syst. Sci. Data, 12, 3341–3356, https://doi.org/10.5194/essd-12-3341-2020, 2020a.

Turney, C. S. M., Fogwill, C. J., Golledge, N. R., McKay, N. P., Van Sebille, E., Jones, R. T., Etheridge, D., Rubino, M., Thornton, D. P., Davies, S. M., Ramsey, C. B., Thomas, Z. A., Bird, M. I., Munksgaard, N. C., Kohno, M., Woodward, J., Winter, K., Weyrich, L. S., Rootes, C. M., Millman, H., Albert, P. G., Rivera, A., Van Ommen, T., Curran, M., Moy, A., Rahmstorf, S., Kawamura, K., Hillenbrand, C.-D., Weber, M. E., Manning, C. J., Young, J., and Cooper, A.: Early Last Interglacial ocean warming drove substantial ice mass loss from Antarctica, Proc. Natl. Acad. Sci., 117, 3996–4006, https://doi.org/10.1073/pnas.1902469117, 2020b.

Ullman, D. J., LeGrande, A. N., Carlson, A. E., Anslow, F. S., and Licciardi, J. M.: Assessing the impact of Laurentide Ice Sheet topography on glacial climate, Clim. Past, 10, 487–507, https://doi.org/10.5194/cp-10-487-2014, 2014.

Ullman, D. J., Carlson, A. E., Hostetler, S. W., Clark, P. U., Cuzzone, J., Milne, G. A., Winsor, K., and Caffee, M.: Final Laurentide ice-sheet deglaciation and Holocene climate-sea level change, Quat. Sci. Rev., 152, 49–59, https://doi.org/10.1016/j.quascirev.2016.09.014, 2016.

Valdes, P. J., Armstrong, E., Badger, M. P. S., Bradshaw, C. D., Bragg, F., Crucifix, M., Davies-Barnard, T., Day, J. J., Farnsworth, A., Gordon, C., Hopcroft, P. O., Kennedy, A. T., Lord, N. S., Lunt, D. J., Marzocchi, A., Parry, L. M., Pope, V., Roberts, W. H. G., Stone, E. J., Tourte, G. J. L., and Williams, J. H. T.: The BRIDGE HadCM3 family of climate models: HadCM3@Bristol v1.0, Geosci. Model Dev., 10, 3715–3743, https://doi.org/10.5194/gmd-10-3715-2017, 2017.

van Aalderen, V., Charbit, S., Dumas, C., and Quiquet, A.: Relative importance of the mechanisms triggering the Eurasian ice sheet deglaciation, EGUsphere, 1–30, https://doi.org/10.5194/egusphere-2023-34, 2023.

van Aalderen, V., Charbit, S., Dumas, C., and Quiquet, A.: Relative importance of the mechanisms triggering the Eurasian ice sheet deglaciation in the GRISLI2.0 ice sheet model, Clim. Past, 20, 187–209, https://doi.org/10.5194/cp-20-187-2024, 2024.

van Calcar, C. J., van de Wal, R. S. W., Blank, B., de Boer, B., and van der Wal, W.: Simulation of a fully coupled 3D glacial isostatic adjustment – ice sheet model for the Antarctic ice sheet over a glacial cycle, Geosci. Model Dev., 16, 5473–5492, https://doi.org/10.5194/gmd-16-5473-2023, 2023.

Vasskog, K., Langebroek, P. M., Andrews, J. T., Nilsen, J. E. Ø., and Nesje, A.: The Greenland Ice Sheet during the last glacial cycle: Current ice loss and contribution to sea-level rise from a palaeoclimatic perspective, Earth-Sci. Rev., 150, 45–67, https://doi.org/10.1016/j.earscirev.2015.07.006, 2015.

Vizcaino, M.: Ice sheets as interactive components of Earth System Models: progress and challenges, WIREs Clim. Change, 5, 557–568, https://doi.org/10.1002/wcc.285, 2014.

Vizcaíno, M., Lipscomb, W. H., Sacks, W. J., Angelen, J. H. van, Wouters, B., and Broeke, M. R. van den: Greenland Surface Mass Balance as Simulated by the Community Earth System Model. Part I: Model Evaluation and 1850–2005 Results, https://doi.org/10.1175/JCLI-D-12-00615.1, 2013.

Waelbroeck, C., Labeyrie, L., Michel, E., Duplessy, J. C., McManus, J. F., Lambeck, K., Balbon, E., and Labracherie, M.: Sea-level and deep water temperature changes derived from benthic foraminifera isotopic records, Quat. Sci. Rev., 21, 295–305, https://doi.org/10.1016/S0277-3791(01)00101-9, 2002.

Waelbroeck, C., Paul, A., Kucera, M., Rosell-Melé, A., Weinelt, M., Schneider, R., Mix, A. C., Abelmann, A., Armand, L., Bard, E., Barker, S., Barrows, T. T., Benway, H., Cacho, I., Chen, M.-T., Cortijo, E., Crosta, X., de Vernal, A., Dokken, T., Duprat, J., Elderfield, H., Eynaud, F., Gersonde, R., Hayes, A., Henry, M., Hillaire-Marcel, C., Huang, C.-C., Jansen, E., Juggins, S., Kallel, N., Kiefer, T., Kienast, M., Labeyrie, L., Leclaire, H., Londeix, L., Mangin, S., Matthiessen, J., Marret, F., Meland, M., Morey, A. E., Mulitza, S., Pflaumann, U., Pisias, N. G., Radi, T., Rochon, A., Rohling, E. J., Sbaffi, L., Schäfer-Neth, C., Solignac, S., Spero, H., Tachikawa, K., Turon, J.-L., and MARGO Project Members: Constraints on the magnitude and patterns of ocean cooling at the Last Glacial Maximum, Nat. Geosci., 2, 127–132, https://doi.org/10.1038/ngeo411, 2009.

Wainer, K. A. I., Rowe, M. P., Thomas, A. L., Mason, A. J., Williams, B., Tamisiea, M. E., Williams, F. H., Düsterhus, A., and Henderson, G. M.: Speleothem evidence for MIS 5c and 5a sea level above modern level at Bermuda, Earth Planet. Sci. Lett., 457, 325–334, https://doi.org/10.1016/j.epsl.2016.10.005, 2017.

Wang, C., Zhang, L., Lee, S.-K., Wu, L., and Mechoso, C. R.: A global perspective on CMIP5 climate model biases, Nat. Clim. Change, 4, 201–205, https://doi.org/10.1038/nclimate2118, 2014.

Weber, S. L.: The utility of Earth system Models of Intermediate Complexity (EMICs), WIREs Clim. Change, 1, 243–252, https://doi.org/10.1002/wcc.24, 2010.

Wekerle, C., Colleoni, F., Näslund, J.-O., Brandefelt, J., and Masina, S.: Numerical reconstructions of the penultimate glacial maximum Northern Hemisphere ice sheets: sensitivity to climate forcing and model parameters, J. Glaciol., 62, 607–622, https://doi.org/10.1017/jog.2016.45, 2016.

Whitehouse, P. L.: Glacial isostatic adjustment modelling: historical perspectives, recent advances, and future directions, Earth Surf. Dyn., 6, 401–429, https://doi.org/10.5194/esurf-6-401-2018, 2018.

Willeit, M. and Ganopolski, A.: The importance of snow albedo for ice sheet evolution over the last glacial cycle, Clim. Past, 14, 697–707, https://doi.org/10.5194/cp-14-697-2018, 2018.

Willeit, M., Calov, R., Talento, S., Greve, R., Bernales, J., Klemann, V., Bagge, M., and Ganopolski, A.: Glacial inception through rapid ice area increase driven by albedo and vegetation feedbacks, Clim. Past, 20, 597–623, https://doi.org/10.5194/cp-20-597-2024, 2024.

Williams, J. H. T., Smith, R. S., Valdes, P. J., Booth, B. B. B., and Osprey, A.: Optimising the FAMOUS climate model: inclusion of global carbon cycling, Geosci. Model Dev., 6, 141–160, https://doi.org/10.5194/gmd-6-141-2013, 2013.

Williamson, D.: Exploratory ensemble designs for environmental models using k-extended Latin Hypercubes, Environmetrics, 26, 268–283, https://doi.org/10.1002/env.2335, 2015.

Williamson, D., Goldstein, M., Allison, L., Blaker, A., Challenor, P., Jackson, L., and Yamazaki, K.: History matching for exploring and reducing climate model parameter space using observations and a large perturbed physics ensemble, Clim. Dyn., 41, 1703–1729, https://doi.org/10.1007/s00382-013-1896-4, 2013.

Williamson, D., Blaker, A. T., Hampton, C., and Salter, J.: Identifying and removing structural biases in climate models with history matching, Clim. Dyn., 45, 1299–1324, https://doi.org/10.1007/s00382-014-2378-z, 2015.

Winsborrow, M. C. M., Andreassen, K., Corner, G. D., and Laberg, J. S.: Deglaciation of a marine-based ice sheet: Late Weichselian palaeo-ice dynamics and retreat in the southern Barents Sea reconstructed from onshore and offshore glacial geomorphology, Quat. Sci. Rev., 29, 424–442, https://doi.org/10.1016/j.quascirev.2009.10.001, 2010.

Wong, C. I. and Breecker, D. O.: Advancements in the use of speleothems as climate archives, Quat. Sci. Rev., 127, 1–18, https://doi.org/10.1016/j.quascirev.2015.07.019, 2015.

Yokoyama, Y. and Purcell, A.: On the geophysical processes impacting palaeo-sea-level observations, Geosci. Lett., 8, 13, https://doi.org/10.1186/s40562-021-00184-w, 2021.

Zeitz, M., Reese, R., Beckmann, J., Krebs-Kanzow, U., and Winkelmann, R.: Impact of the melt–albedo feedback on the future evolution of the Greenland Ice Sheet with PISM-dEBM-simple, The Cryosphere, 15, 5739–5764, https://doi.org/10.5194/tc-15-5739-2021, 2021.

Zeng, P., Sun, F., Liu, Y., Feng, H., Zhang, R., and Che, Y.: Changes of potential evapotranspiration and its sensitivity across China under future climate scenarios, Atmospheric Res., 261, 105763, https://doi.org/10.1016/j.atmosres.2021.105763, 2021.

Zhang, X.-Y., Trame, M. N., Lesko, L. J., and Schmidt, S.: Sobol Sensitivity Analysis: A Tool to Guide the Development and Evaluation of Systems Pharmacology Models, CPT Pharmacomet. Syst. Pharmacol., 4, 69–79, https://doi.org/10.1002/psp4.6, 2015.

Zhu, J., Otto-Bliesner, B. L., Brady, E. C., Gettelman, A., Bacmeister, J. T., Neale, R. B., Poulsen, C. J., Shaw, J. K., McGraw, Z. S., and Kay, J. E.: LGM Paleoclimate Constraints Inform Cloud Parameterizations and Equilibrium Climate Sensitivity in CESM2, J. Adv. Model. Earth Syst., 14, e2021MS002776, https://doi.org/10.1029/2021MS002776, 2022.

Ziemen, F. A., Rodehacke, C. B., and Mikolajewicz, U.: Coupled ice sheet–climate modeling under glacial and pre-industrial boundary conditions, Clim. Past, 10, 1817–1836, https://doi.org/10.5194/cp-10-1817-2014, 2014.

Ziemen, F. A., Kapsch, M.-L., Klockmann, M., and Mikolajewicz, U.: Heinrich events show two-stage climate response in transient glacial simulations, Clim. Past, 15, 153–168, https://doi.org/10.5194/cp-15-153-2019, 2019.

Zwally, H. J., Abdalati, W., Herring, T., Larson, K., Saba, J., and Steffen, K.: Surface Melt-Induced Acceleration of Greenland Ice-Sheet Flow, Science, 297, 218–222, https://doi.org/10.1126/science.1072708, 2002.

Zweck, C. and Huybrechts, P.: Modeling of the northern hemisphere ice sheets during the last glacial cycle and glaciological sensitivity, J. Geophys. Res. Atmospheres, 110, https://doi.org/10.1029/2004JD005489, 2005.